Development of a New Multi-channel Electrode and Signal Processing for Surface Electromyography Signals Feature Extraction

Charles Jeffrey John Kilby

A thesis submitted to
Auckland University of Technology
in fulfilment for the degree of
Doctor of Philosophy

2017

School of Engineering

Abstract

The overall aim of the research reported in this thesis was to build a new multi-channel electrode and to investigate and develop signal processing techniques for sEMG signals, in order to enable the extractions of more useful-features. Analysis of these signal features will assist in the creation of a more effective database for diagnosing muscle ailments and conditions.

The investigation was carried out by observing the fatiguing characteristics of surface electromyography (sEMG) signals collected from the vastus lateralis muscle of the quadriceps of the dominant leg of 40 healthy participants performing an endurance (or fatiguing) task of 50% of their maximum voluntary isometric contraction (MVIC). The signals were collected using a new multi-channel electrode and analysed using an overlapping sliding window algorithm that extracted signal features of the mean frequency (MNF) and muscle fibre conduction velocity (MFCV).

The new multi-channel electrode had 11 pins and each was pre-amplified with a voltage gain of 484 and bandpass filtering from 6.8 Hz to 1.02 kHz to collect monopolar signals. The monopolar signals were then configured by the software as either linear array or Laplacian configuration. A better signal definition in terms of motor unit action potential was achieved with the Laplacian configuration.

This research also investigated a number of different signal processing techniques to extract features for classification purposes of sEMG signals during an endurance or fatiguing task. These included the use of Fast Fourier Transform, Short Time Fourier Transform and Wavelet Transform. Using the Fourier power spectrum, spectral features such as MNF, median frequency (MDF), and temporal features such as root mean square (RMS) and MFCV were determined. The results showed that, of all the signals analysed, the MNF and MDF values showed similar trends and the RMS values showed a linear relationship, which increased over the time period of the signal. The MFCV values meanwhile showed also a similar trend to those of MNF and MDF.

The MNF feature was selected over MDF as it produced a more accurate trend line that closely correlated with the measured values. Statistical analysis was performed on all 40

participants to produce the mean values for determining the range and fatigue times, and determine how much the MNF and MFCV values dropped over the contraction time. The results showed that fatigue times for the 40 participants ranged between 41.6 to 78.8 seconds when performing 50% MVIC. The mean trend lines of the MNF and MFCV features showed a drop in values in the initial and the final fatigue stage. The initial value of MNF dropped by 20.3% of the maximum value during the first 29.8% of the contraction period. The MFCV meanwhile dropped by 20.9% of the maximum value during the first 28.2% of the contraction period. The MNF value dropped by 17.4% at the final fatigue stage whereas the MFCV value dropped by 18.1%.

The findings of this research, which demonstrates new methodologies that can be used for extracting features of sEMG signals, also identify directions for future work in the field of signal classification.

Table of Contents

List of Figures

List of Tables

List of Abbreviations

2D	2-Dimensional
3D	3-Dimensional
ADP	Adenosine Diphosphate
ARV	Average Rectified Value
ATP	Adenosine Triphosphate
CMRR	Common Mode Rejection Ratio
CP (or PCr)	Creatine Phosphate
CWT	Continuous Wavelet Transform
dB	Decibels
DC	Direct Current
DD	Double Differential
DFT	Discrete Fourier Transform
DSP	Digital Signal Processing
EMG	Electromyography
FFT	Fast Fourier Transform
FT	Fourier Transform
HD-sEMG	High-Density Surface Electromyography
HSR-sEMG	High-Spatial-Resolution Surface Electromyography
IED	Inter-electrode distance
MDF	Median Frequency
MFCV	Muscle Fibre Conduction Velocity
MNF	Mean Frequency
MRA	Multi-resolution Analysis
MU	Motor Units
MVC	Maximum Voluntary Contraction
MVIC	Maximum Voluntary Isometric Contraction
NDD	Normal Double Differentiating
PCB	Printed Circuit Board
PSD	Power Spectrum Density
RMS	Root Mean Square
SA	Spike Analysis
SD	Single Differential

sEMG	Surface Electromyography
SENIAM	Surface Electromyography for the Non-Invasive Assessment of Muscles
SNR	Signal Noise Ratio
STFT	Short-Time Fourier Transform
VI	Virtual Instrument
WT	Wavelet Transform
ZCR	Zero Crossing Rate

Attestation of Authorship

I hereby declare that this submission is my own work and that, to the best of my knowledge and belief, it contains no material previously published or written by another person except where explicitly defined in the acknowledgements, nor material which to a substantial extent has been submitted for the award of any other degree or diploma of a university or other institution of higher learning.

Charles Jeffrey John Kilby

February 2017

Acknowledgements

I wish to express my gratitude to my supervisor, Professor Krishnamachar Prasad for his patience, support, guidance and advice throughout this research. I also greatly appreciate the assistance given by Dr Grant Mawston from the Health and Rehabilitation Research Institute, at North Shore Campus of Auckland University of Technology for imparting professional knowledge and information on working with muscle signals.

Sincere thanks are also extended to helpful data collectors Sarah Haddon and Jasmin Gibbs-Grant, all staff of the School of Engineering, in particular the technicians Achala Perera, Justin Matulich and the administration staff for their kindness and encouragement during my studying period at the Auckland University of Technology.

Due to the nature of research involving of human participants, ethics approval (Application Number 12/49) were sought and granted by the Auckland University of Technology Ethics Committee (AUTEC) Ethics on 3 April 2012.

Chapter 1
Introduction

1.1 Background: Overview of Surface Electromyography

'Electromyography' or EMG is the term used for the study of electrical signals that are obtained from muscle activities by means of using sensory electrodes. The word 'electromyography' itself is a combination of three Greek words: *electron*, which associates it with electricity; *myos* meaning 'muscle'; and *graph* meaning 'to write'. Electromyography is therefore the recording and analysing of electrical signals generated by the muscles during their activities. Electrical signals sourced from any biological organism are called *bioelectrical* or *biosignals*. These biosignals are processed and analysed for the purpose of classifications. A classifier-based EMG characterization system has been widely used by researchers and clinicians as a valuable tool for investigating muscle conditions and providing an accurate diagnosis for neuromuscular disorders for further rehabilitations [1, 2].

The study of EMG involves assessment of functionality and efficiency of muscle motor units by way of recording and analysing their bioelectrical activity. EMG is a valuable technique for two types of uses:

1. Kinesiological: in evaluating mechanisms of human movement analysis. This involves investigating neuromuscular physiology or the relationship of muscular function to movement of the body segments and timing of muscle activity with regard to the movements.
2. Clinical: in diagnosing neuromuscular disorders. This focuses on biosignal analysis through comparison of signal patterns and measurements between normal and abnormal muscle activities. This involves characterizing motor unit action potentials during muscle contraction.

EMG signals, also commonly known as myoelectric signals, are obtained from striated or skeletal muscle and record the activity of a muscle as it contracts during movement. Another type of signals such as Electrocardiography (ECG or EKG) are obtained from the heart and record heart activity.

In surface electromyography (sEMG), bioelectrical signals are obtained by surface electrodes placed on the skin overlying the selected muscle. While surface electrodes are non-invasive, another method of EMG uses needle or fine-wire electrodes penetrating into the muscle approximately 2.5-5 mm deep. This method obtains signals that can be focused on a single muscle motor unit and used for targeting small muscles. Advantages of needle or 'indwelling' EMG include its selectivity and its ability to detect other distant muscle activities or 'cross-talk'. However, indwelling EMG can cause stress and pain to the patient involved.

sEMG recordings provide a safe, easy and non-invasive method that can give objective measures from muscle activities. It is not always necessary to penetrate the skin and record from single motor units to obtain useful and meaningful information regarding muscles. sEMG allows the observer to see the muscles' energy at rest and the continuous change over the course of a movement. sEMG obtains signals generated from a group of muscles rather than one single motor unit. With the use of multiple channels electrode and spatial filtering technique, it becomes possible to observe different aspects of activities from a group of muscles or compounded motor unit. The further development of sEMG with regard to multi-channel electrode design and signal processing techniques is the focus of this study.

The basic setup of sEMG signal acquisition includes a set of ordered protocols of some specific activities which detect electrical signals generated by the muscle as it contracts. The signals are detected by the overlying electrode which are then recorded and sent to a computer. The sEMG signals are collected in data files for subsequent processing and analysis, using appropriate mathematical procedures to determine values that are relevant and meaningful within the study of signal processing. The mean and median frequencies and root mean square (RMS) values are among some of the common terms used for measurements in signal analysis.

Much research and development has gone into designing electrodes and sEMG signal processing and analysing techniques. However, the electrodes designed so far tend to be highly specialized for specific sites, limiting both their use for other sites and their analysing capabilities. This research aims to develop improved surface electrodes with more functional means to process the EMG signals using various techniques to provide more useful and detailed signal features, not just from an overall group of muscles but

also from different muscle motor unit components within that group. Multi-channel electrodes expand sEMG signal processing capabilities. As well as being able to measure the useful variable *muscle fibre conduction velocity*, the multi-channel electrode uses a more refined mathematical computation, such as Laplacian filtering, to prevent cross-talk signals. Hence, the signal processing using the multi-channel electrodes will extract more effective and useful signal features that are critical for accurately diagnosing muscle ailments and conditions.

1.2 History of EMG and sEMG

The present state and possibilities of EMG originated with a series of discoveries in physics and physiology. Its further development has occurred with the advent of new technologies, such as recording and signal processing [3].

The study of how electricity is linked with muscle activities can be traced back to the 17th century when Francesco Redi [4; Chapter 1] from Pisa, Italy studied the electric ray fish's energy which was sourced from highly specialized muscle. Giovanni Borelli [5], a professor of mathematics and physics also in Pisa, demonstrated in 1673 that animal motion is produced by contraction of muscles in his historic study of living creatures. Another researcher, the Englishman John Walsh [6], demonstrated in 1775 that an eel's muscle tissue could generate a spark of electricity. In the 1790s the Italian Luigi Galvani [7] obtained direct evidence of the relationship between muscle contraction and electricity from dissected frogs, where discharge of electricity evoked muscle contractions. Alessandro Volta [4, Chapter 1], another Italian, attempted to show Galvani that the muscle contracting was a result of different metals touching the muscle tissue, but Galvani proved otherwise by firing it with a severed nerve rather than metal. Volta continued his work and developed the electric battery which generated electric current and which he used to stimulate muscle, and that technique received wide attention during the late 18th century.

It was not until the early 19th century when the galvanometer, a tool for measuring electrical current, was invented, that many more studies of bioelectrical muscle activities were carried out. In 1838, the Italian Carlo Matteuci [4, Chapter 1] used the galvanometer to demonstrate that an electrical potential between an excised frog's nerve and its

damaged muscle's cell membrane could produce direct electrical current. In 1849, inspired by Matteuci's work, the German physiologist Emil Du Bois-Reymond [4, Chapter 1] discovered the action potential, and provided the first evidence of electrical activity in human muscles during voluntary contraction using a primitive galvanometer. In 1852, his countryman Hermann von Helmholtz invented the myograph and measured the speed of nerve transmission [8].

By the early 20th century, Frederick Pratt [9] had begun to demonstrate that the magnitude of energy associated with muscle contraction was due to the recruitment of individual muscle fibres, rather than the size of the neural impulse. In 1922, Herbert Gasser and Joseph Erlanger [10] used the newly invented cathode-ray oscilloscope to show the signals from muscles on an oscilloscope, and later won the Nobel Prize in 1944. In 1929, Edgar Adrian and Detlev Bronk [11] measured muscle electrical activity by needle electrodes, with the possibility of detecting potentials of single motor units.

As a result of continuing improvements in EMG instrumentation, from the 1930s through to the 1950s researchers more widely began to use *surface* EMG (sEMG), where electrodes were overlaid on the skin, for the study of normal and abnormal muscle function. During the 1960s, John Basmajian [12] discovered the technique of biofeedback and was able to demonstrate a deeper comprehension of EMG and its application. Basmajian first used a type of training that entailed the use of fine-wire electrodes rather than surface electrodes to demonstrate that EMG feedback could be used to train the neuromuscular system down to its most basic element – the single motor unit. Other researchers such as Elmer Green [13], Thomas Budzynski and colleagues [14] then used sEMG with biofeedback technique in their research work, after which the biofeedback arena began to expand rapidly.

In the 1960s clinical use of sEMG for the treatment of more specific disorders emerged. Among the first practitioners to use sEMG were Curtis Hardyck and colleagues [15]. Others such as H. E. Booker and colleagues [16] demonstrated retraining methods for patients with various neuromuscular conditions, whilst H. E. Johnson and W. H. Garton [17] used sEMG to assist in the restoration of function in hemiplegic patients. sEMG with biofeedback techniques was also used by Steven Wolf and colleagues [18, 19] who were among the first to employ it in the assessment and treatment of lower back pain.

Basmajian continued to work through international forums to share more information on sEMG. The International Society of Electrophysiological Kinesiology (ISEK) was formed in 1965 and publishes one of the few journals which specifically address topics on sEMG – the *Journal of Electromyography and Kinesiology*. Among other contributors, substantial work by Carlo DeLuca [20] and colleagues on the spectral analysis of biosignals and muscle fatigue has made an important contributions to the understanding of muscle physiology and methods of measuring it.

In the 21st century the methods for EMG signal detection and processing have been greatly refined. The quantity and quality of information that can be extracted from these recordings is now important for research and clinical applications in a number of fields, including rehabilitation medicine, ergonomics, sport and space medicine and neurophysiology.

1.3 Pros and Cons of sEMG: Considerations of Use

As previously mentioned, sEMG provides is a safe, easy and non-invasive method and allows objective quantification of the energy of muscles. Meaningful information regarding muscles can be obtained without penetrating the skin and with the use of multiple sensor arrays or multiple channels electrodes, it becomes possible to determine how various aspects of muscles differ by viewing signal patterns over a specific muscle in greater details.

Many aspects need to be considered regarding the use of sEMG, including muscle testing, visual observation of posture, and movement. Each aspect also has its limitations. By adding sEMG recording information to the practitioner's fund of knowledge about the muscle function of a particular patient, the practitioner can combine valuable information concerning how the nervous system participates in working with the muscle function.

From testing and signal analysis, sEMG practitioners may be able to answer the following questions: Do the muscles fire early or late in a recruitment pattern? Does a particular exercise actually activate the muscle it is intended to? Does the muscle turn off following a given movement, or does it show irritability following movement?

sEMG's weaknesses relate to the anatomy under study, the instruments used to study and the methods or procedures chosen to study it. It is important that clinicians acknowledge and understand these limitations. One key limitation is the ability to monitor only a few muscle sites. The neuromuscular system is very rich and complex, and to reduce it to one or two channels of sEMG information is very limiting. At a minimum, a four-channel sEMG instrument allows one to study the right and left aspects of two opposing groups [3, Chapter 1]. At this level, the information becomes much more meaningful and practical.

Scanning multiple sets of muscles in their resting state may help the practitioner to decide which regions of the musculature might be of further interest. Another possible shortcoming of sEMG recordings has to do with muscle substitution patterns. The neuromuscular system may express the same movement using different muscle groups. When this occurs, it might lead an experimenter to believe that the sEMG recordings are either inconsistent or unreliable. Thus it is important for practitioners to understand the 'normal' case, so that they can interpret recordings with greater confidence.

Another difficulty with sEMG is the possibility of cross-talk, a phenomenon where energy from one muscle group travels over into the recording field of another muscle group. When this happens, the specificity of sEMG recordings may be affected. Cross-talk might make it difficult or even impossible to isolate the sEMG recordings from a specific muscle. Some electrode placement sites have greater specificity than others. An additional limitation to sEMG is that, to date, there are only a few published guides to electrode placement (one of which is the *Electrode Atlas* [3; Chapter 16]), and none of them has become standard. Results from one researcher or clinic do not tend to correspond to those from another researcher or clinic, due to differences in electrode-placement. The *Electrode Atlas* needs to encourage a more standardized method for sEMG electrode placement. A standardized method would strengthen the interpretation of sEMG recordings at a given muscle site.

The first sEMG electrode atlas was compiled by John Davis in 1959 [21], which provided researchers with electrode placement maps to assist in the standardization of sEMG recordings for the next 20 years. In 1980 John Basmajian and Robert Blumenstein [22] wrote a small book to guide electrode placements. This expanded and updated the initial recommendations of Davis to include more sites relevant to rehabilitation. Jeffrey Cram,

Glenn Kasman and Jonathan Holtz [3, Chapter 17] later produced an electrode atlas of 69 sites, classifying each recording site for the quality of the recording in terms of *specific*, *quasi-specific* and *general* recordings. As sEMG recordings might be subjected to issues of volume conduction from surrounding distant muscles, specific recordings were felt to be relatively free of such contamination. Quasi-specific sites were thought to record from the muscle named, as well as volume-conducted signals from surrounding muscles. General recordings were considered to be recordings from a region rather than from specific muscles. In addition to the sites for placement, sample recordings from standardized movements are presented in both raw sEMG and processed modes. SENIAM (sEMG for a Non-Invasive Assessment of Muscles) was a European project between 1996 and 1999, which developed recommendations for sEMG sensors and sensor placement procedures. SENIAM was coordinated and managed by Hermie Hermens and Bart Freriks [23]. This has created a very concise and well-illustrated book that attempts to set standards on sEMG electrode placements for 27 muscle sites across the areas of the shoulder and neck, the back muscles, the arm and hand, the upper leg and hip and the lower leg. Part 2 of the recent book by Marco Barbero, Roberto Merletti and Alberto Rainoldi [24], *Atlas of Muscle Innervation Zones: Understanding Surface Electromyography and Its Applications* indicates suitable electrode positions for single-pair electrodes.

The practitioner should remember that sEMG is not a measure of force, nor strength or the amount of effort given. It is simply a measure of the electrical energy given off by the muscle. Practitioners must be cautious about how they interpret the sEMG findings, being careful not to over-interpret them. For example, they should not generalize results across different muscle groups, since each has different muscle mass that produces different amplitude to start with. Instead, clinicians might normalize the activity of two different muscle sites as ratios. Using a reference muscle group's maximum voluntary isometric contraction (MVIC) and comparing with different MVICs can be another fair method of determining how well muscles are functioning.

A final shortcoming is that sEMG electrodes are not totally unobtrusive. The electrodes and leads can potentially encumber a movement pattern or make the patient feel self-conscious about a posture or movements. Thus, the sEMG recordings might not perfectly reflect the customary patterns of use for the patient. Practitioners are therefore encouraged to have several different kinds of electrodes on hand, so that they can choose

a type of electrode which is suitable for the muscle and movement pattern that they wish to study.

1.4 Research Objectives and Methodology

As discussed in section 1.3, one limitation of current sEMG systems is due to the ability to monitor only from one or two channel electrodes, which results in a narrow range of information from a specific muscle site. This contributes to having poor spatial selectivity, which does not allow for the separation of the contributions from different muscle motor units [25]. Using electrodes with more than two channels over the muscle of interest produces greater spatial selectivity of information, which allows for more meaningful information to be extracted by the researcher [25; Chapter 4, 26]. In addition, the designs of multi-channel electrodes made so far [27-36] tend to be highly specialized for specific muscle sites, limiting both their use for other sites and their analysing capabilities.

This research aims to develop improved surface electrodes with more functional aspects to process the EMG signals using various techniques. This will show more useful and detailed signal features, not only from the overall muscle but also from different muscle motor unit components within the muscle under investigation. This will be carried out by researching, designing and building multi-channel electrode with a specific array configuration.

Multi-channel electrodes expand the capabilities for processing sEMG signals by using various techniques to extract different signal features from that muscle. By using multi-channel electrodes, a more refined mathematical computation such as the Laplacian filtering can be applied to prevent muscle cross-talk in the signals collected. As explained in section 1.3, cross-talk signal is an interference signal coming from other muscles other than the one under study. The problems that might arise in the specificity of sEMG recordings can be detected and isolated by Laplacian filtering [37-39]. The multi-channel electrodes are also able to measure another useful variable referred to as *muscle fibre conduction velocity* (MFCV), which conveys the information about muscle fibres' firing rates that is a useful additional feature in signal analysis.

Hence the overall aim of this research is to build a new multi-channel electrode that can be used on different skeletal muscle sites of similar size and to develop the processing of sEMG signals to enable the extractions of more useful-features. Analysis of these signal features will assist in the signal classification and creation of a more effective database for diagnosing muscle ailments and conditions.

For any kind of sensors or electrodes to operate, an instrumentation system which includes electrical and computational apparatus is used for data acquisition, signal processing and analysis. The general schematic of the instrumentation system is depicted in Figure 1.1 [40]. The term *measurand* is used for the participant, who provides the physical, property or condition that the system measures. The sensor or in this case the sEMG electrode converts energy or information from the measurand to another form which is electrical. The signal is then processed and displayed for analysis and interpretations.

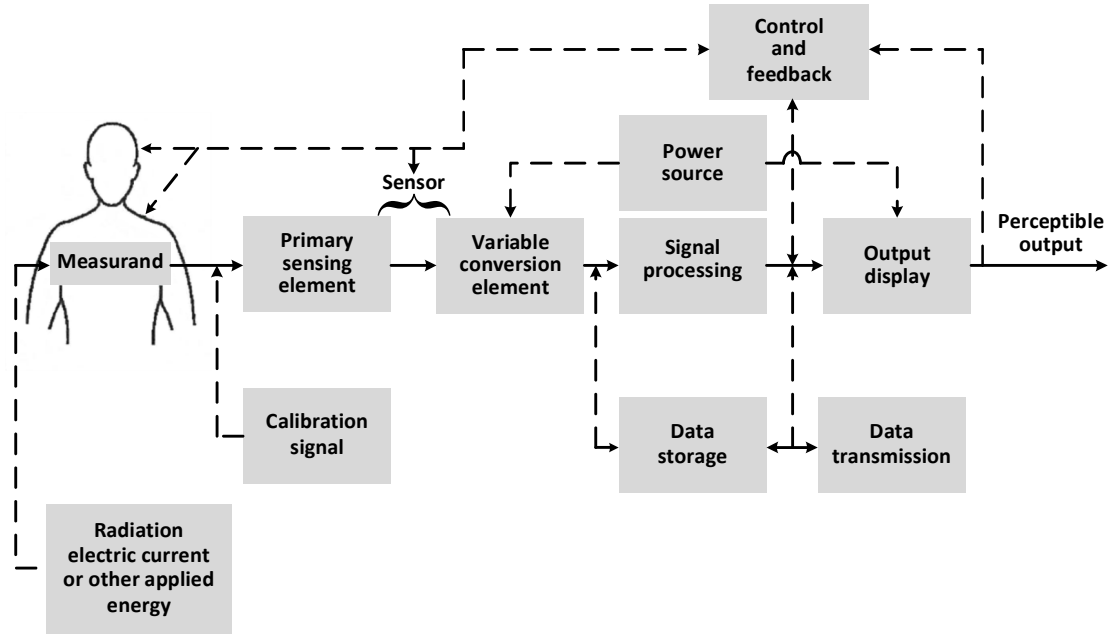

Figure 1.1 General schematic of the instrumentation system [40].

In order to achieve the above aim, this research is divided into a series of objectives and methodologies reflected in the chapters covered. The order of the objectives is as follows:

1. To understand the anatomy of muscles and how muscles functions. Chapter 2 covers relevant, in-depth and visual information with regard to the muscles measured in this research.

2. To design and develop multi-channel electrodes. Chapter 3 covers detailed information on technical design of the new multi-channel electrode.
3. To develop data collection protocols, test and investigate further the new multi-channel electrode's capabilities for signal processing. This firstly includes a pilot study using 5 participants to compare and validate the new multi-channel electrode against readily available surface electrodes before data from the main study of 40 participants are gathered to further explore the analysing capabilities of the multi-channel electrodes. In Chapter 4 a series of experimental setups for data acquisition are described as follows:
   (a) The ethical approval was required for participants involved.
   (b) The design of overall setup, listing all the equipment used, how it is set up, is presented in diagrams.
   (c) Data collection protocol.
4. Signal processing – extensive information on aspects such as sampling rates and different signal processing techniques used are discussed in Chapter 5, including:
   (a) Fourier Transform
   (b) Short-Term Fourier Transform
   (c) Wavelet Transform
   (d) New Sliding Window Algorithm
6. Signal Analysis. Chapter 6 involves signal feature extractions of mean frequency, median frequency, RMS and MFCV. Other aspects involved are normalizing and repeatability. Results of the data collection from the 40 participants are presented in the form of graphs and box-and-whisker diagrams. Statistical analysis is also performed on the results.
7. Discussions of the overall findings, possible future study and conclusions are presented in Chapter 7.

Chapter 2
Muscle Anatomy and Physiology

2.1 Introduction

While sEMG is mainly concerned with skeletal muscle, for the purpose of this research it is necessary to describe the anatomy of human muscle in general and the physiology of muscle contraction. This chapter therefore presents an overview of these areas in order to provide background and context for this research, which aims to build a new multi-channel electrode that can be used on different muscle sites and to develop the processing of sEMG signals to enable extractions of more effective and useful features that are needed for diagnosing muscle ailments and conditions.

Muscles generate force and movement, either for external use around the body's environment or for internal use in regulating organ functions. The basic function of muscle is to contract in order to produce body movement. Muscle cells form a major part of the body and are the sites where chemical energy is turned into force and movement [41-43].

Humans have three types of muscle tissues, which have been classified as [41-43]:

1. *Skeletal muscle* – most of this type of muscle is attached to a bone. Its contraction is responsible for supporting and moving the skeleton. The contraction of skeletal muscle is initiated by impulses sent from neurons to the muscle and is usually under *voluntary* control, which means that movement is controlled by the individual's will. Since the general structure is comprised of elongated stripes and fibre with multiple nuclei, skeletal muscle is referred to as *striated* muscle.
2. *Cardiac muscle* – the muscle of the heart, which is an *involuntary* muscle, regulated by the autonomic nervous system and hormones. Cardiac muscle produces a rhythmic contraction for pumping the blood to circulate around the body. It is also referred to as *striated* muscle but has a branching and single-nucleus cell structure.

3. *Smooth muscle* – mostly found in the walls of internal organs. Smooth muscle, which is also *involuntary* muscle, moves a substance within the body other than the heart, such as the walls of the stomach and intestines in the digestion system, urinary bladder, uterus blood vessels and airways in the trachea and lungs of the respiratory passages. Contractions of smooth muscle cells are responsible for making hairs of the skin stand up and for changing the diameter of the pupil of the eye. Smooth muscles are sheet-like in structure and comprise of single-nucleus cells, and are regulated by the autonomic nervous system, hormones and other local chemical factors which control its contraction.

Through a microscope, the structures of the three types of muscle can be distinguished by patterns of alternating light and dark bands. Figure 2.1 compares the appearance of skeletal muscle cells with that of cardiac and smooth muscles.

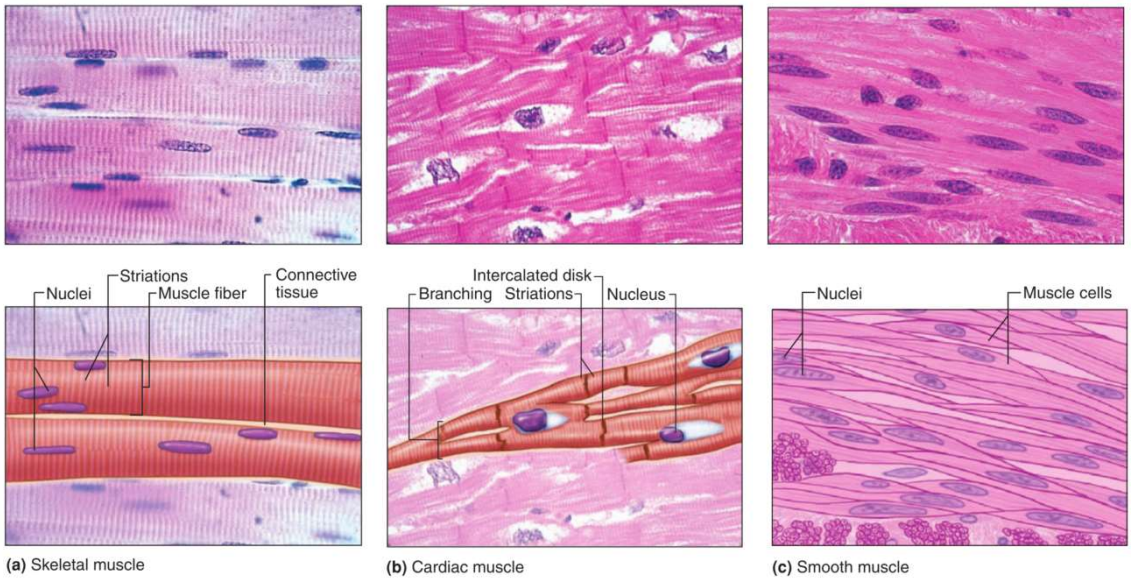

Figure 2.1 Comparison of skeletal muscle with cardiac and smooth muscle as seen with light microscopy (top panels) and in schematic form (bottom panels). Both skeletal and cardiac muscle have a striated appearance. Cardiac and smooth muscle tend to have single-nucleus cells, but skeletal muscle cells are multinucleated [43; Chapter 9].

Muscles have four basic functions:

1. *Producing movement* – muscle contraction produces movement. Skeletal muscle contraction enables body movement, eye movement, facial expressions, and also helps breathing. Smooth muscle contraction moves food through the digestive system and reduces size of blood vessels. Cardiac muscle contraction pumps blood around the body.
2. *Maintaining posture* – muscle contraction opposes the force of gravity to allow the body to remain upright. Refinement of muscle contraction allows the body to assume different positions.
3. *Stabilizing joints* – many muscle tendons in skeletal muscle extend across joints to stabilize them. The skeleton would fall apart if it was not stabilized by muscle tendons and ligaments (connecting bones or cartilage).
4. *Generating heat* – muscle contraction produces heat as well as movement, maintaining posture and stabilizing joints. This heat is used to maintain body temperature.

2.2 Skeletal Muscle Structure

A mass of skeletal muscle, commonly known as flesh, consists of skeletal muscle cells, which are also known as *muscle fibres,* bound and bundled together by connective tissue. A single skeletal muscle cell is soft and fragile, but many thousands of these fibres held together by connective tissues enable the muscle as a whole to exert great force.

Each muscle fibre (cell) is covered by plasma membrane called the *sarcolemma.* A strand of muscle fibre is surrounded by a delicate connective tissue sheath called the *endomysium*. Several of the covered muscle fibres strands are then wrapped by a coarser fibrous membrane called the *perimysium,* to form a collection of fibres called a *fascicle*. A number of the fascicles are bound together by an even tougher outer covering of connective tissue called an *epimysium*, which covers a whole skeletal muscle group. At the ends of the muscle, the epimysium forms strong cordlike bundles of collagen fibres known as a *tendon*. Skeletal muscles are usually attached to bones, cartilage or other connective tissue coverings by these tendons. Figure 2.2 shows the bundling structure of skeletal muscle.

In some muscles, the individual fibres extend the entire length of the muscle, but in most the fibres are shorter, often oriented at an angle to the longitudinal axis of the muscle. Some tendons are very long, with the site where the tendon attaches to the bone being far from the end of the muscle. For example, some of the muscles which move the fingers are in the forearm. These muscles are connected to the fingers by long tendons.

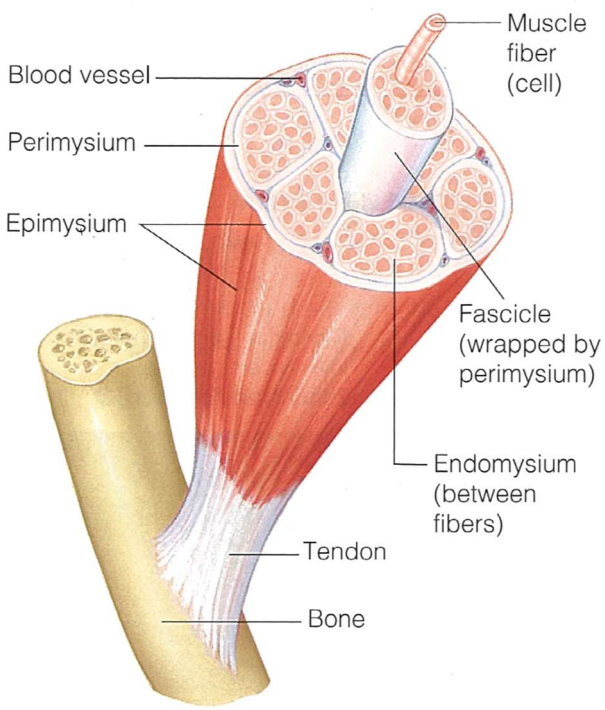

Figure 2.2 Bundling structure of skeletal muscle with connective tissues [41; Chapter 6].

Muscle fibres start to form during pre-birth development, by the fusion of a number of identical mononucleated cells known as *myoblasts* into a single cylindrical multinucleated cell. Skeletal muscle differentiation is completed around the time of birth, and these differentiated fibres continue to increase in size from infancy to adulthood. Compared to other cell types, skeletal muscle fibres are extremely large. Adult skeletal muscle fibres have diameters between 10 and 100 μm and lengths that may extend up to 20 cm [44; Chapter 1]. Key to the maintenance and function of such large cells is the retention of the nuclei from the original myoblasts. Spread throughout the length of the muscle fibre, each myoblast participates in regulation of gene expression and protein synthesis within its local domain.

The cells of skeletal muscles are filled with excitable membrane, whose function is not to transfer or process information but to generate tension. In the general study of human cell biology, *cytoplasm* is a fluid substance that fills the cell around the nucleus. Most of each muscle fibre's cytoplasm is filled with smaller cylindrical bundles called *myofibrils*. Myofibrils are approximately 1 to 2 μm in diameter and are made of *thick* and *thin* filaments in a repeating pattern. Each myofibril extends from one end of the fibre to the other and is linked to the tendons at the ends of the fibre. The thick and thin filaments in each myofibril are arranged in a repeating pattern along the length of the myofibril. One unit of this repeating pattern is known as a *sarcomere*. The *thick* filaments are composed almost entirely of the protein *myosin* while the *thin* filaments are principally composed of the proteins *actin, troponin* and *tropomyosin*, which play important roles in regulating contraction. Figure 2.3 shows the structural organization of skeletal muscle and Figure 2.4 shows a sarcomere within myofibrils at high magnification.

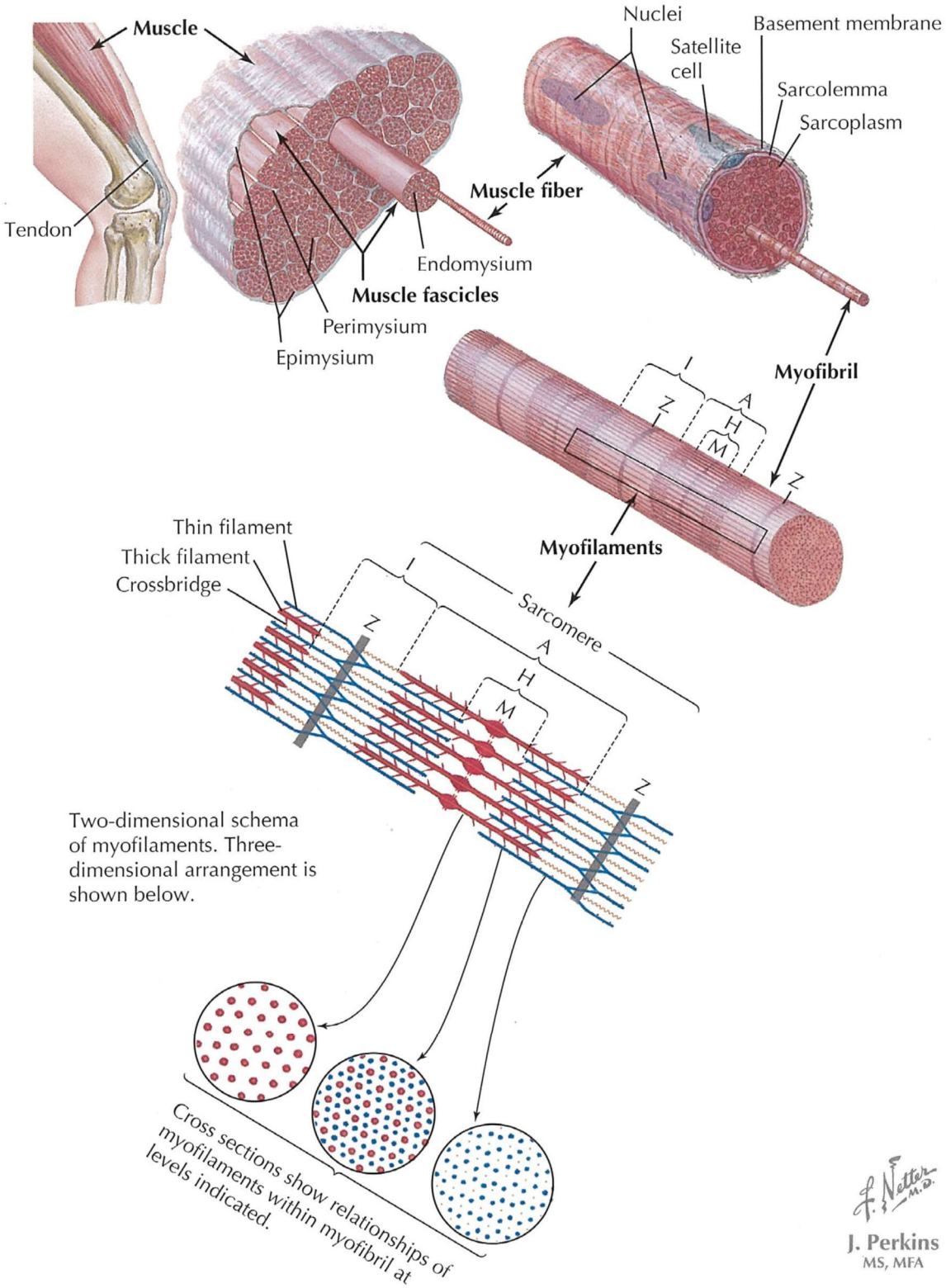

Figure 2.3 Structural organization of skeletal muscle [42; Section 2].

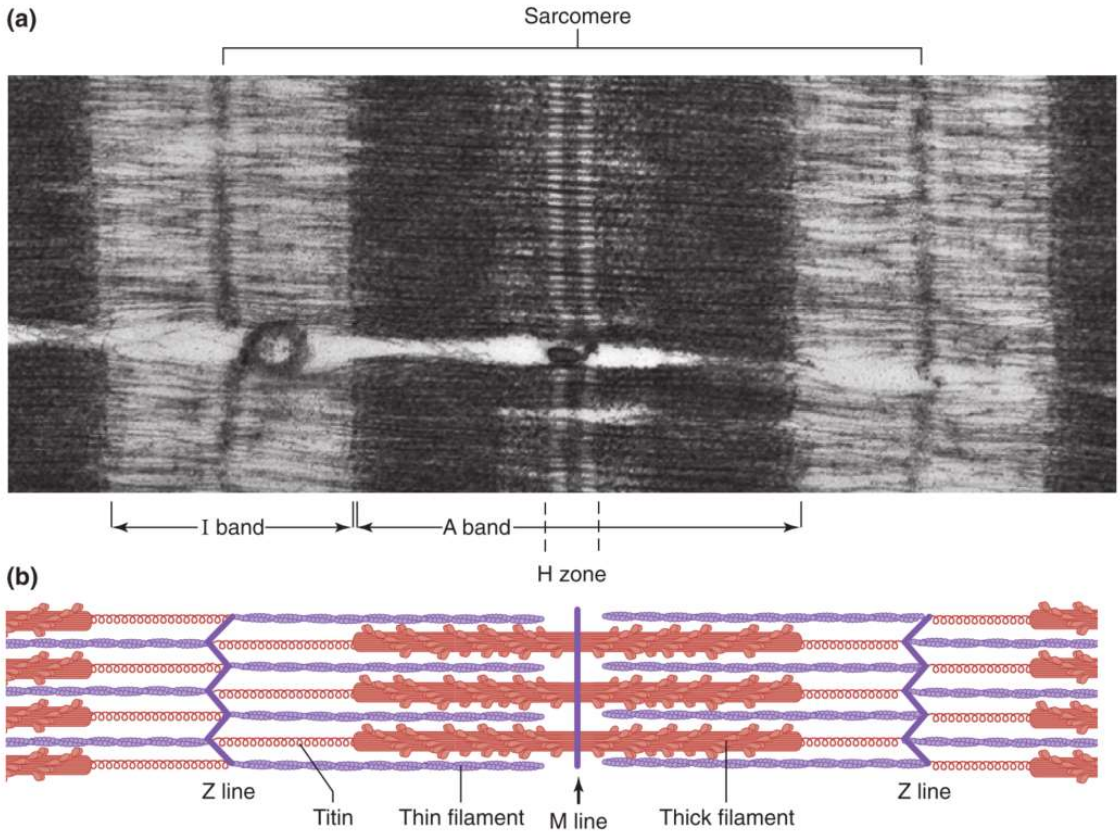

Figure 2.4 (a) High magnification of a sarcomere within myofibrils. (b) Arrangement of the thick and thin filaments in the sarcomere in (a) [43; Chapter 9].

The thick filaments are located in the middle of each sarcomere, where their orderly, parallel arrangement produces a wide, dark band called the *A band* as shown in Figure 2.4 (a). Each sarcomere contains two sets of thin filaments, one at each end, called the *I band*. One end of each thin filament is anchored to a network of interconnecting proteins known as the *Z line*, whereas the other end overlaps a portion of the thick filaments. Two successive Z lines define the limits of one sarcomere. Thus, thin filaments from two adjacent sarcomeres are anchored to the two sides of each Z line. A Z line is only a two-dimensional projection of a cylindrical shape of myofibrils, and its actual shape is approximately circular.

A light band or *I band*, which is bisected by a Z line, lies between the A bands of two adjacent sarcomeres, and contains those portions of the thin filaments which do not overlap the thick filaments. Two additional bands are present in the A band region of each sarcomere which are the *H zone* and the *M line* as shown in Figures 2.3 and 2.4 (b). The H zone is a narrow light band in the centre of the A band. It corresponds to the space

between the opposing ends of the two sets of thin filaments in each sarcomere. The M line is a narrow dark band in the centre of the H zone and is comprised of the proteins that link together the central region of adjacent thick filaments. In addition, filaments composed of the elastic protein *titin* extend from the Z line to the M line and are linked to both the M line proteins and the thick filaments. Both the M line linkage between thick filaments and the titin filament act to maintain the alignment of thick filaments in the middle of each sarcomere.

2.3 Mechanisms of Skeletal Muscle Contraction

The term *contraction* as used in muscle physiology simply refers to activation of the force-generating sites within muscle fibres, which are the *cross-bridges* [42; Section 2]. Cross-bridges are portions of myosin molecules that extend from the surface of the thick filaments towards the thin filaments at the space between overlapping thick and thin filaments as shown in Figure 2.3. During muscle contraction, the cross-bridges make contact with the thin filaments and exert force on them. Following contraction, the mechanisms that generate force are turned off and tension declines, allowing *relaxation* of the muscle fibre.

The generation of motion or force by the muscle is activated when the plasma membrane of a muscle fibre is excited, which leads to cross-bridge activity. An *action potential* then propagates along the surface membrane of the fibre, triggering chemical reactions that in turn cause fibre contraction. When a muscle contracts, the action potentials generate an electric field that can be monitored by means of surface electrodes placed on skin. This field is a result of the contribution of many fibres contracting at different times and with different rates. The signal obtained is EMG, which is a random signal with statistical properties that depend on the muscle function and condition [25; Chapter 10]. An action potential in a skeletal muscle fibre lasts 1 to 2 microseconds, and it is completed before any signs of mechanical activity begin as shown in Figure 2.5. Once begun, the mechanical activity following an action potential may last 100 milliseconds or more.

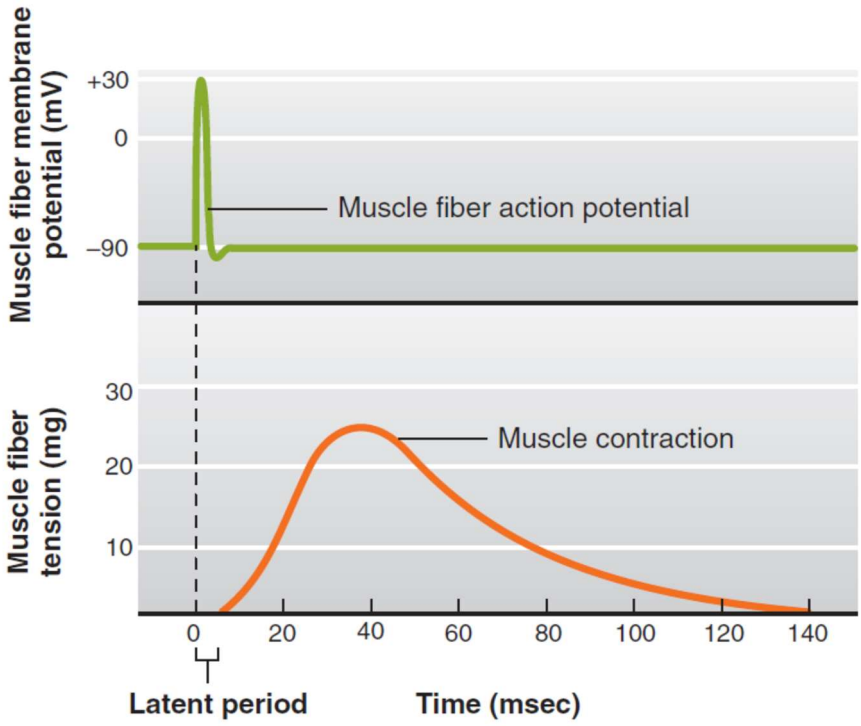

Figure 2.5 Time relationship between a skeletal muscle fibre action potential and the resulting contraction and relaxation of the muscle fibre. The latent period is the delay between the beginning of the action potential and the initial increase in tension [43; Chapter 9].

When force generation produces shortening of a skeletal muscle fibre, the overlapping thick and thin filaments in each sarcomere move past each other, driven by movements of the cross-bridges. During this shortening of the sarcomeres, there is no change in the lengths of either the thick or thin filaments as shown in Figure 2.6. This is known as the *sliding-filament mechanism* of muscle contraction [42; Section 2].

The sequence of events that occurs between the time a cross-bridge binds to a thin filament, the movement made and when it is set to repeat the process is known as a *cross-bridge cycle* [42; Section 2]. Each cycle consists of four steps:

1. Attachment of the cross-bridge to a thin filament
2. Movement of the cross-bridge producing tension in the thin filament
3. Detachment of the cross-bridge from the thin filament
4. Energizing the cross-bridge so that it can again attach to a thin filament and repeat the cycle

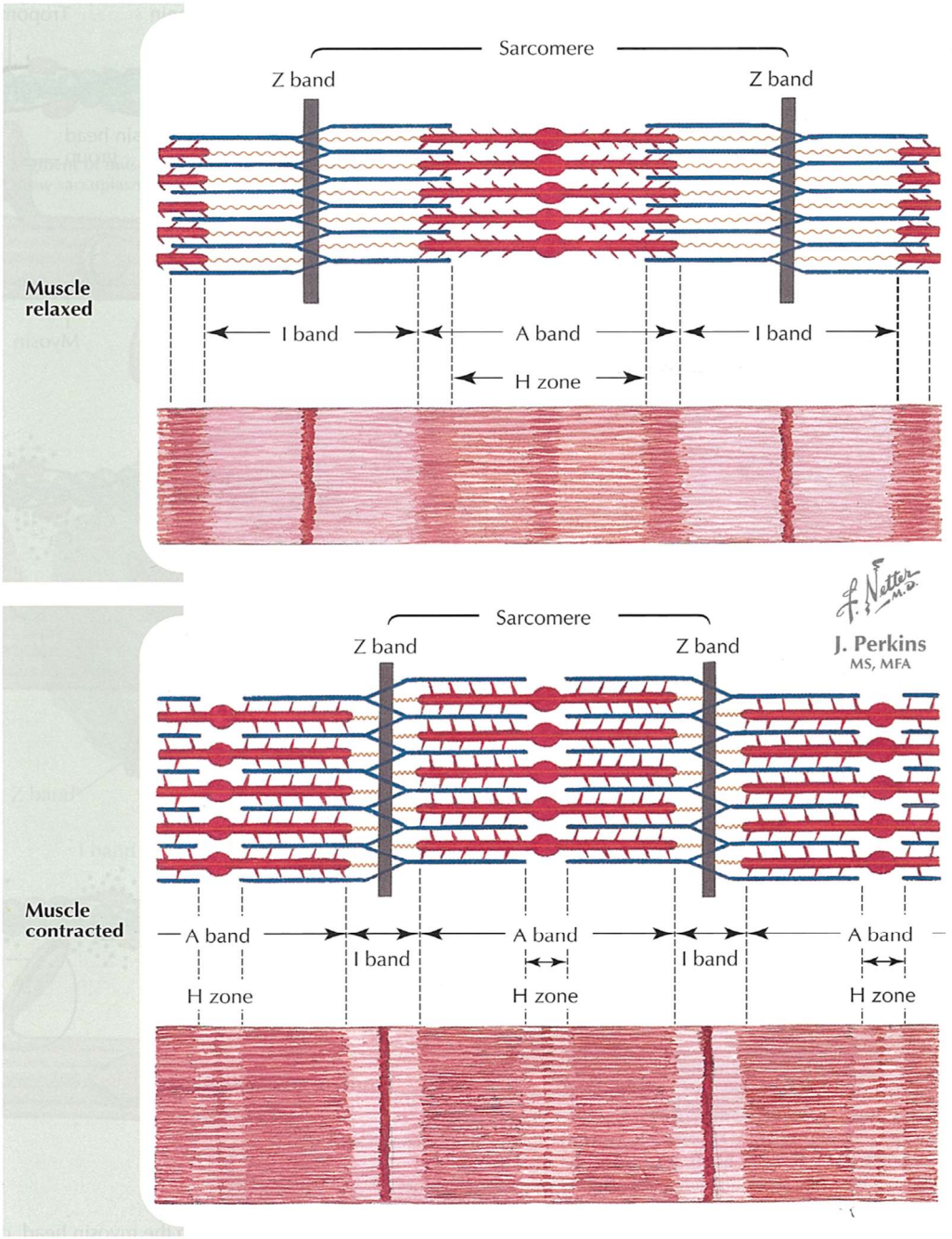

Figure 2.6 The sliding of thick filaments past overlapping thin filaments shortens the sarcomere with no change in thick or thin filament length. The I band and H zone are reduced [42; Section 2].

Each cross-bridge undergoes its own cycle of movement independently of other cross-bridges. At any instant during contraction, only some of the cross-bridges are attached to the thin filaments, producing tension, while others are simultaneously in a detached portion of their cycle.

The molecular mechanism of muscle contraction involves biochemical reactions at each step of the cycle. In a resting muscle fibre, the amount of cytoplasmic calcium ions (Ca^{2+})

is low, and myosin cross-bridges of the thick filaments cannot bind to the actin cross-bridges of the thin filaments. Still bound to myosin, the cross-bridges are in an energized state produced by the hydrolysis of adenosine triphosphate (ATP) into adenosine diphosphate (ADP) and inorganic phosphate. ATP, ADP and inorganic phosphate are natural chemicals within the body, and the hydrolysis of ATP is the reaction responsible for energy production. Cross-bridge cycling is initiated when Ca^{2+} enters the cytoplasm. Then for each step of the cycle, further chemical reactions occur between actin, myosin, ADP, inorganic phosphate and ATP. At the end of the cycle the state is returned back to where the cross-bridges are energized with unbounded myosin. Further details of the biochemical reactions are not discussed in this thesis in order to remain focused on the topic of this research – the development of multi-array surface EMG and its signal processing and analysis. The overview in this section is intended to provide a basic understanding of muscle contraction mechanisms.

2.3.1 Motor Unit Action Potential

As has been previously described, an action potential in the plasma membrane of a skeletal muscle is the signal that triggers contraction. The mechanism that initiates the cross-bridge activities that lead to the action potential of the skeletal muscle is the stimulation of the nerve fibres in skeletal muscle. The neurons of the skeletal muscle are also known as *motor neurons.* An axon, a type of nerve fibre, is the part of a motor neuron that innervates skeletal muscle fibre. The axons of motor neurons of the skeletal muscles are the largest-diameter axons in the body, enabling them to propagate action potentials at high velocities and allowing signals from the central nervous system to travel to skeletal muscle fibres with minimal delay.

Upon reaching a muscle, the axon of a motor neuron divides into many branches and each branch forms a single junction with a muscle fibre. A single motor neuron innervates many muscle fibres, but each fibre is controlled by a branch from only one motor neuron. A motor neuron plus the muscle fibres it innervates is called a *motor unit*, as depicted in Figure 2.7. The muscle fibres in a single motor unit are located in one muscle, but they are scattered throughout the muscle and are not necessarily adjacent to each other. When an action potential occurs in a motor neuron, all the muscle fibres in its motor unit are stimulated to contract.

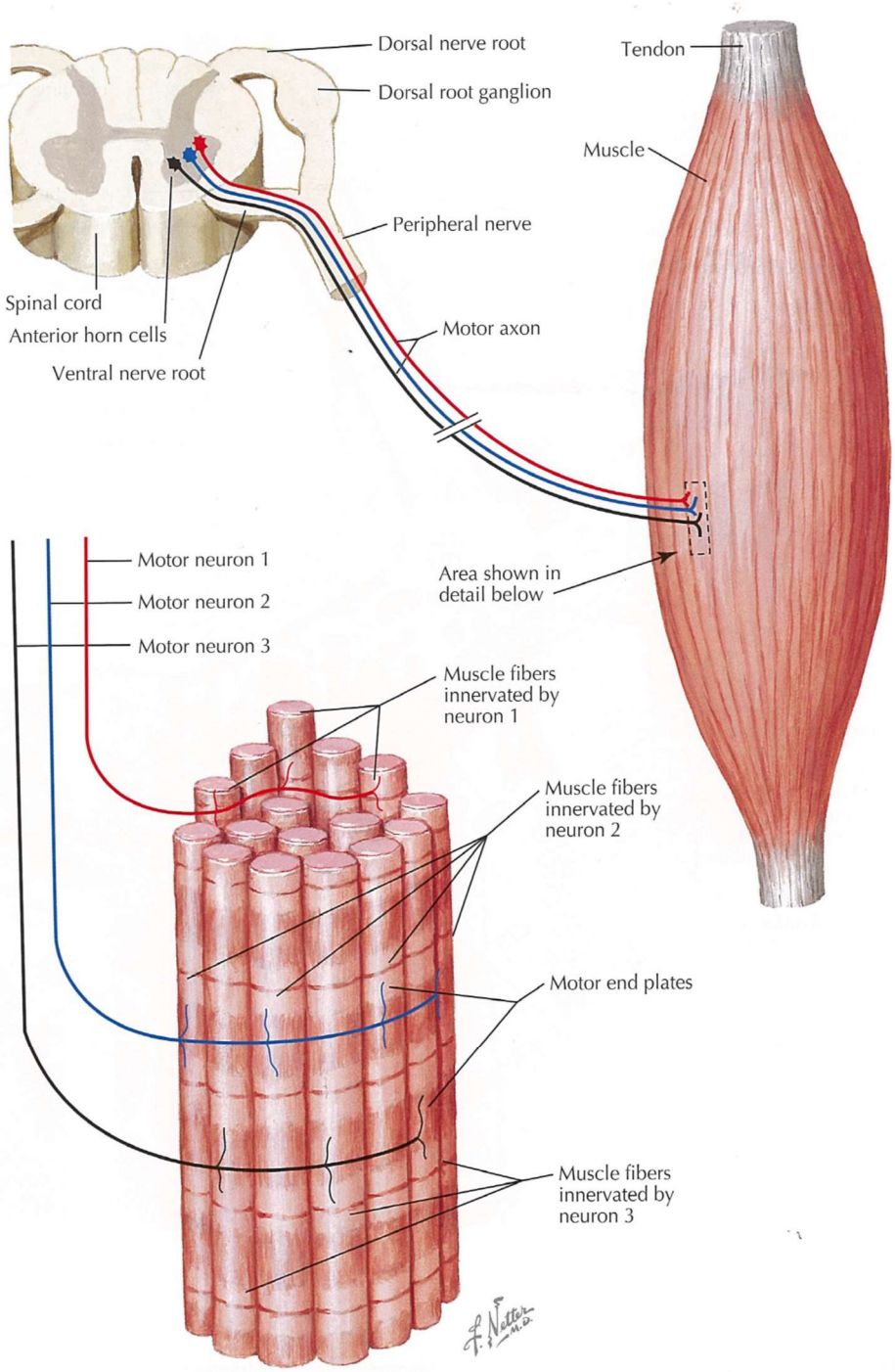

Figure 2.7 Motor units consisting of a single motor neuron and the muscle fibres it innervates [42; Section 2].

The axon divides into a number of short branches that lie embedded in grooves on the muscle fibre surface, as shown in Figure 2.8 (a). The myelin sheath surrounding the axon of each motor neuron ends near the surface of a muscle fibre, see Figure 2.8 (b). The region of the muscle fibre plasma membrane that lies directly under the terminal portion of the axon is known as the *motor end plate.* The junction of an axon terminal with the motor end plate is known as a *neuromuscular junction*.

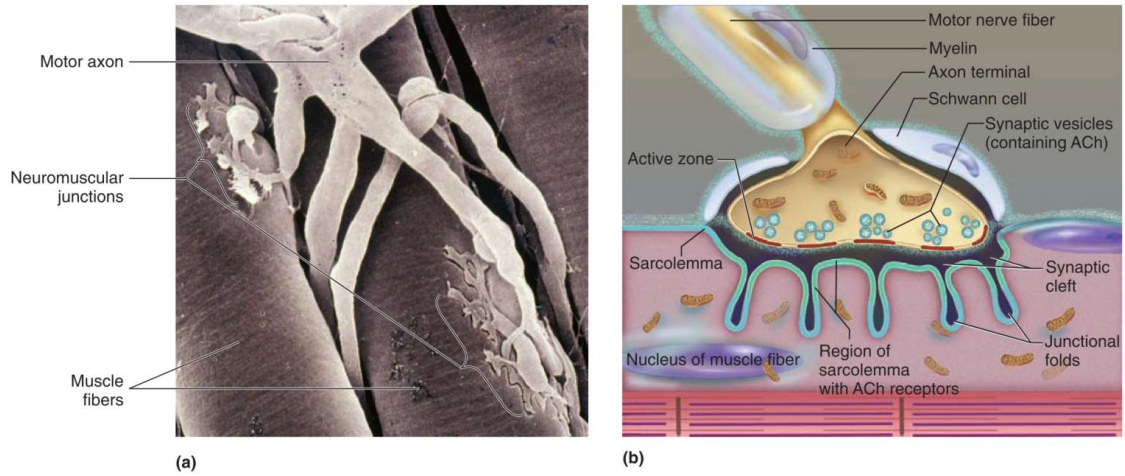

Figure 2.8 The neuromuscular junction. (a) Scanning electron micrograph showing branching of motor neuron axons, with axon terminals embedded in grooves on the muscle fibre's surface. (b) Structure of a neuromuscular junction [43; Chapter 9].

The force exerted on an object by a contracting muscle is known as *muscle tension,* while the force exerted on the muscle by an object is the *load.* Muscle tension and load are opposing forces. Whether a fibre shortens depends on the relative magnitudes of the tension and the load. For muscle fibres to shorten and thereby move a load, muscle tension must be greater than the opposing load.

When a muscle develops tension but does not shorten or lengthen, the contraction is said to be *isometric* [45; Chapter 6, 46; Chapter 1]. Such contractions occur when the muscle supports a load in a constant position or attempts to move an otherwise supported load that is greater than the tension developed by the muscle. A contraction in which the muscle changes lengths while the load on the muscle remains constant is called *isotonic* [45; Chapter 6, 46; Chapter 1].

Depending on the relative magnitudes of muscle tension and the opposing load, isotonic contraction can be associated with either shortening or lengthening of a muscle. When tension exceeds the load, shortening occurs and this is referred to as *concentric* contraction [45; Chapter 6]. On the other hand, if an unsupported load is greater than the tension generated by cross-bridges, the result is an *eccentric* contraction or *lengthening* contraction [45; Chapter 6]. In this situation, the load pulls the muscle to a longer length in spite of the opposing force produced by the cross-bridges. Such lengthening contractions occur when an object being supported by muscle contraction is lowered, as when knee extensors in the thighs are used to lower the body to a seating position from a

standing position. It must be emphasized that in these situations the lengthening of muscle fibres is not an active process produced by the contractile proteins but a consequence of the external forces being applied to the muscle. In the absence of external lengthening forces, a fibre will only *shorten* when stimulated, it will never lengthen, as first shown by the Italian physiologist, physicist and mathematician Giovanni Alfonso Borelli (1608-1679) [5]. All three types of contractions – isometric, concentric and eccentric – occur in the natural course of everyday activities.

The mechanical response of a muscle fibre to a single action potential is known as a *twitch*. Following the action potential, there is an interval of a few milliseconds (known as the *latent period*) before the tension in the muscle fibre begins to increase. During this latent period, the processes associated with excitation-contraction coupling are occurring. The time interval from the beginning of tension development at the end of the latent period to the peak tension is known as the *contraction time*. Not all skeletal muscle fibres have the same twitch contraction time. Some fast fibres have contraction times as short as 10 milliseconds, whereas slower fibres may take 100 milliseconds or longer.

2.3.2 Muscle Fatigue and Skeletal Muscle Types

When a skeletal muscle fibre is repeatedly stimulated, the tension of the fibre develops and eventually decreases even though the stimulation continues. This decline in muscle tension as a result of previous contractile activity is known as *muscle fatigue* [4; Chapter 9, 47]. When muscles are exercised strenuously over a long period of time, muscle fatigue occurs. A muscle is said to be *fatigued* when it is not able to contract, even though it is still being stimulated [4; Chapter 9, 47]. An active or working muscle begins to contract more weakly until it finally ceases reacting and stops.

Muscle fatigue is believed to result from the *oxygen debt* that occurs during prolonged muscle activity. The work that a muscle can do and how long it can work without becoming fatigued depends on how good its blood supply is. When muscles lack oxygen, lactic acid begins to accumulate in the muscle via the anaerobic mechanism. The muscle's ATP supply starts to run low as the acidity in the muscle increases. The lack of ATP causes the muscle to contract less and less effectively, and finally it stops doing so.

Complete muscle fatigue, in which the muscle quits entirely, rarely occurs, because the feeling of fatigue appears long before it occurs and hence slowing down or stopping the activity simply happens. Oxygen debt always occurs to some extent during vigorous muscle activity and it must be paid back, whether or not fatigue has occurred. During the recovery period after an activity, the individual breathes rapidly and deeply. This continues until the muscles have received the amount of oxygen needed to remove the accumulated lactic acid and replenish reserves of ATP phosphocreatine, also known as creatine phosphate (CP or PCr), that serves as a rapidly mobilizable reserve of high-energy phosphates in skeletal muscle and the brain.

Additional characteristics of fatigued muscle are decreased shortening velocity and slower rate of relaxation. The onset of fatigue and its rate of development depend on the type of skeletal muscle fibre that is active, the intensity and duration of contractile activity, and the degree of an individual's fitness. If a muscle is allowed to rest after the onset of fatigue, it can recover its ability to contract upon re-stimulation.

Skeletal muscle fibres do not all have the same mechanical and metabolic characteristics. Different types of fibres can be classified on the basis of:

1. Their maximal velocities of shortening, fast or slow
2. The major pathway they use to form ATP, the chemical responsible for the production of energy, whether it is an oxidative or glycolytic process.

On the basis of these two characteristics, three principal types of skeletal muscle fibres can be distinguished:

1. Slow-oxidative fibres (type I) combine low myosin-ATPase (an enzyme which is responsible for catalyzing the decomposition of ATP into ADP and a free phosphate ion) with high oxidative capacity.
2. Fast-oxidative-glycolytic fibres (type IIA) combine high myosin-ATPase activity with high oxidative capacity and intermediate glycolytic capacity.
3. Fast-glycolytic fibres (type IIB) combine high myosin-ATPase activity with high glycolytic capacity.

Figure 2.9 shows that diameters of glycolytic fibres are generally larger than those of oxidative fibres. This fact has significance for tension development. The number of thick and thin filaments per unit of cross-sectional area is about the same in all types of skeletal

muscle fibres. Therefore, the larger the diameter of a muscle fibre, the greater the total number of thick and thin filaments acting in parallel to produce force, and the greater the maximum tension or greater strength it can develop. Accordingly, the average glycolytic fibre, with its larger diameter, develops more tension when it contracts than does an average oxidative fibre.

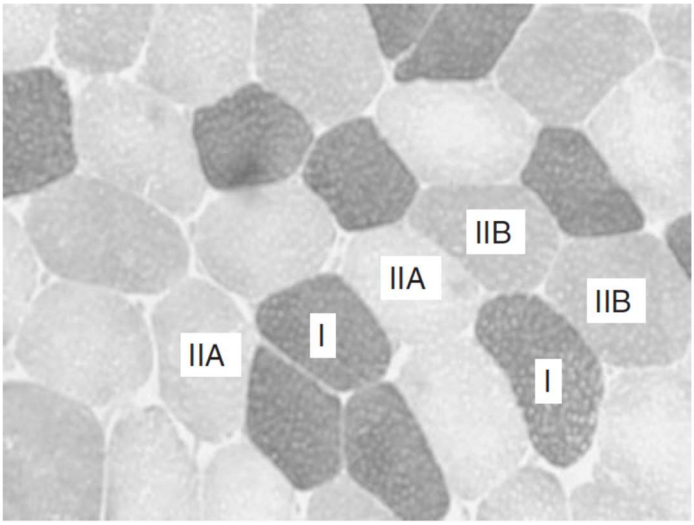

Figure 2.9 Muscle fibre types in normal human muscle, prepared using an ATPase stain. The darkest fibres are slow-oxidative (type I), lighter-coloured fibres are fast-oxidative-glycolytic (type IIA) and fast-glycolytic fibres (type IIB) [25; Chapter 1].

These three types of fibres also differ in their capacity to resist fatigue. Fast-glycolytic fibres fatigue rapidly, whereas slow-oxidative fibres are very resistant to fatigue, which allows them to maintain contractile activity for long periods with little loss of tension. Fast-oxidative-glycolytic fibres have an intermediate capacity to resist fatigue.

All muscle fibres in a single motor unit are of the same fibre type. Hence, fibre designation to the motor unit can be applied and referred to as slow-oxidative motor units, fast-oxidative-glycolytic motor units and fast-glycolytic motor units.

Most skeletal muscles are composed of all three motor unit types interspersed with each other, as shown in Figure 2.10. No muscle has only a single fibre type. Depending on the proportions of the fibre types present, muscles can differ considerably in their maximal contraction speed, strength and fatigability. For example, the muscles of the back, which need to be able to maintain their activity for long periods of time without fatigue while supporting an upright posture, contain large numbers of slow-oxidative

fibres. In contrast, muscles in the arms that are called upon to produce large amounts of tension over a short time period, as when a boxer throws a punch, have a greater proportion of fast-glycolytic fibres. Leg muscles used for fast running over intermediate distances typically have a high proportion of fast-oxidative-glycolytic fibres. Significant variation occurs between individuals. Elite distance runners, for example, on average have greater than 75% slow fibres in the muscle of the lower leg, whereas in elite sprinters the same muscle has 75% fast-twitch fibre types.

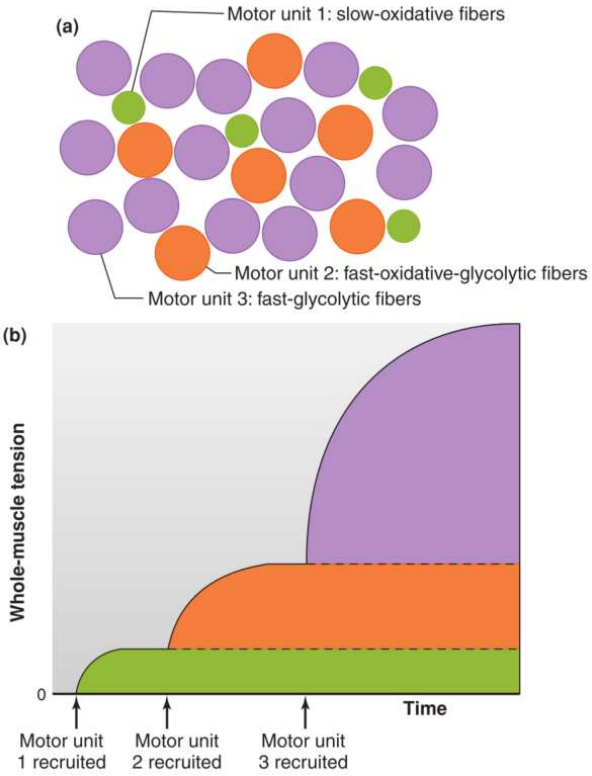

Figure 2.10 (a) Diagram of a cross section through a muscle composed of three types of motor units. (b) Tetanic muscle tension resulting from the successive recruitment of the three types of motor units. Note that motor unit 3, composed of fast-glycolytic fibres, produces the greatest rise in tension because it is composed of large-diameter fibres with the largest number of fibres per motor unit [43; Chapter 9].

The total tension a muscle can develop depends upon two factors:

1. The amount of tension developed by each fibre from action potential frequency, fibre length, fibre diameter and fatigue.
2. The number of active fibres contracting at any time from number of fibres per motor unit and number of active motor units.

By controlling these two factors, the nervous system controls whole-muscle tension as well as shortening velocity.

Motor unit size varies considerably from one muscle to another. The muscles in the hand and eye, which produce very delicate movements, contain small motor units. One motor neuron innervates only about 13 fibres in an eye muscle. In contrast, in the more coarsely controlled muscles of the legs, each motor unit is large, containing hundreds of, and in some cases several thousand, fibres. When a muscle is composed of small motor units, the total tension the muscle produces can be increased in small steps by activating additional motor units. If the motor units are large, large increases in tension will occur as each additional motor unit activated. Thus, finer control of muscle tension is possible in muscles with small motor units.

The force a single fibre produces depends on the fibre diameter, the greater the diameter, the greater the force. A motor unit composed of 100 fast-glycolytic fibres produces more force than a motor unit composed of 100 slow-oxidative fibres. In addition, fast-glycolytic motor units tend to have more muscle fibres. For both of these reasons, activating a fast-glycolytic motor unit will produce more force than activating a slow-oxidative motor unit.

The process of increasing the number of motor units that are active in a muscle at any given time is called *recruitment* [43; Chapter 9]. This is achieved by activating excitatory synaptic inputs in more motor neurons. The greater the number of active motor neurons, the more motor units recruited and the greater the muscle tension. Figure 2.10 shows that slow-oxidative motor units are recruited first due to the smallest motor neurons that innervate them. Then the recruitment is followed by fast-oxidative-glycolytic motor units, and finally, during very strong contractions, by fast-glycolytic motor units. Fast-glycolytic motor units produce the greatest rise in tension, because they consist of large-diameter fibres with the largest number of fibres per motor unit.

Chapter 3
Multi-Channel Surface Electromyography Electrodes

3.1 Introduction

This chapter presents a literature review of existing multi-channel surface electrodes, in terms of their use in acquiring and analysing sEMG signals before presenting in detail the design and development process for the new multi-channel electrode used in this research. The new electrode was configured as either a linear array or Laplacian filtering electrode, using software to extract specific features such as mean frequency (MNF), median frequency (MDF), root mean square (RMS) values and muscle fibre conduction velocity (MFCV) using signal processing techniques covered in Chapter 5.

As explained in Chapter 1, sEMG signals are bioelectrical signals generated by skeletal muscles and detected from the skin surface. These signals provide information that can be used to extract muscle activation characteristics for studying neuromuscular properties where diagnosis for rehabilitation can be made, which is of great importance in the medical field.

Sections 3.2 and 3.3 of this chapter, uses material taken from a published journal paper based on this research titled '*Multi-Channel Surface Electromyography Electrodes: A Review'* [48] co-authored with Krishnamachar Prasad and Grant Mawston.

3.2 Literature Review of Multi-Channel Electrodes for sEMG

A literature review of studies on the use of multi-channel electrodes was carried out by examining peer-reviewed journal papers on electromyography signals or analysis published since the year 2000 in recognized international journals with a high impact factor (IF) [49-51]. The five journals selected that met these criteria were: (1) *European Journal of Applied Physiology* – IF = 2.29, (2) *Journal of Biomechanic*s – IF = 3.14, (3) *Journal of Electromyography and Kinesiology* – IF = 1.75, (4) *Journal of Ergonomics* – IF = 1.6 and (e) Muscle & Nerve – IF = 2.31.

The initial search term 'surface EMG electrode' returned hits in 364 papers across the five journals. Only 62 of those papers [36, 37, 52-111] returned hits for the search term 'multi-channel' as shown in Table 3.1. Out of those 62 papers, only five [36, 52-55] explored the recent progress, application, benefits and limitations of multi-channel electrodes in the field of this research or clinical analysis of sEMG signals.

Table 3.1 shows the yearly distribution of journal papers from 2000 to 2013 that returned hits and were reviewed and classified as using 'multi-channel' electrodes for the collection of 'surface EMG' signals.

Table 3.1 Yearly distribution from 2000 to 2013 of the number of published journal papers relevant to this research for multi-channel sEMG electrodes.

Journal Name	2000	2001	2002	2003	2004	2005	2006	2007	2008	2009	2010	2011	2012	2013	Total
(a) European Journal of Applied Physiology	–	–	2	–	–	3	1	1	2	–	2	1	1	1	14 out of 57
(b) Journal of Biomechanics	–	–	–	–	–	–	–	–	–	–	–	–	–	–	0 out of 14
(c) Journal of Electromyography and Kinesiology	2	–	–	3	–	–	4	3	5	3	–	2	–	2	24 out of 76
(d) Journal of Ergonomics	–	–	–	–	–	–	–	–	–	–	–	1	–	–	1 out of 170
(e) Muscle & Nerve	1	1	1	1	3	2	2	1	1	2	–	2	5	1	23 out of 47
Total	3	1	3	4	3	5	7	5	8	5	2	6	6	4	62 out of 364

Of the 62 relevant papers, 14 were published in the *European Journal of Applied Physiology*, 24 in the *Journal of Electromyography and Kinesiology* and 23 in *Muscle & Nerve*. These papers were generally interested in how muscle functions to produce movement or force. Of the other two journals, the *Journal of Ergonomics* published only one paper that involved multi-channel electrodes and the *Journal of Biomechanics* published none. The majority of papers published in these two journals used standard sEMG electrodes with the conventional two-channel electrodes in bipolar configuration

for traditional data acquisition of sEMG signals. These papers were mainly concerned with the general function of a movement by parts of the body and with not analysing the condition of a muscle, which this research is focused on. The multi-channel electrode which were mentioned in the literature review used more than two channels, either as ***'linear array'*** or a ***'2D array'*** of surface electrodes.

The literature review further showed that different types of multi-channel electrodes have been used in the collection and analysis of sEMG signals, which can be categorized in the following way:

- *Linear-array electrode*: used for motor unit parameters such as amplitude and conduction velocity [56-58, 60, 62, 64, 66, 67, 70-73, 75, 81-83, 86, 87, 89, 92, 93, 95, 98, 104, 106-110].
- *Two-Dimensional (2D) array electrode*: used for motor unit recognition [74, 84, 85, 88, 91, 103, 111].
- *High-Spatial-Resolution surface electrode (HSR-sEMG)* are 2D array-based electrodes: used for improved selectivity of motor unit parameters [37, 61].
- *High-Density surface electrode (HD-sEMG)* are 2D array-based electrodes: used for motor unit recognition or motor unit topology [59, 63, 65, 68, 69, 76-80, 90, 94, 96, 97, 99-102, 105].

Figure 3.1 shows the overall picture of where the multi-channel electrodes sit on the continuum of what can be measured in terms of the muscle physiology using surface or needle electrodes.

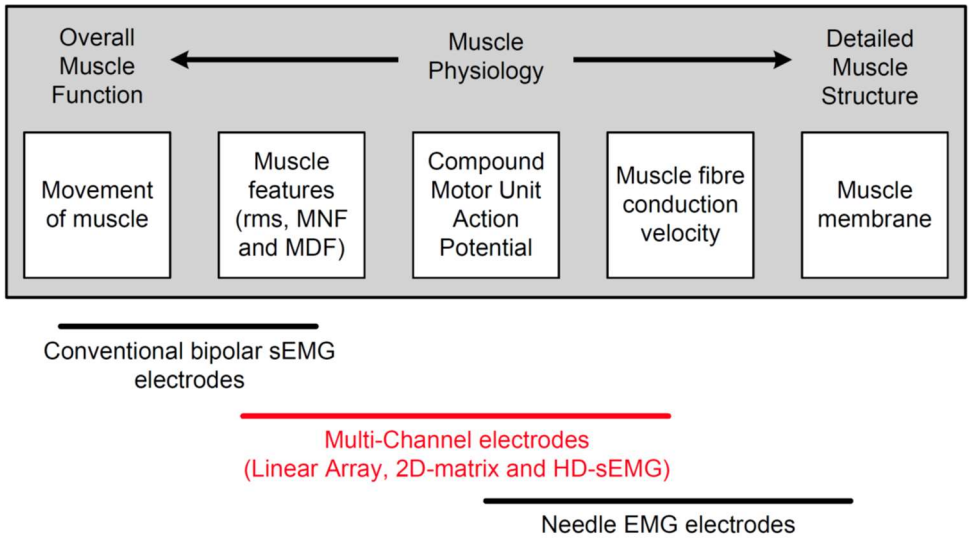

Figure 3.1 Revised diagram showing what various EMG electrodes such as conventional sEMG electrodes, multi-channel sEMG electrodes (indicated in red) and needle EMG electrodes can measure in terms of muscle physiology [54].

A review of the relevant studies [37, 56-111] revealed that important aspects related to multi-channel electrodes were: (a) electrode design and configuration; (b) data acquisition; (c) signal processing techniques used; and (d) testing of the participants. Further considerations for each of these aspects are listed as follows:

(a) ***Electrode Design and Configuration***

- Electrode material, shape and size
- Inter-electrode distance (IED) of the electrodes
- Gelled or dry electrodes
- Electrode configuration
- Filtering used and amplification of the signal

(b) ***Data Acquisition of sEMG signals***

- Sampling frequency
- Bit-resolution of the data acquisition card

(c) ***Signal processing of sEMG signals***

- Signal processing techniques used

(d) ***Testing of the participant***

- Muscles being investigated
- Experimental set-up
- Placement of the electrodes on the skin surface

Electrode design and configuration is covered in this chapter while the remaining aspects are covered in subsequent chapters.

3.3 Surface EMG and Multi-Channel Electrodes

This section first introduces the sEMG design recommended by the European project Surface EMG for Non-Invasive Assessment of Muscles (SENIAM) [112-119] and then describes the configurations of sEMG used by other research. The basic sEMG follows the SENIAM recommendations in terms of materials used and IED. SENIAM recommendations are selected as it is an early and recognized association that substantially studied and researched in the area of sEMG. The next section covers the configurations of electrodes and describes the various types of electrode arrangements used by other research. It discusses how different arrangements can produce different forms of signals which can be further processed and analysed later. As with any type of electronic devices, sEMG electrodes have electrical properties and components which need to be considered. Hence the importance of noise filtering and both the filtering and amplification of the signals detected by electrodes are also covered. All these considerations inform the development of the new multi-channel electrode, which will be presented in the next section of this chapter.

3.3.1 sEMG Electrodes Designs and Recommendations

sEMG electrodes which are placed over the skin surface act as sensors or transducers, detecting bioelectrical signals generated by the skeletal muscles during contractions. Surface electrodes can be classified, based on the materials and technologies implemented in their manufacturing. sEMG electrodes can be distinguished as dry and non-dry or wet electrodes. Dry electrodes include pin or bar electrodes made of noble metals like gold (Au), platinum (Pt) or silver (Ag); silver chloride (AgCl); or sintered silver/silver chloride (Ag/AgCl). Wet electrodes (also called pre-gelled electrodes) consist of dry electrode components and a layer of conductive gel, hydrogel or sponge with an electrolyte solution, and they are often self-adhesive for ease of application. Figure 3.2 shows examples of surface electrodes for sEMG recordings.

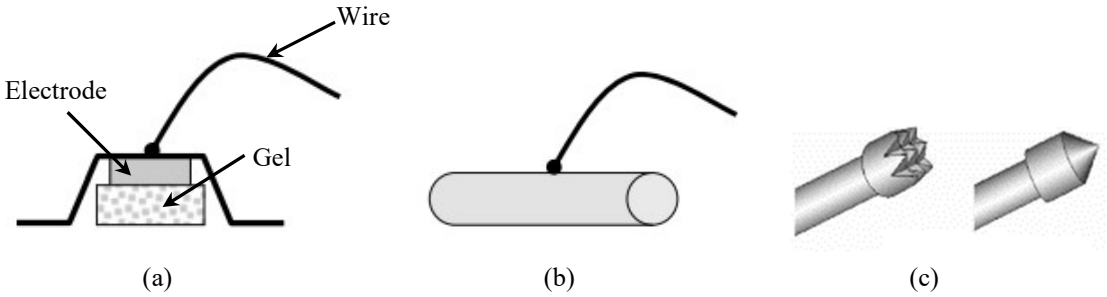

Figure 3.2 Revised figure showing a range of common surface electrodes used: (a) disposable electrode with sponge saturated with an electrolyte gel (wet), (b) solid metal bar electrode (dry) and (c) pin electrodes (dry) [26].

A surface electrode's physical dimensions, shape, technology and constituent materials can strongly influence the recorded sEMG signal [23, 26]. Hence, when choosing a sEMG sensor or electrode, the type, shape, size, IED, material and construction of the sensor have to be carefully considered. SENIAM gives recommendations on sensors design, materials used, IED, placement, signal processing and modelling of sEMG.

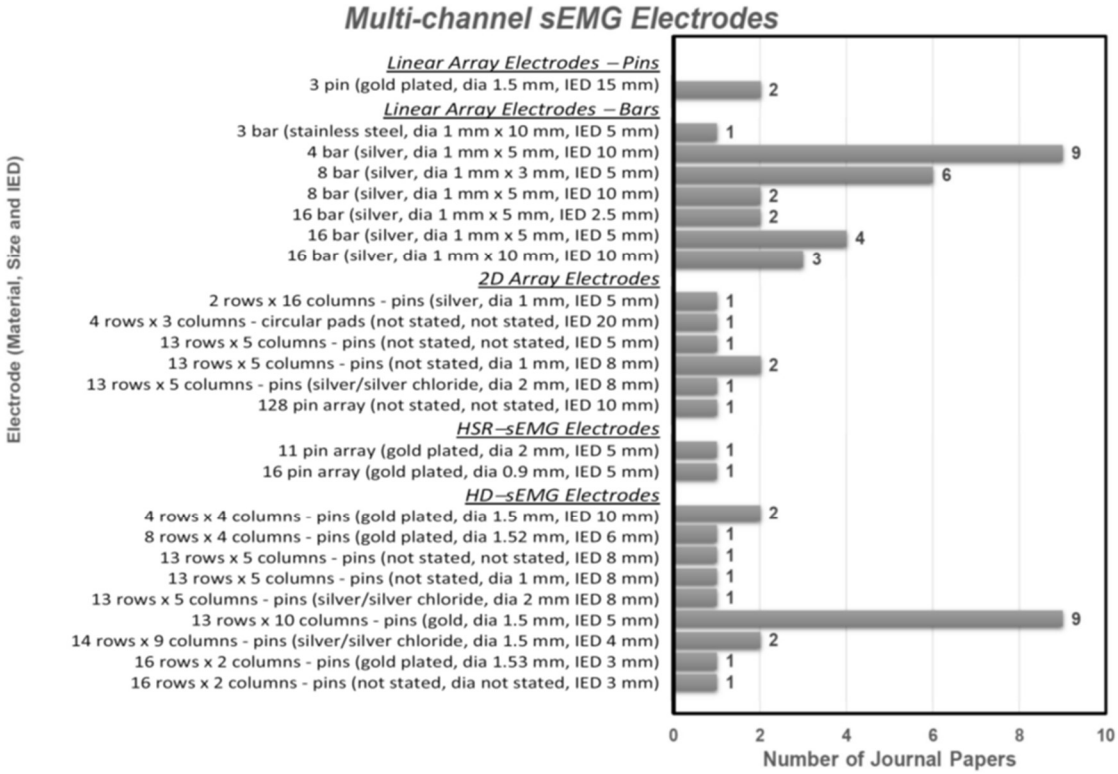

Figure 3.3 Inventory of varying sEMG used in the other research with different configurations, electrode material, size and IED of the multi-channel electrodes determined from the literature review (section 3.2).

The sensor type can be either *monopolar* or *bipolar*. The latter is a sensor consisting of two surface electrodes in either a one- or two-dimensional array. Since most publications meeting the search criteria used bipolar sensors in their sEMG research, the SENIAM recommendations for sEMG sensors are restricted to those of bipolar sensors only [23]. There are no SENIAM design recommendations for multi-channel sEMG electrodes, and there is a need for this information to be included as research has already been carried out using multi-channel electrodes, as mentioned in section 3.2 [36, 52-55]. For bipolar sensors, SENIAM's recommendations include:

- **Electrode shape and size:** the shape and size of the conductive area of sEMG electrodes. Both rectangular (square or bar) and circular (pin) electrodes are used, with not much difference in performance and pick up area. SENIAM recommends that the maximum size of the electrode in the direction of the muscle fibres is circular with a diameter of 10 mm. The literature review showed a wide variation of electrodes were used, with either bar or pins with varying dimensions in terms of diameter and length, as seen in Figure 3.3.
- **Inter-electrode distance (IED):** the centre-to-centre distance between the conductive areas of two bipolar electrodes, as seen in Figure 3.4.

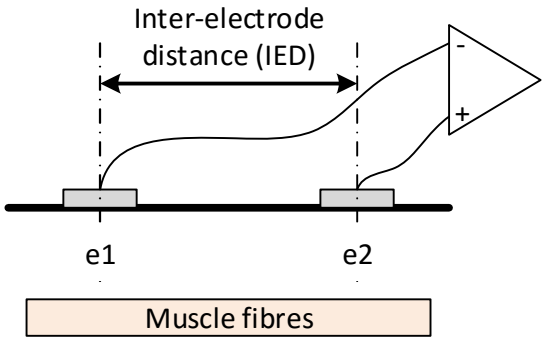

Figure 3.4 The IED between two electrodes (e1 and e2) for a bipolar configuration.

The influence of IED on the pick-up area and cross-talk is relevant due to the difference size of muscles. SENIAM recommends applying bipolar sEMG around the recommended sensor location with an IED of 20 mm. When bipolar electrodes are being applied to a small muscle, the IED should not exceed one-quarter of the muscle fibre length, to avoid unstable recordings due to tendon and motor endplate effects. The IED shown in Figure 3.4 is the distance between the centre of one electrode to the centre of the nearest electrode. These

electrodes may be collecting monopolar signals from individual electrodes. There is a wide range of values, but the most common is either 5 mm or 10 mm.

- **Electrode material:** forms the contact layer with the skin. The good electrode-skin contact exhibits a low electrode-skin impedance and a 'stable' behaviour in time, that is, with respect to impedance and chemical reactions at the skin interface. The literature review showed that the varieties used were silver (Ag), silver chloride (AgCl), sintered Ag/AgCl, gold (Au), Au-plated and others. Electrodes are mostly combined with electrode gel [23, 26]. Electrode gel and paste are used to reduce the electrode-skin impedance. Electrode gel is to be applied properly to a non-gelled electrode before use on a muscle, in order to obtain reliable sEMG recordings. SENIAM recommends using pre-gelled Ag/AgCl electrodes as they were seen to provide stable transition with relatively low noise, and are available commercially [23].

- **Sensor construction**: the mechanical construction used to integrate the electrodes, cables and, if applicable, the preamplifier. SENIAM recommendations are to use a construction with a fixed IED, built from lightweight material which should not directly affect sEMG characteristics. Cables need to be fixed, using tape or elastic band in such a manner to avoid pulling or movement, especially in fast dynamic contractions. There is no specific information on multi-channel sensor construction, but generally the basic wiring stability is required as above.
- **Sensor placement procedure:** a number of sequential steps to ensure location of the sensor in order to obtain reliable sEMG signals. SENIAM has set up a database showing how and where the electrode should be placed on the skin. The database was used in some previous research using multi-channel electrodes for placing the sensor on the muscle of interest [120].

Another classification of the sEMG electrodes is based on their electro-chemical behaviour or their capacitive ability to store charge: that is, whether they are polarizable or non-polarizable [121; Chapter 47, 122]. Polarizable electrodes have a strong capacitive behaviour, due to a double layer of charges at the metal-electrolyte interface. When a voltage is applied, there is no actual charge flow at the electrode-tissue interface, but a change of charge distribution associated to a displacement current occurs. Gold and platinum electrodes come closest to the ideal polarizable behaviour. A polarizable

electrode is not suitable for sEMG recordings with dynamic muscle contractions, since a movement of the metal surface of the electrode with respect to the electrolyte solution or skin can induce a change in the surface potential [121; Chapter 47, 122]. This is also called the *movement artefact* which is typically lower than 20 Hz and partially overlaps with the low-frequency components of sEMG signal, causing loss of information. On the other hand, non-polarizable electrodes allow a free flow of charge across the interface, as they are characterized by mainly ohmic behaviour.

The current most-preferred bipolar electrode for sEMG application is the pre-gelled Ag/AgCl electrode as recommended by SENIAM. It fits the requirement of being non-polarizable as it has very low polarization on current flow. It is also highly stable, since its junction with gel produces a lower noise level than other metallic electrodes [23, 121; Chapter 47, 122]. When pre-gelled electrodes cannot be used, then the electrolyte has to be applied to the electrode metal shortly before the recording. Research on capacitive or polarizable electrodes is ongoing [23, 26], in order to build more effective electrodes which can be used to produce the lowest noise levels and to prevent loss of sEMG signal information. On the other hand, it is not always practical to have pre-gelled non-polarized electrodes when using a multi-channel system, as it consists of an array of numerous pins [37, 59, 61, 63, 65, 68, 69, 74, 76-80, 84, 85, 88, 90, 94, 97, 99-103, 105, 111]. A linear array electrode usually has pre-gelled electrodes [56-58, 60, 64, 67, 70-73, 75, 82, 83, 86, 87, 89, 92, 95, 106, 107], but HSR-sEMG [37, 61] and HD-sEMG use dry pin electrodes [59, 63, 65, 68, 76-80, 84, 90, 94, 97, 99-102, 111].

This research aimed to develop surface electrodes with enhanced functions to extract more signal features with more parameters. These enhanced functions require new design configurations, including setup array for multi-channel electrodes.

3.3.2 Basic Configurations of sEMG Electrodes

When sEMG signals are collected through an electrode placed on the surface of the skin, either during voluntary contraction of the muscle or at rest, the electrode acts as a passive electrical interface between the participant and the recording equipment.

Electrode configuration for sEMG refers to the number of electrodes at the recording site and their arrangement. The two most common configurations are *monopolar (or*

unipolar) and *bipolar (or single differential)* configurations. In both cases, there are usually two detection surfaces and a ground electrode. Any other electrode configurations are extensions of the bipolar configuration. For instance, the bipolar configuration using a single differential amplifier can be expanded to a *double differential* configuration, as shown in Figure 3.5.

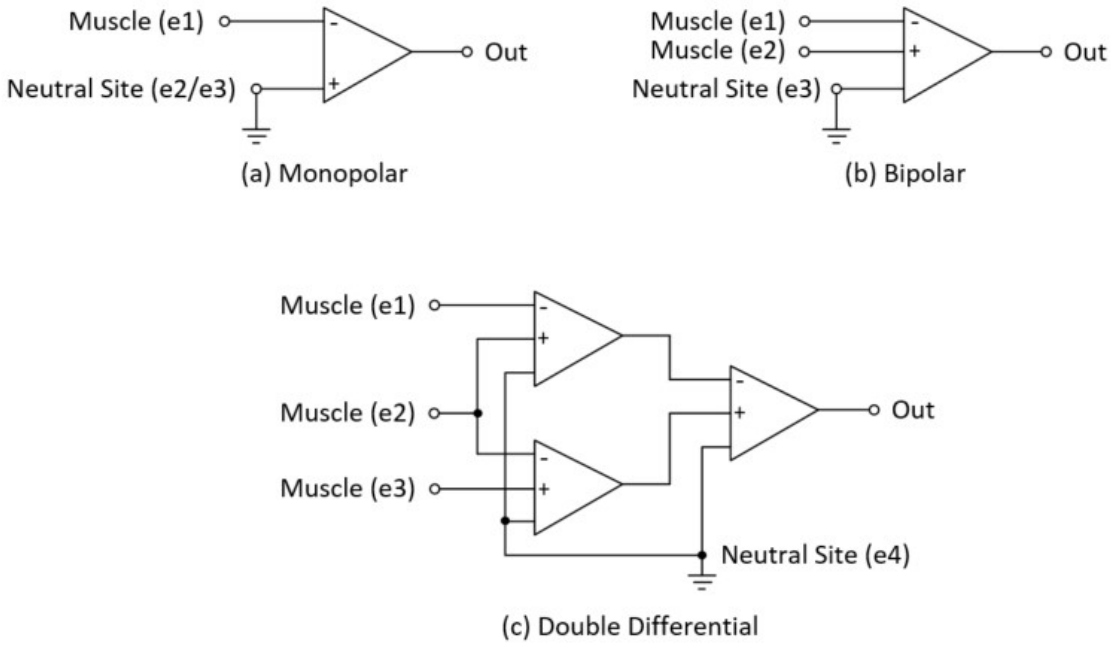

Figure 3.5 The configurations for (a) monopolar, (b) bipolar and (c) double differential for the collection of sEMG signals.

A *monopolar configurations* consists of one electrode (e1) as the active recording surface placed over the muscle and a second electrode (e2) as the reference, which is placed on an electrically neutral location such as the tendon to determine a potential difference. A third electrode (e3) acts as the ground and is placed on a bony surface away from electrodes e1 and e2. Usually e2 is placed at the same location as the ground, and so only two electrodes are needed. Generally, monopolar signals produce lower frequency responses and less spatial selectivity than bipolar signals. Monopolar configuration for surface electrodes is usually used during static contractions or in clinical investigations using needle electrodes.

A *bipolar configuration* has both active electrodes (e1 and e2) placed over the muscle, with another electrode (e3) acting as the ground placed on a bony surface. Signals from the active electrodes are fed into a differential amplifier that records the electrical

difference between the recording electrodes (e1 and e2). So any signal that is common to both inputs of the differential amplifier is greatly attenuated, and removed from the signal. This configuration is designed to minimize unwanted signals from surrounding environment such as radio frequency and electrical activity from power outlets, surround lights and so on [3, 44]. SENIAM recommendations on sEMG were based on bipolar configuration [23].

A *double differential configuration* consists of three active electrodes (e1, e2 and e3) in a row placed over the muscle, and another electrode (e4) for the reference or ground placed on a bony surface. This configuration gives an enhanced rejection of unwanted signals similar to that of the bipolar configuration [3, 25, 36, 44, 123].

3.3.3 Multi-Channel sEMG Electrode Configurations

When multiple of electrodes are placed over the recording sites, the devices are referred to as *multi-channel electrodes* [27, 36]. The basic electrode configurations of monopolar, bipolar and double differential that are used in a multiple number with particular arrangements, form a multi-channel electrode. In this way a montage of information concerning the distribution of the EMG activity over a muscle or the timing relationships between different muscles becomes accessible. In principle, there is no hindrance to increasing the number of surface electrodes over the muscle, the number of channels, or arranging complex montages from different electrodes for each channel.

Some types of the multi-channel configurations are:

- Linear array
- Two-Dimensional (2D) array
- High-Spatial-Resolution sEMG (HSR-sEMG)
- High-Density sEMG (HD-sEMG)

3.3.3.1 Linear Array Electrodes

Connecting several recording electrodes placed in a line results in a linear array recording, as shown in Figure 3.6 [124].

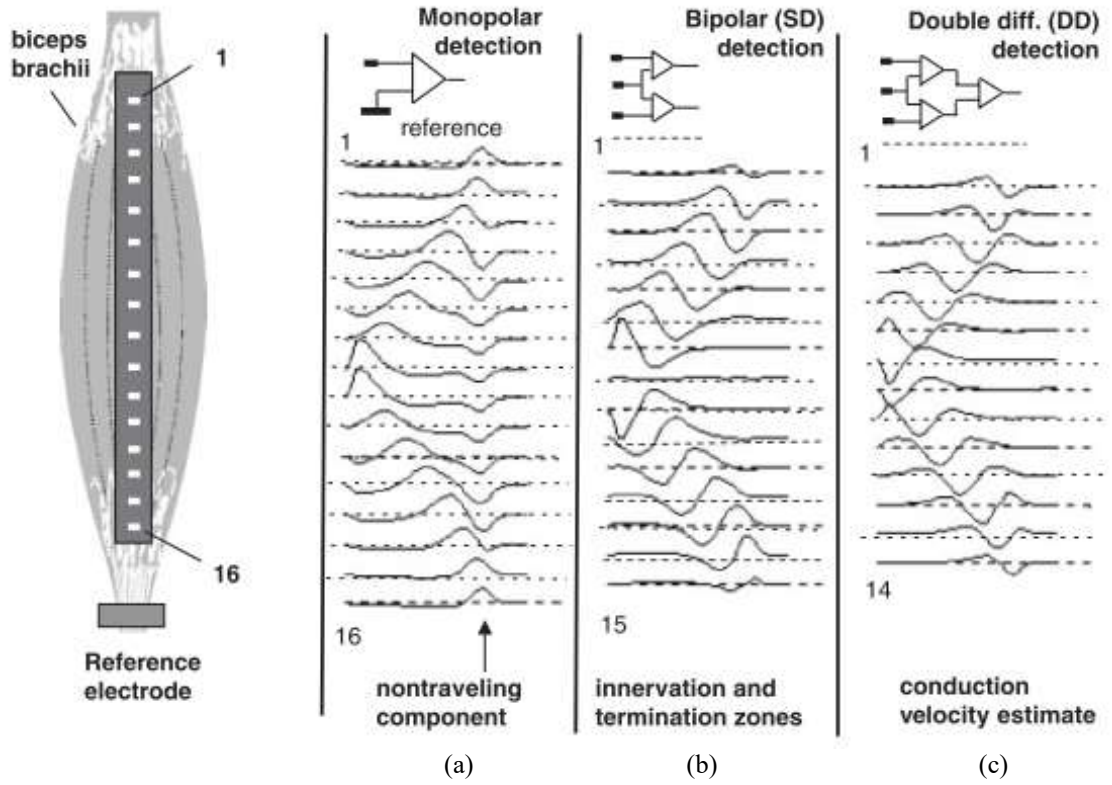

Figure 3.6 Schematic diagram of the three configurations for the detection of sEMG from linear array [124].

Figure 3.6 shows the three configurations. Monopolar detection (a) provides the maximum information available from the signal and includes the fibre-end effects. Bipolar or single differential (SD) detection (b) provides a clear picture of any innervation and tendon zones. Double differential (DD) detection (c) is the most suitable for estimating the muscle fibre conduction velocity (MFCV) [124].

The literature review revealed that 24 of the 62 relevant papers used linear array electrodes, either in the bipolar or double differential configuration mode. The electrodes used in those studies were sourced from the same manufacturer – LISiN-Spes Medica, Italy. They are semi-disposable pre-gelled electrodes made from silver bars. The 2D Array and HD-sEMG electrodes were reusable and made from gold-plated pins.

3.3.3.2 2D Array Electrodes

These sEMG electrodes form a grid or matrix which is covering a portion of the skin surface above one or more muscles [36]. Each of the electrodes collects a monopolar signal, which are further processed for analysis. The 2D array electrodes are the basis for further development to form the HSR-sEMG and HD-sEMG electrodes for specialized research and clinical uses of sEMG signals [36, 52, 125].

3.3.3.3 HSR-sEMG Electrodes

High-Spatial-Resolution surface EMG (HSR-sEMG) is a class of high-pass spatial filters represented by Laplace filters which approximate the second spatial derivative of the surface potential [25; Chapter 7]. Figure 3.7 shows the combination of activities of one electrode with one or several surrounding electrodes close to the muscle, which results in *higher-order derivations* [126]. The classic configuration of two electrodes used over the muscle results in a bipolar recording and double differential recording as presented in Figure 3.7 (a) and (b) respectively. The effect is *spatial (high-pass) filtering* producing a narrowing of the spatial view of the sEMG signal [29, 32, 34, 35, 126-130]. A more complex spatial filtering is achieved by a *normal double differentiating filter (NDD filter)*, referred to as *Laplacian configuration*, where a central electrode is connected with four surrounding electrodes [34, 35]. The weighting factors of the NDD filter (its filter mask) are written as:

$$A = \begin{bmatrix} 0 & +1 & 0 \\ +1 & -4 & +1 \\ 0 & +1 & 0 \end{bmatrix}$$

where the '–4' is the weight of central electrode and the '+1's indicate the four surrounding filters. This NDD or Laplacian configuration is shown in Figure 3.7 (c). The spatial Laplacian filtering is used with monopolar signals obtained from either 2D array or HD-sEMG electrodes [26, 34-36].

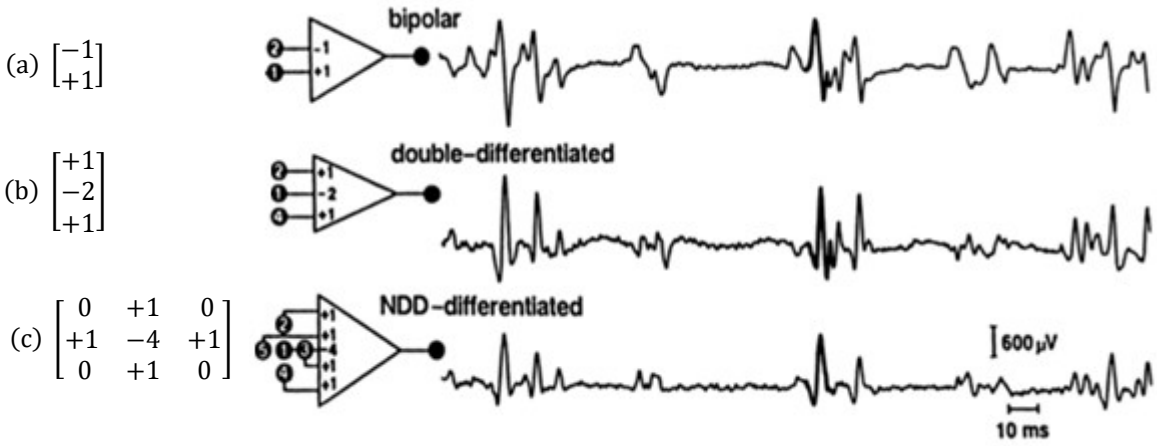

Figure 3.7 Presentation of different EMG electrode configurations recorded from the abductor pollicis brevis muscle at maximum voluntary contraction. One excitation of a motor unit has been emphasized [126].

The exact montage to be used depends on the clinical or research question. It should be realized that the recording area of the electrodes becomes progressively smaller with higher-order derivations, but also with shorter IED. As a natural consequence, the amplitude of the signals usually decreases. An important and often intended consequence of bipolar and higher-order montages, and of a short IED, is the suppression of the far-field activity, originating during the start and extinction of the action potential [29, 32, 34, 35, 126-130].

The array which is applied along the muscle fibre direction is also known to sample the propagating potential at different positions in the space. This can be used to estimate muscle fibre conduction velocity (MFCV) and to determine the location of innervation zones and tendons [53, 131, 132].

3.3.3.4 HD-sEMG Electrodes

High-Density sEMG (HD-sEMG) are arranged in a two-dimensional grid with an arbitrary number of electrodes and IEDs, as shown in Figure 3.8 (a). This configuration enables the localization and size estimation of motor units (MUs) as well as the determination of the position of the endplate zone. With a two-dimensional grid it is also possible to display the sEMG activity in an amplitude map, as shown Figure 3.8 (b) [36].

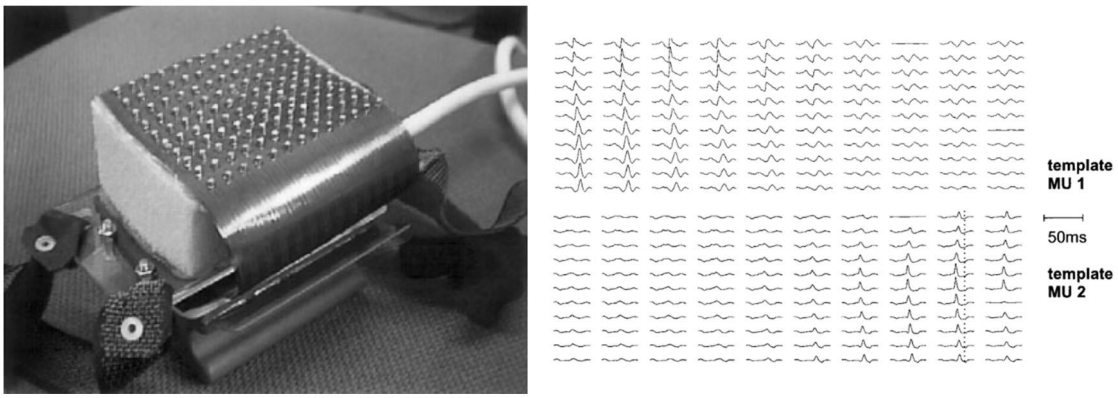

(a) (b)

Figure 3.8 (a) A 126-channel high-density electrode grid developed for the study of the larger skeletal muscles. Three-dimensional surface MU potential templates recorded from two MUs. (b) Signals represented in a monopolar montage [36].

It is therefore recommended for all sEMG measurements, especially for HD-sEMG electrodes, to record and store the signals of the individual electrodes in the array or grid, referenced to a remote electrode in a monopolar fashion. This approach allows versatility with respect to the desired montages, such as bipolar, double differential or Laplacian configuration.

Some previous studies have used HD-sEMG electrodes, all of which collected monopolar signals [59, 63, 65, 68, 69, 76-80, 90, 94, 96, 97, 99-102, 105]. There was a wide variation in the number of pins used. For example, some researchers used a commercially available HD-sEMG electrode supplied by BioSemi, The Netherlands with 126 gold-plated pins, as shown in Figure 3.8 [59, 63, 76-78, 90, 94, 100, 101].

3.3.4 Electrode Impedance, Noise and DC Voltage

With the surface electrode overlying the skin, electrode-skin impedance should be taken into account. Huigen, et al. [133] found that in the range of 0.5 to 500 Hz there was no difference in noise properties between electrodes of different metals when the electrode-gel interface was allowed time to stabilize. Faster stabilization of low noise production was achieved using a silver/silver chloride (Ag/AgCl) electrode compared with other metals, and hence it is preferred for low noise sEMG recordings. Their research was unable to provide a physical explanation for the relationship between the impedance and noise properties of electrodes. However, the input impedance of the

amplifiers used to amplify the biosignal from the electrode was very high (> 100 MΩ), and their input noise current was very low (< 1 ρA_{rms}). Consequently, the impedance of the electrodes does not play a role in the quality of the signal processing [133].

Another aspect to consider is the *battery effect* [25; Chapter 5], which occurs when two similar electrodes are used in a single differential configuration where the two DC voltages would cancel out. Since the contact features of the electrode-skin interface are never the same in two different locations, this battery effect should be considered. Slowly changing voltages or DC are usually present between two points on the skin and may be observed as high as a few hundred mV. This constrains the design of front-end amplifiers whose DC gain must be limited to prevent saturation [25; Chapter 5, 122].

Despite the use of well-designed active electrodes, signal recording instrumentation and careful skin preparation, some noise will always accompany the desired signal. Signal conditioning techniques for further noise reduction using band-pass filtering can be applied [134].

3.4 Design of the New Multi-Channel Electrode

There are a number of aspects that need to be considered when designing electronic hardware for sEMG electrodes. The most important one is selecting the possible range of voltage and frequency values when detecting sEMG signals. Figure 3.9 shows the range of frequencies for sEMG (shown in red), and where it sits in terms of other biosignals that can be found in the human body [122].

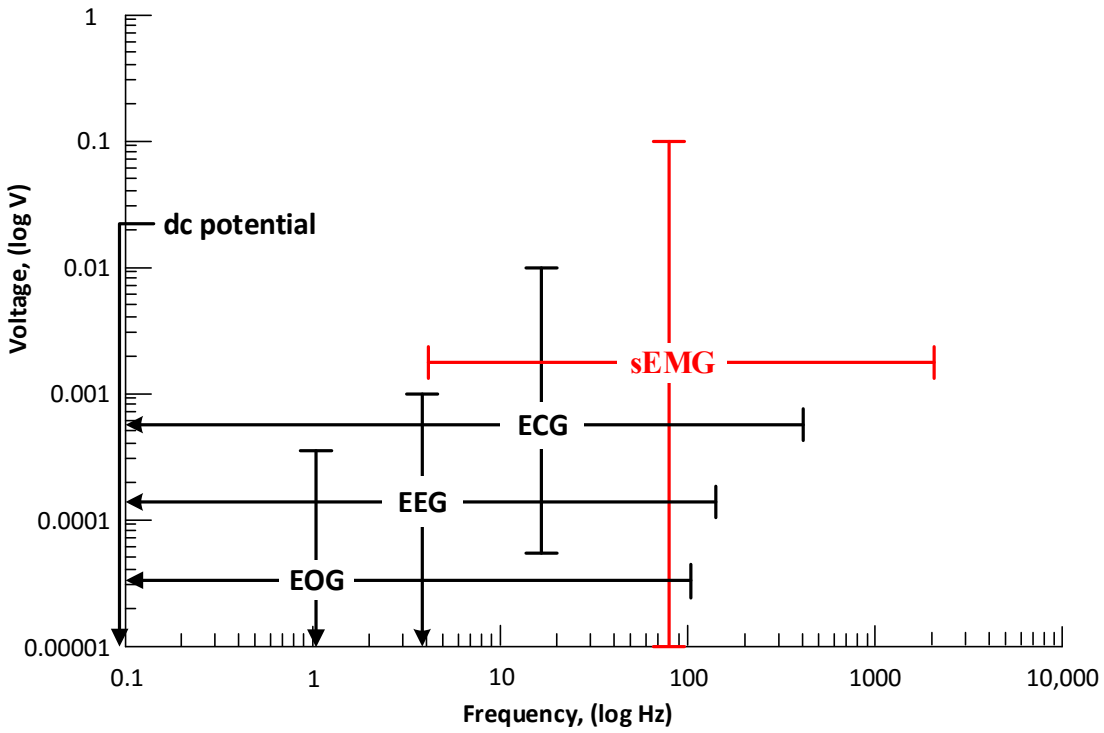

Biosignal	Frequency Range (Hz)	Voltage Amplitude Range (V)
Electrooculography (EOG)	0.01 to 100	50μ to 350μ
Electroencephalogram (EEG)	0.01 to 150	1μ to 1m
Electrocardiography (ECG)	0.01 to 400	15μ to 10m
Electromyography (Surface sEMG)	**5 to 2,000**	**10μ to 100m**

Figure 3.9 A revised graph and table of the range of frequencies of different biosignals found in the human body [122], with sEMG indicated in red.

There are standards and protocols for reporting the EMG data which had been consolidated over the years by the *Journal of Electromyography and Kinesiology* [135], usually referred to as the *golden rules* (see Appendix A). The essential factors with respect to hardware are:

- Electrodes
- Amplification
- Filtering

The design of the electrodes used in this research to collect data for analysis purposes is shown in Figure 3.10. It consists of 11 electrode pins in a combination of linear array and Laplacian configuration.

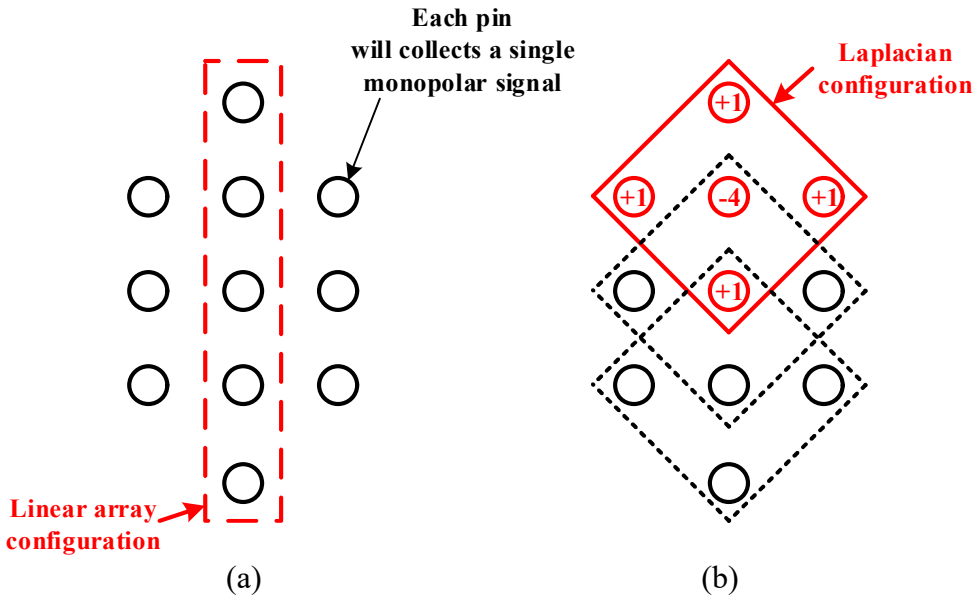

Figure 3.10 Configuration of the 11 electrode pins: (a) the five pins that will be used for the linear array and (b) the pins that will make up the three channels of Laplacian configuration.

Each of the 11 pins collected monopolar sEMG signals from the vastus lateralis muscle of the quadriceps performing an isometric static contraction (detailed protocols are presented in Chapter 4). The signals were further processed online for both the linear array and Laplacian configurations (details of the signal processing are presented in Chapter 5). A better signal definition in terms of motor unit action potential was achieved with the Laplacian configuration.

The selected electrode material was gold-plated pins with a diameter ϕ of 4.8 mm (3/16 inches) and an IED of 10 mm. The signals from each of the active sites were preamplified as near as possible to the skin using an instrumentation amplifier, with a gain of 501 (or 54 dB). The filtering was done using a high-pass filter with a cut-off frequency of 5 Hz before the amplifier, and a low-pass filter after the amplifier with a cut-off frequency of 1 kHz, so that the electrode would have a band-pass filter of 5 Hz to 1 kHz at -3dB [136; Chapter 2].

Three Texas Instruments instrumentation amplifiers from the INA family were considered: the INA118, INA128 and INA333. After conducting simulations, the INA118 amplifier was found the most suitable.

Figure 3.11 shows the schematic circuit for the preamplifier circuit for each of the 11 monopolar signals. Further details about the selection and determination of the amplifier design are given in Appendix B.

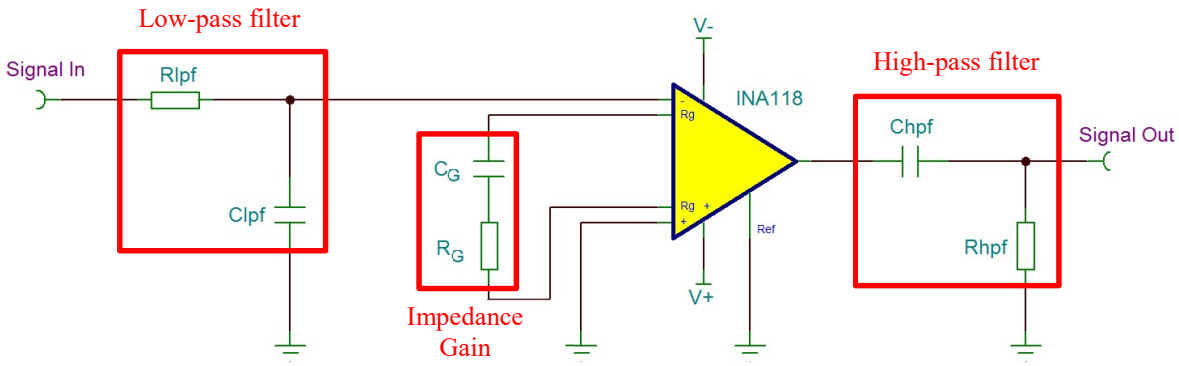

Figure 3.11 Passive components used to make a preamplifier circuit for one monopolar channel for the new electrode.

Before the final components for the filters and setting the impedance gain of the amplifier, a number of different investigations were carried out using the simulation software called TINA-TI, a SPICE based analogue simulation program for the prototyping of circuits on a breadboard, which are then printed on circuit boards. The results are shown in Appendix B. The steps taken were:

(a) Setting the gain of the amplifier without any filtering. This was achieved by placing an initial a resistor of 100 Ω giving a gain of 501 or 53.99 dB (≈54 dB) between pin 1 and 8 of the amplifier. Then a capacitance of 300 μF was connected in series with a 100 Ω resistor, as to ensure that the any DC component in the signal was not amplified to prevent saturation of the output signal. The capacitor creates a high-pass filter in the circuit with a cut-off frequency of 5.3 Hz at -3 dB point, with -20 dB/decade roll rate.

(b) The passive low-pass filter was designed using component values of 1.5 kΩ resistor and a 100 ηF, which has a cut-off frequency of 1.06 kHz at -3 dB point, with a -20 dB/decade roll rate.

(c) The passive high-pass filter was designed using component values of 820 Ω resistor and a capacitor of 100 μF giving a cut-off frequency of 1.94 Hz. Taking into account of the high-pass filtering of capacitor of the input impedance gain setting from (a), the high-pass filter cut-off is approximately the same 5.8 Hz with a better roll-rate of +40 dB/decade.

The above values of the preamplifier circuit for each monopolar signal are shown in Figure 3.12 (a). The frequency response curve obtained by the simulation for the circuit in Figure 3.12 (a) using TINA-TI software is shown in Figure 3.12 (b). The measured values were found by recording a number of readings at known frequencies, working out the gain, and plotting it against the simulated values, as shown in Figure 3.12 (c).

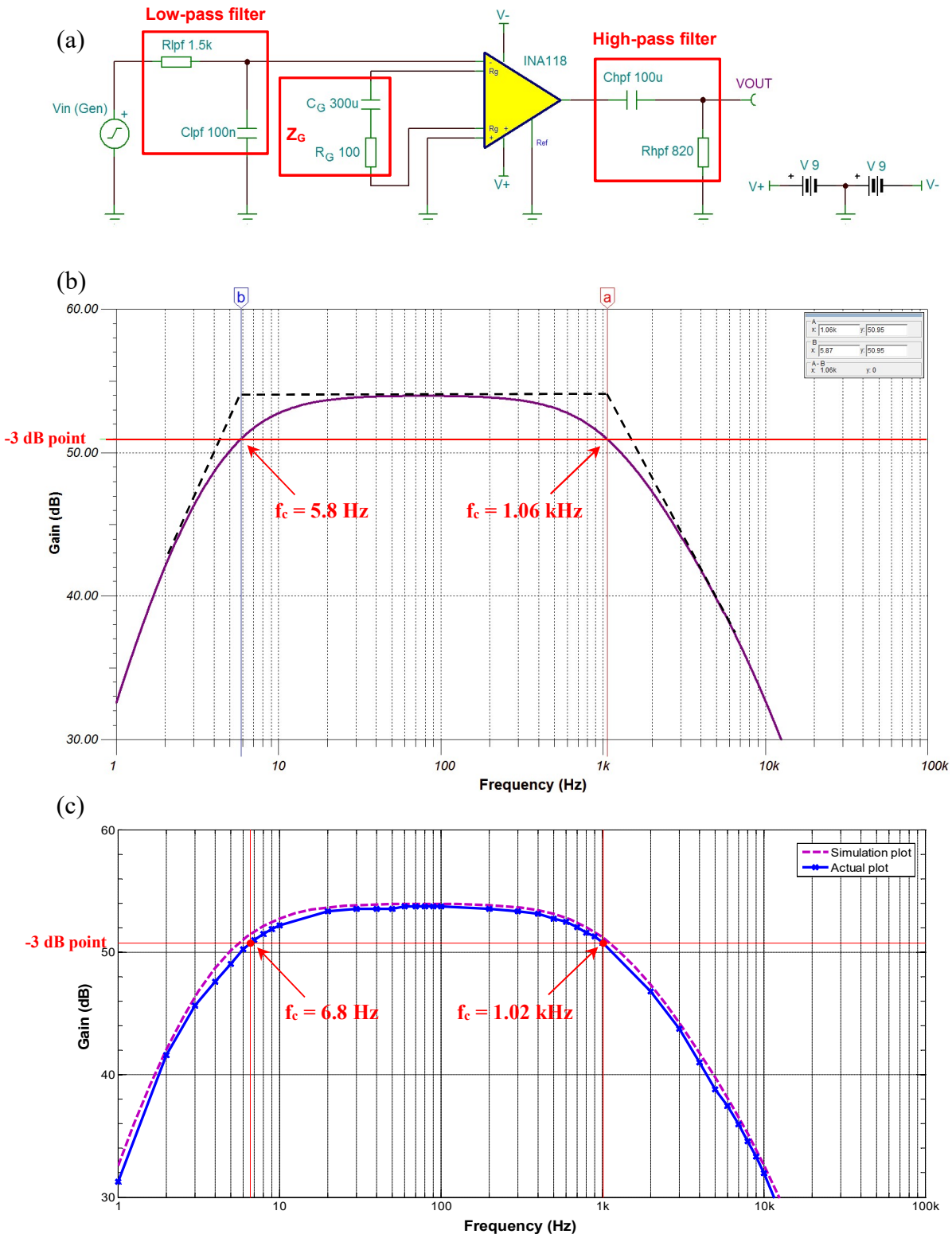

Figure 3.12 (a) TINA-TI simulation circuit. (b) Gain-frequency response plot showing the gain is 498 (53.95 dB), the lower cut-off frequency is 5.8 Hz and the upper cut-off frequency is 1.06 kHz. (c) Plot showing gain-frequency response for both simulated and measured values. The measured values have a maximum gain of 484 (53.7 dB) with a lower cut-off frequency of 6.8 Hz and an upper cut-off frequency of 1.02 kHz.

Table 3.2 shows the simulated and measured values for the gain, lower cut-off and upper cut-off frequencies for the circuit shown in Figure 3.12 (a). The respective values were close to each other indicating that the new preamplifier circuit nearly met the specifications set out for the circuit, which is to have a gain of 500 and a band-pass filter with a low cut-off frequency of 5 Hz and high cut-off frequency of 1 kHz.

Table 3.2 Simulated and measured values for gain, upper cut-off and lower cut-off frequencies for the preamplifier circuit shown in Figure 3.12 (a).

Value	**Simulated**	**Measured**
Gain	498 (53.98 dB)	484 (53.7 dB)
Low cut-off frequency	5.8 Hz	6.8 Hz
High cut-off frequency	1.06 kHz	1.02 kHz

The next step was to make the circuit Figure 3.12 (a) using high precision components to ensure the simulated values are met when the new 11-channel electrode is built. The schematics and PCBs were designed using Altium Design 14 for the multi-channel electrode and the battery power supply unit, and these are as shown in Appendix C. The electrode casing and power supply cover was drawn in SolidWorks 2012 and then built using the 3D printing facilities at the AUT University. The completed electrode is shown in Figure 3.13, where completed dimensions of the electrode casing are 88.5 mm in length by 42 mm wide and 14.5 mm height, with the IED is 10 mm.

The stand-alone battery power supply unit in Appendix C, is designed to supply ± 6 V to each preamplifier circuit from two standard PP3 9 V batteries. The stand-alone battery supply unit eliminates any electrical noise and interference which is more apparent when using a power supply from the mains.

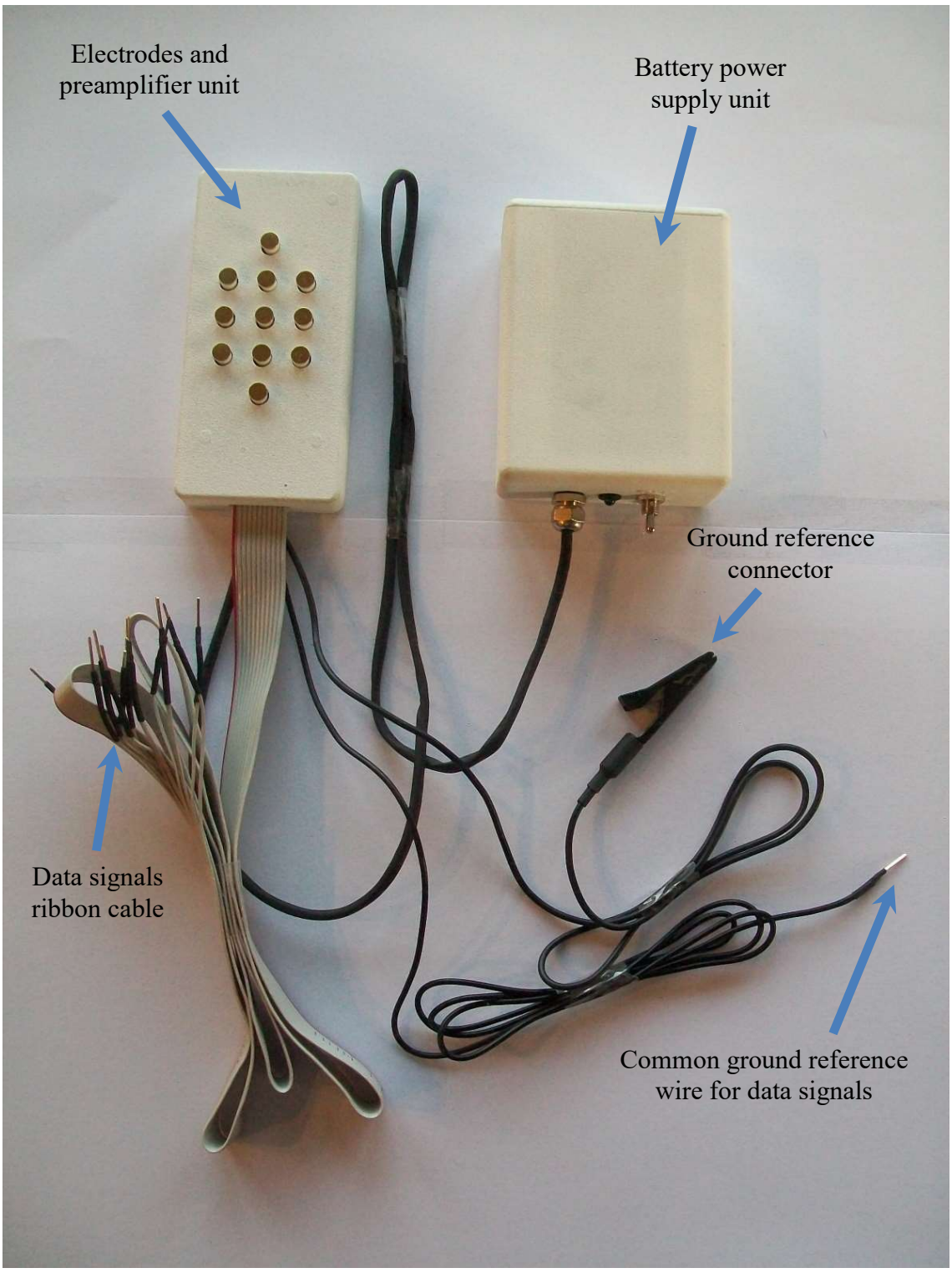

Figure 3.13 The new sEMG multi-channel electrode with separate battery power supply unit.

Chapter 4
Data Acquisition

4.1 Introduction

This chapter details the procedure followed for the data acquisition phase of this research using the newly designed multi-channel electrode described in Chapter 3 section 3.4. First the overall setup for the data acquisition is outlined, along with the equipment used. The data collection involved participants performing specific tasks focusing on their vastus lateralis, the largest muscle of the quadriceps group, while attached to the new multi-channel electrode. Protocols for a series of exercises were determined and described for the purpose of collecting the data via a range of maximum voluntary contractions. Since data obtained from human participants was part of this research, ethics approval by the Auckland University of Technology Ethics Committee (AUTEC) was required. An application for ethics approval was submitted explaining the research aim and procedures.

The setup of equipment included the biofeedback applications for displaying the following information:

- The *force trace*: displayed to both the participant and data collector. Force trace is the amount of force shown in the unit Newton (N) exerted by participant on the load cell during the period of testing.
- Data acquisition of the *force trace* and *sEMG signals*: displayed to the principal researcher and stored for signal processing and analysis, which is covered in Chapter 5.

4.2 Ethics Approval

Ethics approval (Application Number 12/49) was sought and granted by AUTEC on the 3 April 2012. The ethics approval also required the implementation of the three principles of the New Zealand Treaty of Waitangi, which are Partnership, Participation and Protection in the relationships between the researcher and other participants.

Appendix D includes a copy of the completed application form for the ethics approval for this research.

4.3 The Equipment and Setup

This section covers the overall setup for testing each participant's vastus lateralis and lists the equipment used.

The overall layout of the equipment setup involved:

- Testing chair
- Data acquisition cards using customized biofeedback/data acquisition virtual instruments (VIs) developed using LabVIEW software

The overall schematic setup is shown in Figure 4.1. The multi-channel electrode, which had a stand-alone battery power supply unit, was placed on the vastus lateralis muscle of the participant, who sat on the testing chair performing static isometric contractions. The multi-channel electrode was connected to a data acquisition card, which was linked further to a computer that displayed and recorded muscle activities.

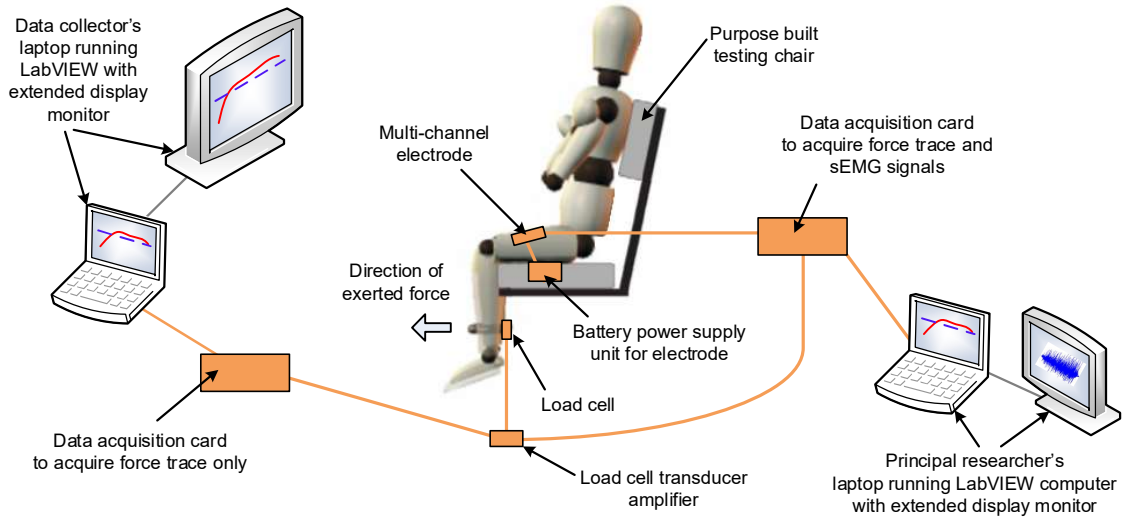

Figure 4.1 The overall setup of data acquisition system.

Two separate laptop computers with extended monitors and data acquisition cards were used to acquire data:

1. The data collector's laptop (Lenovo, T60 model) showed the same force trace to both the data collector laptop monitor and a separate extended monitor for the participant to view simultaneously. The extended monitor only presented biofeedback in terms of showing the force trace generated from the load cell for a particular task being performed. The force trace was measured for the following tasks:
   (a) To find the overall maximum voluntary isometric contraction (MVIC) force of each participant.
   (b) For testing each participant performing predetermined force values, which were set by the data collector, such as holding at 10%, 20% etc. of the participant's MVIC.
   (c) For testing each participant performing a fatiguing task set at 50% of the MVIC force.
2. The principal researcher's laptop (HP, EliteBook 8570p model) showed both the force trace generated and the collected sEMG signals simultaneously. The laptop was connected to an additional monitor to ensure that all data was displayed to the principal researcher.

4.3.1 Testing Chair

Figure 4.2 shows the purpose-built chair used for testing the participants. The chair features had an adjustable back support, restraining straps and an adjustable load cell assembly, which is attached to the participant's leg at the mid-lower part of the shin. The chair's restraining straps allowed the participant to be secured for stability while performing a number of tests.

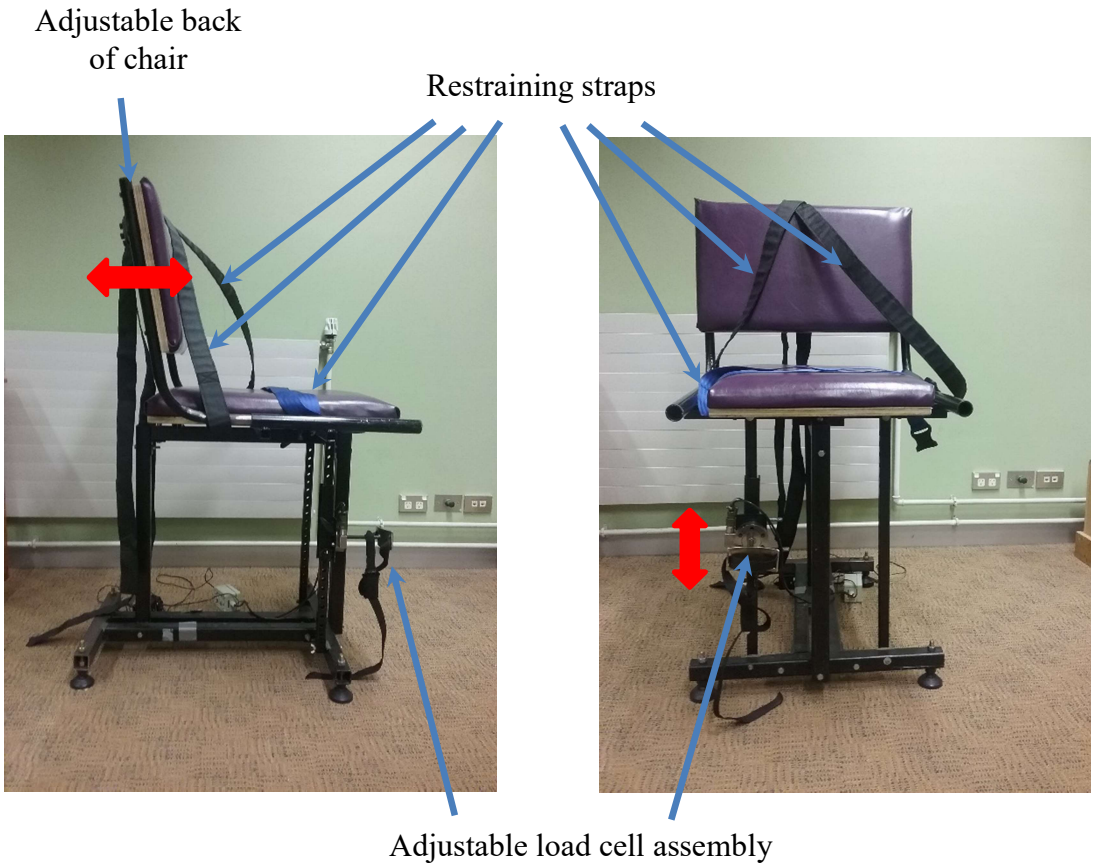

Figure 4.2 Picture of the testing chair, (left) the back of the testing chair was adjustable horizontally as indicated by the red arrow, (right) the load cell assembly is adjustable vertically as indicated by the red arrow.

Figure 4.3 shows the load cell, restraining brackets, transducer amplifier with the data acquisition card, and laptop computer running LabVIEW using the new calibration VI. This allowed the transducer output voltage readings to be converted to force during each of the tests performed and enabled the simultaneous collection of the sEMG signals from the participant's vastus lateralis muscle using the new multi-channel electrode. The load cell assembly with the restraining bracket was designed to be detachable so that it could be used to test both the right and left legs of the participant.

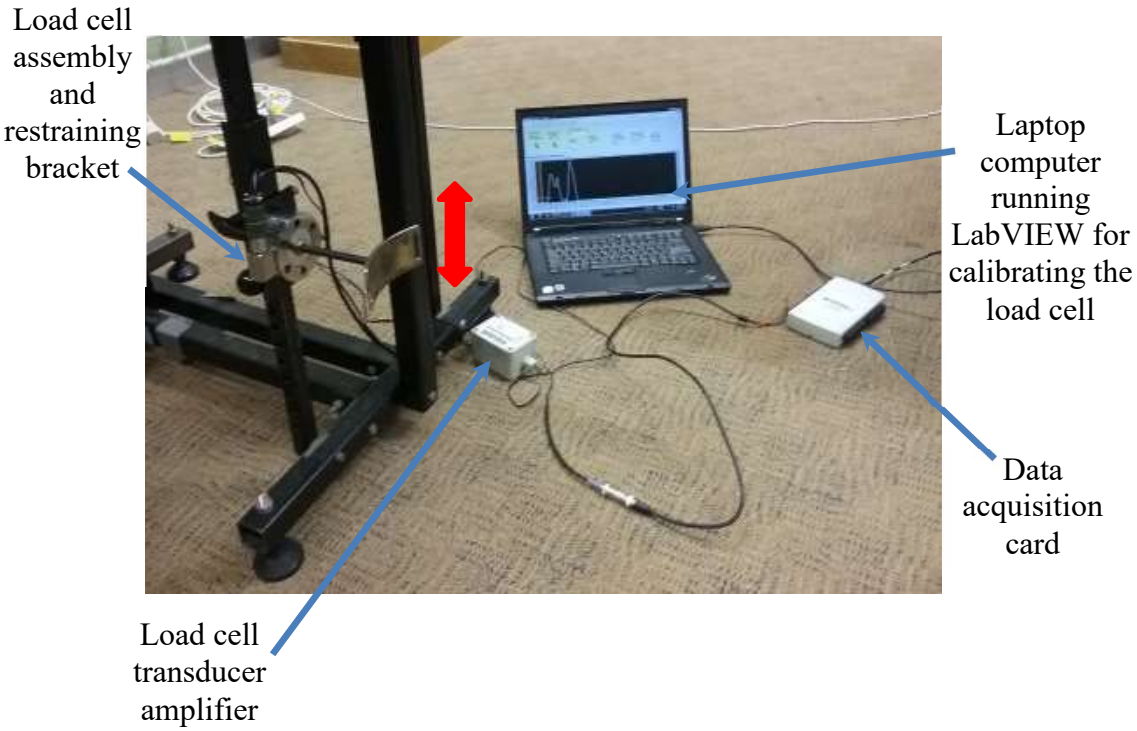

Figure 4.3 Calibration of the load cell assembly with restraining bracket. The red arrow indicates the vertical adjustment of the assembly.

Load cell is a sensor or transducer that is able to detect force exerted to it and used to create an electrical signal in unit voltage, whose magnitude is directly proportional to the force being measured. Transducer amplifier is used to amplify signals obtained by the load cell. Table 4.1 gives the manufacturer details of the equipment for the load cell, transducer amplifier and data acquisition card.

Table 4.1 Load cell, transducer amplifier and data acquisition card specifications

Equipment	Manufacturer
Model 41 Precision Low Profile Load Cell	Honeywell (Minnesota, USA)
Model UV, Universal In-Line Transducer Amplifier	Sensortec Inc. (Indiana, USA)
NI USB-6218 Data Acquisition Card (16–bit)	National Instruments (Texas, USA)

Before any testing was carried out, the load cell needed to be calibrated to determine the scaling factor in terms of force per volts (N/V). In order to do this, a new VI needed to be written for the data acquisition using LabVIEW software to determine the scaling factor. Appendix E shows the calibration procedure, the new VI and scaling factor results.

Figure 4.4 shows an outline figure representing a participant sitting on the testing chair before the new multi-channel electrode is attached. The red lines represent the mechanical axes of the human body related to the sitting position in the testing chair [137; Chapter 7, 138; Chapter 8]. The angle between the back and seat of the chair was set at 80 degrees to ensure that there was no discomfort at the lower part of back during testing [137; Chapter 7]. The angle between the seat and the lower shin of the leg that held and strapped with the load cell was set at 85 degrees. This angle of 85 degrees is referred to as the *flexion of leg at the knee joint* as used in previous studies carried out by Pincivero, et al. [139], Shenoy, et al. [140] and De Ruiter, et al. [141], all of which found that the maximum torque occurred between 80 to 90 degrees.

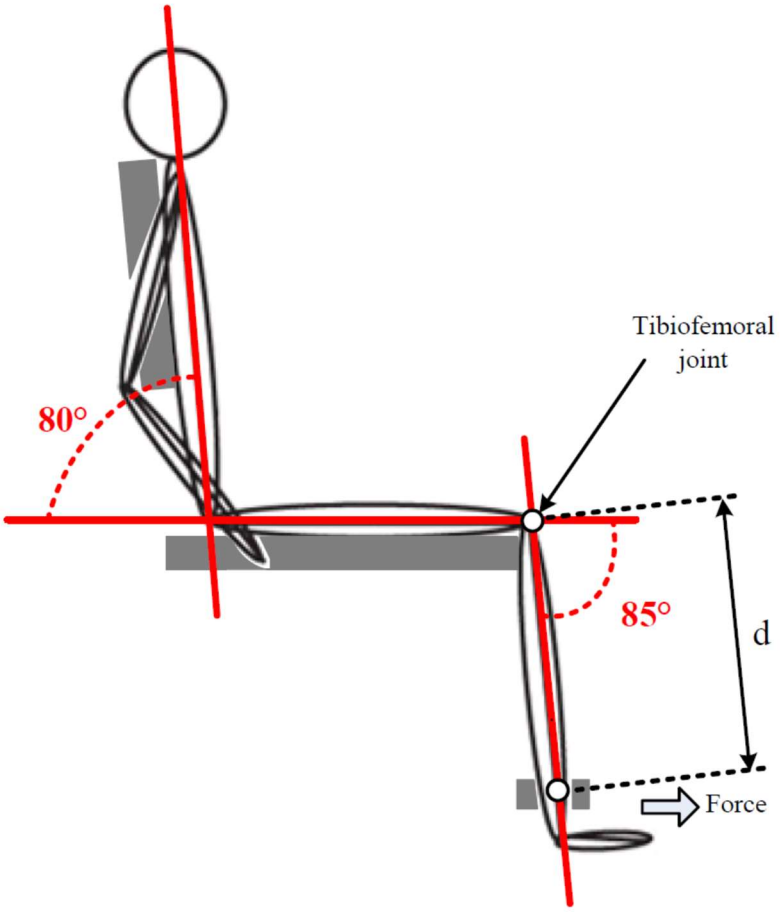

Figure 4.4 Mechanical axes, angles and torque length (d) of the participant in the testing chair.

The strength of the participant's vastus lateralis muscle was determined by taking the exerted force values and multiplying it by the length 'd' between the *tibiofemoral joint* of the knee [138; Chapter 8] and load assembly, as shown in Figure 4.4, to give the torque values in Newton metres (Nm) [137; Chapter 7].

4.3.2 LabVIEW Biofeedback VI

Biofeedback of the force trace being produced needed to be shown in real time to both the participant and data collector. Since the testing had three different tasks, different VIs were required for:

1. Finding the MVIC force
2. Testing the participant performing predetermined percentage values of the MVIC force found in Task 1
3. Testing the participant to hold 50% of MVIC force found in Task 1 for the fatiguing task

The core of the three VIs was structurally the same, with variations to determine the required values for each the above tasks. More details are explained in Appendix F containing the VIs for the force trace shown to the data collector and participant.

Figure 4.5 shows the setup of the equipment for the two biofeedback screens, one for the data collector and the other for the participant performing the tasks.

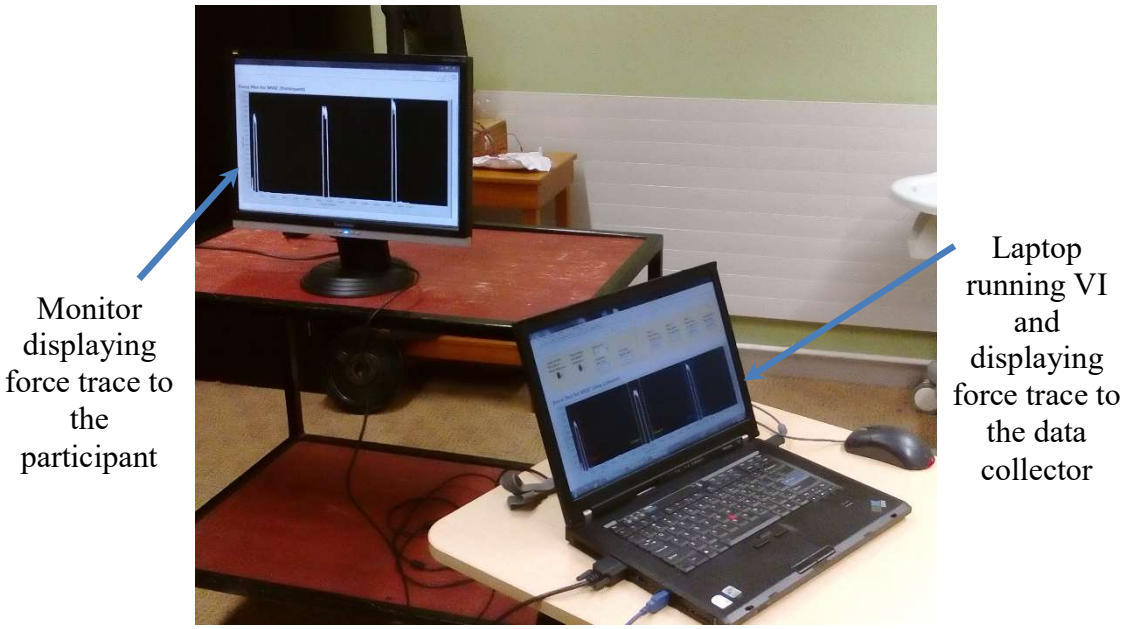

Figure 4.5 Laptop and extended monitor displaying generated force trace to both the data collector and participant.

4.3.3 LabVIEW VI for Data Acquisition of Force Trace and sEMG Signals

The simultaneous collection of the data for the force trace and the sEMG signals required a new customized VI that integrated the multi-channel function. The amount of data was collected from the 12 different channels of the data acquisition card, at a rate of 10,000 samples per second (or 10 kHz) for a maximum possible period of 30-minutes. The data was then stored on the hard drive of the laptop. The 12 channels required to collect the data consisted of:

- One channel for the force trace
- 11 separate channels for the sEMG signals from each pin of the new multi-channel electrode

The VI for the data acquisition of force trace and sEMG signals used by the principal researcher is shown in Appendix G.

The standard data acquisition using LabVIEW proved unsuitable, so a technique using a *producer/consumer* loop was used with *notifiers* and *queues*. Full explanation is described in Appendix G. Figure 4.6 shows the setup of the equipment used by the principal researcher for data collection.

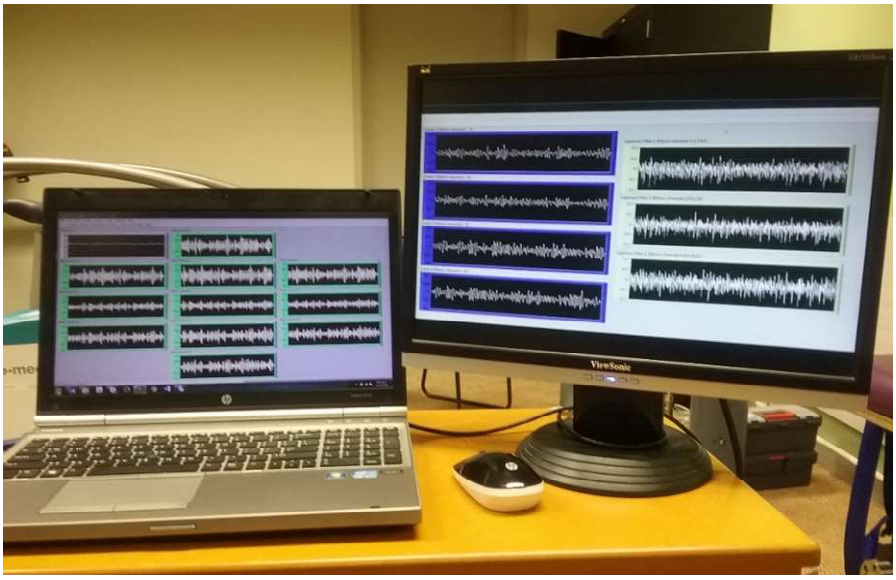

Figure 4.6 (left) Laptop monitor displaying the 11 monopolar channels plus force trace. (right) Extended computer monitor displaying linear array and Laplacian configured signals for principal researcher to view during data acquisition.

4.4 Data Collection

When potential participants agreed to meet with either the principal researcher or data collector, they were initially screened to ensure they met the inclusion or exclusion criteria for the research. If they met the criteria, they were invited to the Auckland University of Technology's School of Physiotherapy and Rehabilitation facilities at a later date for testing.

The data collector, a senior student with a background in human physiology, supported the principal researcher in terms of meeting all necessary requirements before the data acquisition process began. The data collector was responsible for:

- Explaining the testing protocols and obtaining the participant's consent and personal details.
- Physiological measurements of the participant.
- Skin site preparation of the vastus lateralis muscle for the placement of electrodes on the participant.
- Preparing the participant to carry out testing protocols for the data acquisition.

4.4.1 Consents and Personal Details

The following steps were taken before carrying out any testing of the participants:

- The principal researcher explained the purpose of the research and the protocols of the tests, which were designed to measure muscle activity via bioelectrical signals generated in the muscle.
- The data collector allowed each participant to read the Participant Information Sheet and sign the Consent Form, which are included in the Appendix D. Participants were given the opportunity to ask any questions at this stage.
- Before any preparation for the placement of electrode, the data collector recorded each participant's personal details such as name, age and ethnicity. The data sheet used to record those particulars is included in Appendix H.

4.4.2 Physiological Measurements

Before any testing and reporting in electromyography research, a number of physiological measurements need to be taken and recorded [135]. Appendix H shows the form used to obtain these measurements, which included:

- Height and weight
- Dominant leg (left or right leg, when used to kick a ball) [142]
- Measurement of fat thickness of the subcutaneous tissue layer above the muscle at skin site. Two techniques were used (a) skinfold thickness and (b) ultrasound
- Measurement of torque length along the tibia when seated in the testing chair.

4.4.3 Skin Site Preparation for Electrode Placement

Each participant, wearing only sports shorts and shirt with no socks and shoes, was then asked to lie on an electric physiotherapy bed. This enabled the skin surface above the vastus lateralis muscle of the participant's dominant leg to be prepared by the data collector. The positioning of the electrode was determined using the SENIAM recommendations [23, 116]. The new multi-channel electrode would be placed at two-thirds of the distance from the anterior spina iliaca superior to the lateral side of the patella as shown in Figure 4.7, which was the site where the skin preparation and measurement of fat thickness were to be carried out.

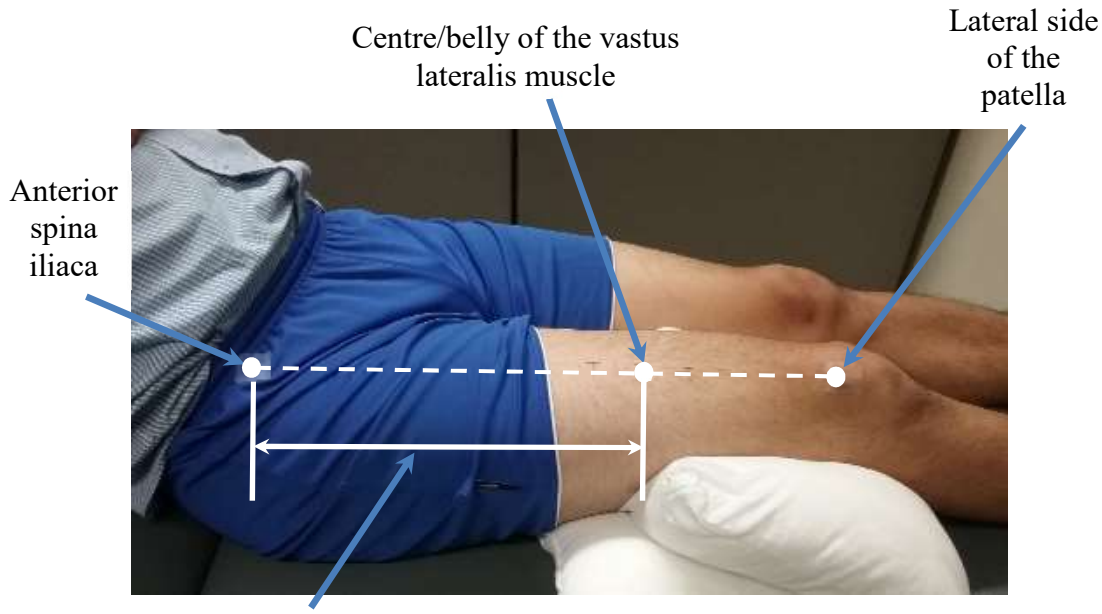

Figure 4.7 Positioning of the multi-channel electrode using the SENIAM recommendations.

Before the electrode was attached, the skin site was prepared to reduce the impedance to a value between 500 Ω and 10 kΩ [24, 135, 143, 144]. This was to ensure that the sEMG signals collected by the new multi-channel electrode would have a high signal-to-noise ratio (SNR) [122]. The steps taken for preparing the skin were:

1. Removing the hair by shaving the skin and rubbing with abrasive gel to remove the dry layer of the skin or dead skin cells [24, 143, 144]
2. Cleaning the skin using alcohol wipes to remove sweat [24, 143, 144] and then leaving to dry naturally
3. Measuring the skin resistance using a reusable bar electrode (DDB-30BSAF, Electrode Store, USA) with an IED space of 30 mm attached to a digital multi-meter (DM35XL, Wavetek, USA) as shown in Figure 4.8.

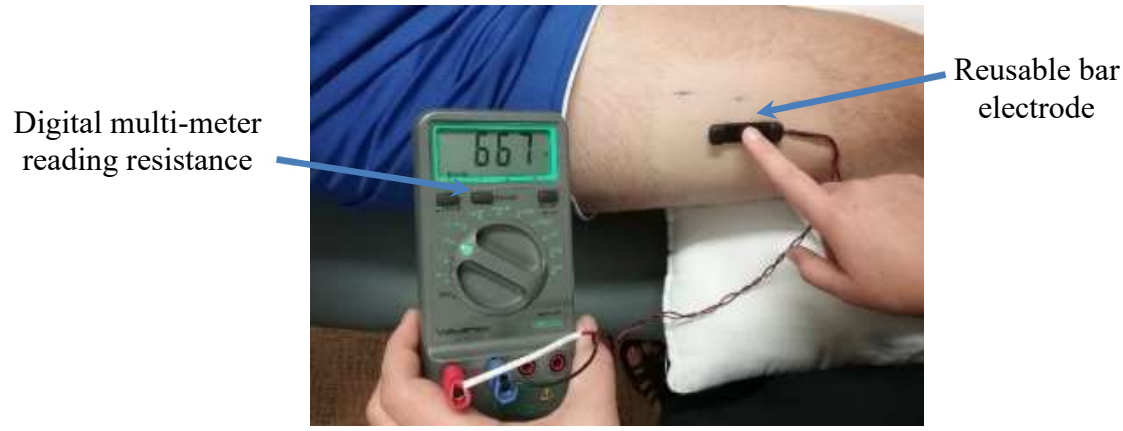

Figure 4.8 Measuring the skin resistance using a multi-meter.

Another physiological factor that affects the SNR of the sEMG signals is the subcutaneous tissue or fat layer of the skin where the electrode is to be placed [145-147]. The fat layer can increase the electrode-to-muscle distance from the electrode, which will affect the SNR of the signal. It had been shown that low fat layer values are associated with high values of SNR [145]. The thickness of the fat layer can account up to 50% of the variance in the signal [146]. The subcutaneous tissue layer was measured in two ways:

1. Skinfold caliper (C-120, Creative Health Products, USA) used by the data collector to measure the values at the site of the electrode, as shown in Figure 4.9.

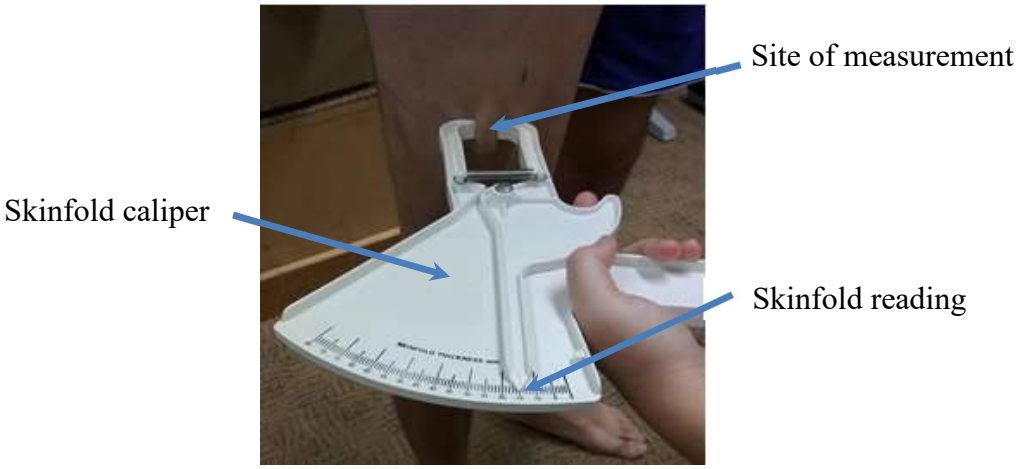

Figure 4.9 Taking skinfold measurement using a caliper.

2. An ultrasound reading was taken by the data collector, using a digital portable ultrasound scanner (Model 8300, Chison Ltd, USA) as shown in Figure 4.10.

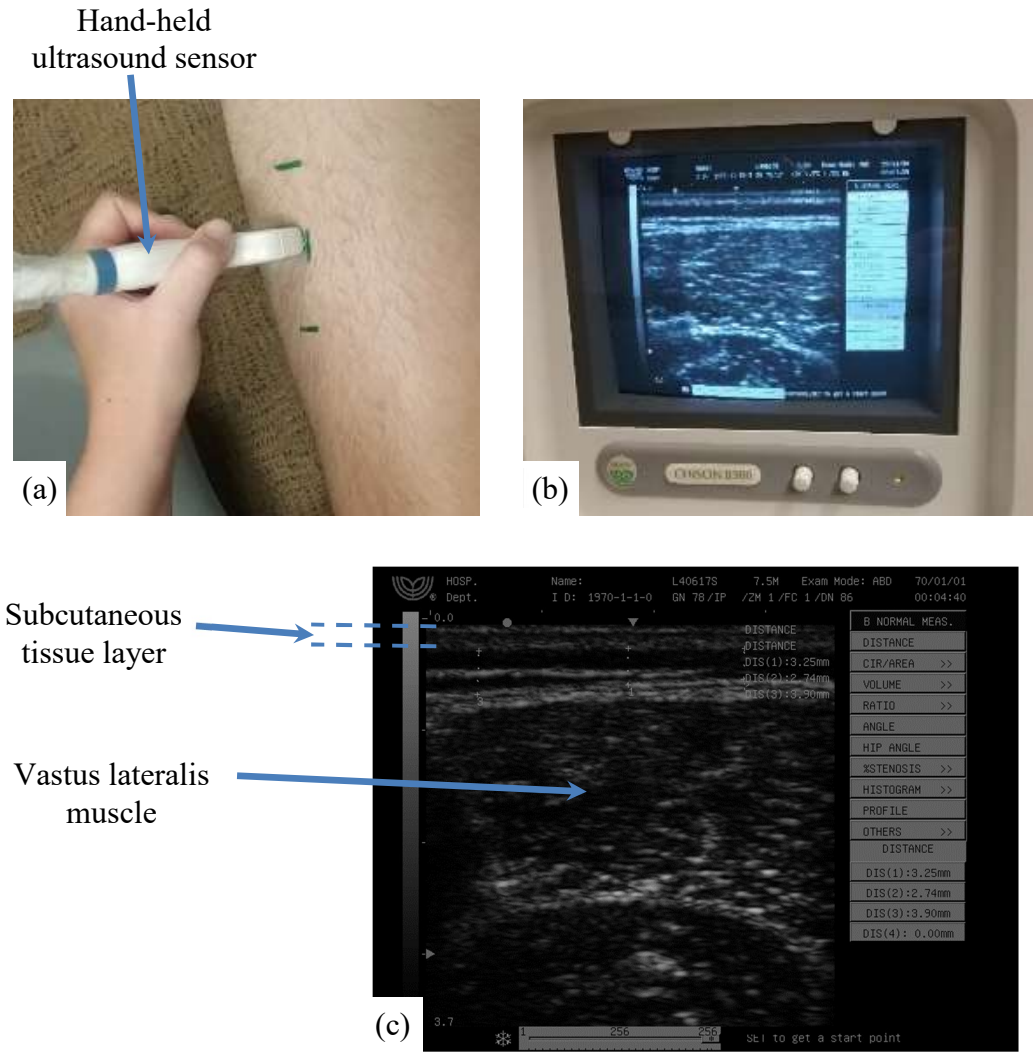

Figure 4.10 Measuring subcutaneous tissue of fat layer thickness using ultrasound (a) Hand sensor placed over the site of the muscle. (b) Image displayed on the scanner display. (c) Scanned image of muscle.

4.4.4 Testing Protocols

Before the participants were ready to be tested and seated in the testing chair, they were required to do a 5-minute warm-up on an exercise bike [139, 141, 148-150]. Once seated and restrained on the chair, the new multi-channel and reference electrodes were attached to the participant. The new multi-channel electrode was placed at two-thirds of the distance from the anterior spina iliaca superior to the lateral side of the patella as previously shown in Figure 4.7. The reference (ground) electrode required zero potential. The standard electrode position for zero potential is the bony landmark of *tibial*

tuberosity, where no electrical activity exists [24, 116]. The torque length was measured and recorded along the participant's tibia bone between the tibiofemoral joint (A) and centre point (B) of the load cell assembly strap, as shown in Figure 4.11.

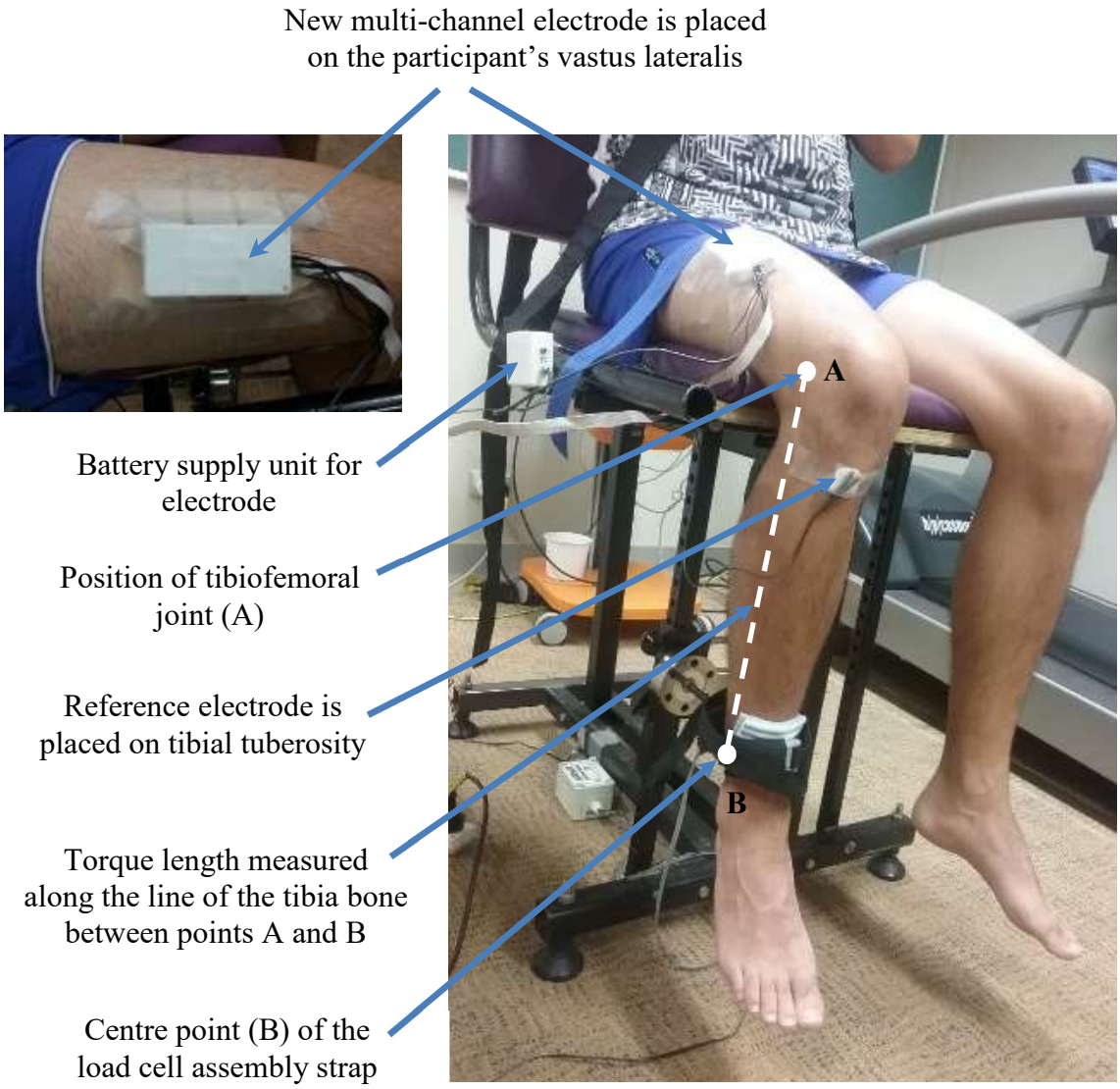

Figure 4.11 Participant sitting on the testing chair, with multi-channel and reference electrodes attached prior to testing.

Figure 4.12 shows a participant preparing to perform one of the MVIC tasks. The participant has restraining straps across his chest and thigh to keep them stabilized on the chair. The participant's arms were placed across his chest to isolate possible extra force from holding on to the chair, which could generate extra unwanted force from the quadriceps muscle of the leg during the testing [139, 141, 148-150].

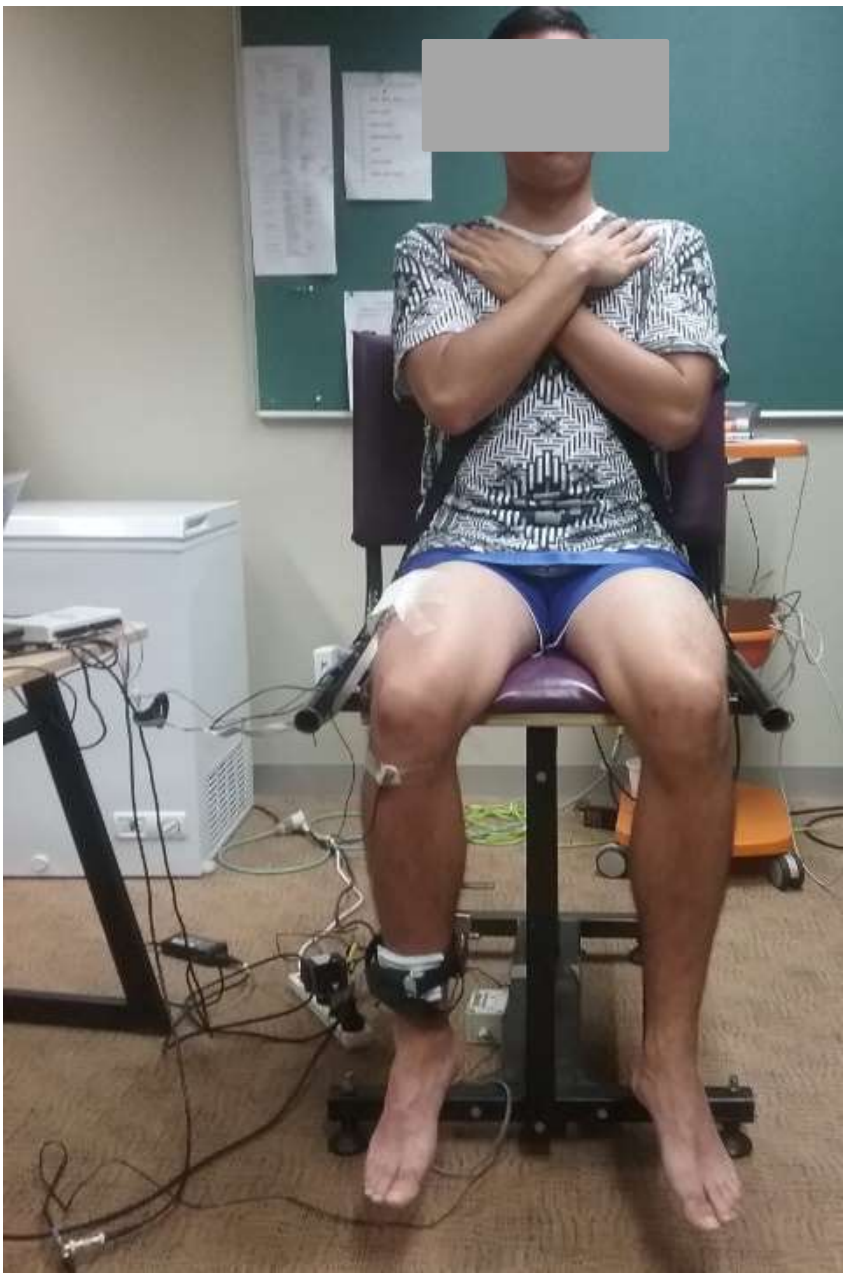

Figure 4.12 Participant in a position ready to perform MVIC tasks.

The MVIC tasks performed were as follows:

1. Participants performed MVIC forces by pushing the load cell away from the chair and holding for at least 10 seconds. Three MVIC forces were performed with a 2-minute rest between each attempt. This was to ensure that the muscle had sufficient time for recovery. The highest of the three MVIC force values was used for all percentage of MVIC force tests (Task 2) and the endurance task (Task 3).

2. Participants performed percentage of MVIC forces, where values of 10%, 20%, 30%, 40%, 50%, 60%, 70%, 80% and 90% were selected randomly by the data collector. The participant held each percentage value of MVIC for at least 10 seconds, with a 2-minute rest between each attempt. The reason for the random values was to ensure that the participant was not able to predict the next force value, and to avoid subconscious self-training that might lead to inconsistent readings [150]. The selected percentages were recorded on the data sheet shown in Appendix H.
3. Before the final endurance task, a 20-minute rest was given to ensure that the muscle had fully recovered and rested before this task. Participants then held a steady 50% MVIC force for as long as they could, until muscle fatigue occurred.

During the tasks, the data collected by the principal researcher's laptop were (a) the force values and (b) sEMG signals. The data were then further processed and analysed offline at a later date, using the signal processing techniques as discussed in Chapter 5.

Chapter 5
Digital Signal Processing Principles

5.1 Introduction

This chapter covers the principles of the digital signal processing techniques (DSP) that were applied to the sEMG signals acquired from the new multi-channel electrode developed for this research. First, biosignals are defined, modelled and their characteristics described before the other important aspects involved in the data acquisition – the sampling rate and quantization of the signal – are outlined.

The theoretical principles underlying the DSP used in the analysis of the sEMG signals for this research are then described, which include the Fourier Transform (FT), Short-Time Fourier Transform (STFT) and Wavelet Transform (WT). The signal features obtained are the mean frequency (MNF) and median frequency (MDF), root mean square values (RMS) and the muscle fibre conduction velocity (MFCV).

5.2 Definition of Biosignals

A signal is a phenomenon that conveys information. Biomedical signals are signals used in the biomedical field mainly for extracting information on a biological system under investigation. Within the scope of biomedical signals and sensors, a biosignal can be defined as a *description of a physiological phenomenon*, irrespective of the nature of this description [151; Chapter 1]. Since the number of physiological mechanisms of interest is nearly unlimited, the number of possible biosignals is also large. In a broad sense, the variety of biosignals extends from visual inspection of the patient up to signals recorded from the human body using sensors.

5.3 Modelling Biosignals

The behaviour of an arbitrary biosignal such as a sEMG signal can be modelled as an equivalent circuit as shown in Figure 5.1.

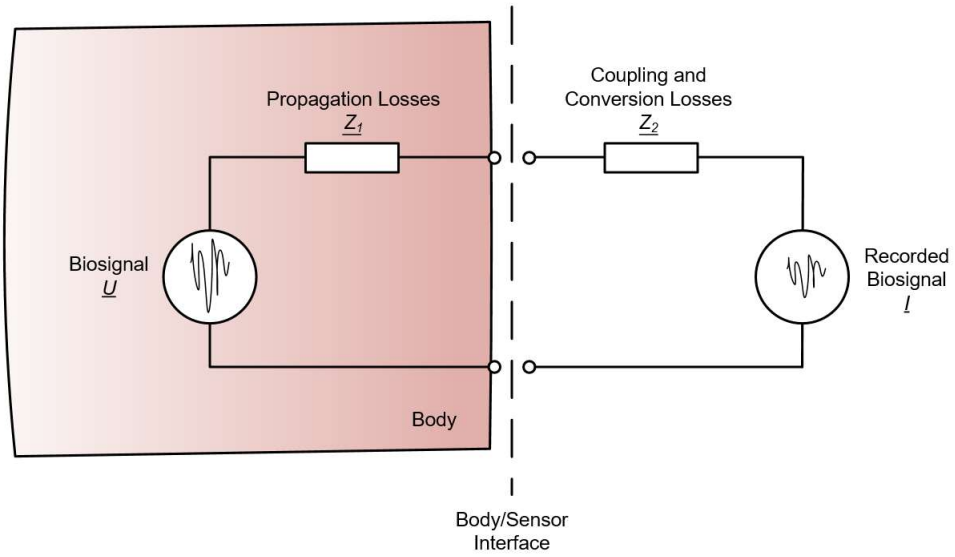

Figure 5.1 Model of biosignal generation, propagation, coupling and recording.

The source of the biosignal usually exhibits non-sinusoidal behaviour. Non-sinusoidal waveforms can be represented as a sum of sinusoidal functions [151: Chapter 1, 152; Chapter 1]. The source of the biosignal in Figure 5.1 can be represented by a sinusoidal voltage source:

$$u(t) = U\cos(\omega t + \varphi_U) \tag{5.1}$$

with a complex amplitude of:

$$\underline{U} = Ue^{j\varphi_U} \tag{5.2}$$

where $\underline{U}$ is the magnitude of the biosignal generated with angular frequency $\omega = 2\pi f$, f is the oscillating frequency with phase of φ_U, and which satisfies:

$$u(t) = Re[\underline{U}e^{j\omega t}] \tag{5.3}$$

The propagation losses are represented by a series impedance:

$$\underline{Z_1} = Z_1 e^{j\varphi_1} \tag{5.4}$$

and the coupling and conversion losses by the impedance:

$$\underline{Z_2} = Z_2 e^{j\varphi_2} \tag{5.5}$$

The recorded biosignal is given by the resulting current:

$$i = Icos(\omega t + \varphi_i) \tag{5.6}$$

with a complex magnitude of:

$$\underline{I} = Ie^{j\varphi_1} \tag{5.7}$$

which satisfies:

$$i(t) = Re\left[\underline{I}e^{j\omega t}\right] \tag{5.8}$$

and according to Ohm's law:

$$\underline{I} = \frac{\underline{U}}{\underline{Z_1} + \underline{Z_2}} \tag{5.9}$$

The higher the losses (e.g. the magnitudes $Z_1(\neq 0)$ and $Z_2(\neq 0)$, which usually are capacitive-ohmic losses in the model), the weaker the recorded biosignal will be in magnitude I. In general, when $\varphi_1 \neq \varphi_2$ and provided that $\varphi_1 \neq 0$ or $\varphi_2 \neq 0$, all the losses can be modelled by real resistances where $\varphi_1 = \varphi_2$ and $I = U/(Z_1 + Z_2)$. It should be noted that the physiological phenomena of interest are hidden not only in $\underline{U}$ but also in $\underline{Z_1}$, as the propagation may influence the resulting $\underline{I}$ in a significant and even advantageous way.

5.4 Classification of Biosignals

Biosignals may be classified in many ways, some of the most important classifications are listed below:

1. *Classification according to source*. Biosignals may be classified according to their source or physical nature [121; Chapter 1]. These sources are sub classified as:
   (a) *Bioelectric signals.* These are unique to biomedical systems and are generated by nerve cells and muscle cells. Its source is the membrane potential, which under certain conditions may be excited to generate an action potential.
   (b) *Bioimpedance signals*. The impedance of the tissue contains important information concerning its composition, blood volume, blood distribution, endocrine activity, automatic nervous system activity, and more.
   (c) *Bioacoustic signals*. Many biomedical phenomena create acoustic noise. The measurement of this acoustic noise provides information about the underlying phenomenon.
   (d) *Bio-magnetic signals*. Various organs, such as the brain, heart, and lungs, produce extremely weak magnetic fields. The measurements of these fields provides information not included in other biosignals.
   (e) *Biomechanical signals*. These include all signals used in the biomedicine fields that originate from some mechanical function of the biologic system.
   (f) *Biochemical signals.* The result of chemical measurements from the living tissue or from samples analysed in the clinical laboratory.
   (g) *Bio-optical signals*. The result of optical functions of the biologic system, occurring naturally or induced by the measurement.

These classifications are generally used when the basic physical characteristics of the underlying process are of interest, for example, when a model for the signal may be desired [121; Chapter 1].

2. *Classification according to biomedical application*. The biomedical signal is acquired and processed with diagnostic, monitoring, or other goals in mind. Classification may be constructed according to the field of application, for example, cardiology or neurology. Such classification may be of interest when the goal is the study of physiological systems [121; Chapter 1].
3. *Classification according to signal characteristics*. From the point of view of signal analysis, this is the most relevant classification method. When the main goal is processing, it is not relevant what the source of the signal is or to which biomedical system it belongs; what matters are the signal characteristics [121; Chapter 1].

Most often in biomedical applications, as in many other applications, the acquisition of the signal is not sufficient. Processing of the acquired signal is needed to obtain the relevant information 'buried' in it. This may be due to the fact that the signal is noisy and thus must be 'cleaned', (or in more professional terminology the signal has to be enhanced) or due to the fact that the relevant information is not 'visible' in the signal [121; Chapter 1]. In the latter case, the signal is usually transformed to obtain the required information.

There are two broad classes of signals: (1) *continuous signals* and (2) *discrete signals*. Continuous signals are described by a continuous function $x(t)$ which provides information about the signal at any given time. Discrete signals are described by a sequence $x[n]$, which provides information at a given discrete point on the time axis. Most of the biomedical signals are continuous. Since current technology provides powerful tools for discrete signal processing, a continuous signal is transformed into a discrete signal by a process known as *sampling*. A given signal $x(t)$ is sampled into the sequence $x[n]$ by:

$$x[n] = x(t)|_{t=nT_s} \tag{5.10}$$

where $n = 0, 1, 2, \ldots$, T_s is the sampling interval and $f_s = 2\pi/T_s$ is the sampling frequency. The classification of signals according to characteristics is shown in Figure 5.2, which applies to both continuous and discrete signals [121; Chapter 1, 151; Chapter 1, 153; Chapter 1].

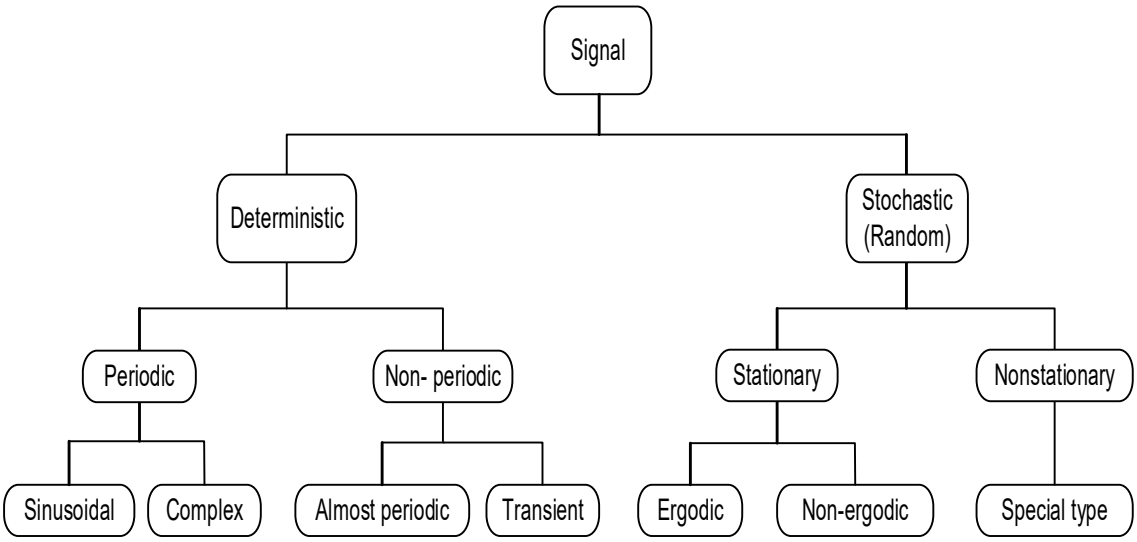

Figure 5.2 Classification of signals according to characteristics.

Signals, whether continuous or discrete, can be divided into two main groups:

1. Deterministic
2. Stochastic

Deterministic signals are signals that can be exactly described mathematically or graphically. If a signal is deterministic and its mathematical description is given, it conveys no information. Real-world signals are never deterministic. There is always some unknown and unpredictable noise added, some unpredictable change in the parameters, and some underlying characteristics of the signal that render it non-deterministic. It is, however, very often convenient to approximate or model the signal by means of a deterministic function. An important family of deterministic signals is the periodic family. A periodic signal is a deterministic signal that may be expressed by:

$$x(t) = x(t + nT) \tag{5.11}$$

where n is an integer and T is the period. The periodic signal consists of a basic wave shape with a duration of T seconds. The basic wave shape repeats itself infinitely on the time axis. The simplest periodic signal is the sinusoidal signal. Complex periodic signals have more elaborate wave shapes.

Most deterministic functions are non-periodic. It is sometimes worthwhile to consider an 'almost periodic' type of signal. The ECG signal can sometimes be considered almost periodic.

Stochastic signals are the most important class of signal. These signals are a sample function of a stochastic or random process. The process produces sample functions, the infinite collection of which is called *the ensemble*. Each sample function differs from the others in its fine details, however, they all share the same distribution probabilities. Stochastic signals cannot be expressed exactly and can be described only in terms of probabilities which may be calculated over the ensemble. Assuming a signal *x(t)*, the N^{th}-order joint probability function can be expressed as:

$$P[x(t1) \leq x1,\ x(t2) \leq s2, \ldots, x(tN) \leq xN] = P(x1, x2, \ldots, xN) \quad (5.12)$$

The signal processing of biomedical signals poses some unique problems. The reason for this is mainly the complexity of the underlying system and the need to perform indirect, non-invasive measurements. There are a large number of processing methods and algorithms available. In order to apply the best method, the user must know the goal of the processing, the test conditions, and the characteristics of the underlying signal.

5.5 Analogue-Digital-Conversion of sEMG Signals

Biosignals at the source are *continuous* and are acquired using a transducer sensor to convert the signal to a voltage that varies over time [121, 122, 151]. Analogue-to-digital conversion (ADC) is the process that allow digital computers to interact with these continuous signals. The conversion of a continuous (analogue) signal to a digital signal shown in Figure 5.3 is a three-step process [153]:

1. Discretization in time – sampling
2. Discretization of amplitude values – quantization
3. Converting the discrete samples to digital samples – coding/encoding

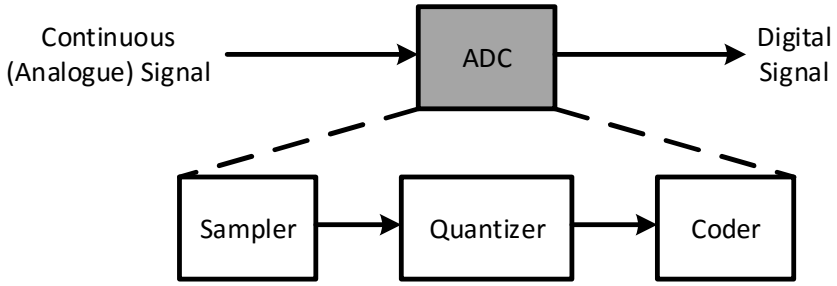

Figure 5.3 Block diagram of the three stages of ADC conversion of a continuous signal to a digital signal.

This digital information is different from its continuous counterpart in two important respects, it is both *sampled* and *quantized*. Both restrict how much information a digital signal can contain, so an understanding of what information needs to be retained or removed is required. In turn, this dictates the selection of the sampling frequency, bit resolution and type of analogue filtering needed for converting between the analogue and digital realms [154; Chapter 3, 155; Chapter 2].

The block diagram in Figure 5.4 shows the ADC of the sEMG signals and force trace moving from the participant to storage on a laptop computer. Force trace is obtained from the load cell showing how much force is exerted by the participant during testing. The hardware used for the ADC in this research was a National Instruments (NI) USB-6218 data acquisition card (DAQ card) with a 16–bit resolution.

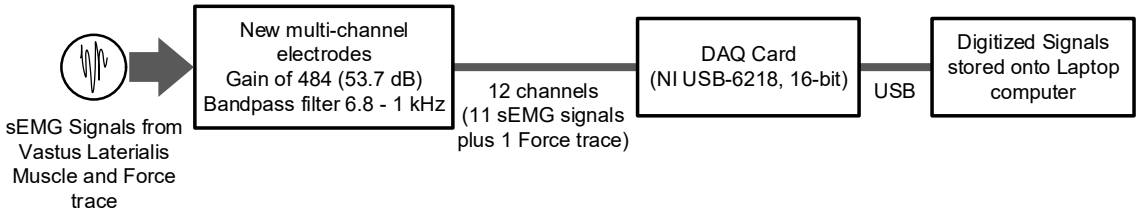

Figure 5.4 Block diagram showing the ADC of the signals being acquired.

5.5.1 Sampling

Continuous signals, whether deterministic or stochastic, are defined at every point in time. To process these signals requires acquiring infinitely many pieces of information. Signal processing of these signals requires the use of computers, which are not able to store infinite data sets. Sampling solves this problem by reducing the data to a more manageable size.

The definition of *proper sampling* can be expressed in the following way:

> *Suppose that you sample a continuous signal in some manner. If you can exactly reconstruct the analogue signal from the samples, you must have done the sampling properly. Even if the sampled data appears confusing or incomplete, the key information has been captured if you can reverse the `process* [154; Chapter 3].

A continuous signal is given by the expression:

$$x(t) \tag{5.13}$$

where t is time, to indicate that it has a value for each instant of time. Sampling the signal is achieved by taking samples of the signal at regular time intervals. The sampled signal is referred to as a digital signal, and is represented by the expression:

$$x[n] \tag{5.14}$$

where n is the sampling instant, to show a value at each sampling point and at times between intervals. The sampling interval T_s is the time in seconds between samples, and the sampling frequency f_s or sampling rate is the number of samples per second measured in Hertz (Hz), which is given by:

$$f_s = \frac{1}{T_s} \tag{5.15}$$

The sampling frequency plays an important role in establishing the accuracy and reproducibility of the sampled signal [156-158]. It is therefore critical to determine what the minimum sampling frequency of a signal should be, in order to correctly reproduce the original signal. To find this value, the *Shannon* or the *Nyquist* sampling theory is used, named after the authors of early 1900s papers on the topic [159-161]. The sampling theory holds that a continuous signal can be properly sampled, *only if it does not contain frequency components above one-half the sampling rate* [153; Chapter 4, 154; Chapter 3, 159-161], so:

$$f_s \geq 2f_{max} \tag{5.16}$$

where f_{max} is the largest frequency component of the continuous signal. If the signal has frequencies of interest above the sampling frequency, *aliasing* will occur. There will be a reduction in amplitude and the high-frequency content will be distorted or aliased downwards [153; Chapter 4, 154; Chapter 3]. Since the digital data is no longer uniquely related to a particular analogue signal, an unambiguous reconstruction is impossible [154; Chapter 3]. To reduce the possible effect of aliasing on the continuous signal, sampling should be bandlimited before the ADC [121; Chapter 2].

The final sampling frequency used in this research was determined by the DAQ card and the signal processing techniques are discussed later in this chapter.

5.5.2 Quantization

The coded binary output of the ADC is a discrete integer, and while the continuous (analogue) signal has a continuous range of values, ADC also requires the analogue signal to be sliced into discrete levels. The process is referred to as *quantization* [121; Chapter 2, 153; Chapter 2, 162; Chapter 1]. Quantization produces a discrete digital signal whose samples can assume only certain values, according to the way they are coded [121; Chapter 2, 153; Chapter 2, 162; Chapter 1].

The digitization of a voltage signal is specified over a particular range, in which the quantization should occur between the maximum and minimum input voltages. By defining the range R of operation for a given n–bit N, the quantization step Q_R or resolution of the quantizer is given by:

$$Q_R = \frac{R}{2^N} \tag{5.17}$$

Using the values from the Technical Specification Sheet for USB NI 6218 DAQ, as shown in Appendix I, the input range is set to ± 10 V, which gives the quantizer a resolution of:

$$Q_R = \frac{(Range\ is + 10\ \text{V}\ to - 10\ \text{V})}{2^{16}}$$

$$Q_R = \frac{20\ \text{V}}{65536} = 305\ \mu\text{V}$$

The number of quantized steps Q_N is given by:

$$Q_N = 2^N\ steps \tag{5.18}$$

$$Q_N = 2^{16} = 65536\ steps$$

Quantization introduces a quantization error Q_E between the samples and their quantized values, which are given by:

$$Q_E = \frac{Q_R}{2} \tag{5.19}$$

$$Q_E = \frac{305\ \mu\text{V}}{2} = 152.5\ \mu\text{V}$$

The quantizer for the DAQ card will have a maximum error between levels of 152.5 μV, since the spacing is uniformly distributed at 305 μV.

Quantizers that have a large number of small steps produce quantization noise which is approximately white [153; Chapter 2]. For the quantization noise to be approximately white, it will require successive input signal samples to be only moderately correlated [153; Chapter 2].

Consider the mean square σ_n^2, of the quantizer for a signal samples for a given signal $x(t)$ with probability density function $p(x)$:

$$\sigma_n^2 = \int_{-x}^{x} [Q(x) - x]^2 p(x) dx \tag{5.20}$$

which can be also written as:

$$\sigma_n^2 = \sum_{i=1}^{N} \int_{x_i-1}^{x} \left(x_{qi} - x\right)^2 p(x) dx \tag{5.21}$$

Note that equations 5.20 and 5.21 describe the variance of the quantization noise.

Assuming that the quantization steps are small, such that $p(x) \approx p\left(x_{qi}\right)$ in the range $x_{i-1} \leq x \leq x_i$. Denote the step $q_i = x_i - x_{i-1}$, then equations 5.20 and 5.21 can be estimated by:

$$\begin{aligned} \sigma_n^2 \approx \frac{1}{12} \sum_{i=2}^{N-1} p\left(x_{pi}\right) q_i^3 + \int_{-\infty}^{x_1} \left(x_{q1} - x\right)^2 p(x) dx \\ + \int_{x_{N-1}}^{\infty} \left(x_{qN-1} - x\right)^2 p(x) dx \end{aligned} \tag{5.22}$$

The last two terms of equation 5.22 are due to the saturation parts of the quantizers. In equation 5.22 it was assumed that $x_0 = -\infty$ and $x_N = \infty$. In general, the input signal is adjusted such that $p(x) \cong 0$ for $x > x_{N-1}$ and $x < x_i$; hence, the last two terms of equation 5.22 are zero and:

$$\sigma_n^2 \cong \frac{1}{12} \sum_{i=2}^{N-1} p(x_{qi}) q_i^3 \tag{5.23}$$

The most common quantizer is the uniform quantizer for which $q_i = q, i = 2, \dots, N-1$ [153; Chapter 2]. For these quantizers, the expression can be further simplified for the noise variance as:

$$\sigma_n^2 = \frac{q^2}{12} \sum_{i=2}^{N-1} p(x_{qi}) q \approx \frac{q^2}{12} \tag{5.24}$$

since:

$$\sum p(x_{qi}) q \simeq \int p(x) dx = 1 \tag{5.25}$$

The approximate value for the quantization noise variation given by equation 5.24 is the most often one used. Uniform quantizers, with small quantitation step q, and with saturation levels can be ignored, have distributed uniform noise, in the range $-q/2 \leq n_q \leq q/2$ with variance $\sigma_n^2 = q^2/12$ [153; Chapter 2].

To justify the assumption that saturation effects can be neglected, make sure the extreme quantization levels x_1 and x_{N-1} are to be some multiple of the input variance.

Define the *loading factor* L_q (for symmetric uniform quantizers) [153; Chapter 2]:

$$L_q = \frac{x_{N-1}}{\sigma_x} = \frac{-x_1}{\sigma_x} \tag{5.26}$$

where σ_x is the standard deviation (root mean square [RMS]) of the input signal. A common choice for loading factor is $L_q = 4$ (*four sigma loading*). For such quantizer, $N - 2$ levels are for $-4\sigma_x \leq x \leq 4\sigma_x$ hence:

$$q = 8\,\sigma_x/(N-2) \tag{5.27}$$

The signal-to-noise ratio (SNR), for the quantizer can be defined by [121; Chapter 2, 153; Chapter 2]:

$$SNR = 10\log\left(\frac{\sigma_x^2}{\sigma_n^2}\right) \tag{5.28}$$

The SNR of the uniform symmetric quantizer is given by introducing equations 5.24 and 5.27 into equation 5.28:

$$SNR = 10\log\left[\frac{12(N-2)^2}{64}\right] \tag{5.29}$$

$$SNR = 10\log[(N-2)^2 \times 0.1875] \tag{5.30}$$

Hence for the 16–bit DAQ card used, the quantization SNR is:

$$SNR = 10\log((2^{16}-2)^2 \times 0.1875)$$

$$SNR = 89.06 \text{ dB}$$

The DAQ card used in this research therefore has a SNR equal to 89 dB, which is high and is suitable for acquiring signals.

5.6 Biomedical Signal Processing Techniques

Using signal processing techniques, sEMG signals are described in terms of amplitude and frequency. Signal amplitude is typically used as a measure of relative force production, and it increases with the number, size and firing rate of active motor units. The frequency content of sEMG is dependent on the characteristics of active muscle fibres, such as size, muscle fibre conduction velocity (MFCV) and firing rate.

The three signal processing techniques for the analysis of biomedical signals are:

1. ***Time domain analysis*** is where the variable of the signal is measured with respect to time [155; Chapter 1]. One commonly used method is RMS.
2. ***Frequency domain analysis*** is the transformation of the signal from the time domain to frequency domain. The most commonly used is the Fourier Transform (FT) [155; Chapter 1].
3. ***Time-frequency*** or ***time-scale transform analysis*** is where both the time and frequency or scale domains are used together, using various time-frequency or scale representations. Methods used include the Short-Time Fourier Transform (STFT) [163] and Wavelet Transform (WT) [163, 164].

All of the signal processing techniques above are executed using a fixed period of time, which is referred to as an *epoch* or a *data window* [24; Chapter 5]. Figure 5.5 shows the simplified outputs for all three signal processing techniques described above.

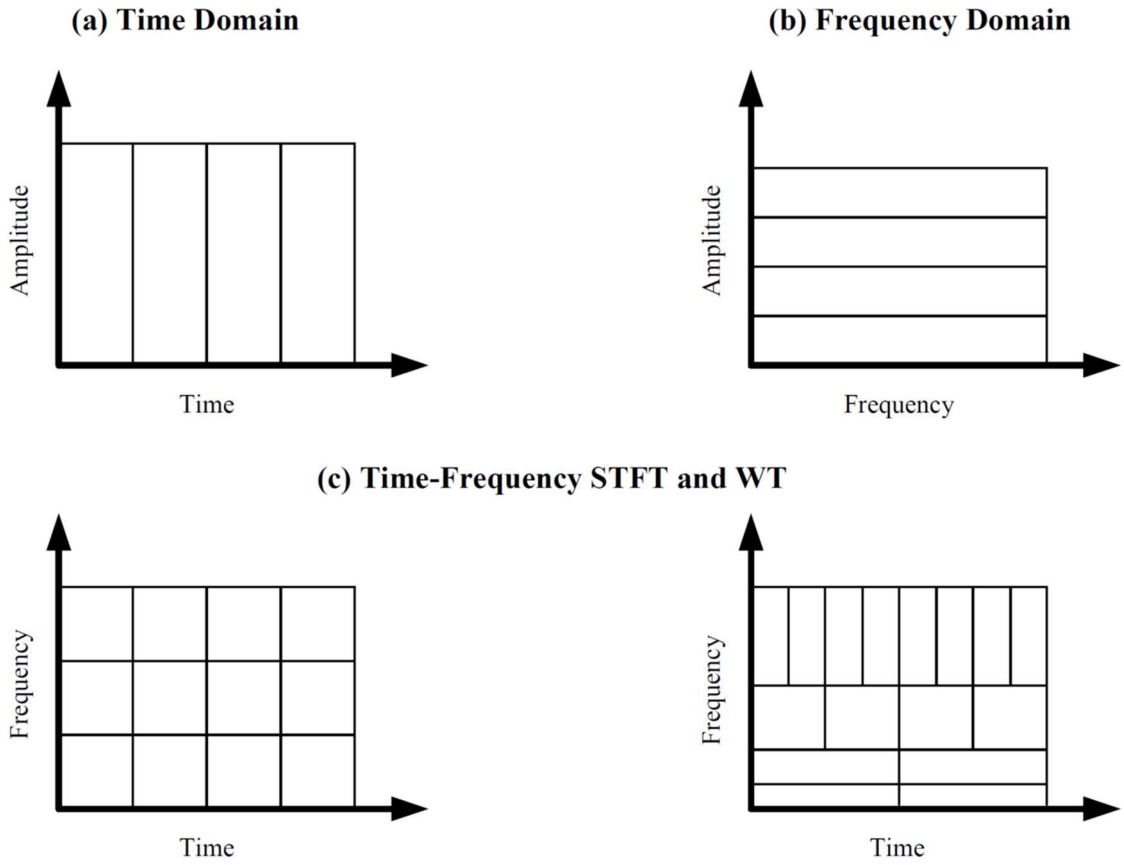

Figure 5.5 Simplified output plots for the (a) time domain, (b) frequency domain and (c) time-frequency or time-scale transform signal processing techniques.

5.6.1 Time Domain Analysis

In the time domain, the dominant change in a sEMG signal is its amplitude due to muscular effort and/or fatigue [3; Chapter 3, 4; Chapter 3, 44; Chapter 4, 165-167]. It has been shown that as muscle effort increases, the sEMG signal strength or amplitude grows [3; Chapter 3, 4; Chapter 3, 44; Chapter 4, 165-167].

The following feature parameters can be used the time domain analysis of sEMG signals [44; Chapter 5]:

- Average Rectified Value (ARV)
- Root Mean Square (RMS)
- Zero-Crossing Rate (ZCR)
- Spike Analysis (SA)

5.6.1.1 Average Rectified Value (ARV)

The ARV is firstly determined by either removing all of the negative phases of the raw sEMG (half-wave rectification) or reversing them (full-wave rectification). The latter option is preferred because it retains all of the signal power [4; Chapter 3, 168]. The integral of the rectified sEMG is then calculated over a time period T, or epoch and the resulting integrated sEMG is finally divided by T to form the ARV equation:

$$ARV = \frac{1}{T}\int_0^T |x(t)|\, dt \tag{5.31}$$

where $x(t)$ is the sEMG signal and T is the time over which the ARV is calculated, with the units measured in μV or mV. For discrete signals, equation 5.31 is rewritten as:

$$ARV = \frac{1}{N}\sum_{n=0}^{N-1} |x_n| \tag{5.32}$$

where n is the sample value and N is the total number of samples within the epoch.

Using just the integrated value of the rectified sEMG signal is a common processing method in its own right, and is referred to as iEMG [44; Chapter 4]:

$$iEMG = \int_0^T |x(t)|\, dt \tag{5.33}$$

for discrete signals, equation 5.33 is rewritten as:

$$iEMG = \sum_{n=0}^{N-1} |x_n| \tag{5.34}$$

The units for iEMG are measured in μVs or mVs. ARV is similar to the numerical integral value in equations 5.33 and 5.34, it is often confused with iEMG, which provides no additional information. iEMG is used to provide an estimate of the total amount of activity [44; Chapter 4, 169; Chapter 5].

Figure 5.6 shows a single sEMG signal collected at 50% maximum voluntary isometric contraction (MVIC) from Laplacian channel 2 (central electrode) of the new multi-channel electrode. The signal has been analysed in the time domain using the ARV technique with the epoch size set to 1 second.

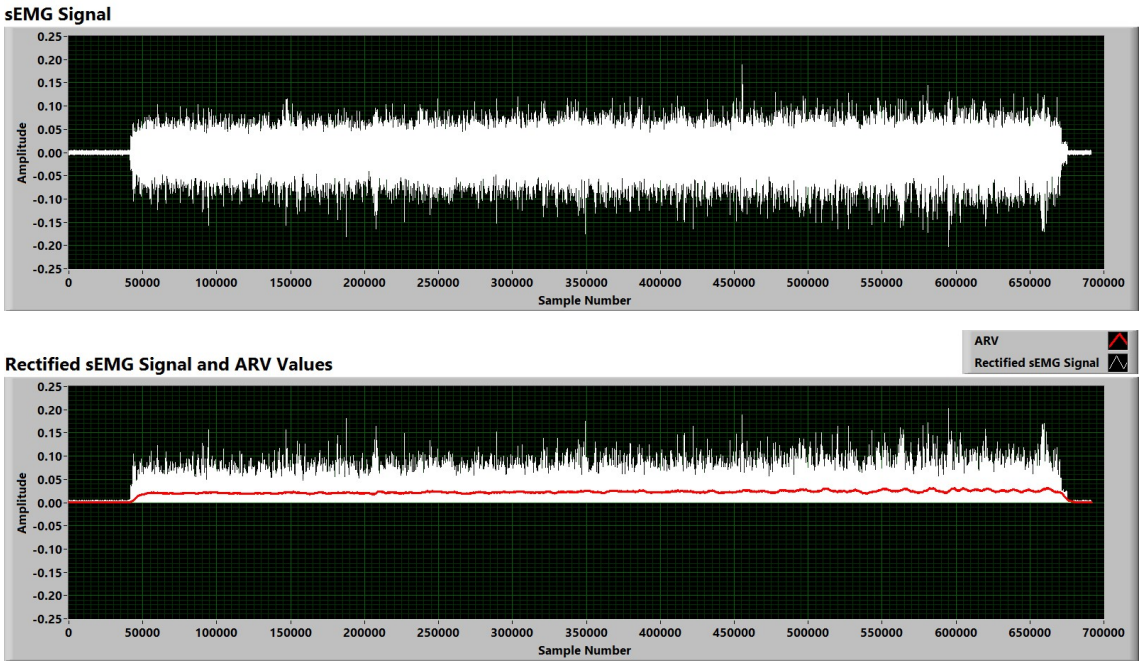

Figure 5.6 The top plot shows a single sEMG signal collected by the new multi-channel electrode with a sampling rate of 10 kHz, which was obtained from Participant No. 13 performing a 50% MVIC endurance task. The bottom plot shows the sEMG signal rectified with the ARV values (red line) and calculated using an epoch size of 1 second.

5.6.1.2 Root Mean Square (RMS)

The RMS value has been used to quantify the electric signal as it is able to reflect the physiological activity in the motor unit during contraction [168]. The RMS is the square root of the mean values squared in an epoch and it reflects the mean power of the signal, which is also called RMS-sEMG [168]:

$$RMS = \sqrt{\frac{1}{N}\sum_{n=0}^{N-1} x_n^2} \tag{5.35}$$

where n is the sample value and N is the total number of samples within the epoch.

Figure 5.7 shows a single sEMG signal collected at 50% MVIC from Laplacian channel 2 (central electrode) of the new multi-channel electrode. The signal has been analysed in the time domain, calculating RMS values with an epoch size set to 1 second.

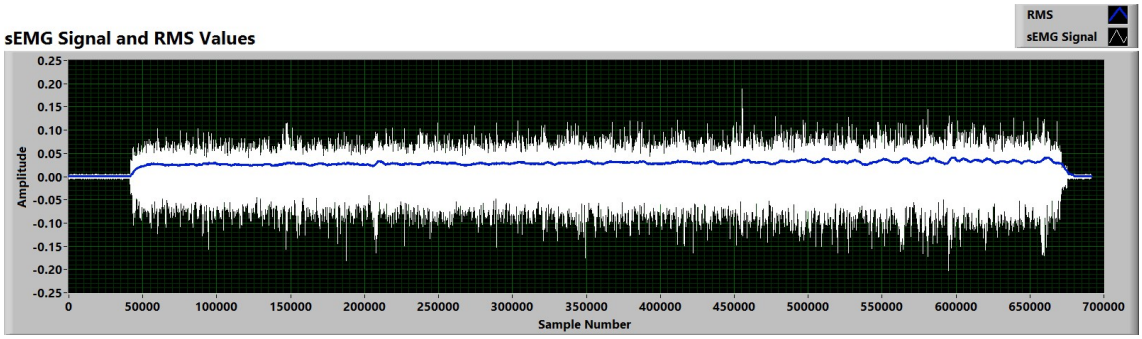

Figure 5.7 The plot shows a single sEMG signal collected by the new multi-channel electrode with a sampling rate of 10 kHz, which was obtained from Participant No. 13 performing a 50% MVIC endurance task. The RMS values (blue line) was calculated using an epoch size of 1 second.

Comparing both the RMS and ARV values for the signal shown in Figure 5.8, there is a little difference in each of their trend lines over time. Both values can be used as an indicator in terms of the signal amplitude in the time domain. RMS is the most reported in terms of signal amplitude since it has both physical and physiological meaning because it is linked with the signal's power (V_{rms}^2) [25; Chapter 6, 44: Chapter 4].

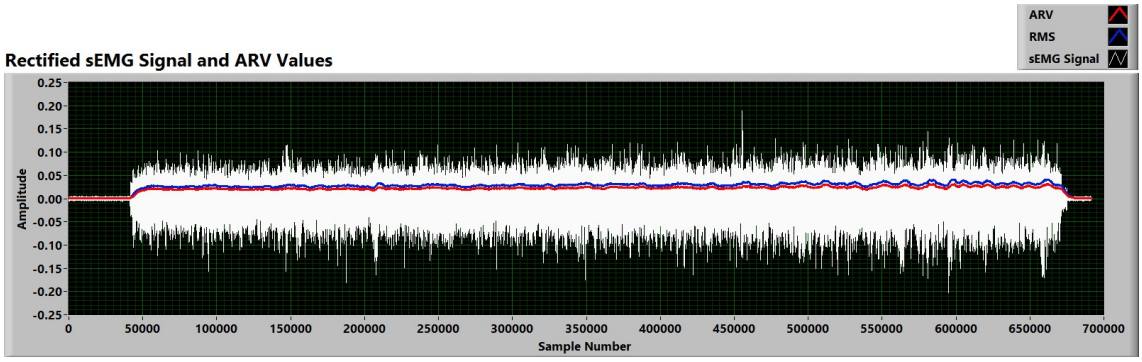

Figure 5.8 The plot shows a single sEMG signal collected by the new multi-channel electrode with a sampling rate of 10 kHz, which was obtained from Participant No. 13 performing a 50% MVIC endurance task. The blue line is the ARV values for the rectified sEMG signal and the red line is the RMS values; both were calculated using an epoch size of 1 second.

5.6.1.3 Zero-crossing Rate (ZCR)

The ZCR, which is sometimes referred to as the zero-cross frequency f_z of a signal $x(t)$, is defined as half the number of zero-crossing of $x(t)$ per second [170, 171]. If both the signal $x(t)$ and its first derivative $x'(t)$ have a Gaussian amplitude, the distribution of the expected zero-crossing rate ZCR (Z) can be calculated as [172, 173]:

$$Z = 2\left[\frac{\int_0^\infty f^2 P(f)\,df}{\int_0^\infty P(f)\,df}\right]^{1/2} \tag{5.36}$$

where $P(f)$ is the power spectral density (PSD) of the signal. For discrete signals, equation 5.36 is rewritten as:

$$Z = 2\left[\frac{\sum_{n=0}^{N-1} k^2 P(k)}{\sum_{n=0}^{N-1} P(k)}\right]^{1/2} \tag{5.37}$$

Hägg and Suurküla [174] showed that the ZCR rate properties are near to both the mean frequency (MNF) and median frequency (MDF) of the PSD. Based on this method, Hägg [170] and Inbar, et al. [171] developed simple real-time fatigue monitors in the early 1980s. Since the ZCR is highly dependent on SNR and sensitive to deviations of the amplitude distribution from the Gaussian one, the use of ZCR has been abandoned [175].

5.6.1.4 Spike Analysis (SA)

SA is most certainly not a newly emerging method in the area of sEMG signal analysis [176]. A peak is any pair of upward or downward deflections within a spike that do not together constitute a discrete spike, except in the case of a spike with a single peak. In this case, the deflections of the spike and the peak are the same. Any deflections that do not constitute discrete spikes as previously defined and are found before, between, or after identified spikes, are assumed to be a background noise and not a sEMG signal. SA can be used to provide similar information as spectral analysis and does not require stationarity. However, contradictory results on the reliability of sEMG spike parameters do not encourage their use [175, 177].

5.6.2 Frequency Domain

The power produced by muscles has a frequency spectrum, on which sEMG signals are transformed from the time domain to frequency domain and displayed to reveal its range of frequencies [3; Chapter 3, 25; Chapter 6, 44; Chapter 4, 162; Chapter 3]. The PSD or power spectrum (PS) plot produced by the FT presents the range of frequency components as a function of the probability of their occurrence [3; Chapter 3].

The frequency content of sEMG signals is used to provide both physiological and non-physiological information [44; Chapter 4]. Physiological aspects of the sEMG signal provided by frequency analysis include MFCV, and to a lesser extent, motor unit firing rates [44; Chapter 4]. Non-physiological information can relate to certain types of noise contamination within the sEMG signal, which can be easily identified [44; Chapter 4].

Fourier Transform (FT)

A FT calculates the frequency, amplitude and phase of each sine wave needed to make up any given signal. It is a linear transform from the time to frequency domain, and it can be used to analyse the spectral component of a signal [152].

The FT $F(\omega)$ of an input signal is defined as the following:

$$F(f) = \int_{-\infty}^{\infty} x(t) e^{-j2\pi f t} dt \tag{5.38}$$

where $x(t)$ is the time domain signal and $2\pi f$ is the angular frequency with f equal to the input frequencies.

The FT $F(k)$ for discrete signals is given as:

$$F(k) = \sum_{n=0}^{N-1} x[n] e^{-j2\pi kn/N} \tag{5. 39}$$

where $x[n]$ is the input sequence, $2\pi k$ is the angular frequency of input sequence frequency $k = 0, 1, 2 \ldots . N - 1$ and N is the number of samples in both discrete-time and the discrete frequency domains.

A FT is executed using either of the two following ways:

1. Fast Fourier Transform (FFT)
2. Discrete Fourier Transform (DFT)

The term *fast* in FFT relates to the computation method to produce the frequency spectrum, which is greatly reduced if the data segment (*N*) used is limited to the powers of 2 (e.g. 256 points, 512 points, etc.). This determines the sampling frequency of the collected sEMG signal. If the data is not sampled to the power of 2, the data segment will need to be *zero-padded* up to the next power of 2. *Zero-padding* of the data is adding a string of zeros either at the beginning or end of the data segment.

DFT is used for signal processing using any data segment that does have a value to the power of 2, but at the expense of computational time.

Since the computation power of computing has vastly increased over the years, there is now no need for setting the data segment length to the power of 2 [178; Chapter 2, 179]. Modern DAQ cards are unable to sample accurately at rates of the power of 2, and only sample at values to the power of 10 [178; Chapter 2, 179]. The NI USB 6218 DAQ card used in this research was found to sample more accurately using values to the power of 10 than to the power of 2. Hence for this research, a high sampling rate of 10 kHz was used to acquire the sEMG signals from the multi-channel electrode.

Doing a FT on a data segment taken from signals such as sEMG signals, involves forcing the fundamental and its harmonics to fit into the period *T* [152; Chapter 2]. Each data segments will contain some waveform patterns from the adjacent segments of the signal and these will give false frequency components [152; Chapter 2]. The results of values in the FT will appear spread out, which is called as *spectral leakage*, also known as *Gibbs phenomenon* [152; Chapter 2].

Windowing pre-multiplies the input data before the FT with a value that smoothly decreases to zero at each end of the data. The purpose is to reduce *leakage* abnormalities in the FT that are introduced by sudden changes at the start and end of data. The problems with data windowing in biomedical signals such as sEMG is that they have a noise-like appearance [152; Chapter 2]. To avoid the spectral leakage when performing a FT on a data window of sEMG signals, a *Hanning window* is commonly used, rather than the other windows that are available for signal processing [152; Chapter 2].

Figure 5.9 shows a single sEMG signal collected at 50% MVIC from Laplacian channel 2 (central electrode) of the new multi-channel electrode. The signal has been Fourier transformed from the time domain to the frequency domain using a Hanning window for a data window segment of 5 seconds. The two Fourier plots show the magnitude of the absolute values from the Fourier transform for the full range of frequencies from 0 to 5 kHz and an expanded view showing that the main frequency components lie between 0 to 500 Hz [168].

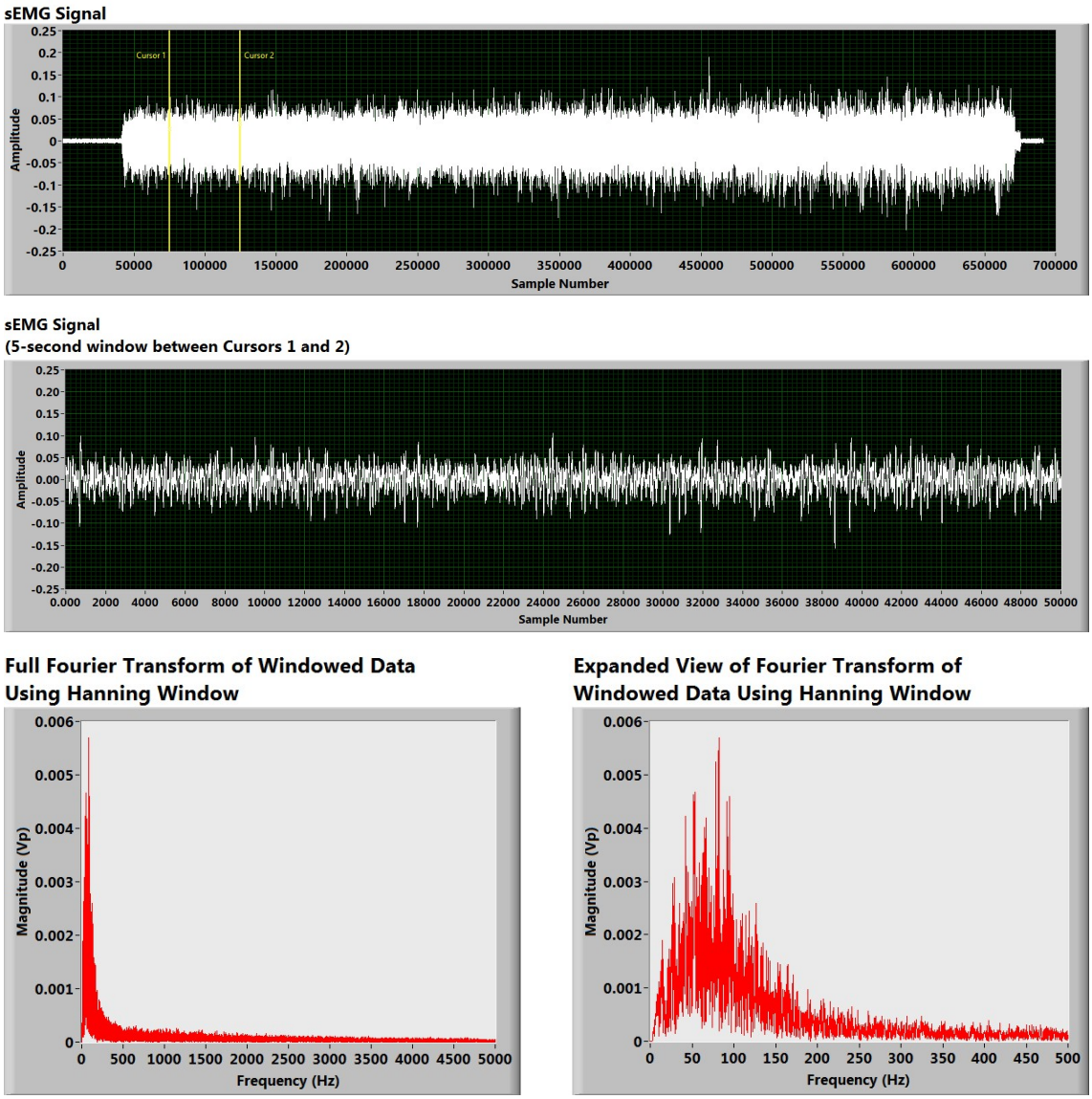

Figure 5.9 The top plot shows a single sEMG signal collected from the new multi-channel electrode with a sampling rate of 10 kHz, which was obtained from Participant No. 13 performing a 50% MVIC endurance task. The middle plot shows the 5-second data window segment taken from the overall sEMG signal between cursors 1 and 2. The left-hand bottom plot shows the overall FT of the 5-second data window and the right-hand plot shows an expanded view of the FT from 0 to 500 Hz.

The FT frequency spectrum of a sEMG is not generally used for analysis due to the sEMG signal being stochastic, and so PSD is used instead [44; Chapter 7]. By definition, the power spectrum of a signal is the magnitude values squared of its FT [152; Chapter 2], which is given by:

$$P(f) = \left| \int_{-\infty}^{\infty} x(t) e^{-j2\pi f t} dt \right|^2 \tag{5.40}$$

or

$$P(k) = \left| \sum_{n=0}^{N-1} x[n] e^{-j2\pi k t/N} \right|^2 \tag{5.41}$$

Figure 5.10 shows the 5-second data window segment taken from the sEMG signal shown in Figure 5.9 and the PSD plots. The two PSD plots show the full range of frequencies from 0 to 5 kHz and an expanded view with the main frequency components of the PSD being between 0 to 250 Hz.

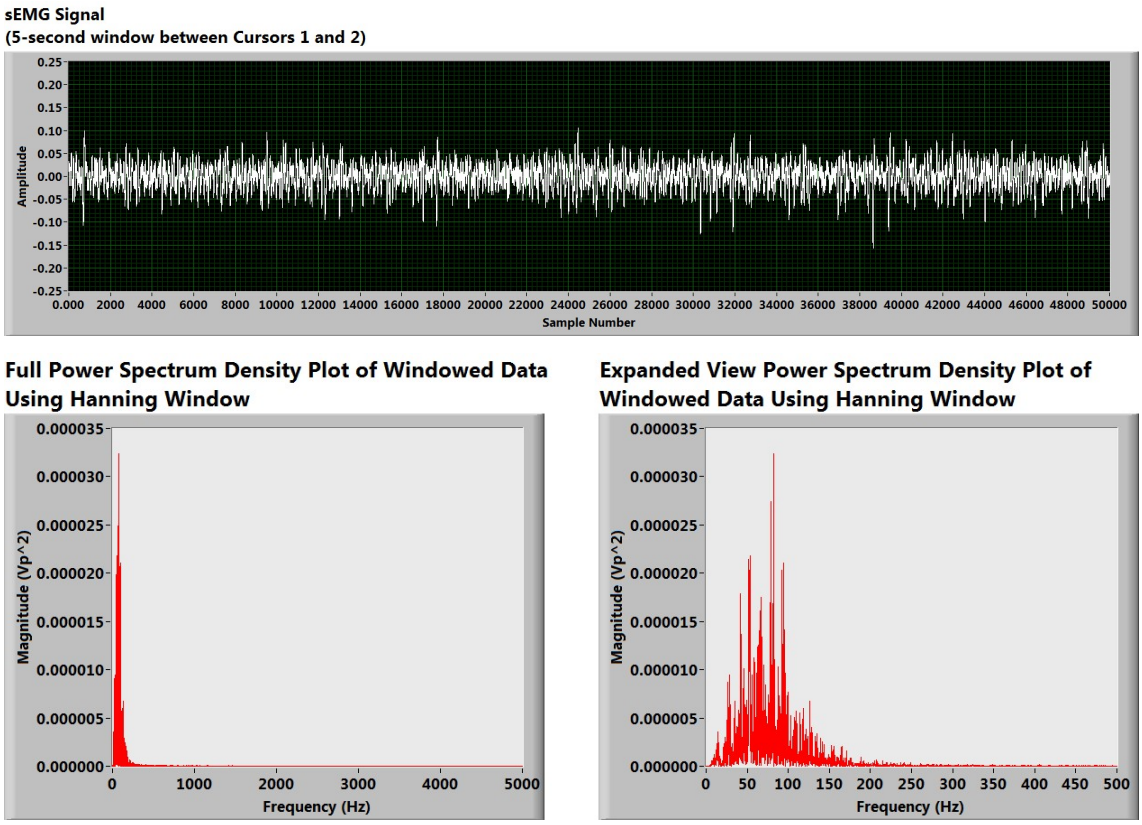

Figure 5.10 The top plot shows the 5-second data window segment taken from the overall sEMG signal shown in Figure 5.9 between cursors 1 and 2. The left-hand bottom plot shows the overall PSD plot of the 5-second window and the right-hand plot shows an expanded view of the PSD plot from 0 to 500 Hz.

Lindstrom and Magnusson [180] and Stulen and De Luca [181] showed by using PSD that two important frequency domain features can be found, which are:

1. Mean frequency (MNF)
2. Median frequency (MDF)

Both have become useful and popular frequency domain features used for the assessment of muscle activity and fatigue in sEMG signals along with the RMS value from the time domain of the signal.

MNF is the average frequency of the power spectrum, given by:

$$MNF = \frac{\int_0^{\infty} fP(f)df}{\int_0^{\infty} P(f)df} \tag{5.42}$$

or

$$MNF = \frac{\sum_{n=0}^{N-1} kP(k)}{\sum_{n=0}^{N-1} P(k)} \tag{5.43}$$

MDF is the frequency at which the power spectrum is divided into two areas of equal power, and is given by:

$$MDF = \int_0^{f_{MDF}} P(f)df = \int_{f_{MDF}}^{\infty} P(f)df = \frac{1}{2}\int_0^{\infty} P(f)df \tag{5.44}$$

or

$$MDF = \sum_{n=0}^{n=MDF} P(k) = \sum_{n=MDF}^{N-1} P(k) = \frac{1}{2}\sum_{n=0}^{N-1} P(k) \tag{5.45}$$

Figure 5.11 shows the 5-second data window segment taken from the sEMG signal shown in Figure 5.9, and the expanded PSD plot showing the main frequency that lie between 0 to 500 Hz. The bottom plot shows the values of both the MNF and MDF of the PSD.

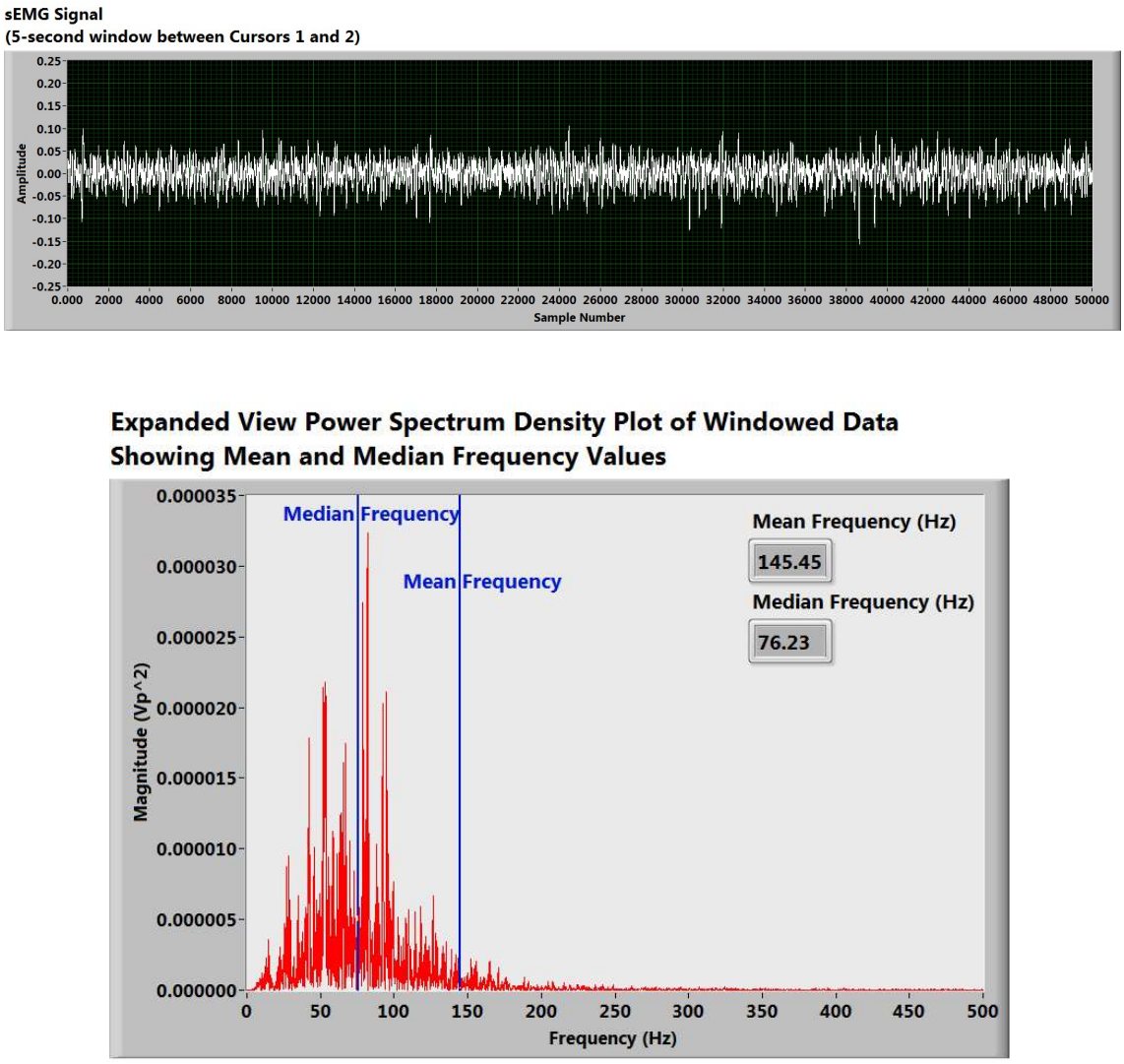

Figure 5.11 The top plot shows the 5-second data window segment taken from the overall sEMG signal shown in Figure 5.9 between cursors 1 and 2. The bottom plot shows an expanded view of the PSD plot from 0 to 500 Hz obtaining values of MNF equal to 145.45 Hz and MDF equal to 73.23 Hz.

5.6.3 Time-Frequency or Time-scale Transform Analysis

For many signals, frequency domain analysis is extremely useful because a signal's frequency content is of great importance. By using a FT, the frequency spectrum of any signals, including sEMG signals, is clarified and recognized by breaking down the signal into its corresponding sinusoidal components of different frequencies. However, using a FT has a serious drawback because in transforming to the frequency domain, the signal is assumed to be stationary and hence time information is lost. When examining a FT of a signal, it is impossible to tell when a particular frequency content of the signal took place in time [152; Chapter 5]. For signal properties which do not change much over time, such as for stationary signal, this drawback is not significant. But it will be a

significant drawback with many biomedical signals such as sEMG, which are stochastic or random. Biomedical signals also contain numerous non-stationary or transitory characteristics: drift, trends, abrupt changes, and beginnings and ends of events. These characteristics are often the most important part of the signal, and FT analysis alone is not suitable in detecting, processing and analysing them. Hence, other signal processing techniques need to be used in order to include the time component of the signals. These techniques are:

- Short-Time Fourier Transform (STFT).
- Wavelet Transform (WT).

5.6.3.1 Short-Time Fourier Transform (STFT)

In an effort to correct this deficiency of FT in terms of the time resolution, Gabor [182] adapted the FT to analyse only a small section of the signal at a time using a technique called *windowing*. This adaptation is called the Short-Time Fourier Transform (STFT), also known as the windowed FT. It maps a signal into a two-dimensional function of time and frequency. The STFT represents a useful compromise between the time-domain and frequency-domain views of a signal.

The STFT involves simply multiplying the time domain signal $x(t)$, which is to be analysed, with an analysis window $\gamma^*(t-\tau)$ where τ is the time delay, and then compute the FT of the windowed signal, expressed as [183; Chapter 7]:

$$F_x^{\gamma}(\tau, f) = \int_{-\infty}^{\infty} x(t)\gamma^*(t-\tau)e^{-j2\pi ft}dt \tag{5.46}$$

where $F_x^{\gamma}(\tau, f)$ is the STFT of time domain signal $x(t)$ and f is the input frequency.

The STFT of a discrete-time signal $x[n]$ is given by:

$$F_x^{\gamma}\left(m, e^{j2\pi k}\right) = \sum_{n=0}^{N-1} x[n]\,\gamma^*(n - mN)e^{-j2\pi kn} \tag{5.47}$$

the frequency f is normalized to the sampling frequency f_s.

The short-time spectrum is a function of the discrete parameter m and the continuous parameter $2\pi f$, where in practice the discrete frequencies used are:

$$2\pi f_k = \frac{2\pi k}{M} \tag{5.48}$$

where $k = 0, 1, \ldots \ldots M - 1$, then the discrete values of the short-term spectrum are given by:

$$F_x^{\gamma}\left(m, e^{j\frac{2\pi k}{M}}\right) = \sum_{n=0}^{N-1} x[n]\,\gamma^*(n - mN)e^{-j\frac{2\pi kn}{M}} \tag{5.49}$$

Since the STFT is complex-valued, the *spectrogram* is used for display purposes or further processing [183; Chapter 7]. This is determined by the squared magnitude of the STFT, which is given by:

$$S_x(\tau, f) = \left|F_x^{\gamma}(\tau, f)\right|^2 = \left|\int_{-\infty}^{\infty} x(t)\gamma^*(t - \tau)e^{-j2\pi f}\,dt\right|^2 \tag{5.50}$$

or

$$S_x\left(m, e^{j2\pi k}\right) = \left|F_x^{\gamma}\left(m, e^{j2\pi k}\right)\right|^2 = \left|\sum_{n=0}^{N-1} x[n]\,\gamma^*(n - mN)e^{-j2\pi kn}\right|^2 \tag{5.51}$$

The spectrogram represents the distribution of signal power in the time-frequency domain [25; Chapter 10].

However, this information is obtained with limited precision, and that precision is determined by the size of the window. While the STFT compromise between the time-domain and frequency domain views of a signal can be useful, the drawback is that once a particular size for the time window is selected, that window is the same for all frequencies. Many signals require a more flexible approach in which the window size can be varied. In general, choosing a narrow window gives good time resolution but poor frequency resolution and a wide window results in poor time resolution but good frequency resolution [183; Chapter 7].

The cause of this condition is due to the time and frequency, which are dependent according to the Heisenberg uncertainty principle [183; Chapter 7], which states that the product of the standard deviation in time and frequency is limited by:

$$\Delta_{2\pi f}\Delta_t \geq \frac{1}{2} \tag{5.52}$$

This means that decreasing the deviation in frequency or increasing the resolution must result in an increase in the deviation in time or decrease in resolution and vice versa. This is the fundamental weakness of the STFT. The boundary of the Heisenberg uncertainty principle is reached if a Gaussian window is used. Another serious drawback of STFT is that it also assumes that signal stationarity is within the window size, hence it is not suitable for processing biomedical signals which normally are non-stationary in nature [163].

Figure 5.12 shows the 5-second data window segment (top plot) taken from the sEMG signal shown in Figure 5.9 and two STFT spectrograms (middle and bottom) generated using windows sizes of 0.5 seconds (or 5000 samples) with each overlapping 0.25 seconds (or 2500 samples). The shaded regions displayed on both spectrograms represent the signal power; the darker the shading the higher the values of the signal power for the corresponding frequency and time [183; Chapter 7].

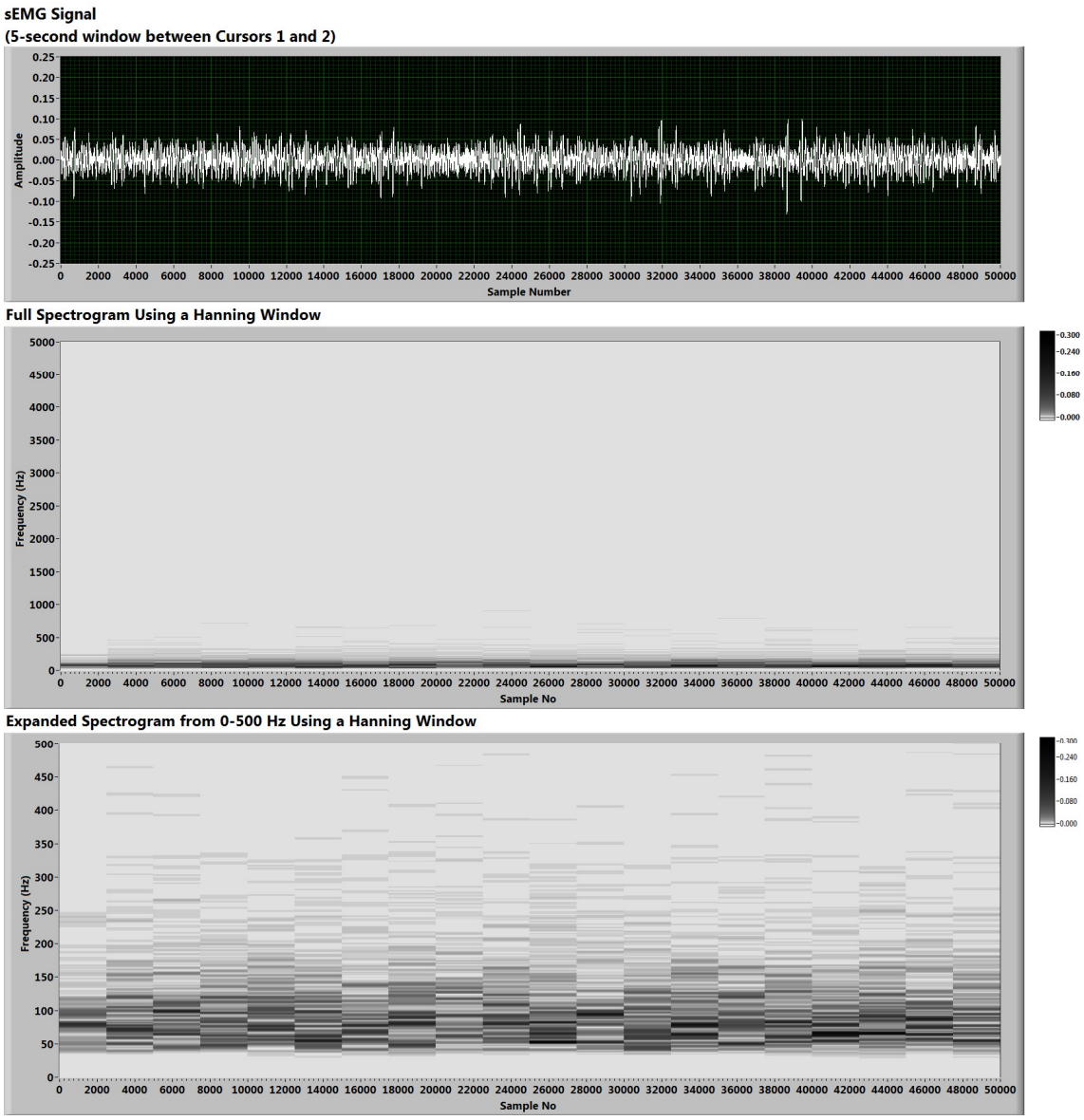

Figure 5.12 The top plot shows the 5-second data window segment taken from the overall sEMG signal shown in Figure 5.9 between cursors 1 and 2. The middle plot shows a full generated STFT spectrogram and the bottom plot is the spectrogram from 0 to 500 Hz.

5.6.3.2 Wavelet Transform (WT)

The inherent problem of the STFT is the inability to combine a good time resolution with a good frequency resolution. Once the window size is selected, the time and frequency resolution of the STFT remains throughout the signal [184; Chapter 9]. This resolution problem suggests that there is a need to use variable lengths in analysing windows, with short ones for high frequencies and long ones for low frequencies [184; Chapter 9]. Wavelet transform (WT) is a suitable method which is able to accommodate this with the use of related time-scale analysis, thus providing a flexible time-frequency resolution.

The WT analysis does not use a time-frequency domain, but a time-scale domain [163, 164; Chapter 1, 184; Chapter 9].

WT analysis uses local wavelike functions known as *wavelets*. A few examples of commonly used wavelets, which are referred to as *mother wavelets*, are shown in Figure 5.13.

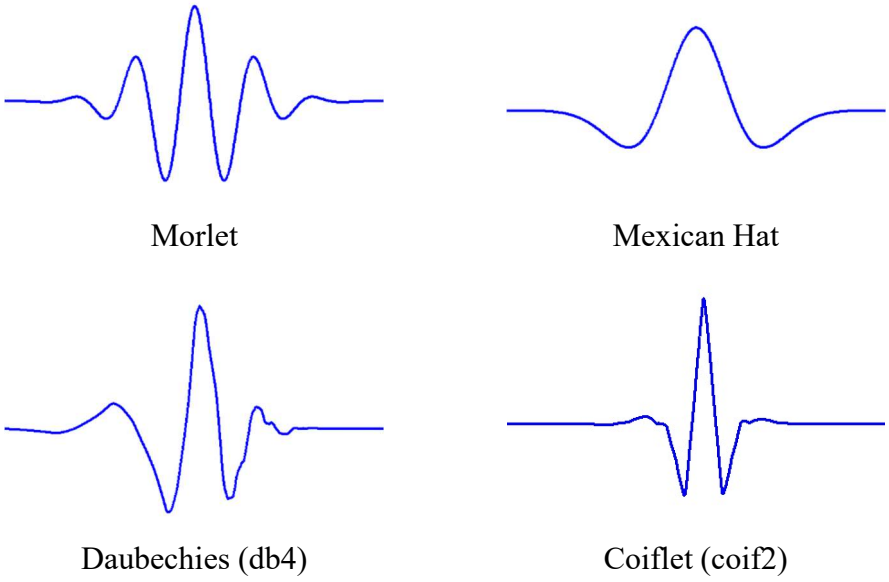

Figure 5.13 Examples of commonly used wavelets.

The wavelets in Figure 5.13 plus many more are used to transform the signal under investigation into a time-scale representation [155, 163, 164, 184]. Mathematically, the WT is a convolution of the wavelet function with the signal. The wavelet is manipulated in two ways: (a) it is moved to a various location (or time) in the signal; and (b) it is either dilated (stretched) or compressed (squeezed), as shown in Figure 5.14.

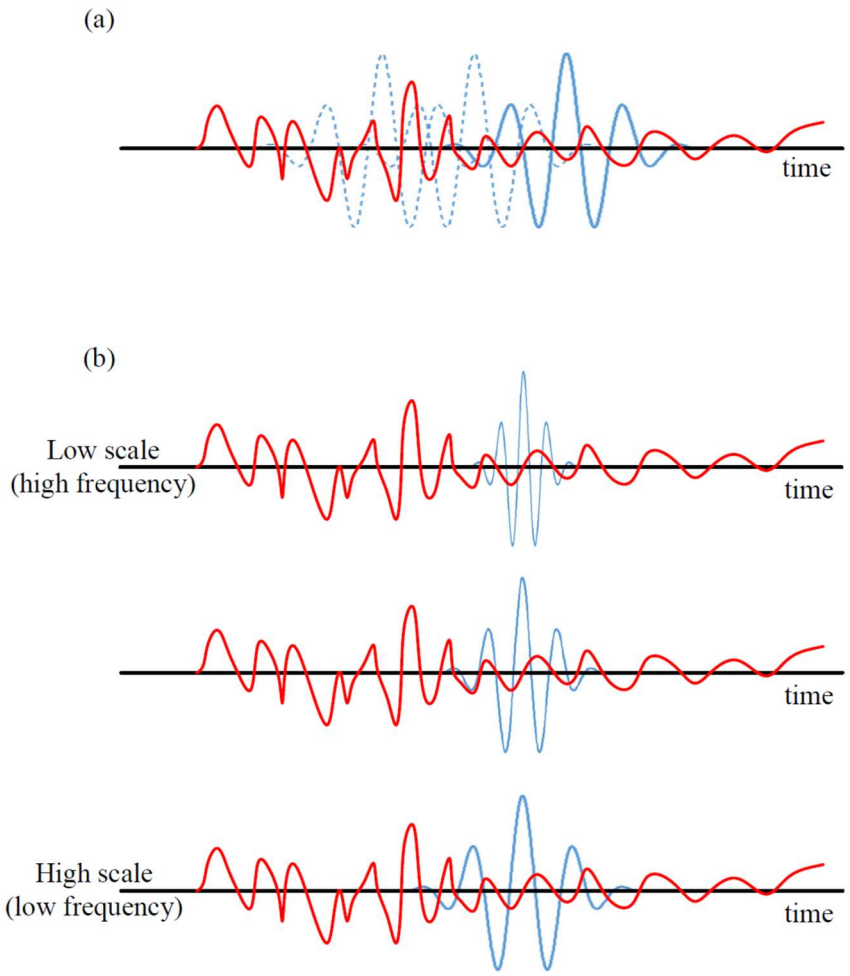

Figure 5.14 A Morlet wavelet being passed through a signal (a) at different locations or time and (b) how it is dilated or squeezed at different scales.

Figure 5.15 shows a schematic of the wavelet transform of a signal using a Morlet wavelet. The top plot shows that if the wavelet matches the shape of the signal at a specific scale and location (or time), then a high transform value is obtained. If the wavelet and the signal do not correlate well, a low transform values is obtained. These values are then plotted into a two-dimensional transform, as shown at the bottom plot of Figure 5.15. The plot, which is also called the *scalogram*, is constructed by computing these transform values from the wavelet and signal at various locations (or time) and for various scales.

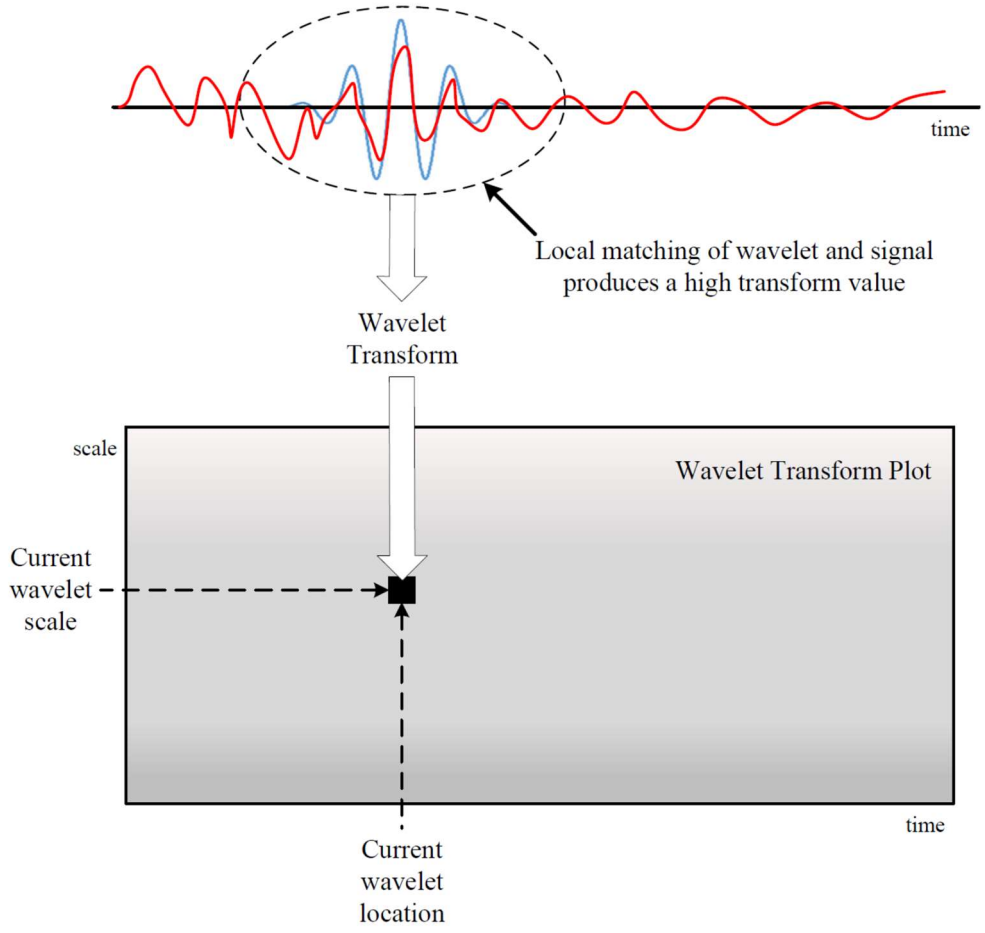

Figure 5.15 The top plot shows a scaled Morlet wavelet being matched with the signal, giving a high transform. The bottom plot shows the transform value plotted on the WT plot.

A WT is in fact an infinite set of various transforms, depending on the function used for its computation. The general features of a WT are based on the *orthogonality* of the wavelets: either *non-orthogonal* or *orthogonal* wavelets are used in a particular type of WT. There are two main types of WTs:

1. ***Continuous Wavelet Transform (CWT)***, which is an implementation of the WT using arbitrary scales and wavelets. The wavelets used are non-orthogonal and the data obtained by this transform are highly correlated.
2. ***Discrete Wavelet Transform (DWT)***, which is an implementation of the WT using a discrete set of the wavelet scales and translations obeying some defined rules. In other words, this transform decomposes the signal into mutually orthogonal set of wavelets, which is the main difference from the CWT.

Continuous Wavelet Transform (CWT)

The word 'continuous' in CWT indicates its ability to operate at any scale and positions, from that of the original signal up to some maximum scale determined by the application needed for detailed analysis with available computational power. The translation of CWT is also continuous during computation, as the analysing wavelet is shifted smoothly over the full domain of the analysed function.

Similarly, the CWT is defined as the sum over all time of the signal multiplied by scaled, shifted versions of the wavelet basis function. Given the input signal $x(t)$ the CWT is defined by equation:

$$\mathcal{W}_x(a,\tau) = \int_{-\infty}^{\infty} x(t)\, \psi^*_{a,\tau}(t) dt \tag{5.53}$$

where a represents the scale parameter, τ represents the translation diameter of time shifting, and the basis function $\psi^*_{a,\tau}$ is obtained by scaling the wavelet $\psi(t)$ at time τ and scale a. The asterisk indicates that the complex conjugate of the wavelet function is used in the transform. The mathematical expression for a wavelet family, which consists of members or mother wavelets, $\psi_{a,\tau}$ is obtained by scaling and time shifting of the wavelet $\psi(t)$ defined by:

$$\psi_{a,\tau}(t) = \frac{1}{\sqrt{|a|}} \psi\left(\frac{t-\tau}{a}\right) \tag{5.54}$$

When a becomes large, the wavelet basis function $\psi_{a,\tau}$ becomes a dilated version of the wavelet bias function, which emphasizes the low-frequency components. Small values of a compress the wavelet basis function $\psi_{a,\tau}$, which emphasizes the high-frequency components. However, the shape of the wavelet basis function will always remain unchanged.

Since $\psi_{a,\tau}$ is defined in equation 5.54, equation 5.53 can be written in equation as:

$$\mathcal{W}_x(a,\tau) = \frac{1}{\sqrt{|a|}} \int_{-\infty}^{\infty} x(t) \psi^* \left(\frac{t-\tau}{a}\right) dt \tag{5.55}$$

Figure 5.16 shows the 5-second data window segment (top plot) from the sEMG signal shown in Figure 5.9 and the CWT plot (bottom). The grey shading indicates the transform of the signal with a Morlet wavelet; the darker the shading the higher the values of the transform for the corresponding scales and time of occurrence.

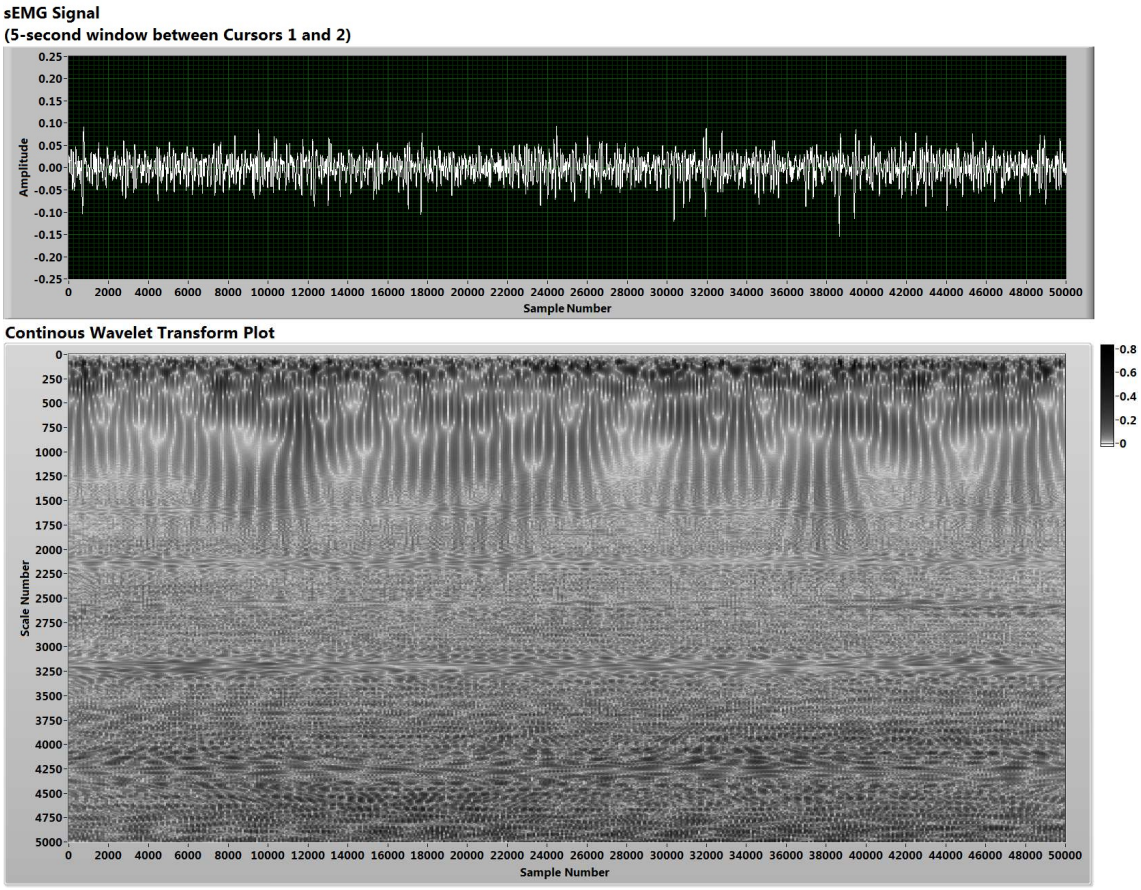

Figure 5.16 The top plot shows the 5-second data window segment taken from the overall sEMG signal shown in Figure 5.9 between cursors 1 and 2. The bottom plot is the CWT of the sEMG signal using the Morlet wavelet between scale values from 1 to 5000.

The WT plot that displays results of the CWT is generally plotted as a scalogram [25; Chapter 10, 183; Chapter 7, 184; Chapter 4], which is the squared magnitude or power of the WT and is given by:

$$P\mathcal{W}_x(\tau, a) = |\mathcal{W}_x(\tau, a)|^2 = \left| \left| \frac{1}{\sqrt{a}} \right| \int_{-\infty}^{\infty} x(t) \psi^* \left(\frac{t - \tau}{a} \right) dt \right|^2 \qquad (5.56)$$

A scalogram, like a spectrogram, is commonly represented as a two-dimensional plot in which power intensity is expressed using different shades of grey. Figure 5.17 shows the 5-second data window segment (top plot) from the sEMG signal shown in Figure 5.9 and the scalogram plot (bottom). The grey shading indicates the transform of the signal with a Morlet wavelet; the darker the shading the higher the values of the signal power for the corresponding scales and time of occurrence.

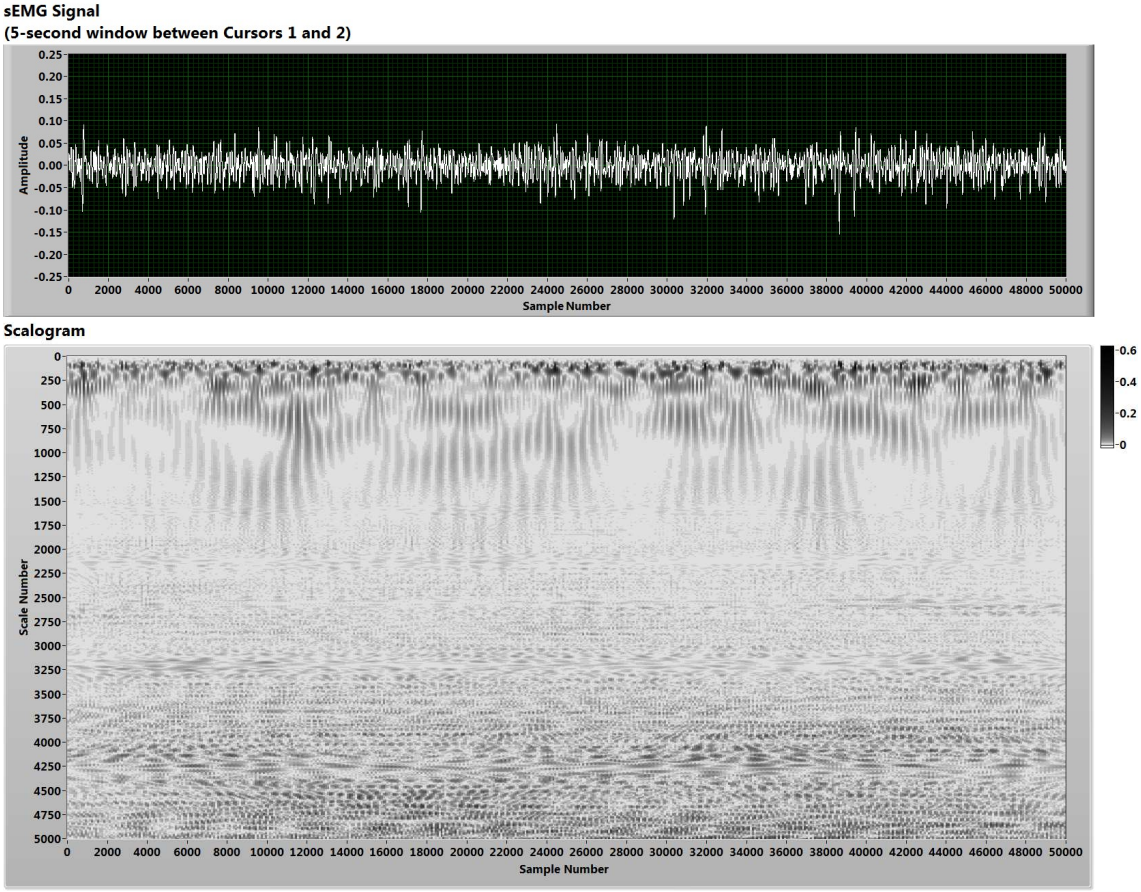

Figure 5.17 The top plot shows 5-second data window segment taken from the overall sEMG signal shown in Figure 5.9 between cursors 1 and 2. The bottom plot is the scalogram of the sEMG signal using the Morlet wavelet between scale values from 1 to 5000.

Both the CWT and scalogram plots are a time-scale view of the sEMG signal and are different from a PSD plot and not related to it [164; Chapter 2, 183; Chapter 9, 184; Chapter 8]. It is also important to understand the nature of scales and the fact that WT analysis does not produce a time-frequency view of a signal is not a weakness but a strength of the technique [185]. Not only is a time-scale a different way to view data, it is a very natural way to view data deriving from a great number of natural phenomena [185]. However, in the case of biomedical signals such as sEMG, it is essential to convert

or connect scales to frequencies where information can be of relevance [185]. The relationship between scale and frequency can only be given in a broad sense. This frequency is called the *pseudo-frequency* that corresponds to a scale [185].

To convert from scales to frequencies is to compute the centre frequency F_c of the wavelet and to use the following relationship expressed by:

$$F_a = \frac{F_c F_s}{a} \tag{5.57}$$

where a is the scale number, F_s is the sampling frequency in Hz, F_c is the centre frequency of a wavelet in Hz, and F_a is the pseudo-frequency in Hz corresponding to the wavelet bias scale a.

The centre frequency F_c is originated from the frequency maximizing the FFT of the wavelet modulus. By processing the mother wavelet using FFT, the centre frequency F_c is obtained from the dominant frequency appearing in the frequency spectrum. A sinusoidal wave is generated at this centre frequency which maps onto the mother wavelet oscillations [185]. Figure 5.18 shows a generated sinusoidal wave at centre frequency in red mapping and translating along the mother wavelet function in blue. The mother wavelet detects the dominant frequency of the sinusoidal signal by a wavelet decomposition followed by conversion of scale to frequency as in equation 5.57. Thus the centre frequency is a convenient and simple characterization of the leading dominant frequency of the wavelet at a given scale [185]. In this research relating to biomedical signals, the Morlet mother wavelet is used with a centre frequency of 0.8125 Hz [185].

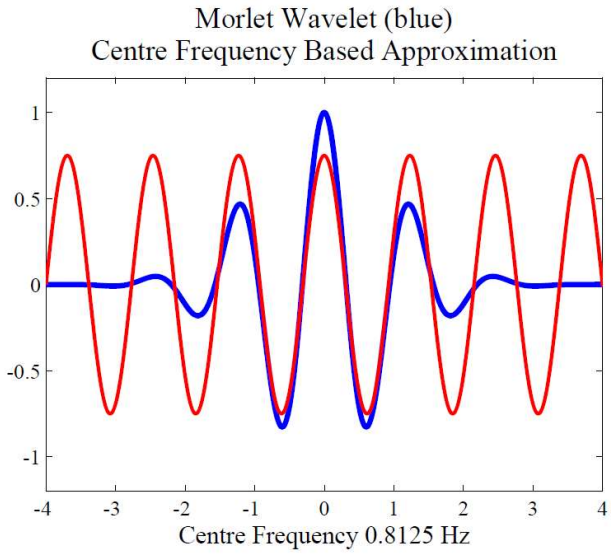

Figure 5.18 Centre frequency-based sinusoidal wave at 0.8125 Hz mapped and translated along a Morlet mother wavelet.

The scalogram shown in Figure 5.19 is an interpolation of the scalogram shown in Figure 5.17, with the vertical scale showing the pseudo-frequency values. The scalogram has been expanded to show frequency values between 0 and 500 Hz.

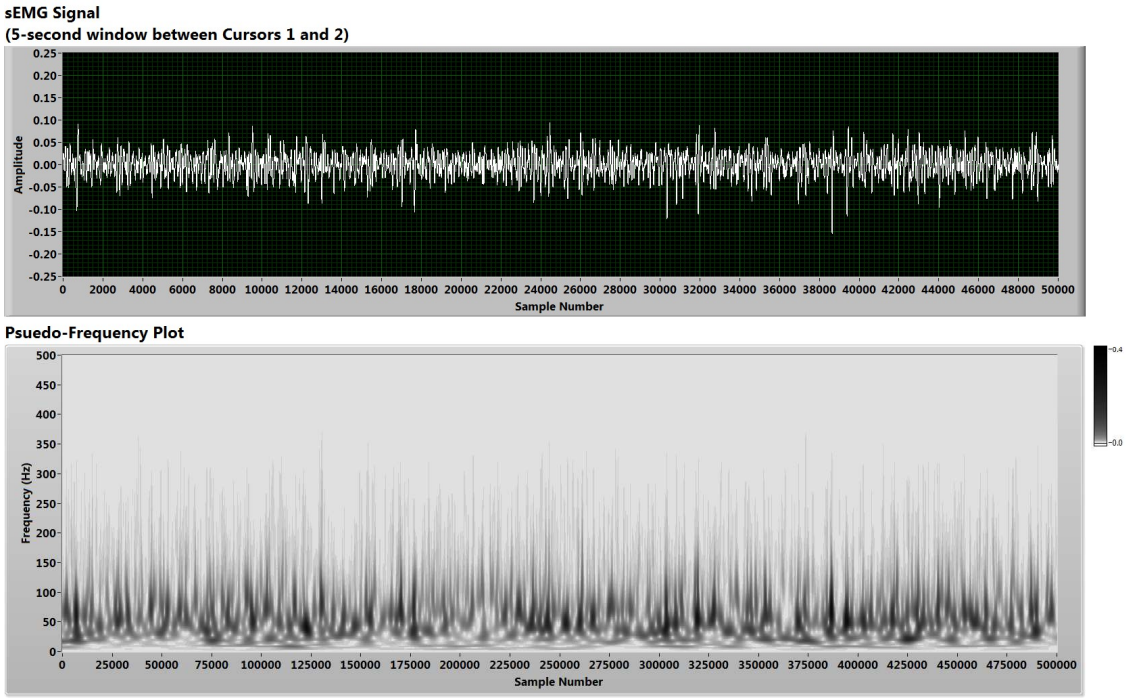

Figure 5.19 The top plot shows the 5-second data window segment taken from the overall sEMG signal shown in Figure 5.9 between cursors 1 and 2. The bottom plot is the scalogram of the sEMG signal using the Morlet wavelet showing pseudo-frequency values from 0 to 500 Hz.

Discrete Wavelet Transform (DWT)

DWT uses the *multi-resolution analysis* (MRA), which is based on multi-rate filter banks, and was developed by Meyer, Dauchechies and Mallat [186-189]. While the translation of CWT is carried out in a smooth continuous fashion, DWT is done in discrete steps.

The wavelets used in DWT are discrete versions of the continuous wavelets used in CWT. Transforming wavelets to discrete signals partially depends on the chosen algorithm. However, it does not explicitly calculate a digitized version of a mother wavelet $\psi(t)$. Rather, DWT acts as a bank of low-pass and high-pass filters that decompose a signal into multiple signal bands. The decomposition process can be iterated, with successive approximations being decomposed in turn, so that one signal is broken down into many lower resolution components. This is called the wavelet decomposition tree, as shown in Figure 5.20.

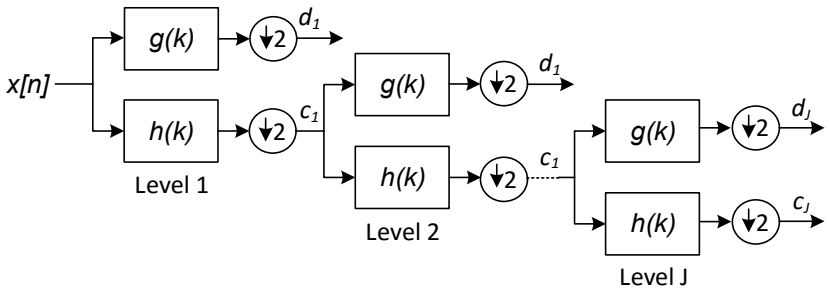

Figure 5.20 Wavelet decomposition tree or analysis filter bank using the DWT pyramid algorithm, where input signal $x[n]$ is filtered recursively with pairs of low-pass $h(k)$ and high-pass $g(k)$ filters. The output from each filter is subjected to down-sampling by a factor of 2, denoted by '↓2'.

The level of decomposition or analysis to show the frequency content of a signal $x[n]$ by DWT is referred to as the *scale index*. Since the analysis process is iterative, in theory it can be continued indefinitely. The output from the low-pass filter $h(k)$ is a smoothed version of the input signal $x[n]$, where the high-frequency components of the signal are removed. The high-pass filter $g(k)$ removes the low-frequency components and the result is a signal containing high-frequency component details of the input signal.

In a digital operation, when the original signal $x[n]$ passes through the two filters, the output emerges as two signals with the same number of data. Thus the number of output

data obtained will be twice the number at the start. In order to avoid this, *down-sampling* the filtered sequences by a factor of two or on a dyadic grid 2^J is performed.

MRA theory uses the ideas similar to subband decomposition and coding. A signal is divided into a set of frequency bands, which are introduced by sampling of dyadic grid. This, however, means that the frequency domain is divided into octave subbands.

The mathematical derivation of scaling function for DWT is defined by having given a discrete signal $x[n]; n = 1, \dots, N$ with its DWT up to level J depth, it maps the vector $(x[1], \dots, x[N])$ to a set of N wavelet coefficients containing output sequences $c_{J,k}$ and $d_{j,k}$ where $j = 1, 2, \dots, J$, of the wavelet series approximation. Such a MRA deviation becomes clear if a second function, called a *scaling function*, is put alongside the wavelet functions.

Scaling Function

A scaling function $\varphi(t)$ gives a set of approximations of the signal as a set of resolution levels j, by projecting it on a set of subspaces V_j. These subspaces V_j are generated by dilation using low-pass filter $h(k)$ and translated versions of $\varphi(t)$. For a given level j, the subset V_j is spanned by the base of scaling functions:

$$\varphi_{jk}(t) = \frac{1}{\sqrt{2^j}} \varphi\left(\frac{t - k2^j}{2^j}\right), \qquad k \in Z \tag{5.58}$$

The approximation coefficients yield:

$$c_{jk} = \langle x, \varphi_{jk} \rangle \tag{5.59}$$

Hence, by setting the stretching factor to 2 or on a dyadic grid, scaling function $\varphi(t)$ corresponds to:

$$\varphi(t) = \sqrt{2} \sum_k h\,[k] \varphi(2t - k) \tag{5.60}$$

where

$$h[n] = \left\langle \frac{1}{\sqrt{2}}\varphi(t), \varphi(2t-n) \right\rangle \tag{5.61}$$

MRA, which is the decomposition of a signal on the subspaces V_j, is completely defined by the function $\varphi(t)$ or equivalently by the sequence $h[n]$ from the low-pass filter function $h[n]$ from equation 5.61. The signal is decomposed or band-filtered to the frequency subbands, where the scale function always defines the low-frequency signal components. The complementary high-frequency band is, however, obtainable by the wavelet function.

Wavelet Function

The information lost between two successive approximations is called a *detail*. It is obtained by projecting the signal on the complement of V_j, denoted by W_j, ($W_j + V_j = V_{j-1}$), and defined by the wavelet functions:

$$\psi_{jk}(t) = \frac{1}{\sqrt{2^j}}\psi\left(\frac{t-k2^j}{2^j}\right), \qquad k \in Z \tag{5.62}$$

where $\psi(t)$ is the mother wavelet defined by:

$$\psi(t) = \sqrt{2}\sum_k g\,[k]\varphi(2t-k) \tag{5.63}$$

with

$$g[n] = \left\langle \frac{1}{\sqrt{2}}\psi(t), \varphi(2t-n) \right\rangle \tag{5.64}$$

The detail coefficients are computed as follows:

$$d_{jk} = \langle x, \psi_{jk} \rangle \tag{5.65}$$

and they correspond to the DWT as generated by the MRA:

$$d_{jk} = DWT_{\psi x}(j,k) = \langle x, \psi_{jk} \rangle \tag{5.66}$$

The Morlet wavelet does not allow for orthogonal wavelets, which is a requirement for DWT analysis in terms of translations and scaling. Based on previous research on the signal decomposition of a sEMG signal and reconstruction, it was found that the Daubechies wavelet (db05) is the most suitable for performing DWT of sEMG signals [190]. An example of a signal analysed by DWT with a mother wavelet Daubechies (db05) is illustrated in Figure 5.21.

The top box (a) in Figure 5.21 shows the 5-second data window segment taken from the overall sEMG signal shown in Figure 5.9 between cursors 1 and 2, and below it is the DWT plot with scale number of 4 using the Daubechies wavelet (db05). The bottom box (b) shows various plots as the sEMG signal is filtered through from scale 1 to 4. The red dotted lines pointed from the region where the signal was originated from the DWT plot in box (a).

DWT separates and retains the signal features in one or more subbands as shown in Figure 5.21. The level of decomposition shown in Figure 5.21 is to scale index 4, and it shows the subbanding obtained from a discrete signal sampled at 10 kHz and has 50,000 samples (5 seconds). This subbanding of the DWT is variable, which means the feature of band varies such that the frequency resolution is proportional to the centre frequency. This subbanding has been shown to be appropriate for many physical signals, but the partition is still fixed.

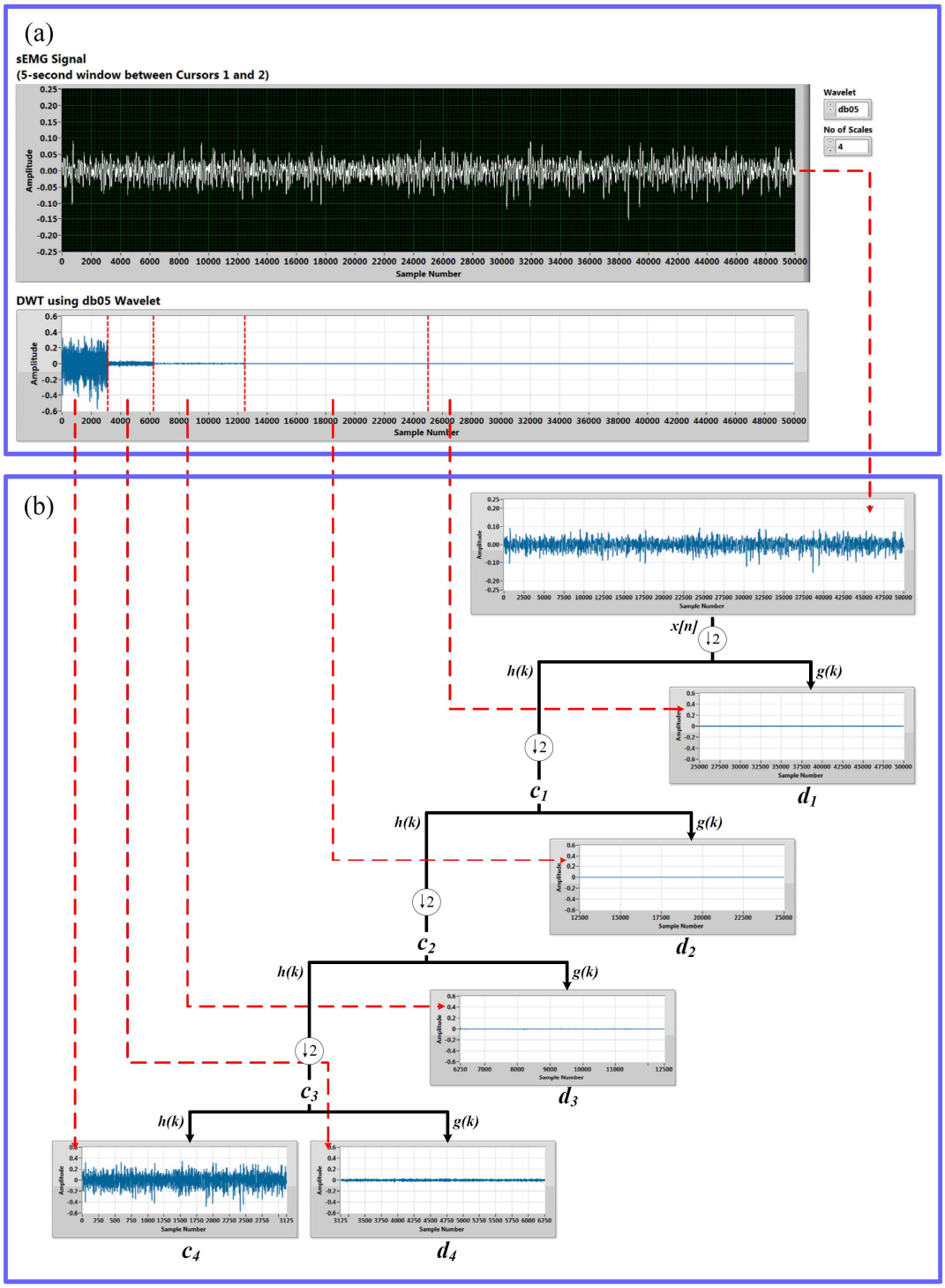

Figure 5.21 (a) The 5-second data window segment taken from the overall sEMG signal shown in Figure 5.9 between cursors 1 and 2 and the DWT plot at scale 4 using the Daubechies wavelet (db05). (b) The decomposition of the sEMG signal through scales 1 to 4.

Since the DWT signal is being down-sampled at each successive frequency scale, it becomes a sparse transform at lower frequency scales. It is expected that CWT can overcome this problem and gives an additional method of sEMG signal frequency analysis [191].

5.7 Muscle Fibre Conduction Velocity (MFCV)

An important muscle feature that can be determined by using a multi-channel electrode is the muscle fibre conduction velocity (MFCV). MFCV is a basic physiological parameter that greatly affects the myoelectric signal, whether it is detected by indwelling or surface electrodes, and is referred to as the velocity of propagation of action potentials along the muscle fibres [4; Chapter 8, 192].

MFCV values can range from 2.5 to 5 ms^{-1} for most human skeletal muscles, and vary depending on the electrode location measured [193, 194]. MFCV is assumed constant over the length of the muscle and is determined by simultaneously recording sEMG signals at two positions above the muscle [192-195].

The traditional method for finding the MFCV of a muscle is the cross-correlation technique which uses two sEMG signals $x(t)$ and $y(t)$ given by [196]:

$$R_{xy}(\tau) = \frac{1}{T}\int_0^T x(t)y(t+\tau)\,dt \tag{5.67}$$

where T is the time period of the signal and τ is the time delay, or:

$$R_{xy}(\tau) = \frac{1}{N}\sum_{n=1}^{N}[x(n)y(n+\tau)] \tag{5.68}$$

where N is the number of samples of the signal and τ is the sample delay.

To quantify this, $R_{xy}(\tau)$ is normalized to have values between −1 and +1:

$$R'_{xy}(\tau) = \frac{R_{xy}(\tau)}{\sqrt{R_{xx}(0)R_{yy}(0)}} \tag{5.69}$$

where $R_{xx}(0)$ is the auto-correlation of $x(t)$ at $\tau = 0$, and $R_{yy}(0)$ is the auto-correlation of $y(t)$ at $\tau = 0$.

Using the cross-correlation shift Δt between the two signals or the action potential of the muscle and the inter-electrode distance (IED) of the electrode d, MFCV is given by:

$$MFCV = \frac{d}{\Delta t} \tag{5.70}$$

The cross-correlation of sEMG signals is obtained by using signals collected from a pair of electrodes. The sampling frequency is related to sEMG signals, as described in section 5.7.1, where the main frequency components are between 0 to 500 Hz. The Nyquist sampling theorem states that the minimum sampling rate f_s should be double the maximum frequency component, which will be 1 kHz. Taking the value for the IED to be 10 mm (= 0.01 m) and that for MFCV to be f_s=5 ms^{-1}, Δt will be the time taken of the muscle signal to travel from one electrode to another, or the *action potential* of the muscle, and is calculated as:

$$\Delta t = \frac{d}{MFCV} = \frac{0.01\ m}{5\ s} = 0.002\ seconds$$

The sampling period t_s would be:

$$t_s = \frac{1}{f_s} = \frac{1}{1000\ Hz} = 0.001\ seconds$$

Using the values above for Δt and t_s, the number of samples N obtained would be:

$$N = \frac{\Delta t}{t_s} = \frac{0.002\ seconds}{0.001\ seconds} = 2\ samples$$

Using only two samples is insufficient to find the MFCV using the cross-correlation method, and there are two ways this can be improved. One way is to interpolate the cross-correlation to a higher sampling so that the lag τ represents a smaller division of time [197]. The other method is to sample the sEMG signals at a higher rate to ensure adequate resolution [198]. As noted earlier in this chapter, for this research the sampling rate was increased to 10 kHz, which ensures there are 10 times the number of points for the cross-correlation of two sEMG signals to find the MFVC. There is no standard minimum value for the cross-correlation coefficient that is acceptable for analysis for sEMG signals, but Broman, et al. [199] found that values between 0.6 and 0.9 were acceptable.

The top three plots in Figure 5.22 show the 5-second data window segments for three Laplacian channels for Participant No. 13, taken from the overall sEMG signal similar to that shown in Figure 5.9 between cursors 1 and 2. The bottom plots show the normalized cross-correlated plots and expanded views for cross-correlation between (a) channel 1 and 2; and (b) channel 2 and 3 of the Laplacian signals. The cross-correlation plot for the sEMG signals from channel 1 and 2 shows a maximum coefficient value of 0.723 and a MFCV of 4.45 ms^{-1}. The cross-correlation plot for the sEMG signals from channel 2 and 3 shows a maximum coefficient value of 0.676 and a MFCV of 4.5 ms^{-1}.

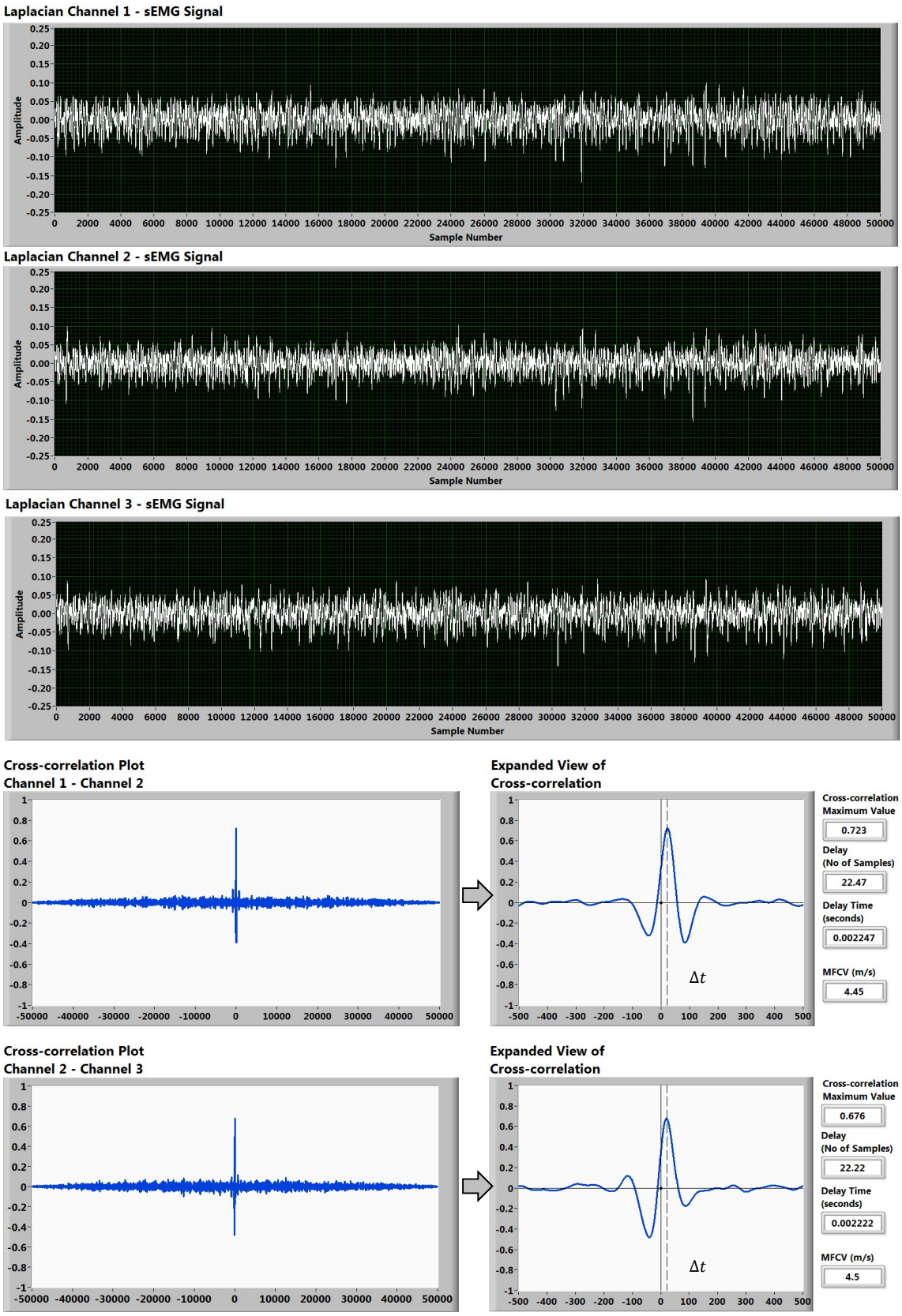

Figure 5.22 The top three plots show all three Laplacian channels collected from the new multi-channel electrode for a 5-second window (note that channel 2 is the signal from Figure 5.9). The bottom plots are the cross-correlation plots with expanded views for the top three plots of the sEMG signals.

This chapter has covered majority of the points that need to be considered for acquiring biomedical signals such as sEMG signals, as well as the various DSP techniques. Various DSP techniques can be used in the (a) time domain, (b) frequency domain or (c) time-scale (or time-frequency) domain. Each of the DSP techniques covered in this chapter was applied to sEMG signals collected from a participant performing the 50% MVIC endurance task covered in Chapter 4, and the analysis outputs were presented for each. This research is focused on analysing signals that have been collected from the newly designed multi-channel electrode described in Chapter 3. The next chapter will discuss the new algorithm developed using some of the DSP techniques, and report the results obtained from the analysis of the Laplacian signals collected from the new multi-channel electrode for the 50% MVIC endurance task carried out on 40 participants.

Chapter 6
Data Analysis and Results

6.1 Introduction

This chapter presents the results obtained from the analysis of the Laplacian signals collected from the new multi-channel electrode during a 50% MVIC endurance task carried out on 40 participants. An initial pilot study was carried out with five participants using a three-channel Laplacian electrode. Once the pilot study was completed and all of the technical issues resolved, the main study of 40 participants was then executed using the new multi-channel electrode. As described in Chapter 5, the signal processing techniques used were in the time domain, frequency domain and time-frequency (or scale) domain. Because the research was investigating sEMG signals for the endurance task to identify characteristics that exist in terms of time, only the signal processing techniques that produced a time element were used. A new signal processing algorithm was developed using a sliding window technique, which was passed through the sEMG signals to find the values for the MDF, MNF, RMS and MFCV.

6.2 Pilot Study

In the early stages of this research, a pilot study was carried out using an existing Laplacian electrode from the Health and Rehabilitation Research Institute at the North Shore Campus of Auckland University of Technology. This electrode had originally come from the University of Technology of Compiègne, France.[37, 38] and is pictured in Figure 6.1.

Figure 6.1 Three-channel Laplacian electrode (right) and amplifier/power supplier (left) used in pilot study [37, 38].

Each Laplacian channel of this electrode was amplified with a gain of 100 and a bandpass filter of 8 Hz – 15 kHz. The raw sEMG signals collected for the pilot study were collected at a sampling rate of 10 kHz using a 16–bit resolution DAQ (NI PCI-6024E) in the ±5 V range using LabVIEW. It was found that the amplification of the electrode was too low and further amplification was achieved using a Grass model P511 amplifier (Grass Instruments Company, USA) where signals collected were amplified by 5 to 10 with a given overall gain of 500 or 1000. The signals collected were stored on a computer hard drive for further processing offline using the power spectrum density of a FT as defined in section 5.7.1.

Further analysis of the signals collected from this pilot study established that the existing DC component was amplified and had to be removed from the signal before further processing could be carried out. This was performed in LabVIEW using a technique referred to as *demeaning* the signal [25; Chapter 5, 26]. This was done by first finding the mean value of the overall signal and then subtracting it from the original signal. If this was not done, the power spectrum density showed a large DC component in the transform and was unable to show valid information concerning the signal's power.

Another issues identified by the pilot study were the positioning and orientation of the electrode on the participant's muscle. Unless the electrode was positioned on the centre of the muscle and parallel with it, the signals collected were unable to be processed and analysed to give meaningful information [116, 200, 201].

The pilot study showed there was a need for a new multi-channel electrode to be developed to obtain signals that can be used for the various signal-processing techniques covered in this research.

6.3 New Signal Processing Algorithm

A new algorithm was developed using an overlapping sliding window technique, and the following values were calculated:

(a) Power spectrum using a Hanning window to find the MNF and MDF (described in section 5.6.2).
(b) RMS of the signal (described in section 5.6.3).
(c) MFCV using cross-correlation of two signals (described in section 5.7).

The new algorithm used to obtain the values for MNF, MDF, RMS and MFCV is described and shown in Appendix J. The schematic diagram showing how the sliding window is passed through the sEMG signal to find the values for MNF, MDF, RMS and MFCV is shown in Figure 6.2. Using the algorithm, different overlapped window sizes were used and passed through the signal. It was found that a window size of 1 second or 10,000 samples, and the overlap of 0.25 seconds or 2,500 samples, gave the most meaningful results in terms of time resolution for analysing the three Laplacian signals.

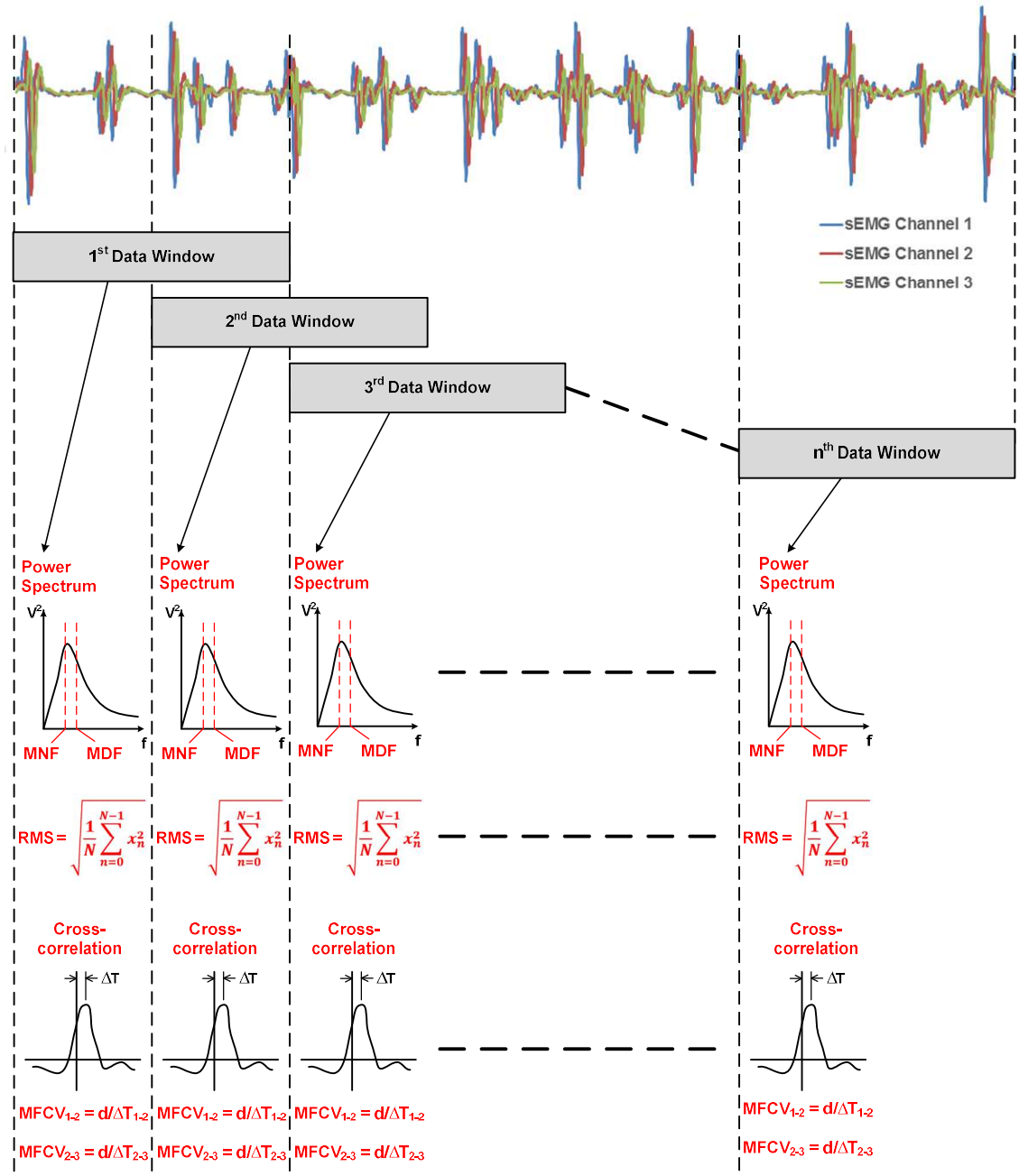

Figure 6.2 Schematic diagram showing how the sliding window is passed through the sEMG signal to find the values for MNF, MDF, RMS and MFCV.

6.4 Results of the Main Study

The results of the main study relate to the three Laplacian signals that were generated from the 11 pin multi-channel electrode that were collected from 40 participants. The research focused on the endurance task of holding 50% MVIC, as described in section 4.4.1. This section provides a summary of physiological feature measurements and a set of results obtained from one participant using the new signal processing algorithm described in the previous section.

6.4.1 Physiological Features

Table 6.1 shows histogram plots and box-and-whisker diagrams for the summary of physiological features recorded before testing the participants. The full record of these physiological features is included in Appendix K.

The box-and-whisker diagram for each feature shows the data in terms of quartiles. The box represents the data that lies between the lower and upper quartile, which is the interquartile range of the data [202; Chapter 3]. The horizontal line in the middle of the box represents the median of the data [202; Chapter 3]. The whiskers on the plot mark the full range of the data and are drawn on either side of the box, representing the minimum and maximum values [202; Chapter 3].

Table 6.1 Summary of physiological features of participants

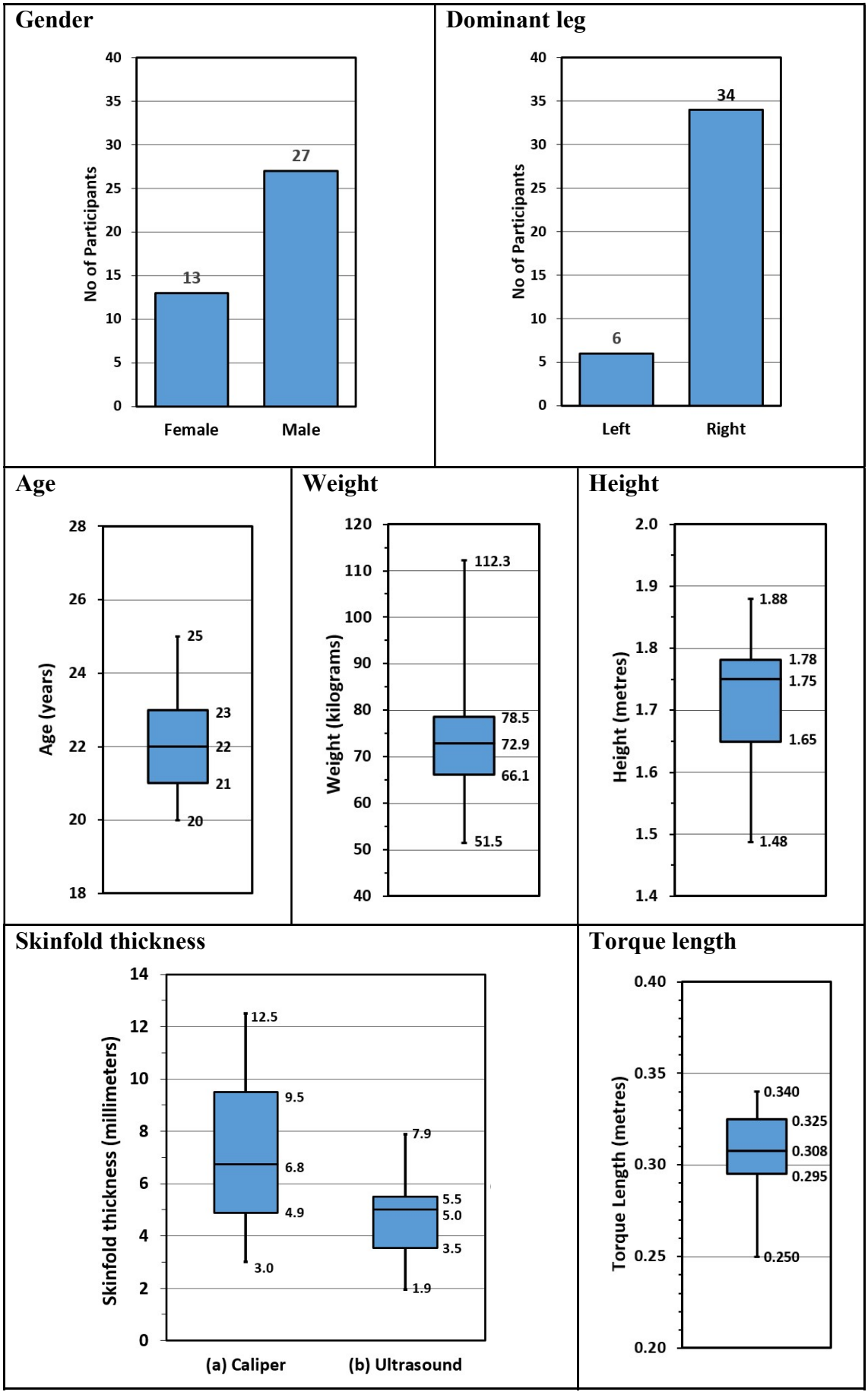

There were two methods used to find the subcutaneous tissue layer or fat of the skin: (a) the skinfold thickness technique using a skinfold caliper and (b) the ultrasound scan (both explained in section 4.4.3). From the box-and-whisker diagrams, it can be seen that the ultrasound scan gives more precise measurement of the subcutaneous layer, and is therefore the preferred method with a smaller range of values (6 mm) compared to a range of 9 mm for the skinfold caliper. Studies carried out by Nordander et al [146] and Selkow et al [147] revealed that although the skinfold caliper can still be used when the ultrasound scan is unavailable, it overestimates the measurement of the subcutaneous layer, and it should only be used for determining the Body Mass Index (BMI).

6.4.2 Analysed Results of a Single Participant

This section describes how the data were analysed and presented for Participant No. 13. Figure G.1 in Appendix G showed the signals by Laplacian configuration, as a more refined mathematical computation, Laplacian filtering produced better signal definition than by linear array. After the Laplacian signals were obtained from the data collection, they were analysed offline in LabVIEW using the new signal processing algorithm to determine the values for MNF, MDF, RMS and MFCV. These values were then plotted using MATLAB 8.1, R2013a (MathWorks Inc., USA). Trend lines were added to each plot using the *polyval* function with a 5th order polynomial, which produced the best trend line in MATLAB for visual observation of features in the signal.

To find the trend line reliability to the plot values, the *coefficient of determination* or the *R-squared value* was calculated. This indicates the proportionate amount of variation of variable y from the independent variables x in a regression model [203; Chapter 8]. The larger the R-squared value (i.e. at or near 1), the less is the variability of the trend line from the measured values. The trend lines were characterized as *polynomial* functions for the plots [203; Chapter 8].

Figures 6.3–6.5 show plotted values for the MNF, MDF and RMS features of the Laplacian signals for Channel 1, 2 and 3 (Ch1, Ch2, Ch3) respectively. Also shown for each feature is the polynomial trend line with the R-squared value.

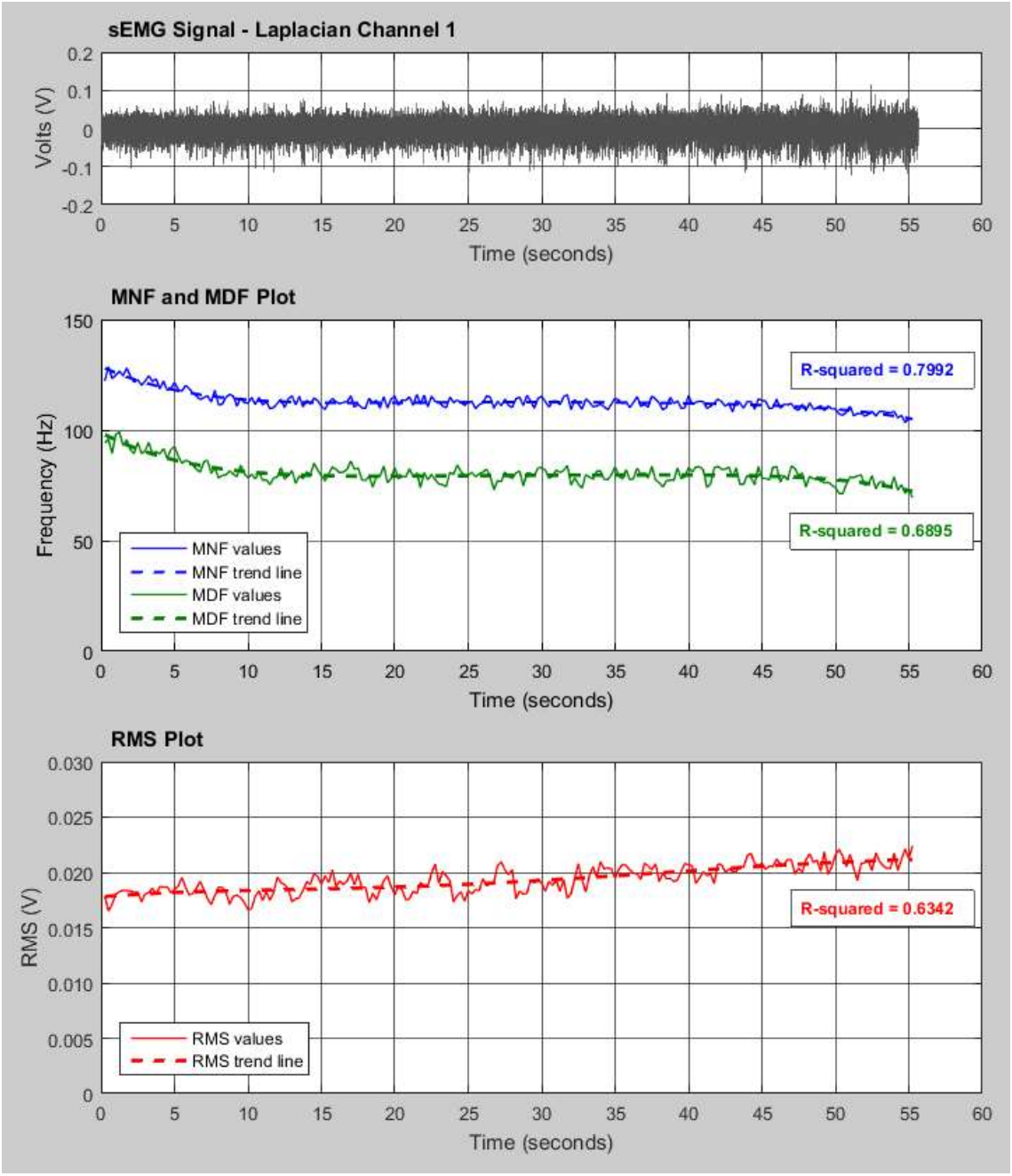

Figure 6.3 Plotted values and trend lines with their R-squared values for MNF, MDF (middle) and RMS (bottom) from Ch1 Laplacian signal for Participant No. 13 (top).

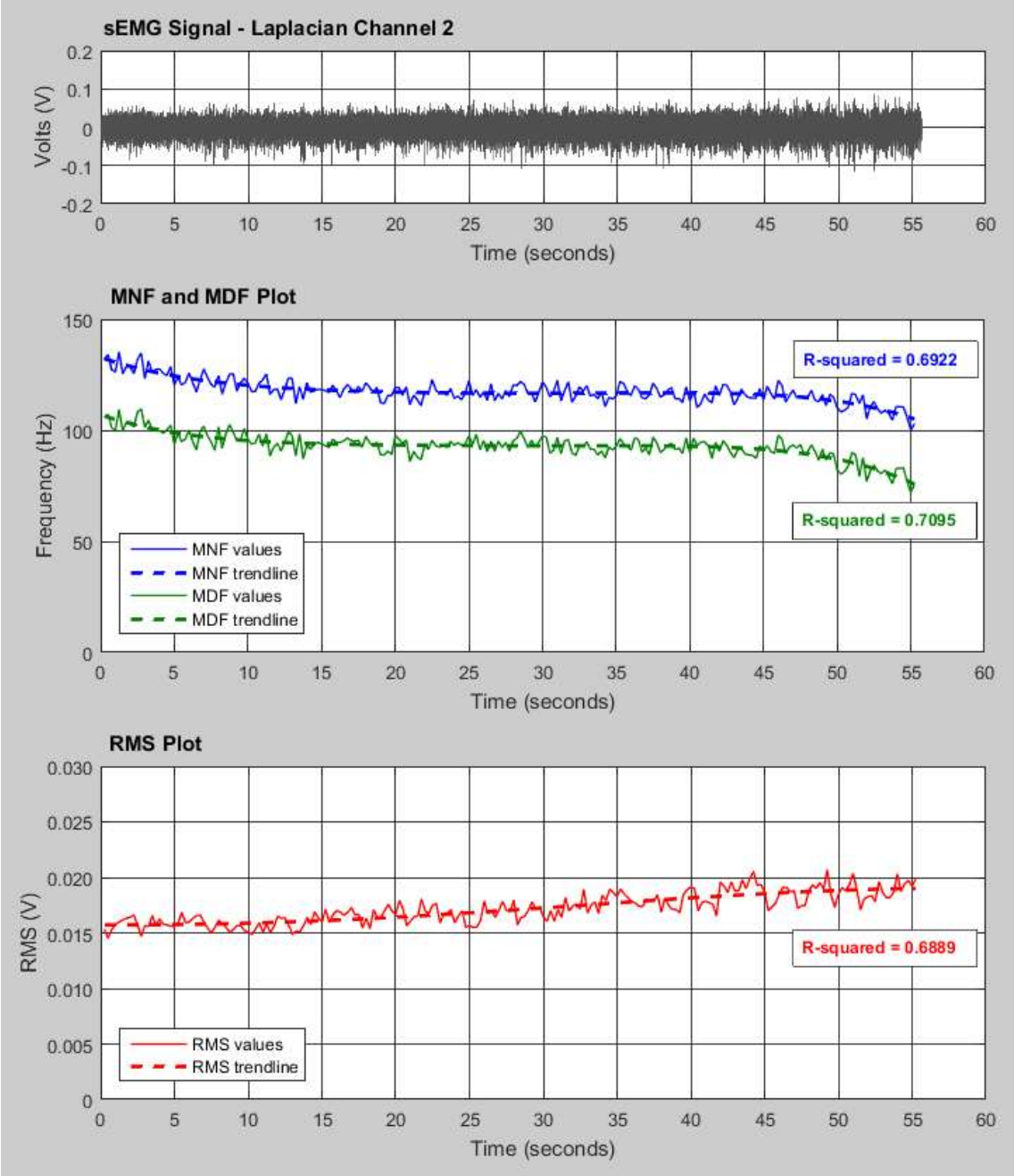

Figure 6.4 Plotted values and trend lines with their R-squared values for MNF, MDF (middle) and RMS (bottom) from Ch2 Laplacian signal for Participant No. 13 (top).

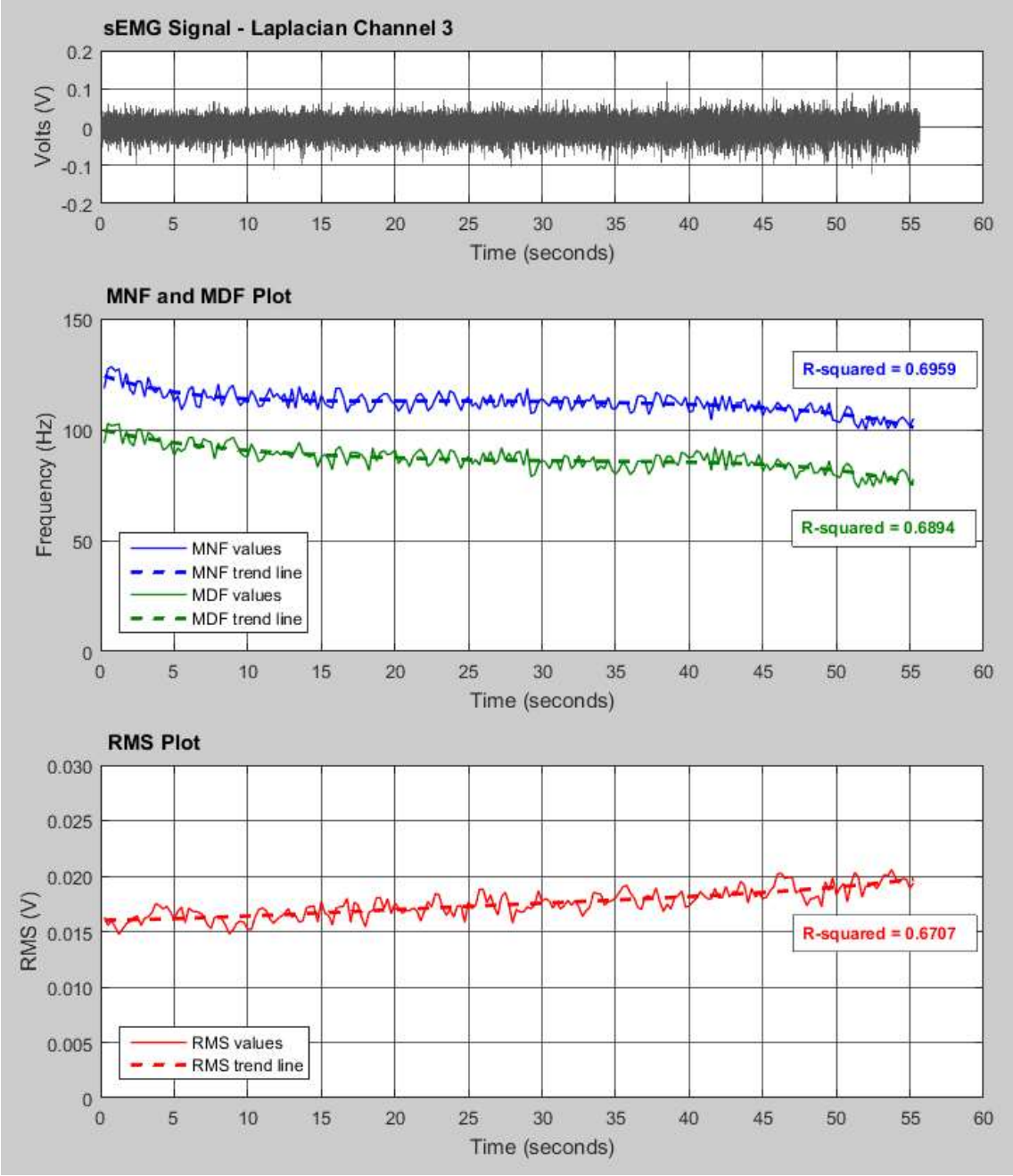

Figure 6.5 Plotted values and trend lines with their R-squared values for MNF, MDF (middle) and RMS (bottom) from Ch3 Laplacian signal for Participant No. 13 (top).

The trend lines for the MNF, MDF and RMS features for each of the three Laplacian signals shown in Figures 6.3–6.5 were then plotted with a *mean trend line*, shown in Figure 6.6. Finding the mean trend lines for all these features allows a comparison to be made between all the data collected from all participants who were part of this research.

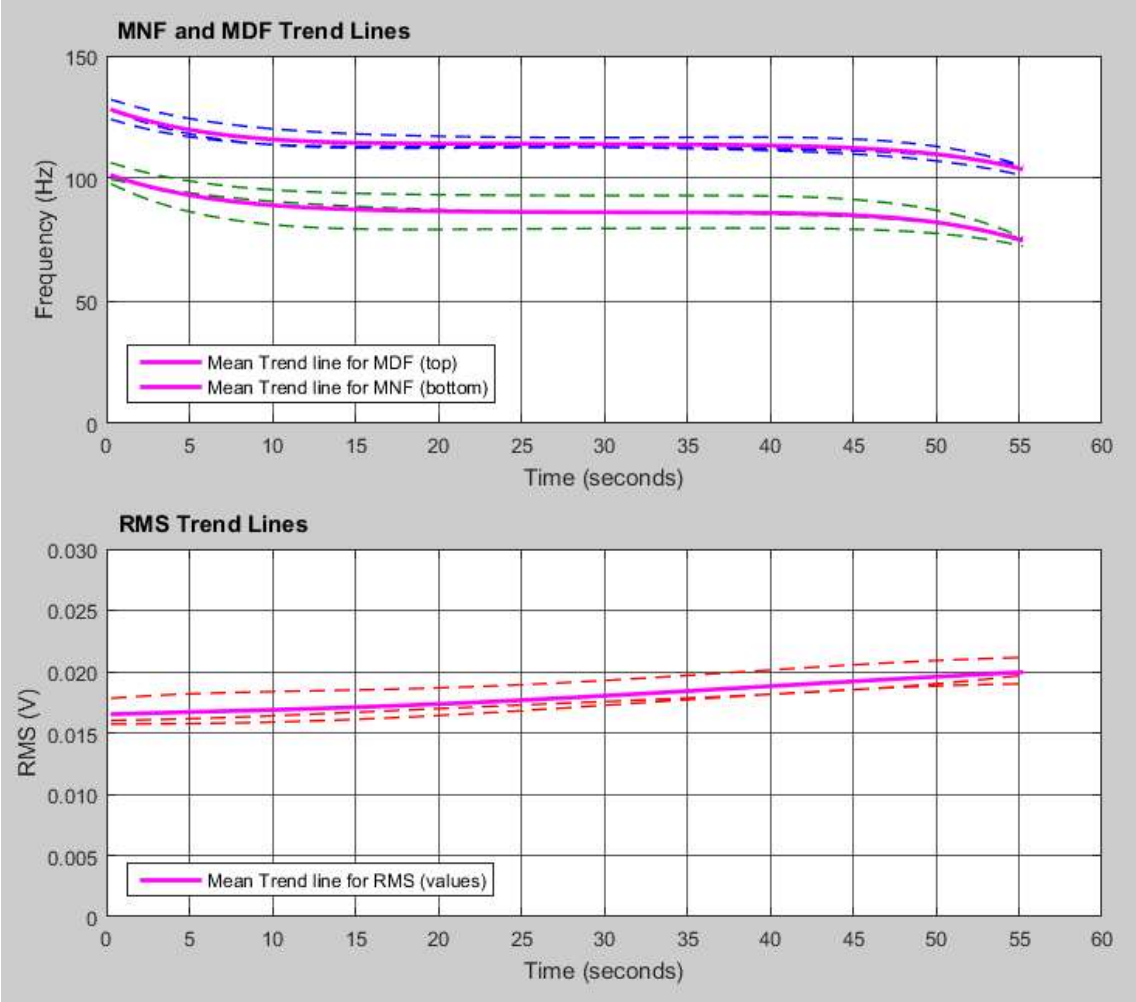

Figure 6.6 Plotted values of the trend lines from Figures 6.3–6.5 and the mean trend lines for MNF and MDF (top) and RMS (bottom).

Figure 6.6 shows that the MDF values are lower in values than the MNF values and the mean trend lines for both MDF and MNF follow the same trend. As previously discussed in Chapter 5, the power spectrum density for each of the data windows was skewed to the left, where lower frequencies are more dominant in the signal (shown previously in Figure 5.11).

By examining the mean trend lines (purple line) in the top plot of Figure 6.6, it can be seen that both MDF and MNF values show a similar trend to the individual trend lines of MDF (blue-dotted lines) and MNF (dark green-dotted lines), as shown in Figures 6.3–6.5 for each of the Laplacian signals (Ch1, Ch2 and Ch3). During the first 10–25 seconds, both MDF and MNF values dropped to about 10%, after which they remained steady from 10–15 to 45 seconds. After 45 seconds and until complete fatigue of the muscle occurred (around 55 seconds), the fall was about 8% of their initial value.

The mean trend line (purple line) for RMS values in the top plot of Figure 6.6 increased in a linear fashion and showed a similar trend to the individual trend lines for RMS (red-dotted lines), as shown in Figures 6.3– 6.5 for each of the Laplacian signals (Ch1, Ch2 and Ch3). The RMS increased to about 20% in value from its initial value at the start of the endurance task.

The MFCV obtained by the new algorithm is covered in section 6.3 and Appendix J. The MFCV used the signals from the Laplacian signals for Ch1 and Ch2 with an IED of 10 mm. Figure 6.7 shows these signals (top and middle plots) and MFCV values were plotted with the polynomial trend line and R-squared value (bottom plot). The same was done for the MFCV of the signals from the Laplacian signals from Ch2 and Ch3 as shown in Figure 6.8.

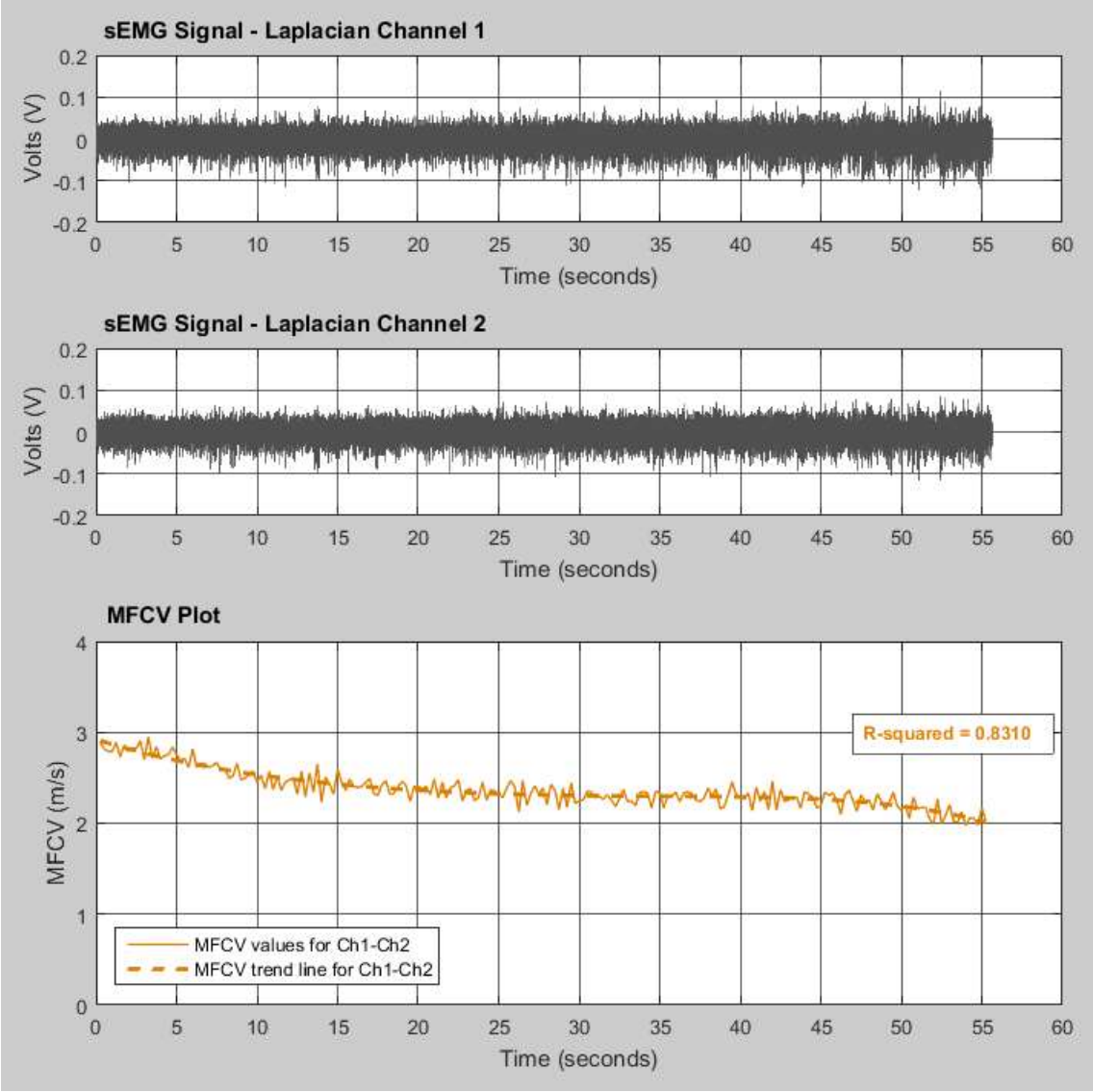

Figure 6.7 Plotted MFCV values and trend line with its R-squared value (bottom) using Laplacian signals from Ch1 (top) and Ch2 (middle) for Participant No. 13.

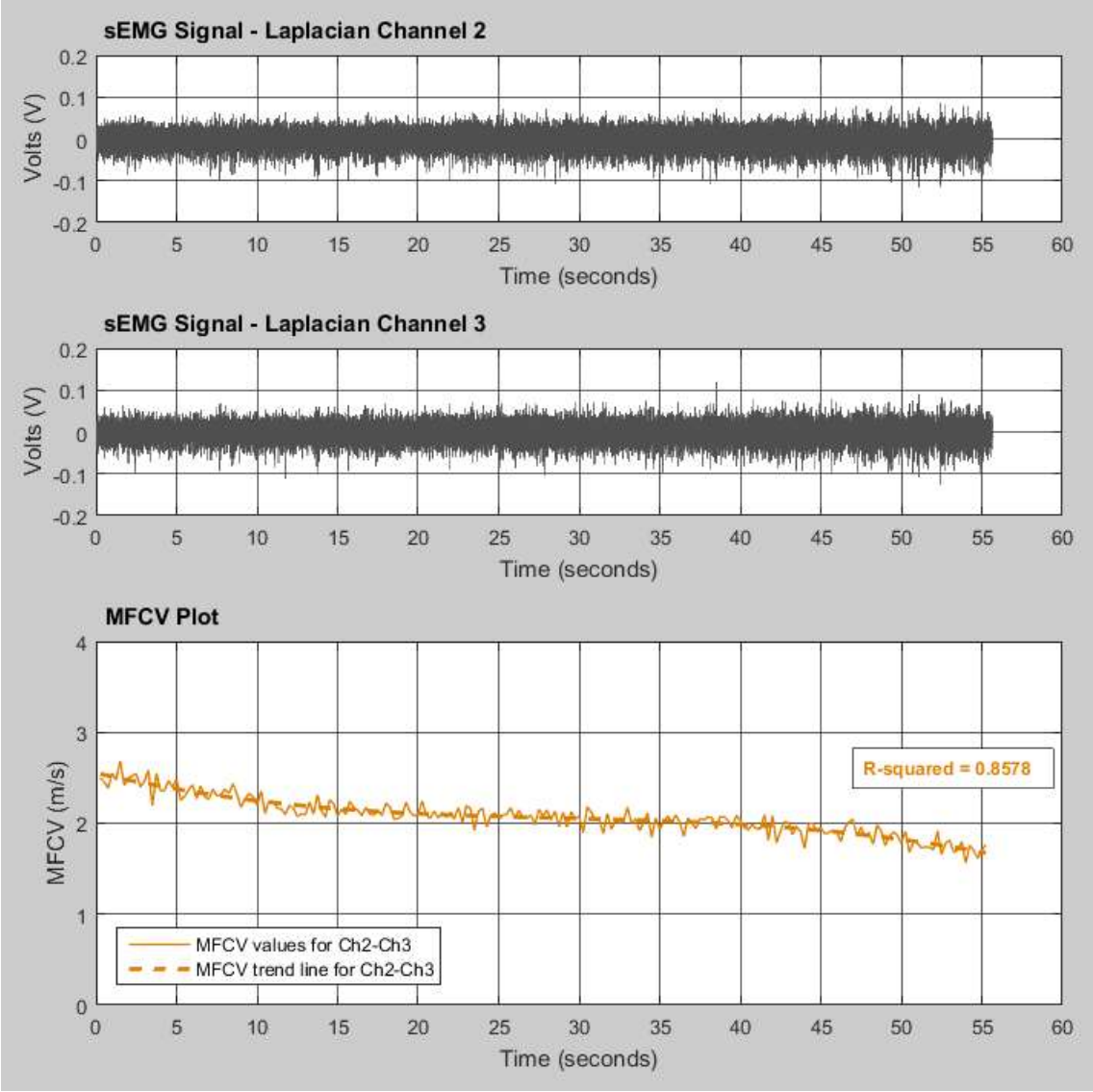

Figure 6.8 Plotted MFCV values and trend line with its R-squared value (bottom) using Laplacian signals from Ch2 (top) and Ch3 (middle) for Participant No. 13.

The mean trend line for the MFCV values was then determined and is shown as the purple line in Figure 6.9. The dotted lines, which represent the measured MFCV values from Figures 6.7–6.8, are also shown in Figure 6.9. Finding the mean trend line for this feature allows a comparison to be made between all the data collected from all other participants that were part of this research.

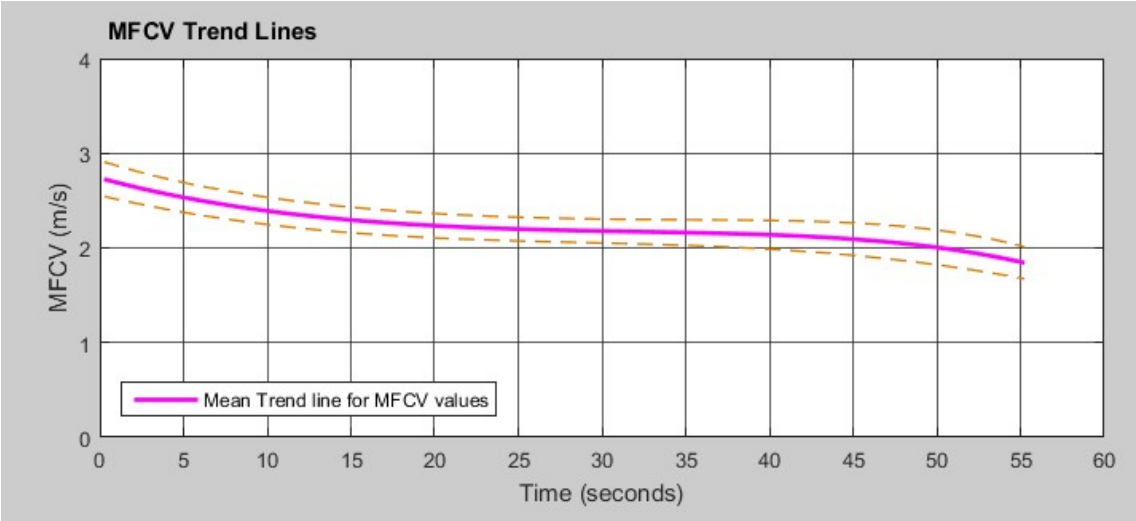

Figure 6.9 Plotted values of the trend lines for MFCV (brown-dotted line) from Figures 6.7–6.8 and the mean trend line (purple line).

The mean trend line for MFCV shows a similar trend to the individual trend lines for MFCV (brown dotted lines). During the first 15 seconds, the MFCV values dropped about 15%, after which they remained steady from 15 to 40 seconds. After 40 seconds and until complete fatigue of the muscle occurred (around 55 seconds), the fall was about 10% of their initial value.

6.4.3 Overall Analysis of Research Results

From the analysis of the previous section, it was decided to use only two features of the Laplacian signals collected from the 40 participants – the MNF and MFCV mean trend lines – for the subsequent analysis. The main reason for using only the MNF, and not both the MNF and MDF, was that they always followed the same trend in each participant. Also, the R-squared value of MNF was generally higher than the R-squared value of the MDF, indicating that the trend line of MNF followed the measured values more closely than those of the MDF.

The RMS plots did not present any useful trend lines for observing features in the signal. The RMS trend line generally showed a linear increase, even when a polynomial-based generated trend line was used. Hence, only the MNF and MFCV mean trend lines for all the participants were generated and used for the subsequent analysis of this research.

Table 6.2 shows a summary of the torque values and the fatigue times at 50% MVIC as the box-and whisker diagrams for the results shown in Appendix L. Therefore, the results by this research methodology showed that 40 participants of age 18–35 with healthy knees have their fatigue times ranged between 41.6 and 78.8 seconds when performing 50% MVIC tasks.

Table 6.2 Summary of the torque values and fatigue times at 50% MVIC

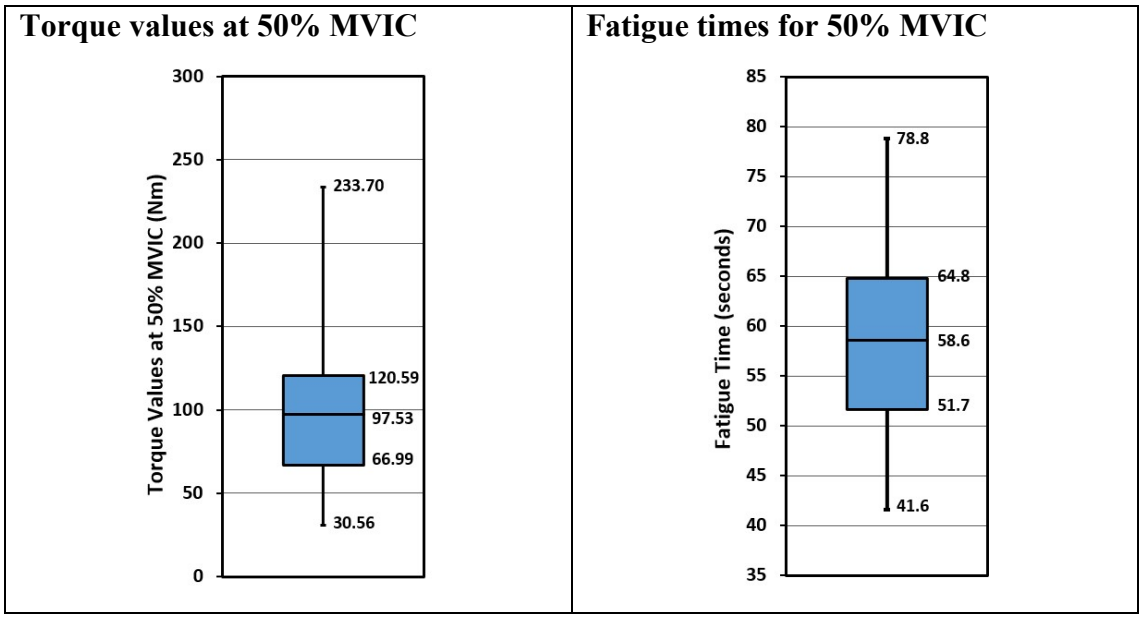

Appendix M includes the MNF and MFCV mean trend lines for each participant in terms of their fatigue times, for the:

- Lower quartile range
- Interquartile range
- Upper quartile range

The summary plots for the MNF and MFCV mean trend lines of each quartile range were also plotted and are included in Appendix M. These summary plots were redrawn for the mean trend lines values, each was normalized by taking the maximum values and equating them to a value of 1 (or 100%). To normalize the rest of the values for each mean trend line, the values were divided by the maximum value of that particular trend line. The normalized mean trend lines are also included in Appendix M. The significant benefit of normalization is the rescaling to a percentage of a reference value which is unique and standardized for all subjects within a study [143]. Normalization eliminates any varying influence of local signal detection conditions. It allows a direct quantitative comparison of sEMG findings between subjects [143]. The normalized plots show that there is very close correlation for both MNF and MFCV mean trend lines at the lower quartile, interquartile and upper quartile range of the different fatigue times.

By examining the individual mean trend lines of the MNF and MFCV for all participants, it was found that there are three significant regions, which are:

1. The initial region, which started from a maximum value and then dropped to a steady value.
2. The middle region, which was generally a steady value.
3. The final region, which dropped from a steady value to a point where fatigue had occurred.

Statistical analysis was performed on the mean trend lines of all 40 participants to produce the mean values for the following overall results:

1. The initial value of MNF dropped by 20.3% of the maximum value during the first 29.8% of the contraction period. The MFCV dropped by 20.9% of the maximum value during the first 28.2% of the contraction period.
2. The MNF value dropped by 17.4% in the final region where values dropped from steady values, whereas the MFCV value dropped by 18.1%.

Details of this statistical analysis data are included in Appendix N.

Chapter 7
Conclusion

The overall aim of the research reported in this thesis was to build a new multi-channel electrode and to investigate and develop signal processing techniques for sEMG signals in order to enable the extraction of more useful-features. Analysis of these signal features will assist in the creation of a more effective database for diagnosing muscle ailments and conditions.

After a thorough review of existing literature, a new multi-channel electrode was designed and built for this research. The literature review identified a number of different multi-channel electrodes that had been developed, none of which was commercially available. Hence a new design multi-channel electrode had to be built in order to collect more signals and which could be used in different configurations. The new multi-channel electrode has 11 pins and each is pre-amplified with a voltage gain of 484 and bandpass filtering from 6.8 Hz to 1.02 kHz to collect monopolar signals. The monopolar signals were then configured by the software as either *linear array* or *Laplacian* configuration. A better signal definition in terms of motor unit action potential was achieved with the Laplacian configuration.

This research used signals collected from the vastus lateralis muscle of the quadriceps of the dominant leg of 40 healthy participants performing an endurance (or fatiguing) task of 50% of their maximum voluntary isometric contraction (MVIC). The participants were aged between 18 and 35 years old with no previous knee injuries or ailments.

Before data collection, ethical approval was needed from the Auckland University of Technology Ethics Committee due to the involvement of human participants. In the application, a detailed testing protocol was described, including what physiological features were to be measured and recorded.

The data for the endurance task were acquired from 12 channels consisting one of from the load cell (shown as the force trace) and 11 monopolar signals from the newly designed multi-channel electrodes. A large amount data needed to be recorded and stored on a

laptop computer. For this purpose, a new data acquisition code was written in LabVIEW using a technique referred to as *producer/consumer loop* with a sampling rate of 10 kHz for a maximum of 120 seconds (2 minutes). The signals collected were analysed offline using a new developed algorithm with a sliding window technique, which passed through the signals to extract useful features or information for classification purposes.

A number of signal processing techniques were investigated to analyse the generated Laplacian signals in either the frequency, time or time-frequency domains. For classification purposes, a time-frequency technique domain was developed further and a new algorithm was written to extract signal features. These features were the mean frequency (MNF) and the median frequency (MDF) values from the power spectrum density. The sliding window that had the best time-frequency resolution, was a 1-second data window with 0.25-second overlap. Other temporal features, such as the root mean square (RMS) value of the signal and the muscle fibre conduction velocity (MFCV), were also determined for each window that was passed through the signals.

The MNF and MDF values showed the same trend through all the analysed signals. However, because the MNF trend line followed the measured values better than the MDF, the MNF was selected to be used for further statistical analysis. For the RMS values, the trend lines in all cases showed a linear increase from the muscle contraction until fatigue stage. However, there was no noticeable trend in the values and so RMS was not considered to be a useful feature to this research at this stage. The MFCV values showed similar trend lines to those of the MNF and MDF values. This indicated that these features were linked in terms of muscle fibre behaviour throughout the contraction time from the start of the endurance task to the finish.

Statistical analysis was performed on all 40 participants to produce the mean values for determining the range and fatigue times, and determine how much the MNF and MFCV values dropped over the contraction time. The results showed that fatigue times for the 40 participants ranged between 41.6 to 78.8 seconds when performing 50% MVIC. The mean trend lines of the MNF and MFCV features showed a drop in values in the initial and the final fatigue stage. The initial value of MNF dropped by 20.3% of the maximum value during the first 29.8% of the contraction period. The MFCV meanwhile dropped by 20.9% of the maximum value during the first 28.2% of the contraction period. The

MNF value dropped by 17.4% at the final fatigue stage, whereas the MFCV value dropped by 18.1%.

The testing protocol used for this research was limited to healthy participants from the age of 18 to 35. There is therefore a need for the future research to investigate (a) different age groups, (b) repeatability of the same group over period of time, and (c) participants with different muscle alignments. Due to the limited number of data available, the building of a database of sEMG signals from other specific muscles would be of great use for future researchers.

Using the mean trend lines, a future study could focus on the initial portion of the endurance task and use either the MNF or MFCV values, or both together, to predict the time of fatigue by performing the same task over a shorter period of time. This would avoid any possible discomfort and hence speed up the recovery time for the participant performing the task.

The signal processing techniques covered in this research show the global aspects of the muscle contraction in terms of spectral and temporal domains of the sEMG signals. It was found that MNF and MFCV were useful features. A potentially useful study would be to develop means for the observer to obtain more detailed information of how motor unit action potentials are activated during muscle contraction, or the so-called *'recruitment process'* which generates force. This could include Independent Component Analysis (ICA) and Principal Component Analysis (PCA) using the readily available data from this research from all the monopolar signals collected. The knowledge gained from this research therefore opens doors to whole new areas of research. Extracting more detail using ICA or PCA to find information about muscle contraction would be a potential tool to analyse the large datasets obtained from recording sEMG signals from multi-channel electrodes.

The new multi-channel electrode used in this this research had a fixed configuration in the number of pins, and inter-electrode distance with a sampling rate of 10 kHz. By changing these parameters, different or additional information may be produced by the muscle contraction being measured. Hence, a study in investigating these properties of sEMG signals would be potentially useful.

The signals generated were configured using different montages for spatial filtering of the monopolar signals as linear array or Laplacian configuration. Future work could be carried out to investigate different spatial filtering to determine which one is likely to give a better spatial selectivity of sEMG signals. In addition to the present weighting factor arrangement of the new multi-channel electrodes, other arrangements of weighting factors of filter masks and their effects on signals could also be explored.

In conclusion, this research has demonstrated methodologies that can be used for extracting features of sEMG signals and identified directions for future work in the field of signal classification.

Appendix A: Standards for Reporting EMG Data

Authors are advised that the following protocols must be observed and supplied in the Methods section of all submitted manuscripts. To avoid delay or return of manuscripts, the requirements below should be considered when preparing the manuscript.

Electrodes:

Reports on surface recording of EMG should include:

- electrode material (e.g., Ag/AgCl)
- electrode geometry (discs, bars, rectangular)
- size (e.g., diameter, radius, width, length)
- use of gel or paste, alcohol applied to cleanse skin, skin abrasion, shaving of hair, etc.
- inter-electrode distance
- electrode location, orientation over muscle with respect to tendons,
- motor point and fibres direction.

Intramuscular wire electrodes should be described by:

- wire material (e.g., stainless steel)
- if single- or multi-strand
- insulation material
- length of exposed tip
- method of insertion (e.g., hypodermic needle)
- depth of insertion
- if single or bipolar wire
- location of insertion in the muscle
- inter-electrode distance
- type of ground electrode used, location.

Needle electrodes and their application should be described and include material, size of conductive contact points at the tip, depth of insertion and accurate location in the muscle.

Amplification:

Amplifiers should be described by the following:

- if single, differential, double differential, etc.
- input impedance
- Common Mode Rejection Ratio (CMRR)
- signal-to-noise ratio
- actual gain range used.

Filtering of the raw EMG should be specified by:

- low- and/or high-pass filters
- filter types (e.g., Butterworth, Chebyshev, etc.)
- low- and/or high-pass cut-off frequencies.

Since the power density spectra of the EMG contains most of its power in the frequency range of 5-500 Hz at the extremes, the journal will not accept reports in which sEMG was filtered above 10 Hz as a low cut-off, and below 350 Hz as the high cut-off; e.g., 10-350 Hz is preferred for *surface* recording. Filtering in the band of 10-150 Hz or 50-350 Hz, for example, is not acceptable as portions of the signal's power above 150 Hz and below 50 Hz are eliminated. This should be kept in mind when designing a study's protocol. Exceptions will be made only in rare cases that carry full scientific justification.

Intramuscular recording should be made with the appropriate increase of the high frequency cut-off to a minimum 450 Hz. A bandpass filter of 10-450 Hz is therefore required.

Needle recording should have a bandwidth of 10-1,500 Hz.

Rectification: A note should be made if full or half-wave rectification was carried out.

EMG Processing:

There are several methods of EMG processing. *Smoothing* the signal with a low-pass filter of a given time constant (normally 50 to 250 ms) is best described as 'smoothing with a low-pass filter of *x* ms'. Alternatively, one can describe it as a 'linear envelope'

or ‘the Mean Absolute Value’, while giving time constant type and order of the low-pass filter used.

Also acceptable is determination of the root mean square (RMS). Authors should include the time period over which the average RMS was calculated.

Integrated EMG is sometimes reported, but the signal is actually integrated over time, rather than just smoothed. Such procedure allows observation of the accumulated EMG activity over time, and should be presented with information as to whether time or voltage was used to reset the integrator and at what threshold it was reset.

Power Density Spectra presentation of the EMG should include:

- time epoch used for each calculation segment
- type of windows used prior to taking the Fast Fourier Transform (FFT) (e.g., Hamming, Hanning, Tukey, etc.)
- taking the algorithm (e.g., FFT)
- number of zero padding applied in the epoch and the resultant resolution
- equation used to calculate the mean frequency (MNF) and the median frequency (MDF).
- the muscle length or fixed joint angle at the time of recording.

Other processing techniques, especially novel techniques, are encouraged if accompanied by full scientific description.

Sampling EMG into the Computer:

Computer processing of the EMG is encouraged if authors observe these important factors:

1. It is advisable that the raw EMG (e.g., after differential amplification and bandpass filtering) be stored in the computer before further analysis in case modification of the protocol is required in the future. In this case, the minimal acceptable sampling rate is at least twice the highest frequency cut-off of the bandpass filter, e.g., if a bandpass filter of 10-350 Hz was used, the minimal sampling rate employed to store the signal in the computer should be 700 Hz (350 × 2), and *preferably higher* to improve accuracy and resolution. Sampling rates below twice the highest frequency cut-off will not be accepted.

2. If smoothing, with a low-pass filter was performed with hardware prior to sampling and storing data in the computer, the sampling rate could be drastically reduced. Rates of 50-100 Hz are sufficient to introduce smoothed EMG into the computer.
3. It is also advisable that authors consider recording the raw EMG (prior to bandpass filtering) in the computer; in such cases a sampling rate of 2500 Hz or above could be used. Yet, to avoid aliasing of high-frequency noise, bandpass filtering (written in software) in the range prescribed above should be performed prior to any further processing of the signal. This approach allows authors to perform EMG recording with minimal hardware and maximal flexibility. Yet, it may be at the expense of computer memory space and speed.
4. Number of bits, model and manufacturer of A/D card used to sample data into the computer should be given.

Normalization:

In investigations where the force/torque was correlated to the EMG, it is common to normalize the force/torque and its respective EMG, relative to the values at maximal voluntary contraction (MVC). Authors should be aware that obtaining true MVC from participants requires some preliminary training. Without training, the MVC could be as much as 20-40% less of that obtained after appropriate training. The journal, therefore, will not accept reports in which participants were not properly trained to elicit true MVC.

Normalizing the force/torque with respect to its MVC is commonly performed with MVC as 100% of the force/torque, and other force levels are expressed as the appropriate percentage of MVC. Similarly, the EMG associated with 100% MVC is designated as 100%. Both force/torque and EMG normalization should include other relevant information such as joint angle(s) and/or muscle length(s) in isometric contractions, and range of joint angle, muscle length, velocity of shortening/elongation, and load applied for non-isometric contractions.

Normalization of data collected from one experimental condition with respect to other contractile conditions can be performed for comparative purposes and will be accepted by the journal only if full description is given.

In summary, the following information should be provided when normalizing data:

- how participants were trained to obtain MVC
- joint angle or muscle length
- angles of adjoining joint, e.g., for studies on elbow flexion, the position of the wrist and shoulder joints should be provided
- rate of rise of force
- velocity of shortening/elongation
- changes in muscle length
- ranges of joint angle/muscle length in non-isometric contraction
- load applied in non-isometric contractions.

EMG Cross-talk:

Authors should demonstrate that significant effort was made to determine that EMG cross-talk from muscles near the muscle of interest did not contaminate the recorded signal. Selecting the appropriate electrode size, inter-electrode distance and location of recordings over the muscle should be carefully planned, especially when working on area where many narrow muscles are tightly gathered (e.g., forearm), or when working with superficial/thin muscles (e.g., trapezius). The work of Winter, et al.[3] and Fuglevand, et al.[1] should be consulted if doubts exist. Care also should be employed when recording surface EMG from areas with subcutaneous adipose tissue as it is known that adipose tissue enhances cross-talk[2] (e.g., abdomen, buttocks, chest, etc.).

[1] Fuglevand AJ, Winter DA, Patala AE, Stashuk D. Detection of motor units' action potentials with surface electrodes - influence of electrode size and spacing, Biological Cybernetics 1992; 67:143-153.

[2] Solomonow M, Baratta R, Bernardi M, Zhou B, Lu Y, Zhu M, Acierno S. Surface and wire EMG, crosstalk in neighbouring muscles, Journal of Electromyography and Kinesiology 1994; 4:131-142.

[3] Winter DA, Fuglevand AJ, Archer SE. Crosstalk in surface electromyography: theoretical and practical estimates, Journal of Electromyography and Kinesiology 1994; 4:15-26.

Appendix B: Design of New Multi-Channel Electrode

The reason for using an instrumentation amplifier (in-amp) for the preamplifier circuit of each electrode is in-amps are precision gain blocks that have a differential input and an output [204; Chapter 2], which may be configured either as bipolar (differential) or monopolar (single-ended with respect to a reference terminal). These devices amplify the difference between two input signal voltages while rejecting any signals that are common to both inputs. In-amps are widely used in many industrial, measurement, data acquisition, and medical applications where DC precision and gain accuracy must be maintained within a noisy environment, such as when large common-mode signals are present with the ac power line frequency of either 50 Hz or 60 Hz. Additional advantages of using in-amps include producing a very low DC offset, low noise and very high input impedance, which is suitable for dealing with small bioelectrical signals generated from the muscle.

The design specification for the in-amp was set to have a lower cut-off frequency of 5 Hz and an upper cut-off frequency of 1 kHz with a gain of 500 [136; Chapter 4]. There were three possible in-amps available to use; INA118, INA128 and INA333. The INA118 was selected as the most suitable out of the three possible in-amps because:

- With simulations, INA118 has an upper cut-off frequency of 13.82 kHz at -3dB gain which covers all the frequencies up to 1 kHz, meaning it meets the requirements of the design specification. INA128 in this case also meets the design specification with an upper cut-off frequency 47.32 kHz, but not INA33, as it only goes up to 770 Hz, which is less than 1 kHz.
- INA118 has quiescent current and requires lower supply voltage than INA128, which is ideal for a stand-alone battery-powered operated device and limits electrical noises from the mains and surroundings.

Figure B.1 shows the basic connections of the INA118 taken from datasheet, which is available from the Texas Instruments website [205].

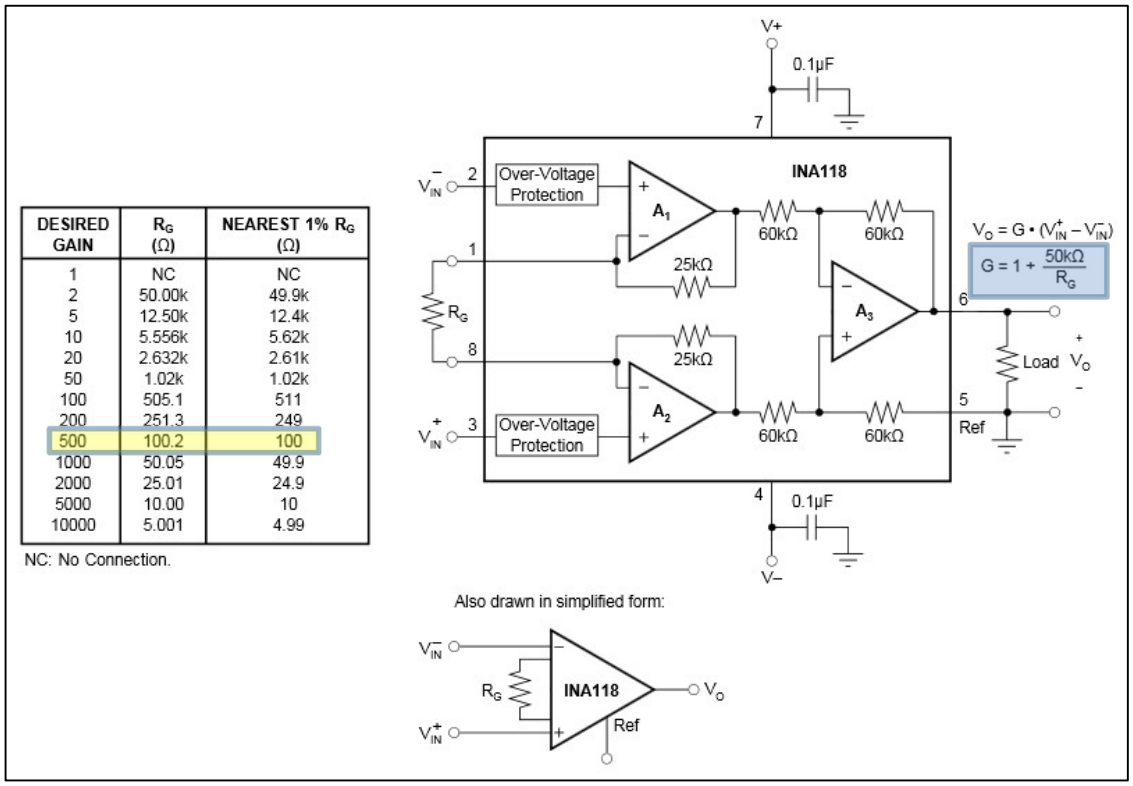

DESIRED GAIN	R_G (Ω)	NEAREST 1% R_G (Ω)
1	NC	NC
2	50.00k	49.9k
5	12.50k	12.4k
10	5.556k	5.62k
20	2.632k	2.61k
50	1.02k	1.02k
100	505.1	511
200	251.3	249
500	100.2	100
1000	50.05	49.9
2000	25.01	24.9
5000	10.00	10
10000	5.001	4.99

NC: No Connection.

Figure B.1 Image taken from the INA118 datasheet showing the basic connection for the INA118. The table shows commonly used gains and the resistor values needed for R_G.

A resistor value R_G needs to be determined for INA118 in order to produce a set amount of gain. The gain was set to the highest value possible without saturating the output of the amplifier, which in this case was 500 (53.96 dB). From the table in Figure B.1, the resistance value shown highlighted in yellow box to achieve the gain of 500 is 100.2 Ω. The use of a 100 Ω resistor is therefore best for this purpose. The equation given in the datasheet for calculating the gain of the in-amp is determined by using equation (1), highlighted in the blue box in Figure B.1:

$$G = 1 + \frac{50\ k\Omega}{R_G} \tag{1}$$

so substituting R_G = 100 Ω into equation (1), the gain is:

$$G = 1 + \frac{50\ k\Omega}{R_G} = 1 + \frac{50,000}{100} = 501\ (53.99dB \quad 54dB$$

With the gain set at 501 (or 54 dB), the circuit as in Figure B.2 (a), was placed in TINA-TI simulation software and the frequency response curve was produced as shown in Figure B.2 (b). The circuit created a low-pass filter effect with an upper cut-off

frequency at 13.8 kHz. The circuit was then built on a prototype board and the values for gain were measured and calculated at fixed frequency values. Figure B.2 (c) shows both the simulated and the measured values.

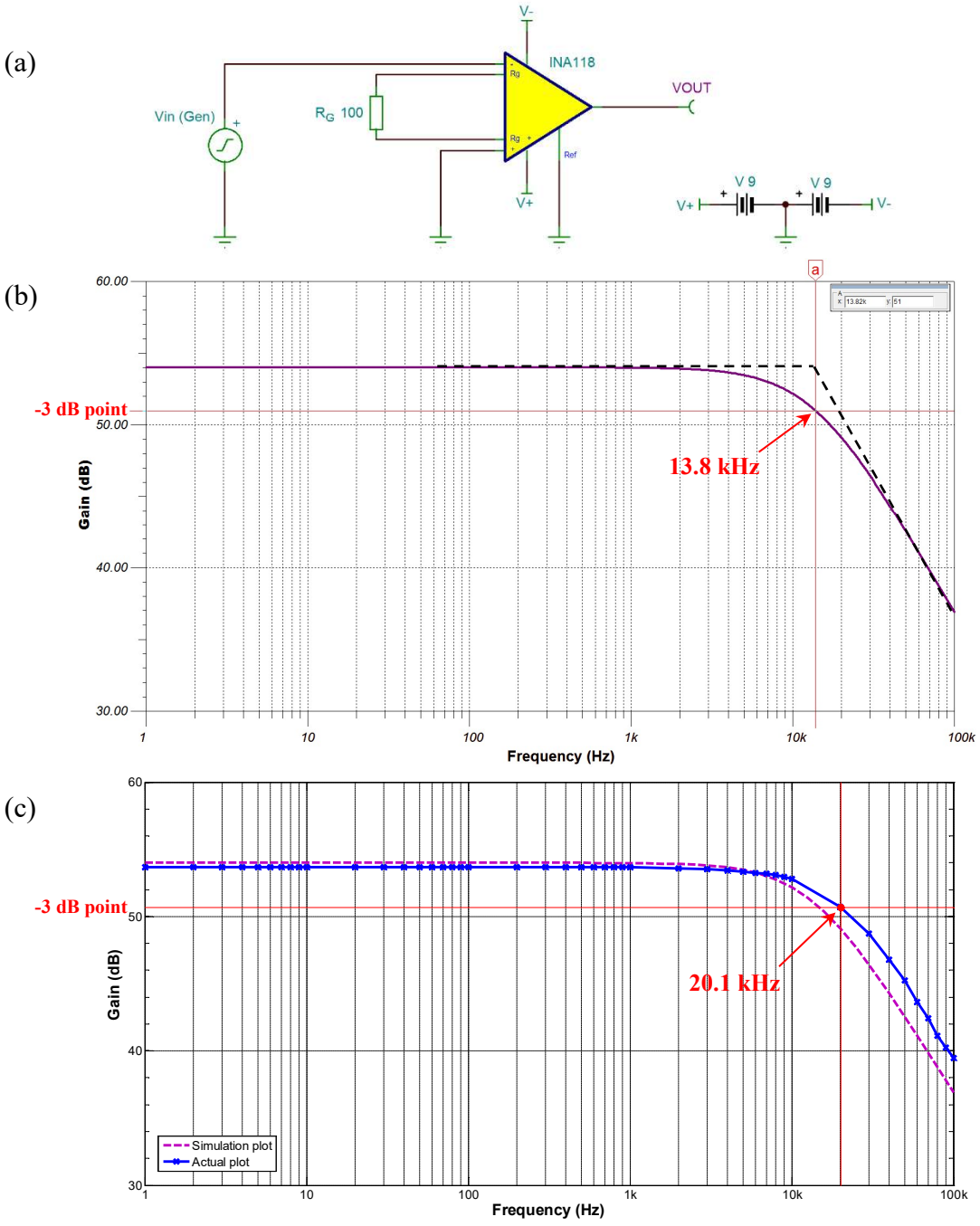

Figure B.2 (a) TINA-TI simulation circuit. (b) Gain-frequency response plot showing the maximum gain of 501 (54 dB) and an upper cut-off frequency of 13.8 kHz at -3dB with a -20 dB/decade roll-rate, shown by black dotted line. (c) Plot shows gain-frequency response for both simulated and measured values. The measured values have a maximum gain of 484 (53.7 dB) with an upper cut-off frequency of 20.1 kHz at -3dB with a -20 dB/decade roll-rate.

The simulated and measured values vary marginally due to the component value for R_G not being precisely 100 Ω. The measured values showed the maximum gain was 484 (53.7 dB) with an upper cut-off frequency of 20.1 kHz, as shown in Figure B.2 (c).

Since all bioelectrical signals have a small DC offset component, saturation of the output signal is likely to occur when amplified. The DC component values found in the signal from sEMG can range from 10 µV to 100 mV, which when amplified with a gain of 500 will be 5 mV to 50 V. This will saturate at 18V, as indicated in the INA118 product's 'Features' list shown in Figure B.3 highlighted in yellow box, where its wide supply range used can be from ±1.35 to ±18 V.

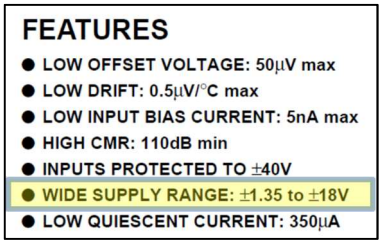

Figure B.3 Electrical features of INA118 amplifier taken from the datasheet.

As the gain in Figure B.2 is purely resistive, the way to remove any DC component of the input signal is to add a high-pass filter to the input of the in-amp [206; Chapter 1], but this is not a reliable method and so it may still be amplified. To ensure the DC offset is not amplified by the in-amp, a capacitor C_G is added in series with resistor R_G to form a complex impedance gain (Z_G) that will act as a high-pass filter for setting the gain of the in-amp as shown in Figure B.4.

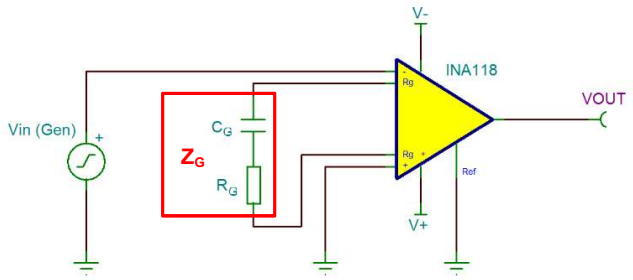

Figure B.4 Shows the complex impedance (Z_G) components, consisting of a resistor (R_G) in series with a capacitor (C_G).

So the impedance gain (Z_G) of the in-amp is set by,

$$Z_G = R_G + X_{CG} \tag{2}$$

where $X_{CG} = \frac{1}{2\pi f C_G}$, so

$$Z_G = R_G + \frac{1}{2\pi f C_G} \tag{3}$$

The transfer function for the circuit can be shown to be given by equation (4):

$$H(f) = 1 + \frac{2\pi f R_1 C_G}{2\pi f R_G C_G + 1} \tag{4}$$

The magnitude response of the transfer function from equation (4) was plotted using MATLAB and this is shown in Figure B.5. The value R_1 = 50 kΩ is taken from equation (1), where R_G = 100 Ω and C_G = 300 µF.

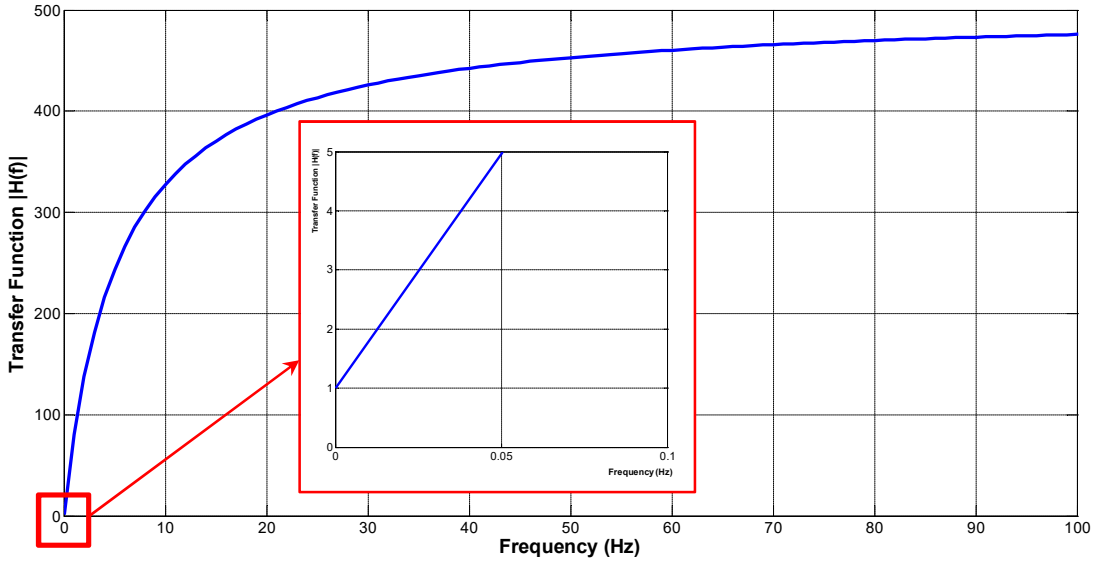

Figure B.5 Magnitude response curve for the transfer function given in equation (4) using values of R_1 = 50 kΩ, R_G = 100 Ω and C_G = 300 µF.

With a complex impedance Z_G, the magnified view of the plot for the transfer function in Figure B.5 shows the gain at 0 Hz has a magnitude of 1, which will allow any DC offset component of the sEMG signal to pass through the circuit without being amplified. Hence later processing by demeaning the signal will remove any DC value that may exist from the original sEMG signal of the muscle.

The circuit in Figure B.6 (a) shows the similar circuit of Figure B.3 with the added value of complex impedance gain Z_G consisting of a 100 Ω resistor in series with a 100 µF capacitor. The circuit were then placed in TINA-TI simulation software and the frequency response curve was produced as shown in Figure B.6 (b).

(a)

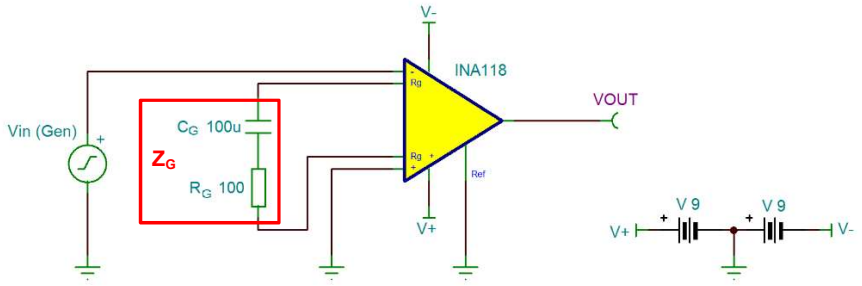

(b)

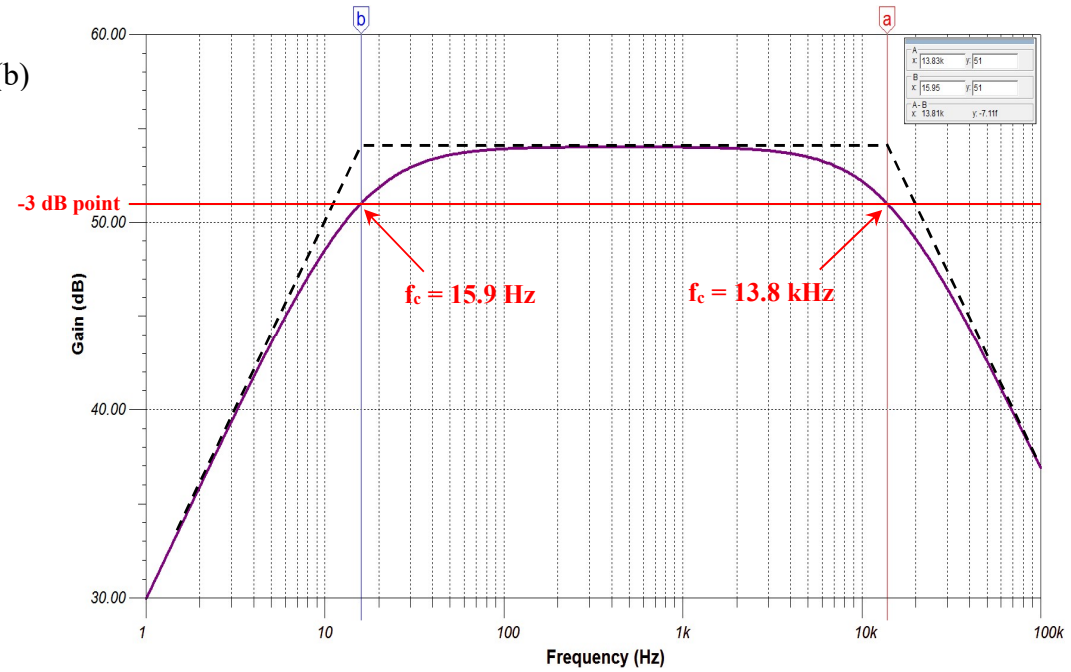

Figure B.6 (a) TINA-TI simulation circuit. (b) Gain-frequency response plot. The upper cut-off frequency remained the same at 13.8 kHz and the maximum gain is 501 (54 dB), as shown in Figure B.2 (b). The complex impedance Z_G has created a high-pass filter effect with a lower cut-off frequency of 15.9 Hz at -3dB with a +20 dB/decade roll-rate.

It was mentioned earlier that the overall design specification requirements of the frequency range for the new preamplifier are to have a lower cut-off frequency at 5 Hz and an upper cut-off frequency of 1 kHz. The complex impedance Z_G for the gain setting created a high-pass filter. To achieve the lower cut-off frequency of 5 Hz, the capacitor values or capacitance can be altered while the resistor value or resistance is kept constant at 100 Ω to maintain the gain of 501 (54 dB). Capacitance was therefore increased from 100 µF to 200 µF and finally to 300 µF. The simulated results using TINA-TI software for 200 µF and 300 µF capacitors showed that both the upper cut-off frequency remained constant at 13.8 Hz with both capacitance values. The lower cut-off frequency was reduced to 7.9 Hz using a 200 µF capacitor, and 5.3 Hz using a capacitor 300 µF. Figures B.7 and B.8 show the use of 200 µF and 300 µF capacitors with their gain-frequency response plots respectively.

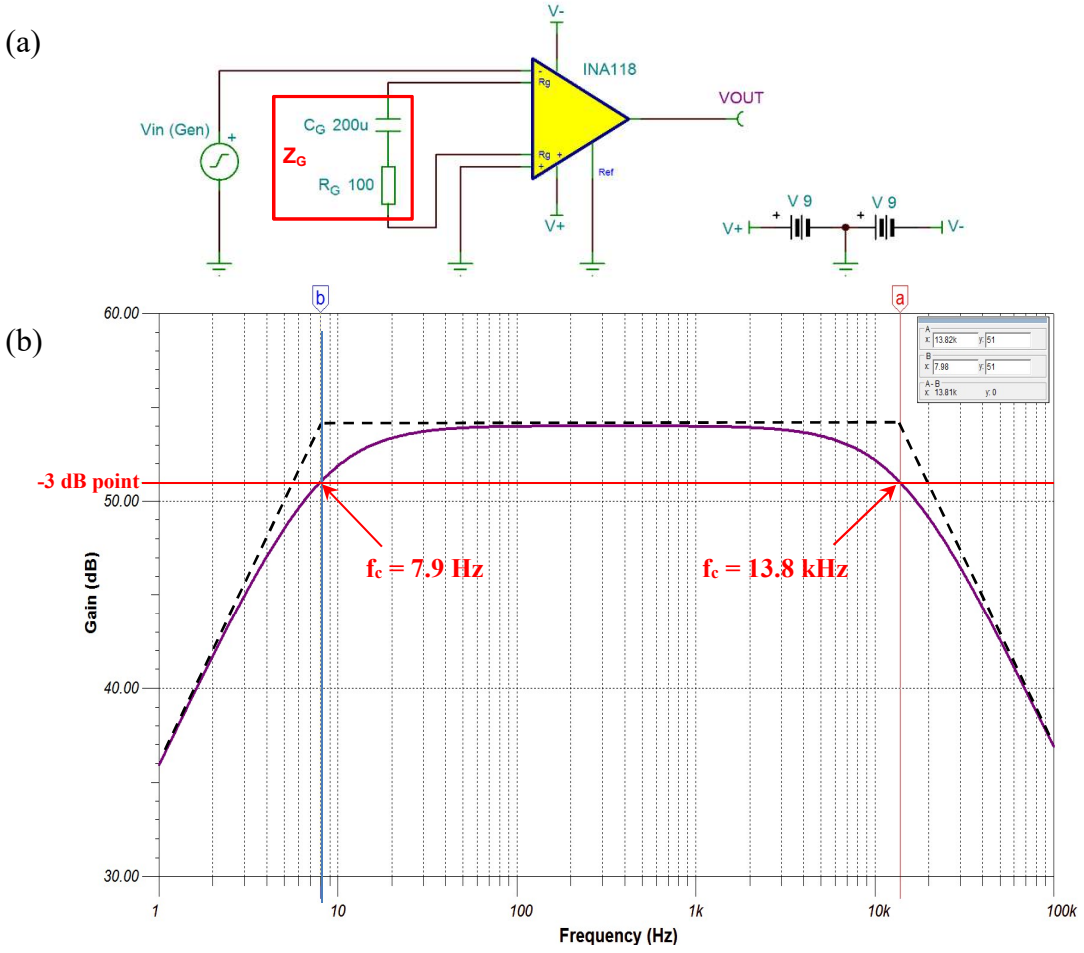

Figure B.7 (a) TINA-TI simulation circuit. (b) Gain-frequency response plot. The upper cut-off frequency remained the same at 13.8 kHz and the maximum gain is 501 (54 dB) as shown in Figure B.2 (b). The complex impedance Z_G has created a high-pass filter effect with a lower cut-off frequency of 7.9 Hz at -3dB with a +20 dB/decade roll-rate.

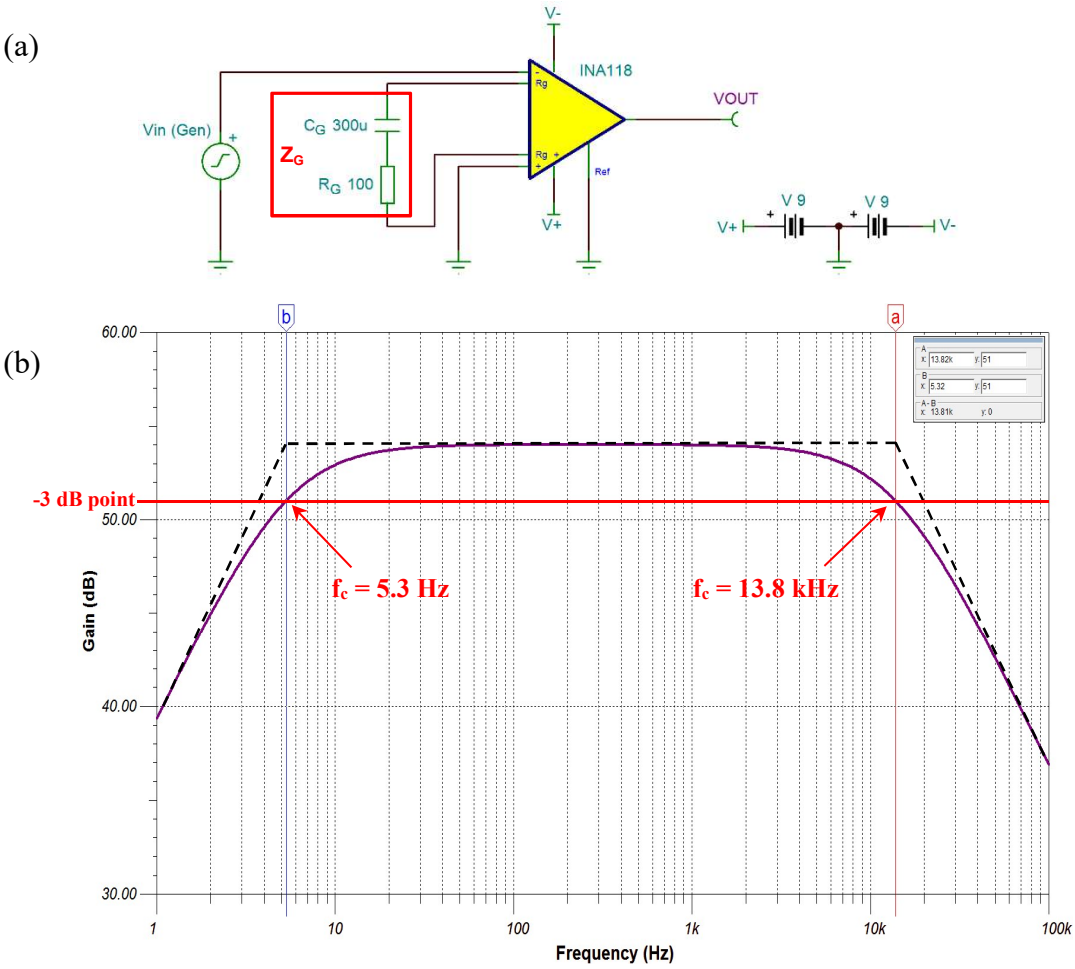

Figure B.8 (a) TINA-TI simulation circuit. (b) Gain-frequency response plot. The upper cut-off frequency remained the same at 13.8 kHz and the maximum gain is 501 (54 dB) as shown in Figure B.2 (b). The complex impedance Z_G has created a high-pass filter effect with a lower cut-off frequency of 5.3 Hz at -3dB with a +20 dB/decade roll-rate.

The next step was to add another filter in order to achieve an upper cut-off frequency of 1 kHz, so any frequency above this would be attenuated. This is done by adding a passive low-pass RC filter [44; Chapter 3] to the in-amp circuit, as in Figure B.9 (a).

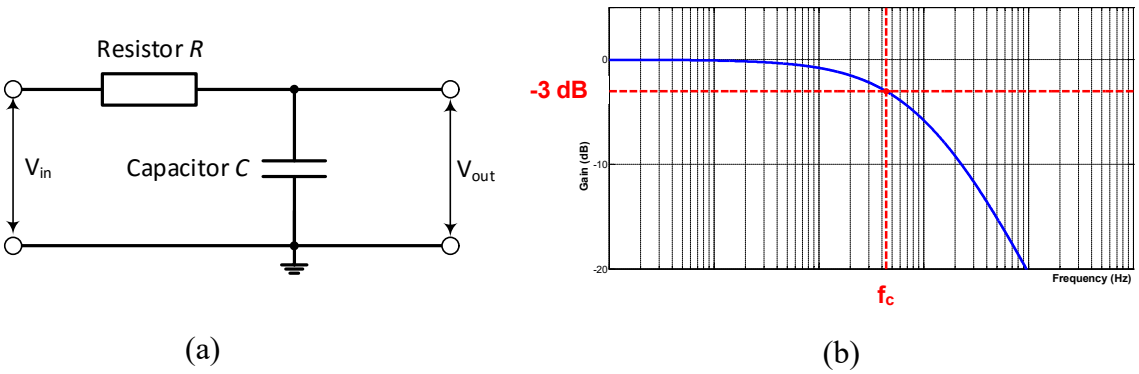

(a) (b)

Figure B.9 (a) The circuit and (b) frequency response plot for a RC low-pass filter.

The cut-off frequency (f_c) is determined by using the standard RC passive filter formula given by equation (5):

$$f_c = \frac{1}{2\pi RC} \tag{5}$$

This type of filter is generally known as a *first-order filter* or *one-pole filter* with a roll rate of ± 20 dB/decade as it has only one reactive component, which is the capacitor in the circuit [206; Chapter 1].

To ensure the filter has little or no loading effect on the amplifier, the value of the capacitor must be kept extremely low. For this amplifier, the capacitor was set at 100 ηF. By rearranging equation (5), it is possible to calculate a suitable resistor value to give a cut-off frequency (f_c) of 1 kHz:

$$R = \frac{1}{2\pi C f_c} \tag{6}$$

so C = 100 ηF and f_c = 1 kHz, then R is:

$$R = \frac{1}{2\pi \times 100 \times 10^{-9} \times 1 \times 10^{3}} = 1591\ \Omega$$

The nearest available lowest resistor is 1.5 kΩ, anything greater than the calculated value will give a cut-off frequency less than 1 kHz. So the new value for f_c using equation (3) is calculated to be:

$$f_c = \frac{1}{2\pi \times 1.5 \times 10^{3} \times 100 \times 10^{-9}} = 1061\ \text{Hz} = 1.06\ \text{kHz}$$

which is sufficiently close to the set 1 kHz for the upper cut-off frequency of the in-amp INA118. Hence R_{lpf} is 1.5 kΩ and C_{lpf} is 100 ηF.

The low-pass filter was placed before the in-amp as shown in Figure B.10 (a). The indicated values of R_{lpf} and C_{lpf} respectively correspond to the R and C in equation (5). The frequency response plot in Figure B.10 (a) is shown in Figure B.10 (b) using the simulation software TINA-TI.

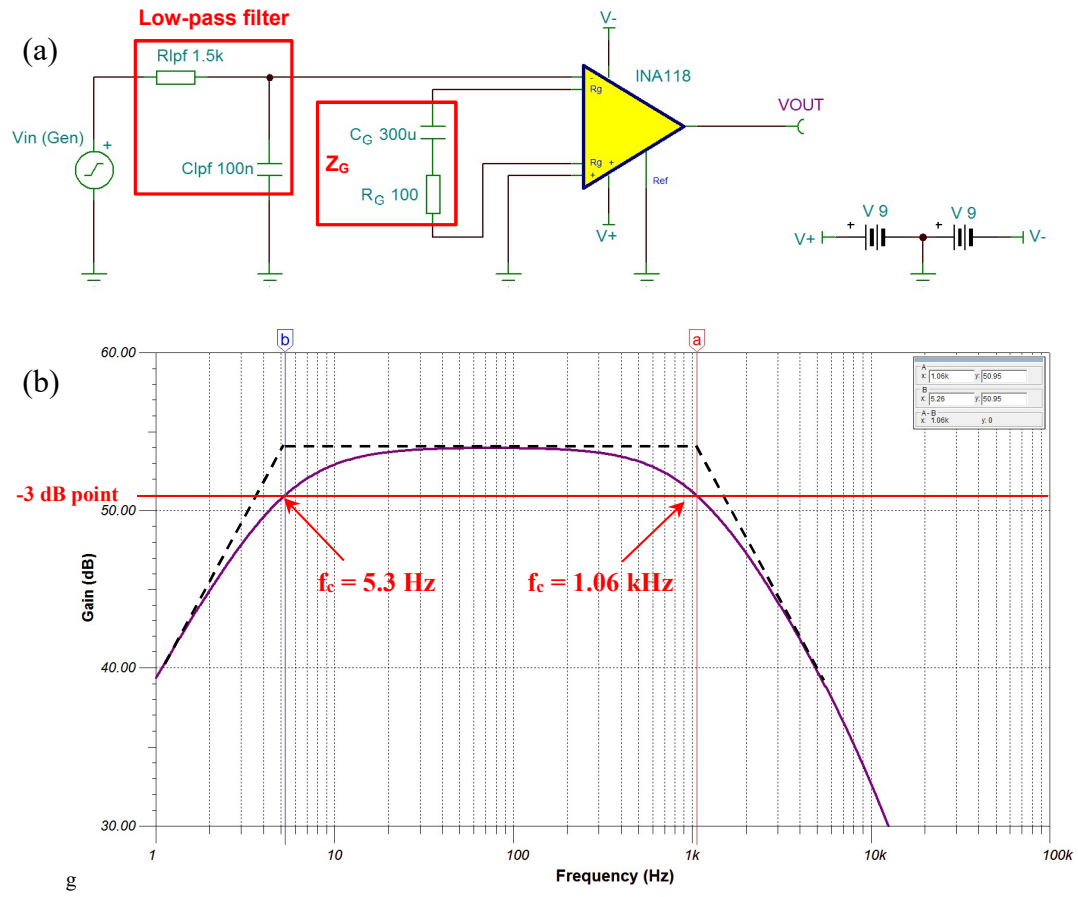

Figure B.10 (a) TINA-TI simulation circuit. (b) Gain-frequency response plot. The lower cut-off frequency remained the same at 5.3 Hz as shown in Figure B.8 (b). The low-pass filter has reduced the upper cut-off frequency to 1.06 kHz at -3dB with a -20 dB/decade roll-rate and the gain has dropped to 498 (53.95 dB).

The transfer function for the circuit can be shown to be given by equation (7):

$$H(f) = \left[\frac{1}{2\pi f R_{lpf} C_{lpf} + 1}\right]_{lpf} \left[1 + \frac{2\pi f R_1 C_G}{2\pi f R_G C_G + 1}\right]_{int-a} \tag{7}$$

The last step was to add a high-pass filter in order to achieve a steeper roll-rate of +40 dB/decade for a cut-off frequency of 5 Hz, so any frequency below this would be attenuated. This was done by adding a passive high-pass RC filter [44; Chapter 3], as shown in Figure B.11 (a).

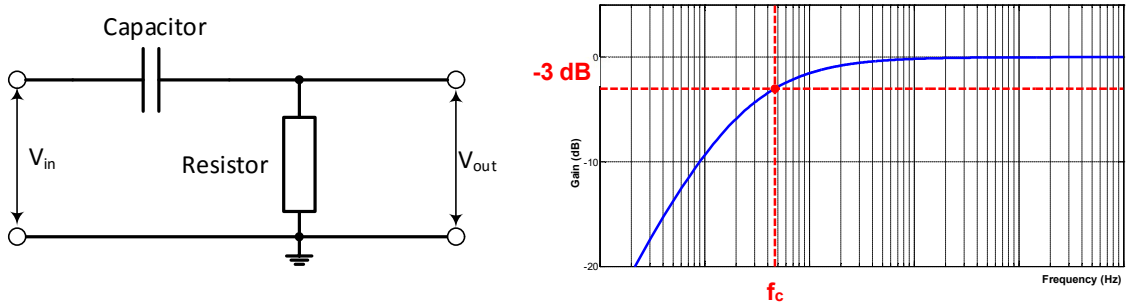

(a) (b)

Figure B.11 (a) The circuit and (b) frequency response plot for a RC high-pass filter.

To ensure the filter has little or no loading effect on the data acquisition output signal from the preamplifier circuit (discussed further in Chapter 4), the value of the resistor must be kept extremely low. The aim of this filter was to obtain a steeper roll rate of +40 dB/decade and to maintain the lower cut-off frequency at 5 Hz. This filter together with the high-pass filter effect from the complex impedance made the high-pass filter of the overall circuit a *second-order filter* or *two-pole filter*. By trial and error, the values used for the resistor and capacitor were set at 100 µF and 820 Ω respectively. Using the standard RC passive filter given by equation (5), the cut off-frequency was calculated to be:

$$f_c = \frac{1}{2\pi \times 820 \times 100 \times 10^{-6}} = 1.94 \text{ Hz}$$

The high-pass filter was placed at the output of the circuit, and the simulation of the circuit in Figure B.12 (a) was carried out using TINA-TI software with the indicated values of R_{hpf} and C_{hpf}, which respectively correspond to the R and C in equation (5). The simulated frequency response plot in Figure B.12 (b) shows the lower cut-off frequency of the circuit changed marginally from 5.3 Hz to 5.8 Hz, with an improved roll-rate of +40 dB/decade at -3 dB point.

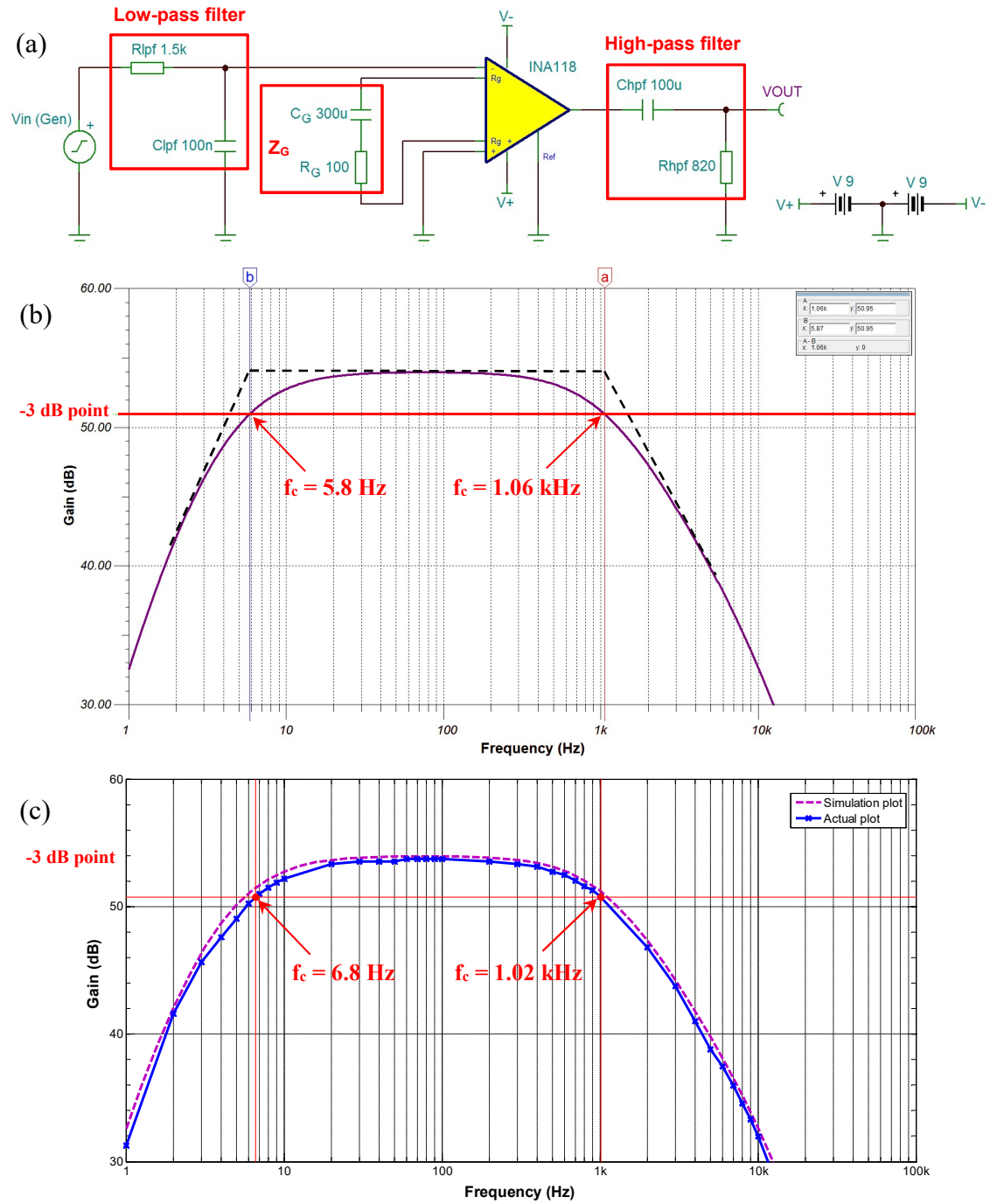

Figure B.12 (a) TINA-TI simulation circuit. (b) Gain-frequency response plot showing the gain has dropped to 498 (53.95 dB), the lower cut-off frequency is 5.8 Hz at -3 dB with a roll-rate of +40 dB/decade and the upper cut-off frequency is 13.8 kHz at -3dB with a -20 dB/decade roll-rate, both shown by black dotted lines. (c) Plot showing gain-frequency response for both simulated and measured values. The measured values have a maximum gain of 484 (53.7 dB) with a lower cut-off frequency of 6.8 Hz and an upper cut-off frequency of 1.02 kHz.

The simulated and measured values varied marginally due to the component values for the complex gain and both the filters not being precisely what is stated. The measured

values showed the maximum gain was 484 (53.7 dB) with a lower cut-off frequency of 6.8 Hz and an upper cut-off frequency of 1.01 kHz, as shown in Figure B.12 (c).

The transfer function for the circuit can be shown to be given by equation (8):

$$H(f) = \left[\frac{1}{2\pi f R_{lpf} C_{lpf} + 1}\right]_{lpf} \left[1 + \frac{2\pi f R_1 C_G}{2\pi f R_G C_G + 1}\right]_{int-a} \quad \left[\frac{2\pi f R_{hpf} C_{hpf}}{2\pi f R_{hpf} C_{hpf} + 1}\right]_{hpf} \tag{8}$$

Appendix C: New Multi-Channel Electrode Drawings

The new multi-channel electrode consists of two main components:

1. Electrode and preamplifier unit
2. Battery power supply unit

C.1 Electrodes and Preamplifier Unit

The following figures show the schematics of the printed circuit boards for the electrodes and preamplifiers. Figure C.1 (a) shows the schematic for a single preamplifier circuit and (b) shows the connections of all of the preamplifiers to the electrode pins. The preamplifiers are encased, indicated by the green box, where each preamplifier channel (CH1-CH11) connects to an electrode pin (labelled A-K).

(a)

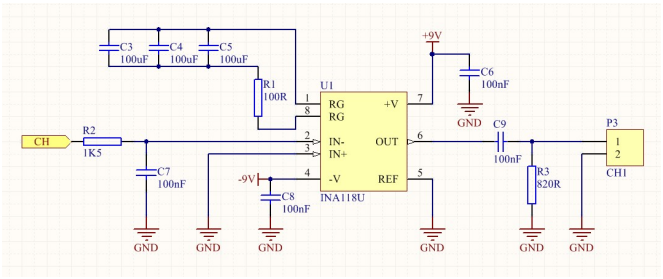

(b)

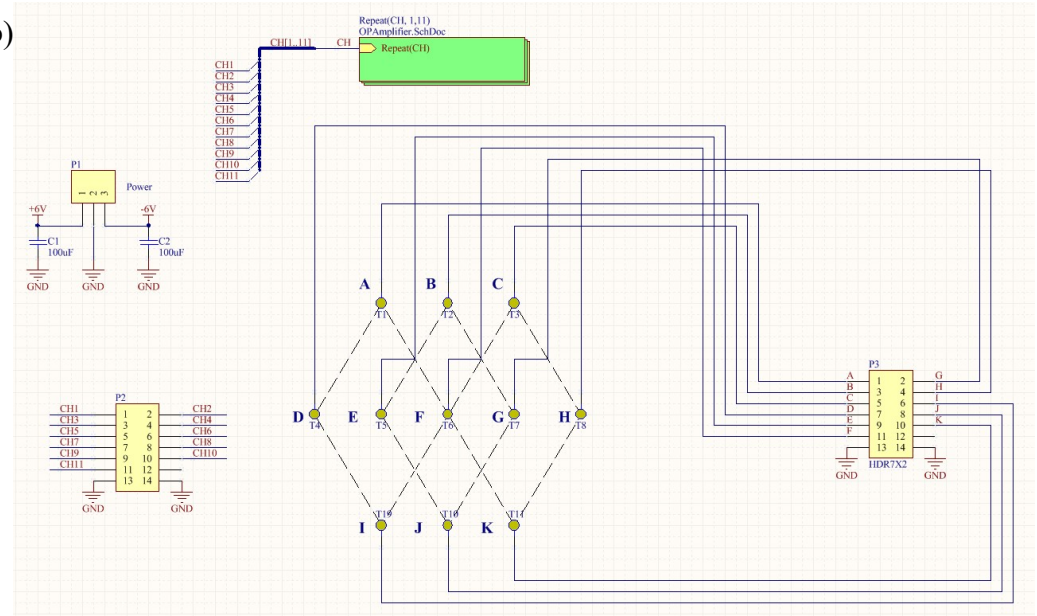

Figure C.1 (a) Schematic of a single preamplifier circuit. (b) Overall schematic circuit for the new multi-channel electrode.

Figure C.2 shows the two separate printed circuit boards for the multi-channel electrode (a) preamplifier board and (b) surface electrodes board. The final assembly of boards (a) and (b) is shown in (c).

(a)

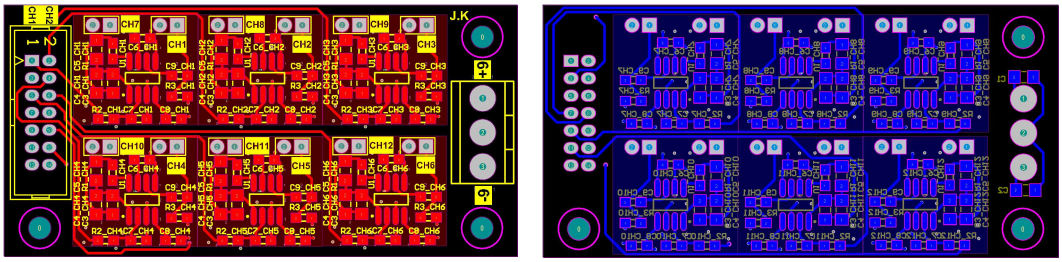

Top layer Bottom layer

(b)

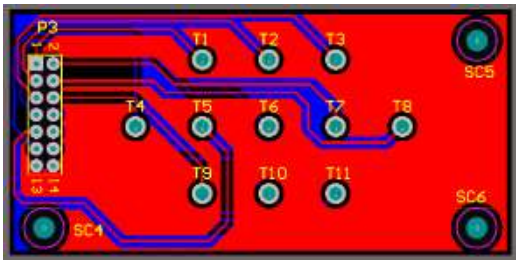

(c)

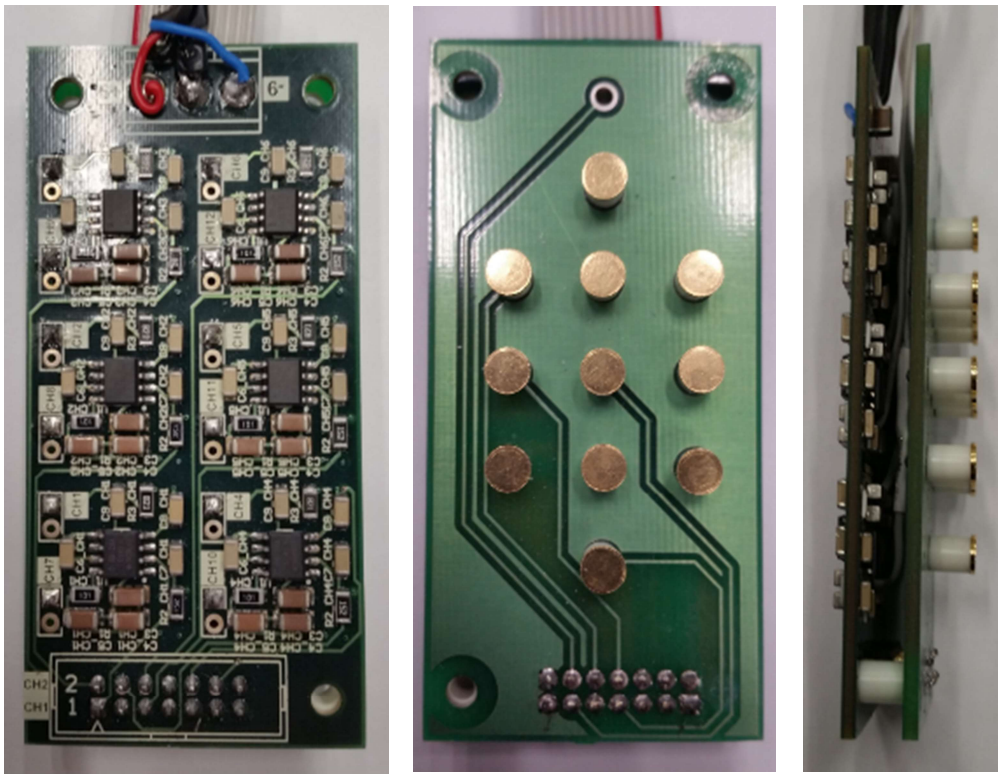

Figure C.2 The printed circuit boards for the (a) preamplifier, (b) electrodes and (c) the final assembled boards for the multi-channel electrode unit.

Figure C.3 shows the (a) SolidWorks drawing and (b) the assembled multi-channel electrode.

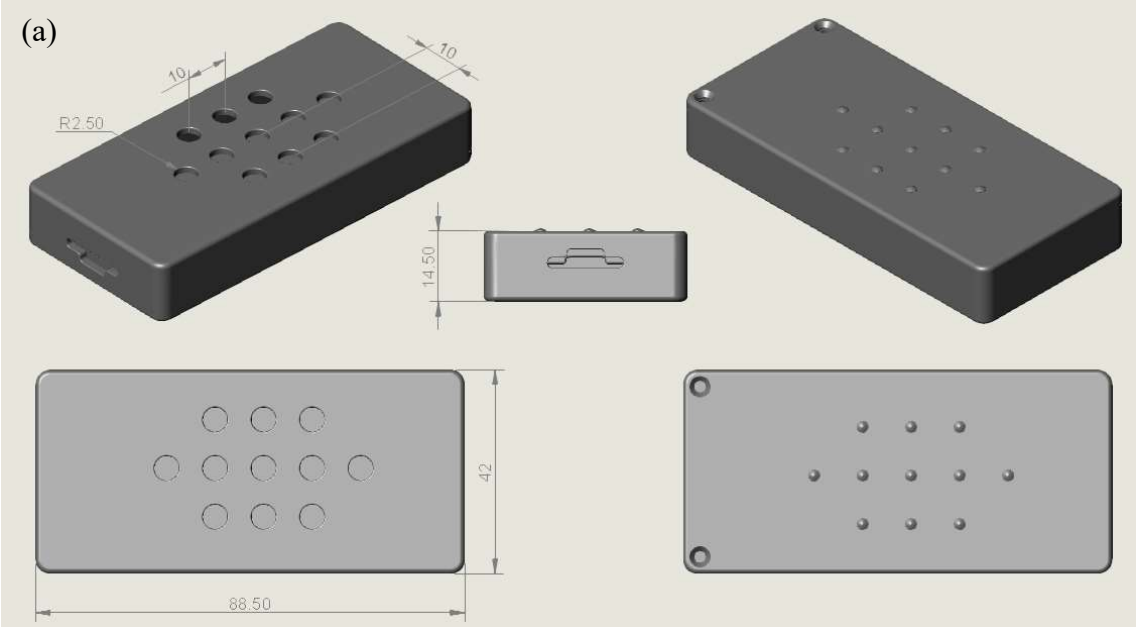

(b)

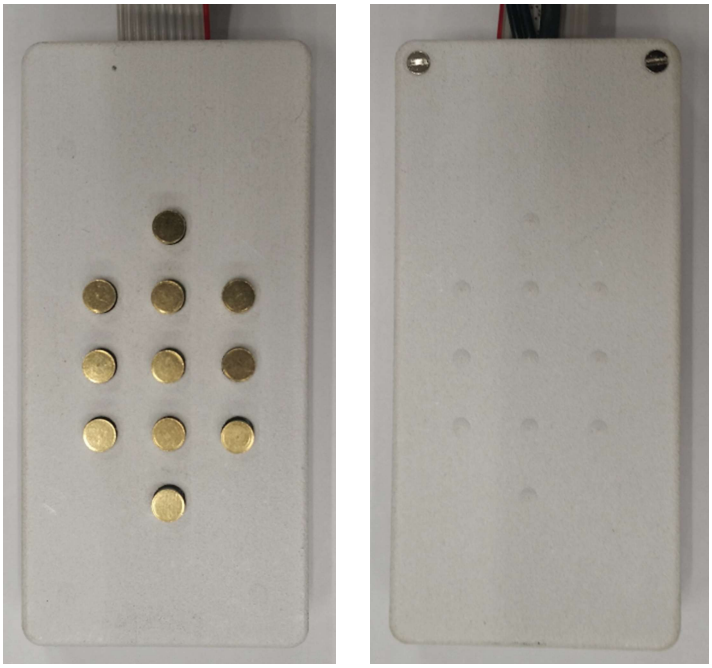

Figure C.3 (a) SolidWorks drawings. (b) Final assembly of the multi-channel electrode unit.

C.2 Power Supply Unit

Figure C.4 shows the voltage regulator printed circuit board for the separate battery power supply unit for the multi-channel electrode. The board ensures the regulated DC supply of ± 6 V is supplied to the preamplifier circuits.

(a)

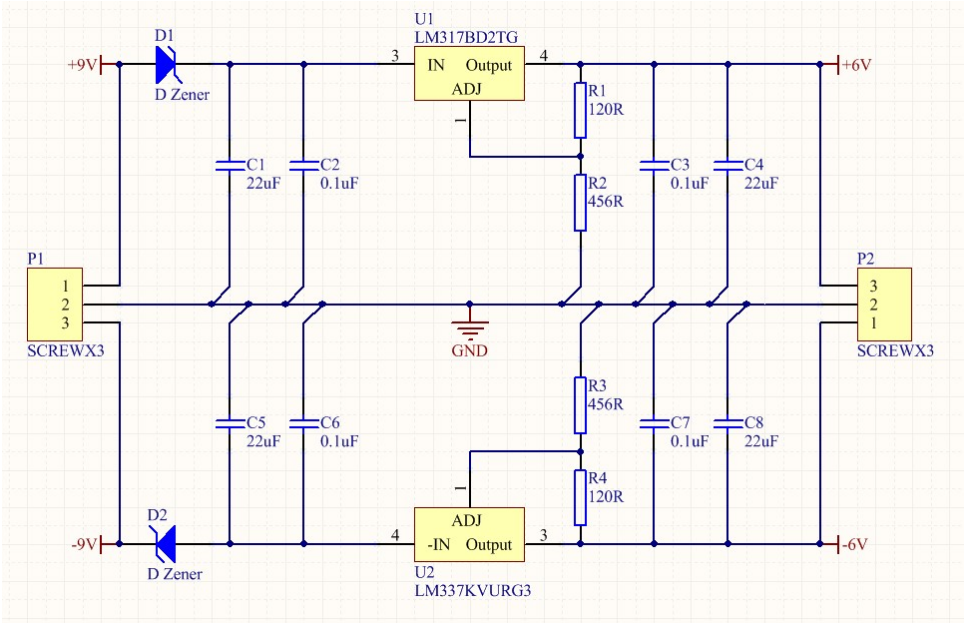

(b)

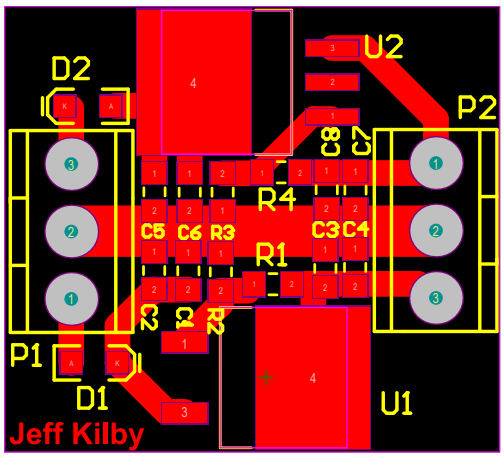

(c)

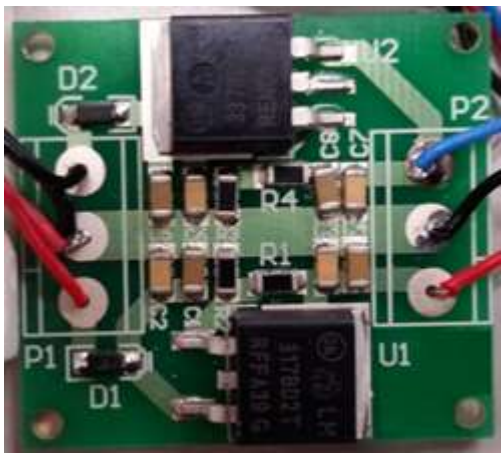

Figure C.4 (a) Schematic diagram, (b) printed circuit board layout diagram and (c) final assembled board for the voltage regulator of the stand-alone power supply unit.

Figure C.5 shows the (a) SolidWorks drawing and (b) the actual assembled unit for battery supply, which houses two standard PP3 9 V batteries and a voltage regulator.

(a)

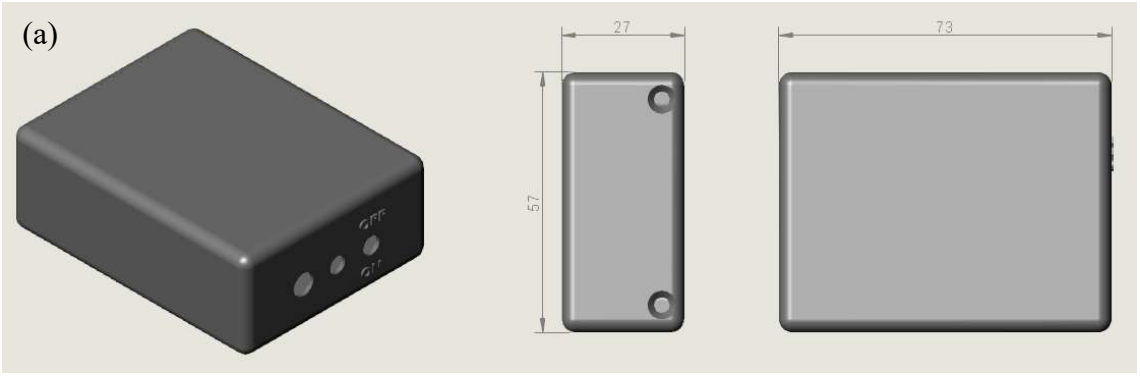

(b)

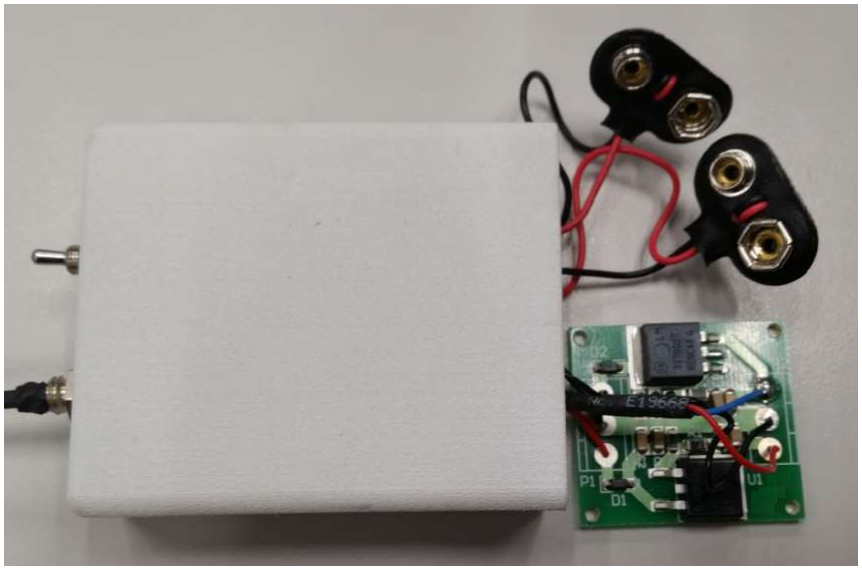

Figure C.5 (a) SolidWorks drawings. (b) Final assembly of the stand-alone battery power supply.

Appendix D: Approval Forms for Data Collection

Section D–1: Completed Auckland University of Technology Ethics Committee Application Form (EA1)

Section D–2: Participant Information Sheet

Section D–3: Consent Form

Section D–4: Advertising Poster

Section D–5 Acceptance Letter Granting Ethical Approval

Section D–1: Completed Auckland University of Technology Ethics Committee Application Form (EA1)

Auckland University of Technology Ethics Committee (AUTEC)

EA1

APPLICATION FOR ETHICS APPROVAL FOR RESEARCH PROJECTS

AUT UNIVERSITY
TE WĀNANGA ARONUI O TAMAKI MAKAU RAU

12/49

Comprehensive information about AUT's ethics approval processes may be found online at http://www.aut.ac.nz/research/research-ethics/ethics. Please read the notes at the end of the form before submitting this application.

A. General Information

A.1. Project Title

If you will be using a different title in documents to that being used as your working title, please provide both, clearly indicating which title will be used for what purpose.

Collection and Classification of Surface Electromyography Signals

A.2. Applicant Name and Qualifications

When the researcher is a student (including staff who are AUT students), the applicant is the principal supervisor. When the researcher is an AUT staff member undertaking research as part of employment or a staff member undertaking research as part of an external qualification, the applicant is the researcher. Staff should refer to Section 11.4 of Applying for Ethics Approval: Guidelines and Procedures *to check requirements for ethics approval where they are studying at another institution.*

Professor Krishnamachar Prasad

A.3. Applicant's School/Department/Academic Group/Centre

School of Engineering/Department of Electrical and Electronics/ Signal and Systems Group

A.4. Applicant's Faculty

Design and Creative Technologies

A.5. Student Details

Please complete this section only if the research is being undertaken by a student as part of an AUT qualification.

A.5.1. Student Name(s):

Jeffrey Kilby

A.5.2. Student ID Number(s):

0015566

A.5.3. Completed Qualification(s):

Master in Engineering (Honours)

A.5.4. E-mail address:

jkilby@aut.ac.nz

A.5.5. School/Department/Academic Group/Centre

School of Engineering/Department of Electrical and Electronics/Signal and Systems Group

A.5.6. Faculty

Design and Creative Technologies

A.5.7. Name of the qualification for which this research is being undertaken:

PhD

A.5.8. Research Output

Please state whether your research will result in a thesis or dissertation or a research paper or is part of coursework requirements.

Thesis

A.6. Details of Other Researchers or Investigators

Please complete this section only if other researchers, investigators or organisations are involved in this project. Please also specify the role any other researcher(s), investigator(s) or organisation(s) will have in the research.

A.6.1. Individual Researcher(s) or Investigator(s)

Please provide the name of each researcher or investigator and the institution in which they research.

A.6.2. Research or Investigator Organisations

Please provide the name of each organisation and the city in which the organisation is located.

A.7. Are you applying concurrently to another ethics committee?

If your answer is yes, please provide full details, including the meeting date, and attach copies of the full application and approval letter if it has been approved.

No

A.8. Declaration

The information supplied is, to the best of my knowledge and belief, accurate. I have read the current Guidelines, published by the Auckland University of Technology Ethics Committee, and clearly understand my obligations and the rights of the participant, particularly with regard to informed consent.

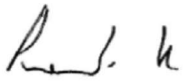

Signature of Applicant — 27th February 2012 — Date

(*In the case of student applications the signature must be that of the Supervisor)*

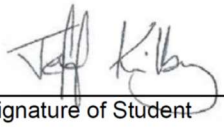

Signature of Student — 27th February 2012 — Date

(*If the research is a student project, both the signature of the Supervisor, as the applicant, and the student are required)*

A.9. Authorising Signature

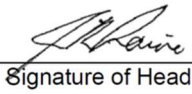

Signature of Head — School of Engineering — Name of Faculty/Programme/School/Centre — 27th February 2012 — Date

B. General Project Information

B.1. Project Duration

B.1.1. Approximate Start Date of Primary Data Collection

March 2012 (Once AUTEC approval is granted)

B.1.2. Approximate Finish Date of Complete Project

July 2015

B.2. Are funds being obtained specifically for this project?

If your answer is yes, then you must complete section G of this Application Form.

No

B.3. Types of persons participating as participants

Please indicate clearly every one of the following categories that applies to those participating in your research.

B.3.1. Researcher's students

No

B.3.2. Adults (20 years and above)

Yes

B.3.3. Legal minors (16 to 20 years old)

Yes

B.3.4. Legal minors (under 16 years old)

No

B.3.5. Members of vulnerable groups

e.g. persons with impairments, limited understanding, etc. If your answer is yes, please provide a full description.

No

B.3.6. Hospital patients

No

B.3.7. Prisoners

No

B.4. Does this research involve use of human remains, tissue or body fluids which does not require submission to a Regional Ethics Committee?

e.g. finger pricks, urine samples, etc. (please refer to section 13 of the AUTEC Guidelines). If your answer is yes, please provide full details of all arrangements, including details of agreements for treatment, how participants will be able to request return of their samples in accordance with right 7 (9) of the Code of Health and Disability Services Consumers' Rights, *etc.*

No

B.5. Does this research involve potentially hazardous substances?

e.g. radioactive materials (please refer to section 15 of the AUTEC Guidelines). If your answer is yes, please provide full details.

No

B.6. Research Instruments

B.6.1. Does the research include the use of a written or electronic questionnaire or survey?

If your answer is yes, please attach to this application form a copy of the finalised questionnaire or survey in the format that it will be presented to participants.

Yes included on the Consent Form.

B.6.2. Does the research involve the use of focus groups or interviews?

If the answer is yes, please indicate how the data will be recorded (e.g. audiotape, videotape, note-taking). When interviews or focus groups are being recorded, you will need to make sure there is provision for explicit consent on the Consent Form and attach to this Application Form examples of indicative questions or the full interview or focus group schedule.

No

B.6.3. Does the research involve the use of observation?

If the answer is 'Yes', please attach to this application a copy of the observation protocol that will be used.

No

B.6.4. Does the research involve the use of other research instruments such as performance tests?

If the answer is yes, please attach to this application a copy of the protocols for the instruments and the instruments that will be used to record results.

Yes

B.6.5. Who will be transcribing or recording the data?

If someone other than the researcher will be transcribing the interview or focus group records or taking the notes, you need to provide a confidentiality agreement with this Application Form.

Jeffrey Kilby

B.7. How does the design and practice of this research implement each of the three principles of the Treaty of Waitangi (Partnership, Participation and Protection) in the relationships between the researcher and other participants?

Please refer to Section 2.5 of AUTEC's Applying for Ethics Approval: Guidelines and Procedures *(accessible in the Ethics Knowledge Base (http://www.aut.ac.nz/research/research-ethics/ethics) and to the relevant Frequently Asked Questions section in the Ethics Knowledge Base.*

This research will implement Partnership, Participation and Protection principles of the Treaty of Waitangi by having consistent intercommunication between the partnerships of researcher with all participants.

Partnership: From the point of first contact with the researcher, necessary information and Consent Form for participation will be provided to the participants. Participants can ask questions and may withdraw any time from the research. The researcher will provide reports of each participant's own results and overall results on requests.

Participation: This will be reflected by providing equal opportunities of participation for all genders, race and culture within the criteria which has to be set for consistent statistical purpose. The criteria only require age group limitation between 18-35 years of age and certain condition of the knee muscles which has no previous knee injury within the last one year or knee surgeries.

Protection: Individual report of participant's own result and overall results can be made available on requests. Overall summary of results is produced without anyone identified. Privacy of data and results will be kept, protected and secured by the researcher (Jeffrey Kilby's office) for ten years which then will be destroyed. Participants may withdraw any time before and during the data collection process as to protect and not disadvantage participants in any way.

B.8. Does this research target Maori participants?

No

B.8.1. If 'Yes", what consultation has been undertaken when designing the research?

Please identify the group(s) with whom consultation has occurred and provide evidence of their support and any impact this consultation had on the design of the research. Researchers are advised to read the Health Research Council's Guidelines for researchers on health research involving Maori, *available via the Ethics Knowledge Base.*

B.9. Does this research target participants of particular cultures or social groups?

Please refer to Section 2.5 of AUTEC's Applying for Ethics Approval: Guidelines and Procedures *(accessible in the Ethics Knowledge Base (http://www.aut.ac.nz/research/research-ethics/ethics) and to the relevant Frequently Asked Questions section in the Ethics Knowledge Base.*

No

B.9.1. If 'Yes" please identify which cultures or social groups are being targeted and how their cultures or social groups are being considered in the research design.

B.9.2. If your answer to B.9 was 'Yes", what consultation has occurred with these cultures or social groups in the design of the research?

Please identify the group(s) with whom consultation has occurred and provide evidence of their support and any impact this consultation had on the design of the research.

B.10. Is there a need for translation or interpreting?

If your answer is 'Yes', please provide copies of any translations with this application and any Confidentiality Agreement required for translators or interpreters.

No

C. Project Details

Please describe the project details in language which is, as far as possible, free from jargon and comprehensible to lay people.

C.1. Aim of project:

Please explain the broad scope and purpose of the project and state concisely how the type of information being sought will achieve the project's aims. Please give the specific hypothesis(es), if any, to be tested.

To process and analyse muscle signals using new signal processing analysis techniques. Information required are muscle signals to be collected from 50 people by the use of surface electrodes.

This project is part research that enhances a field of research presently being carried out at AUT University that has a potential for further research in the field of surface electromyography (EMG) signals.

One of the research areas in the Electrical and Electronics Department within the Faculty of Design and Creative Technologies and School of Engineering at AUT University is the Signal and Systems Group. The proposed project is in coherence with other projects which are being investigated in this Faculty.

This research will provide the theoretical and experimental basis as well as a designed method for future work in the area of EMG signal processing.

C.2. Why are you proposing this research?

(ie what are its potential benefits to participants, researcher, wider community, etc?)

Research benefits are to establish more accurate analysis or technique in detecting normal and abnormal muscles for the use in health, rehabilitation and sports science application. This will widen and develop future research opportunities within the Electrical and Electronic Department at AUT University.

C.3. Background:

Please provide sufficient information, including relevant references, to place the project in perspective and to allow the project's significance to be assessed. Where appropriate, provide one or two references to the applicant's (or supervisor's) own published work in the relevant field.

A muscle is comprised of many small fibres. When a muscle contracts, electrical activity is sent down a nerve, which stimulates the small fibres within the muscle to contract. The more fibres that are stimulated the stronger the muscle contracts and a greater force is produced.

Through the application of surface electromyography (EMG) the combination of electrical activity (action potentials) from the numerous muscle fibres that contribute to a muscle contraction can be collected and analysed [1]. The EMG signal from the muscle is sensed by electrodes place on the skin surface overlying the muscle and then sent to a computer. The collected EMG signal can then be analysed using newly developed signal processing techniques, which allow the frequencies within the EMG signal to be broken down into measures that represent the electrophysiological characteristics of the muscle fibres contributing a muscular contraction [2]. These measures can also be related to force production [3], muscle fatigue [4] and deficits in the musculoskeletal system [5].

In the proposed research project, newly developed signal processing techniques will be used to develop a normative database with respect to muscle fibre firing patterns and electrophysiological characteristics muscle during varying levels of force production. The newly developed signal processing can also be used to rebuild the EMG signal that has been measured from the muscle. The rebuilding process of many signals from many subjects would create a normative database of muscle firing characteristics that would typically be expected occur during normal muscular contraction at various levels of force production. A normative database is important with respect to differential diagnosis of neurological and musculoskeletal disorders. Evidence clearly indicates that when any type a neurological or muscle injury occurs, the recruitment and electrophysiology of the muscle is altered [6-8]. In the future the normative database produced from this proposed research project could be used as a diagnostic tool for determining whether an individual may have a specific neurological and musculoskeletal disorder. The advantage of such a technique is that it is non-invasive and relatively inexpensive. This has implications to the whole community in terms of aiding early diagnosis of neurological and musculoskeletal disorders. Such technique can also be used to monitor the progression or regression, and the effect of rehabilitation on musculoskeletal [9] and neurological disorders [10].

C.4. Procedure:

C.4.1. Explain the philosophical and/or methodological approach taken to obtaining information and/or testing the hypothesis(es).

Procedures

When potential participants make contact with the researcher they will be screened for inclusion and exclusion criteria. If appropriate to participate in the study, they will receive a verbal explanation of what is involved. Prior to assessment, procedures will be explained to the participant and time will be given for the participant to have any remaining questions answered before written consent is obtained.

C.4.2. State in practical terms what research procedures or methods will be used.

Maximal strength test:

Participants will perform a five-minute generalised warm up that will include riding an exercise-cycle at a self-selected pace and performing range of motion exercises for the lower limbs. After the general warm-up is completed, participants will be seated in the upright chair of the HUMAC®/NORM™ Testing and Rehabilitation System (Computer Sports Medicine, Inc) with their knee bent to 80 degrees and attached to load cell that measures voluntary isometric force of the quadriceps. The upper body and upper thigh of the subject will be securely strapped to the chair and the leg will be strapped to the load cell at mid-shin level. The subject will then perform a specific warm-up and familiarisation of a series of three sets of short (five seconds) sub-maximal isometric knee extensions. The intensity of the contractions will be gradually increased against the resistance of the load cell and within the subject's own limits. A one-minute rest will follow each set of warm-up contractions. The subject will then rest for three minutes before the maximal voluntary isometric force (MVIF) of the quadriceps is measured. Three MVIF's will be measured and recorded for a five second period. There will be a two-minute rest period between each MVIF test and the highest MVIF will be selected for analysis. Standardised verbal encouragement will be given throughout the test from the force-to-failure point.

Ramped isometric knee extension test:

Following the Maximal strength test participants, will perform the ramped force production test. Force data from the maximal strength test will be transferred to a computer software programme that will calculate individual force values for 10%, 20%, 30%, 40%, 50%, 60%, 70%, 80%, 90% and maximal force. The force data for each level (10%, 20%, 30%, 40%, 50%, 60%, 70%, 80%, 90% and MVIF) will be displayed on the screen for feedback to the participant. The participant will then be required to perform and sustained isometric contraction of the knee for a given force level for a period of 10 seconds. A two-minute rest period will be given between each of the force values.

Endurance isometric knee extension test:

The subjects will be rested for a further period of 20 minutes following the ramped test before completing the endurance test. In this test the subjects will be asked to maintain a sub-maximal contraction at 50% MVIF. Exhaustion is defined as when the subject cannot hold within 5% of the 50% MVIF contraction. Subjects will be instructed prior to and during the test using standardised verbal encouragement to endure the contraction.

Electromyography (EMG) Measures:

Muscle activity will be recorded via new multi-channel surface electrode plus amplifier. The equipment is electrically isolated and all cables are specifically shielded and grounded for human use. There is no risk of electric shock to the researcher or subject. Routine maintenance ensures the safety and accuracy of the amplifier. This maintenance includes: regular calibration with an oscilloscope to check output signals and regular cable integrity checks made by a registered electronics technician. Following appropriate skin preparation (the skin is shaved, then gently abraded and cleaned with alcohol) the surface electrodes will be place on the skin surface overlying the vastus lateralis muscle of the thigh using standardised procedures.

C.4.3. State how information will be gathered and processed.

The EMG signal from the surface electrode will be amplified with a gain of 500, bandwidth filtered between 5 and 1 kHz. Raw analogue signals will then be converted to digital data and recorded via LabVIEW data acquisition software program at a frequency of 10 kHz, for a period of 10 seconds for each muscle contraction.

C.4.4. State how your data will be analysed.

The data will then be transferred to LabVIEW and MATLAB software using standard and newly developed signal processing analysis technique to analyse the frequency component and characteristics of the EMG signals.

C.4.5. Provide the statistical or methodological justification for this.

Fast Fourier Transform (FFT) and Short Time Fourier Transform (STFT) used for standard signal processing techniques, and the newly developed enhanced signal processing algorithm will also be used to analyse the collected data using both LabVIEW and MATLAB software. These are to enable classification of the EMG signals collected.

C.5. References

Please include the references for your responses to this section in the standard format used in your discipline.

1. Basmajian, J.V. and C.J. De Luca, *Muscles alive: their functions revealed by electromyography*. 5th ed. 1985, Baltimore: Williams and Wilkins.
2. Brody, L.R., et al., *pH-induced effects on median frequency and conduction velocity of the myoelectric signal.* J Appl Physiol, 1991. **71**(5): p. 1878-85.
3. Karlsson, S. and B. Gerdle, *Mean frequency and signal amplitude of the surface EMG of the quadriceps muscles increase with increasing torque--a study using the continuous wavelet transform.* J Electromyogr Kinesiol, 2001. **11**(2): p. 131-40.
4. Knaflitz, M. and P. Bonato, *Time-frequency methods applied to muscle fatigue assessment during dynamic contractions.* J Electromyogr Kinesiol, 1999. **9**(5): p. 337-50.
5. De Michele, G., et al., *Cross-correlation time-frequency analysis for multiple EMG signals in Parkinson's disease: a wavelet approach.* Med Eng Phys, 2003. **25**(5): p. 361-9.
6. Hodges, P.W. and C.A. Richardson, *Altered trunk muscle recruitment in people with low back pain with upper limb movement at different speeds.* Arch Phys Med Rehabil, 1999. **80**(9): p. 1005-12.
7. Mannion, A.F., *Fibre type characteristics and function of the human paraspinal muscles: normal values and changes in association with low back pain.* J Electromyogr Kinesiol, 1999. **9**(6): p. 363-77.
8. Riley, N.A. and M. Bilodeau, *Changes in upper limb joint torque patterns and EMG signals with fatigue following a stroke.* Disabil Rehabil, 2002. **24**(18): p. 961-9.
9. Panagiotacopulos, N.D., et al., *Evaluation of EMG signals from rehabilitated patients with lower back pain using wavelets.* J Electromyogr Kinesiol, 1998. **8**(4): p. 269-78.
10. Strambi, S.K., et al., *Effect of medication in Parkinson's disease: a wavelet analysis of EMG signals.* Med Eng Phys, 2004. **26**(4): p. 279-90.

D. Participants

D.1. Who are the participants?

One hundred subjects with no previous history of knee or severe musculoskeletal injury will participate in the study. Subjects will be students recruited from both AUT University City and North Shore Campuses. Request notices will be posted on notice boards. Subjects will be male or female between the ages of 18 and 35 with no history of knee injury within the last year.

D.1.1. What criteria are to be used in recruiting the participants?

Subjects will be male or female between the ages of 18 and 35 with no history of knee injury within the last year.

D.1.2. What criteria are to be used for selecting participants from those recruited?

None

D.1.3. Are there any potential participants who will be excluded?

If your answer is yes, please detail the criteria for exclusion.

Yes.

Individuals will be excluded if they have had a knee injury within the last year, had any previous knee surgery, and have any current cardiovascular, neurological, cognitive or musculoskeletal ailments.

People with knee injury or leg muscles or any form of medication that may seem relevant to give an unsatisfactory result related to this research.

D.2. Are there any potential conflicts of interest or possible coercive influences in the professional, social, or cultural relationships between the researcher and the participants (e.g. dependent relationships such as teacher/student; parent/child; employer/employee; pastor/congregation etc.)?

No

D.2.1. If your answer was 'Yes', please identify the nature of the relationships concerned and provide full information about the processes being incorporated into the research design to mitigate any adverse affects that may arise from them.

D.3. How many participants will be selected?

5-10 as the first phase for development.

40 - 50 as the second phase for verification.

D.3.1. What is the reason for selecting this number?

It is essential for experiment rigour of relational database related to project that will be set up for this research.

D.3.2. Provide a statistical justification where applicable, if you have not already provided one in C.4 5. above.

Not applicable (50 sets data is sufficient to represent a certain population).

D.3.3. Is there a control group?

If your answer is yes, please describe and state how many are in the control group.

No

D.4. Describe in detail the recruitment methods to be used.

If you will be recruiting by advertisement or email, please attach a copy to this Application Form

This will be achieved by placing advertising posters at AUT City and North Shore campuses asking for volunteers to participate in this research project.

D.5. How will information about the project be given to participants?

(e.g. in writing, verbally). A copy of information to be given to prospective participants is to be attached to this Application Form. If written information is to be provided to participants, you are advised to use the Information Sheet exemplar.

Information about the project will be given to participants in writing.

D.6. Will the participants have difficulty giving informed consent on their own behalf?

Consider physical or mental condition, age, language, legal status, or other barriers. If the answer is yes, please provide full details.

No

D.6.1. If participants are not competent to give fully informed consent, who will consent on their behalf?

D.6.2. Will these participants be asked to provide assent to participation?

If the answer is yes, please attach a copy of the assent form which will be used. Please note that assent is not the same as consent (please refer to the Glossary in Appendix A of the AUTEC Guidelines and Procedures.

D.7. Will consent of participants be gained in writing?

If the answer is yes, please attach a copy of the Consent Form which will be used. If the answer is No, please provide the reasons for this.

Yes

D.8. Will the participants remain anonymous to the researcher?

Please note that anonymity and confidentiality are different. If the answer is yes, please state how, otherwise, if the answer is no, please describe how participant privacy issues and confidentiality of information will be preserved.

At the time of data collection, participants will not be anonymous to the researcher as both will be interacting. However, no participants will be individually identified in the writing up of the research results. All written consent forms and personal data on external data storage devices will be held in secure location in the Jeffrey Kilby's office at AUT University for ten years.

D.9. In the final report will there be any possibility that individuals or groups could be identified?

If the answer is yes, please explain how and why this will happen.

No

D.10. Will feedback or findings be disseminated to participants (individuals or groups)?

If the answer is yes, please explain how this will occur and ensure that this information is included in the Information Sheet.

Yes

D.11. Will the findings of this study be of particular interest to specific cultures or social groups?

If your answer is 'Yes', please identify how the findings will be made available to them.

No

E. Other Project Details

E.1. Where will the project be conducted?

Please provide the name/s of the Institution/s, town/s, city or cities, region or country that best answers this question.

The testing of the participants will be carried out at North Shore Campus of AUT University, Auckland.

E.2. Who is in charge of data collection?

Jeffrey Kilby

E.3. Who will interact with the participants?

Jeffrey Kilby

E.4. What ethical risks are involved for participants in the proposed research?

Please consider the possibility of moral, physical, psychological or emotional risks to participants, including issues of confidentiality and privacy. Researchers are urged to consider this issue from the perspective of the participants, and not only from the perspective of someone familiar with the subject matter and research practices involved.

Minimum risk

E.4.1. Are the participants likely to experience any discomfort, embarrassment (physical, psychological, social) or incapacity as a result of the research's procedures?

To prepare participants for data collection, the subject's left and right legs will be shaven around the areas of the intended muscles. This is to ensure good skin-electrode contact. It will next be gently abraded with skin preparation cleanser (Green Prep), then cleansed with 70% alcoholic swab and let to dry before attaching the newly developed multi-channel surface electrode. This surface electrode are the main sensory contacts attached to the subject for muscle activity. They are disposable or one-off use as surfaces are self-adhesive and preferred for time efficiency and hygiene.

The only discomfort maybe a slight stinging feeling of the skin when cleaning the skin with the alcoholic swab which last a few seconds.

Possible embarrassment will be the patches of shaven area of hair on the participant's legs, which will be of concern to the male subjects due to the time taken for the hair to grow back.

E.4.2. If there are risks, please identify their probability and describe how they will be mitigated.

Please describe how these will be minimised or mitigated (e.g. participants do not need to answer a question that they find embarrassing or they may terminate an interview or there may be a qualified counsellor present in the interview or the findings will be reported in a way that ensures that participants cannot be individually identified, etc.) Possible risks and their mitigation should be fully described in the Information Sheets for participants.

No

E.4.3. If the participants are likely to experience any discomfort, embarrassment, or incapacity, what provision for counselling has been made, either with AUT Counselling (who also provide an online service) or with other counselling professionals (this is to be at no charge to the participants)?

Please refer to section 2.3 of AUTEC's Applying for Ethics Approval: Guidelines and Procedures *in the Ethics Knowledge Base. If the answer is No, please explain the arrangements which have been made to have qualified personnel available to deal with unexpected adverse physical or psychological consequences?*

Participants will be made aware of the skin preparation for the data collection of the muscle activity in the Information Sheet.

E.5. What risks are involved for the researcher(s) in the proposed project (such as physical, social, psychological, or safety risks)?

If this project will involve interviewing participants in private homes, undertaking research overseas, or going into similarly vulnerable situations, then a Researcher Safety protocol should be designed and appended to this application.

None

E.6. Will there be any other physical hazards introduced to AUT staff and/or students through the duration of this project?

If the answer is yes, please provide details of management controls which will be in place to either eliminate or minimise harm from these hazards (e.g. a hazardous substance management plan).

No

E.7. Is deception of participants involved at any stage of the research?

If the answer is yes, please provide full details of and rationale for the deception. Please refer to Section 2.4 of AUTEC's Applying for Ethics Approval: Guidelines and Procedures *when considering this question.*

No

E.8. How much time will participants have to give to the project?

40-60 minutes

E.9. Will any information on the participants be obtained from third parties?

If the answer is yes, please provide full details. This includes use of third parties, such as employers, in recruitment.

No

E.10. Will any identifiable information on the participants be given to third parties?

If the answer is Yes, please provide full details.

No

E.11. Provide details of any payment, gift or koha and, where applicable, level of payment to be made to participants.

Please refer to Section 2.1 of the AUTEC's Applying for Ethics Approval: Guidelines and Procedures *and Appendix A of that document for AUTEC's policy on Payment and Koha, especially in relation to recruitment.*

A small gift of snack bars will be offered to say thank you to the participant for volunteering their time in taking part in the research.

F. Data and Consent Forms

F.1. Who will have access to the data?

Jeffrey Kilby and Professor Krishnamachar Prasad

F.2. Are there plans for future use of the data beyond those already described?

The applicant's attention is drawn to the requirements of the Privacy Act 1993 (see Appendix I). If there are future plans for the use of the data, then this needs to be explained in the Information Sheets for participants.

No

F.3. Where will the data be stored once the analysis is complete?

Please provide the exact storage location. AUTEC normally requires that the data be stored securely on AUT premises in a location separate from the consent forms. If you are proposing an alternative arrangement, please explain why.

All written consent forms and the EMG data is to be stored on external data storage devices will be held in a secure location in the Jeffrey Kilby's office at AUT University for ten years at AUT University City Campus.

F.4. For how long will the data be stored after completion of analysis?

AUTEC normally requires that the data be stored securely for six years. If you are proposing an alternative arrangement, please explain why.

Yes, as the data is health related in terms of rehabilitation.

F.5. Will the data be destroyed?

If the answer is yes, please describe how the destruction will be effected. If the answer is no, please provide the reason for this.

Yes by erasing all the data collected and analysed from the computer data after ten years.

F.6. Who will have access to the Consent Forms?

Jeffrey Kilby and Professor Krishnamachar Prasad

F.7. Where will the completed Consent Forms be stored?

Please provide the exact storage location. AUTEC normally requires that the Consent Forms be stored securely on AUT premises in a location separate from the data. If you are proposing an alternative arrangement, please explain why.

All written consent forms and personal information on data storage devices will be held in a secure location at AUT University, City Campus for ten years in Jeffrey Kilby's office.

F.8. For how long will the completed Consent Forms be stored?

AUTEC normally requires that the Consent Forms be stored securely for six years. If you are proposing an alternative arrangement, please explain why.

Ten years.

F.9. Will the Consent Forms be destroyed?

If the answer is yes, please describe how the destruction will be effected. If the answer is no, please provide the reason for this.

Yes after ten years the consent forms will be shredded at the same time the data is erase from the data storage devices.

G. Material Resources

G.1. Has an application for financial support for this project been (or will be) made to a source external to AUT or is a source external to AUT providing (or will provide) financial support for this project?

No

G.1.1. If the answer to G.1 was 'yes', please provide the name of the source, the amount of financial support involved, and clearly explain how the funder/s are involved in the design and management of the research.

G.2. Has the application been (or will it be) submitted to an AUT Faculty Research Grants Committee or other AUT funding entity?

If the answer is yes, please provide details.

Yes

G.2.1. If the answer to G.2 was 'yes', please provide the name of the source, the amount of financial support involved, and clearly explain how the funder/s are involved in the design and management of the research.

In the process of applying for a contestable research grant from the School of Engineering.

G.3. Is funding already available, or is it awaiting decision?

Please provide full details.

Application for funding is being prepared for a contestable research within the School of Engineering.

G.4. Please provide full details about the financial interest, if any, in the outcome of the project of the researchers, investigators or research organisations mentioned in Part A of this application.

The outcome of the project may not create financial interest in the near future.

H. Other Information

H.1. Have you ever made any other related applications?

If the answer is yes, please provide the AUTEC application / approval number(s)

No

I. Checklist

Please ensure all applicable sections of this form have been completed and all appropriate documentation is attached as incomplete applications will not be considered by AUTEC.

Section A	General Information Completed	✓
	Signatures/Declaration Completed	✓
Section B	Project General Information Completed	✓
Section C	Project Details Completed	✓
Section D	Participant Details Completed	✓
Section E	Other Project Details Completed	✓
Section F	Data & Consent Forms Details Completed	✓
Section G	Material Resources Completed	✓
Section H	Other Information Completed	✓

Spelling and Grammar Check (please note that a high standard of spelling and grammar is required in documents that are issued with AUTEC approval)	✓

Attached Documents (where applicable)

Participant Information Sheet(s)	✓
Consent Form(s)	✓
Questionnaire(s)	✓
Indicative Questions for Interviews or Focus Groups	
Observation Protocols	
Recording Protocols for Tests	✓
Advertisement(s)	✓
Hazardous Substance Management Plan	
Any Confidentiality Agreement(s)	

Other Documentation

None

Before submitting this application, please note the following:

- *Incomplete or incorrectly formatted applications will not be considered by AUTEC;*
- *Please check online for the most recent version of this form before submitting your application;*
- *Please do not alter the formatting of this form or delete any sections. If a particular question is not applicable to your research, please state that as your response to that question;*

This form needs to be submitted, along with all associated documents as follows:

- *In printed form;*
- *With the required signatures in sections A.8 and A.9;*
- *Single sided;*
- *Using clips rather than staples;*
- *By 4 pm on the agenda closing date at:*

The AUTEC Secretariat
Room WA505D, WA Building
55 Wellesley Street East, City Campus.

- *The Internal Mail Code is D-89. If sending applications by Internal Mail, please ensure that they are posted at least two days earlier to allow for any delay that may occur.*

Section D–2: Participant Information Sheet

Participant Information Sheet

Date Information Sheet Produced:

27th February 2012

Project Title

Collection and Classification of Surface Electromyography (EMG) Signals

An Invitation

I, Jeffrey Kilby, Senior Lecturer at AUT University in the School of Engineering, am presently conducting a research for completing my PhD degree. I would like to invite you to participate in my research in signal processing of surface electromyography or muscle signals. For any of you who have not had previous knee injuries within the past year or knee surgeries, you are welcome to volunteer to be a participant in my research. A part of my research is to collect signals from leg muscle using a load cell and surface electrodes placed on the muscles during a series of set activities.

What is the purpose of this research?

This project is part research that enhances a field of research presently being carried out at AUT University that has a potential for further research in the field of surface electromyography (EMG) signals.

One of the research areas in the Electrical and Electronics Department within the Faculty of Design and Creative Technologies and School of Engineering at AUT University is the Signal and Systems Group. The proposed project is in coherence with other projects which are being investigated in this faculty.

This research will provide the theoretical and experimental basis as well as designed methods for future work in the area of EMG signal processing.

How was I identified and why am I being invited to participate in this research?

The participants would have made contact with the researcher and then they will be screened for inclusion and exclusion criteria. If suitable to participate in the study, the participants will receive verbal explanation of what is involved. Prior to assessment, procedures will be explained to the participants and time will be given for the participants to have any remaining questions answered before written consent is obtained.

What will happen in this research?

Participant will perform a five-minute generalised warm up that will include riding an exercise-cycle bike at self-selected pace and performing range of motion exercises for the lower limbs. After the general warm-up is completed, participant will be seated in a testing and rehabilitation upright chair with one of their knees bent to 80 degrees and attached to a load cell that measures voluntary isometric force of the quadriceps. The upper body and upper thigh of the subject will be securely strapped to the chair and the ankle will be strapped to the load cell at mid-shin level. The participant will then perform specific movement activities with the load cell in a series of three sets of short sub-maximal isometric knee extensions.

Force data from the maximal strength test will be transferred to a computer software programme that will calculate individual force values for 10%, 20%, 30%, 40%, 50%, 60%, 70%, 80%, 90% and maximal force. The force data for each level (10%, 20%, 30%, 40%, 50%, 60%, 70%, 80%, 90% and MVIF) will be displayed on the screen for feedback to the participant. The participant will then be required to perform and sustained isometric contraction of the knee for a given force level for a period of 10 seconds. A two-minute rest period will be given between each of the force values.

Participant will be rested for a further period of 20 minutes following the ramped test before completing the endurance test. In this test the subjects will be asked to maintain a sub-maximal contraction at 50% MVIF. Exhaustion is defined as when the subject cannot hold within 5% of the 50% MVIF contraction. Subjects will be instructed prior to and during the test using standardised verbal encouragement to endure the contraction.

What are the discomforts and risks?

To prepare for data collection, the participants' left and right legs will be shaven around the areas of the intended muscles. This is to ensure good skin-electrode contact. The skin then will be gently abraded with cleanser (Green Prep), then cleansed with 70% alcoholic swab and let to dry before attaching the surface electrodes. The surface electrodes are the main sensory contacts for muscle activity. They are disposable or one-off use as surfaces are self-adhesive and preferred for time efficiency and hygiene.

The only discomfort may be a slight stinging feeling of the skin when cleaning with the alcoholic swab which should only last a few seconds.

The possible embarrassment will be the patches of shaven area of hair on the participants' legs, which may be of concern to the male participants due to the time taken for the hair to grow back.

How will these discomforts and risks be alleviated?

Participants will be informed and made aware of the necessity of skin preparation prior to signing the Consent Form. This should allow them to make informed decision and prepare the participants of any embarrassment of the shaven areas of skin and also for possible stinging feeling that may occur when cleaning the skin with the alcoholic swab. Both of these will not have ever lasting effect after completing the task in this research.

What are the benefits?

The benefit of this research is for the completion of my PhD studies and developing research within the AUT's School of Engineering.

How will my privacy be protected?

All written consent forms and the EMG data are to be stored in the external data storage devices which will be held in a secured location in the Jeffrey Kilby's office at AUT University for ten years at AUT University City Campus. After ten years they will be destroyed by erasing the data from the external devices and shedding the consent forms.

What are the costs of participating in this research?

The cost of participating in this research is the participant's willingness is to give up approximately 90 minutes of their time in order to take part in this research.

What opportunity do I have to consider this invitation?

The participant will have the opportunity to participate until the end of July 2014.

How do I agree to participate in this research?

A Consent Form will need to be completed before the participant can take part in this research. Participants may withdraw from the research at any time.

Will I receive feedback on the results of this research?

In the Consent Form questions will be asked whether the participant wants feedback on the results obtained from this research. This will be given in the form of small report to show how their individual results are reflected and compared with the overall results.

What do I do if I have concerns about this research?

Participants may withdraw from the research at any time.

Any concerns regarding the nature of this project should be notified in the first instance to the Project Supervisor, Professor Krishnamachar Prasad, *kprasad@aut.ac.nz* ext 6229.

Concerns regarding the conduct of the research should be notified to the Executive Secretary, AUTEC, Dr Rosemary Godbold, *rosemary.godbold@aut.ac.nz*, 921 9999 ext 6902.

Whom do I contact for further information about this research?

Researcher Contact Details:

Jeffrey Kilby, *jkilby@aut.ac.nz,* 921 9999 ext 8748.

Project Supervisor Contact Details:

Professor Krishnamachar Prasad, *kprasad@aut.ac.nz* ext 6229.

Approved by the Auckland University of Technology Ethics Committee on 3rd April 2012, AUTEC Reference number 12/49.

Section D–3: Consent Form

Consent Form

Project title: *Collection and Classification of Surface Electromyography Signals*
Project Supervisor: *Professor Krishnamachar Prasad*
Researcher: *Jeffrey Kilby*

- ○ I have read and understood the information provided about this research project in the Information Sheet 27th February 2012.
- ○ I have had an opportunity to ask questions and to have them answered.
- ○ I understand that I may withdraw myself or any information that I have provided for this project at any time and without being disadvantaged in any way.
- ○ I am not suffering from heart disease, high blood pressure, any respiratory conditions.
- ○ I have not had a knee injury within the last year, or had any previous knee surgery, and do not have any current cardiovascular, neurological, cognitive or musculoskeletal ailments.
- ○ I agree to take part in this research.
- ○ I wish to receive a copy of the report from the research (please tick one): Yes○ No○

Participant's Signature: .....

Participant's Name: .....

Participant's Contact Details (if appropriate):

.....

.....

.....

.....

Date:

Approved by the Auckland University of Technology Ethics Committee on 3rd April 2012 AUTEC Reference number 12/49

Note: The Participant should retain a copy of this form.

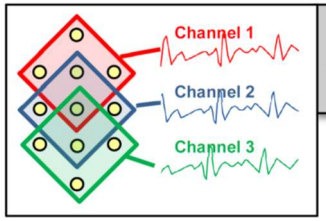

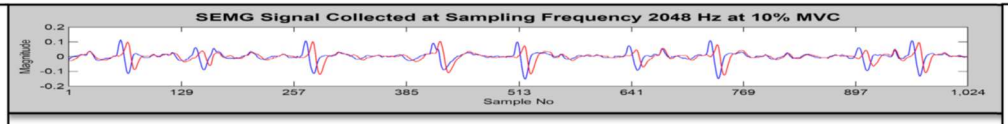

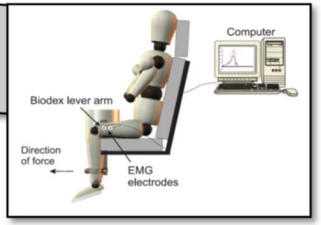

VOLUNTEERS NEEDED

FOR RESEARCH IN ELECTROMYOGRAPHY (MUSCLE) SIGNALS

Be a part of AUT's latest research in Signals and Systems Group of the School of Engineering

If you are between 18-35 years of age with no knee injuries or knee surgeries within the past year, you are welcome to volunteer and participate in this research

For further details please contact Jeffrey Kilby, email: jkilby@aut.ac.nz, phone 9219999 extension 8748

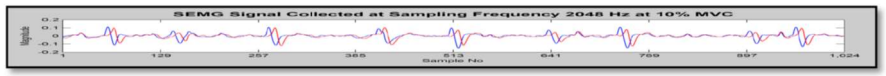

AUT UNIVERSITY ENGINEERING

Section D–5: Acceptance Letter Granting Ethical Approval

MEMORANDUM

Auckland University of Technology Ethics Committee (AUTEC)

To: Krishnamachar Prasad
From: **Dr Rosemary Godbold** Executive Secretary, AUTEC
Date: 3 April 2012
Subject: Ethics Application Number 12/49 **Collection and classification of surface electromyography signals.**

Dear Krishnamachar

Thank you for providing written evidence as requested. I am pleased to advise that it satisfies the points raised by the Auckland University of Technology Ethics Committee (AUTEC) at their meeting on 12 March 2012 and I have approved your ethics application. This delegated approval is made in accordance with section 5.3.2.3 of AUTEC's *Applying for Ethics Approval: Guidelines and Procedures* and is subject to endorsement at AUTEC's meeting on 30 April 2012.

Your ethics application is approved for a period of three years until 3 April 2015.

I advise that as part of the ethics approval process, you are required to submit the following to AUTEC:

- A brief annual progress report using form EA2, which is available online through http://www.aut.ac.nz/research/research-ethics/ethics. When necessary this form may also be used to request an extension of the approval at least one month prior to its expiry on 3 April 2015;
- A brief report on the status of the project using form EA3, which is available online through http://www.aut.ac.nz/research/research-ethics/ethics. This report is to be submitted either when the approval expires on 3 April 2015 or on completion of the project, whichever comes sooner;

It is a condition of approval that AUTEC is notified of any adverse events or if the research does not commence. AUTEC approval needs to be sought for any alteration to the research, including any alteration of or addition to any documents that are provided to participants. You are reminded that, as applicant, you are responsible for ensuring that research undertaken under this approval occurs within the parameters outlined in the approved application.

Please note that AUTEC grants ethical approval only. If you require management approval from an institution or organisation for your research, then you will need to make the arrangements necessary to obtain this.

To enable us to provide you with efficient service, we ask that you use the application number and study title in all written and verbal correspondence with us. Should you have any further enquiries regarding this matter, you are welcome to contact me by email at ethics@aut.ac.nz or by telephone on 921 9999 at extension 6902. Alternatively, you may contact your AUTEC Faculty Representative (a list with contact details may be found in the Ethics Knowledge Base at http://www.aut.ac.nz/research/research-ethics/ethics).

On behalf of AUTEC and myself, I wish you success with your research and look forward to reading about it in your reports.

Yours sincerely

Dr Rosemary Godbold
Executive Secretary
Auckland University of Technology Ethics Committee

Cc: Jeffrey Kilby jkilby@aut.ac.nz

From the desk of …
Dr Rosemary Godbold
Executive Secretary
AUTEC

Private Bag 92006, Auckland 1142
New Zealand
E-mail: ethics@aut.ac.nz

Tel: 64 9 921 9999
ext 8860
Fax: 64 9 921 9902

Appendix E: Calibration of Load Cell

Section E–1: Custom-built LabVIEW Virtual Instrument (VI) for Calibration of Load Cell

Section E–2: Calibration Procedure and Results of Load Cell

E1: Custom-built LabVIEW™ Virtual Instrument (VI) for Calibration of Load Cell

Figure E.1 (a) shows the VI's front panel/user interface and (b) shows the VI's block diagram/graphical code used for calibrating the load cell assembly. The VI runs in two steps using two *while loops*. The first while loop allows the continuous data acquisition of the force trace to be displayed on the front panel during the zeroing and applying of the 100 N load. When the calibration force of the load cell is completed, the first while loop is stopped and the second while loop runs. The second while loop allows cursors to be moved along the force trace to obtain both voltage values for zero and 100 N load. These voltage values were used to calculate the calibration scale factor and saved as a global variable to be used by the other VIs. The second while loop is stopped when the VI stops being executed.

(a) Front panel

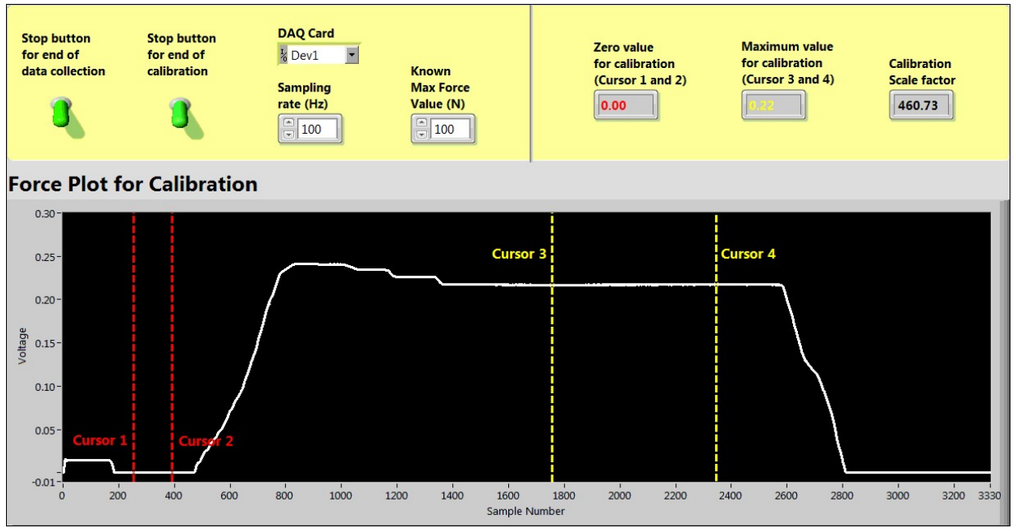

(b) Block diagram

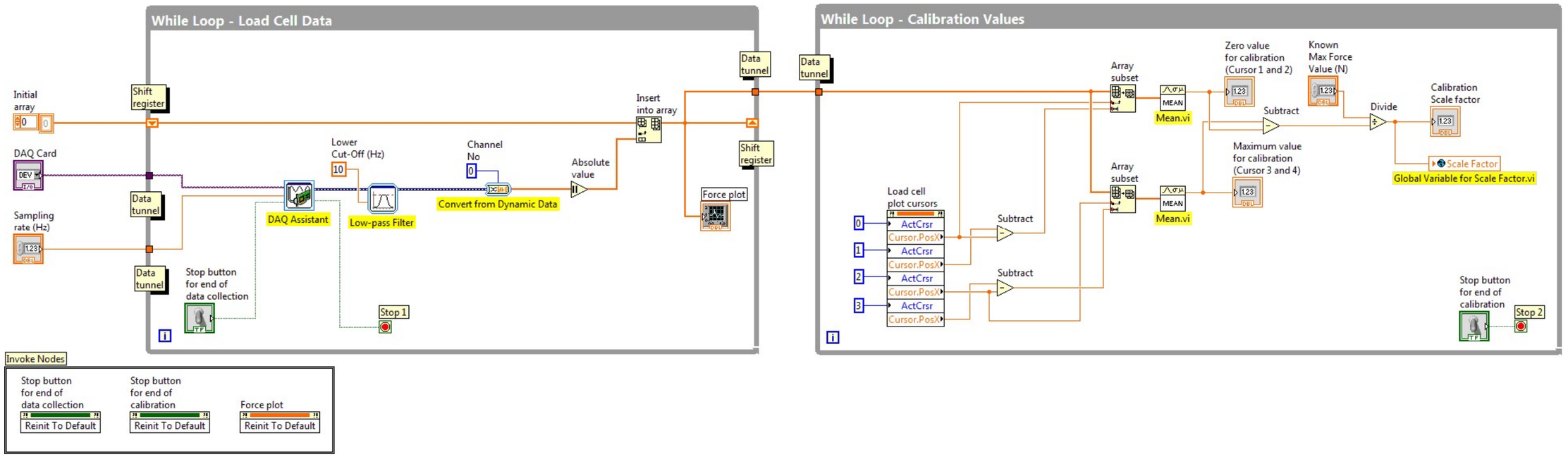

Figure E.1 Custom-built VI for calibration of load cell assembly. (a) Front panel. (b) Block diagram.

E2: Calibration Procedure and Results of Load Cell

The LabVIEW force calibration VI created in section E1 was running on a laptop computer (Lenovo, T60 model) and a data acquisition card was attached to the load cell assembly. Calibration was carried out in two steps:

1. With no load applied, the universal in-line transducer was adjusted to ensure zero voltage was at the output of the transducer. This was to remove any drift and creep [207, 208] that might have occurred since the last calibration of the load cell with the restraining bracket.
2. With a known force of 100 N applied using a DFE Series Digital Force Gauge (Chatillon, Germany), as shown in Figure E.2.

Figure E.2 Force of 100 N applied to the load cell assembly using a Digital Force Gauge.

From these two steps, a force trace was produced on the VI, which outputs the calibration scaling factor in Newton per volts (N/V) in order to convert the voltage output of the load cell to a force value. Figure E.3 shows a calibration force trace output from the VI.

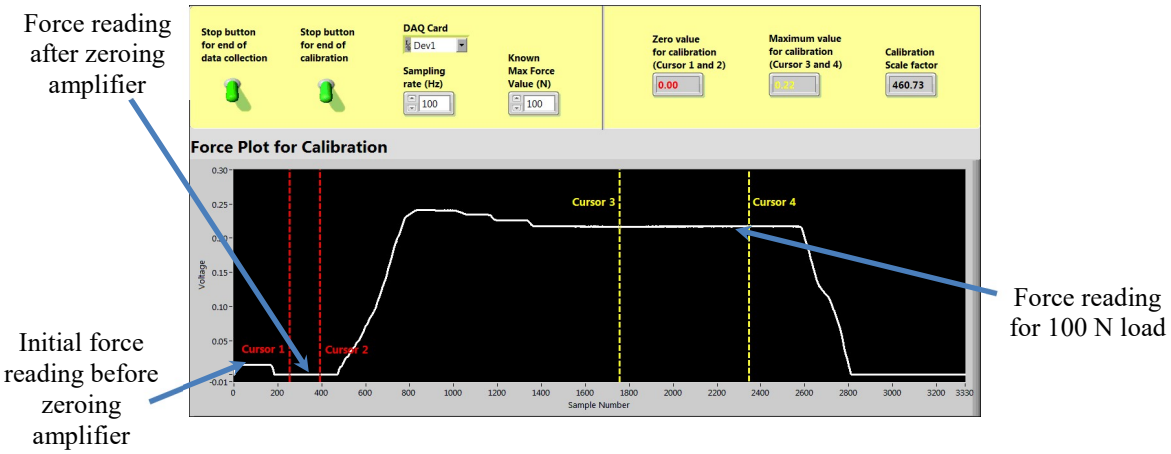

Figure E.3 VI showing a calibration force trace from the load cell assembly to find the scaling factor (N/V).

Appendix F: Biofeedback VIs of Force Trace for Data Collector and Participant

Section F–1: Custom-built VI to Find Maximum Voluntary Isometric Contraction (MVIC) Force of the Participant

Section F–2: Custom-built VI for Testing the Participant Performing Predetermined Tasks at Fixed Percentage Values of Their MVIC Force

Section F–3: Custom-built VI for Testing the Participant Performing the Endurance (or Fatiguing) Task at 50% of Their MVIC Force

Section F–1: Custom-built VI to Find Maximum Voluntary Isometric Contraction (MVIC) Force of the Participant

Figure F.1 (a) shows the VI's front panel/user interface and (b) shows the VI's block diagram/graphical code to determine the maximum overall MVIC force that was produced from three separate attempts by the participant, with a 2-minute rest in-between each attempt. This VI code uses two while loops and a two-event sequence structure. The first while loop allows for continuous data acquisition of the force trace produced by the participant. Data are displayed on the front panel as two separate waveform graphs shown in the top view of Figure F.1. The left-hand view shows what is displayed on the data collector's laptop monitor and the right-hand view shows what is displayed on the participant's monitor. Both monitors displaying the waveform of the force trace are identical and simultaneously shown to the data collector and participant. When all three possible maximum MVIC force tasks are completed, the first while loop is halted, the data acquisition of the force trace stops, and the trace remains displayed on the front panel. The second while loop in the first event of the sequence structure allows each cursor to be moved in the front panel of the data collector monitor to determine the maximum value of each MVIC force and display it. When the second loop is halted, the data from the force trace is saved and stored in a file in the second event of the sequence and the VI stops being executed. The overall maximum MVIC force found is displayed on the data collector's laptop monitor and stored as a global variable to be transferred to the other VIs. Figure F.1 (a) shows a set of measured results obtained from a participant who performed three maximum MVIC forces.

(a) Front panel

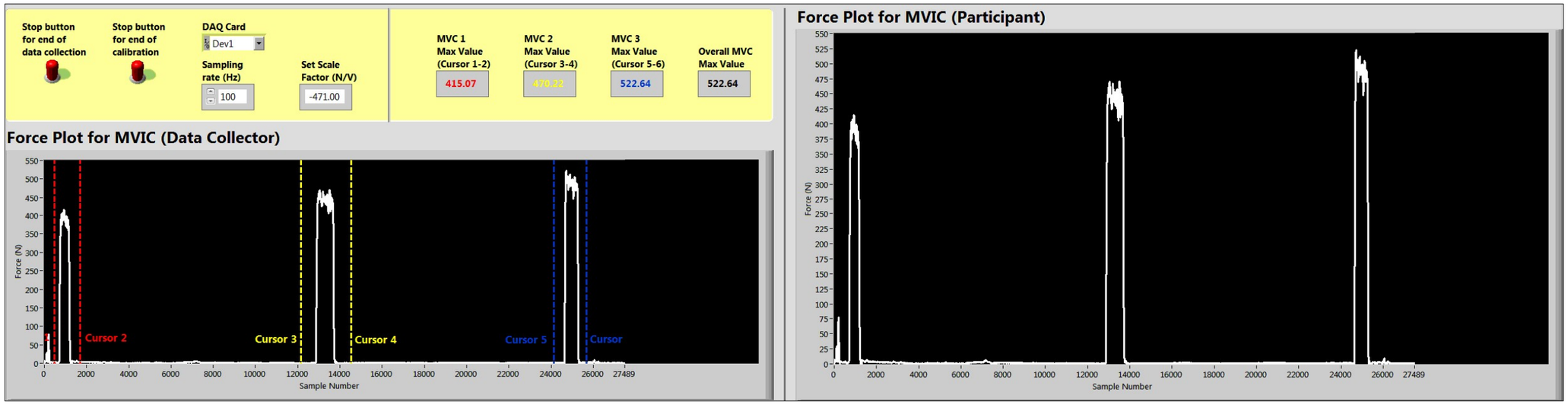

(b) Block diagram

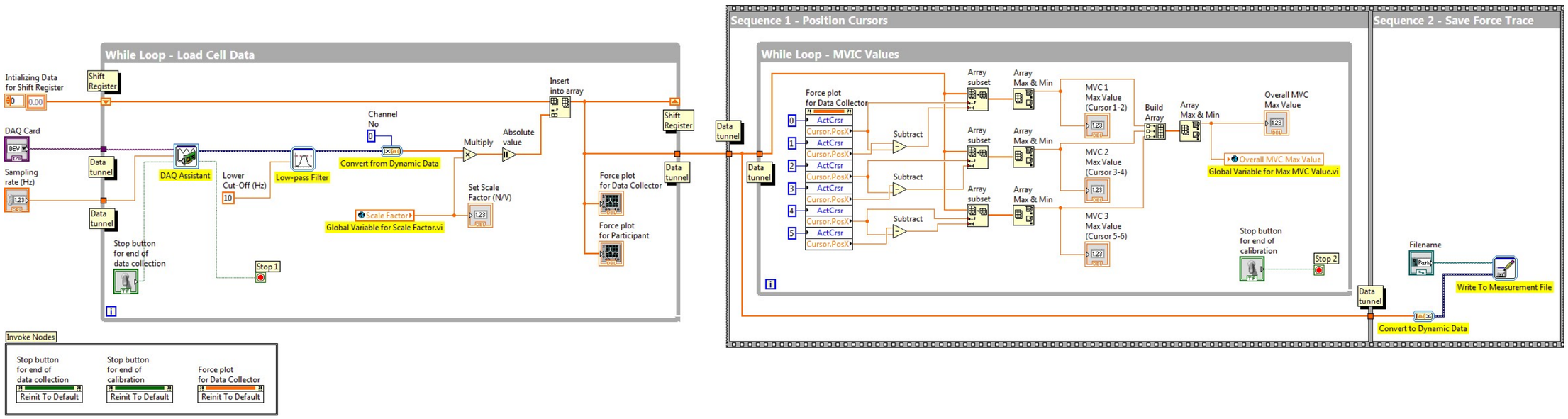

Figure F.1 Custom-built VI to find the MVIC force of the participant. (a) Front panels for the data collector and participant. (b) Block diagram.

Section F–2: Custom-built VI for Testing the Participant Performing Predetermined Tasks at Fixed Percentage Values of Their MVIC Force

Figure F.2 (a) shows the VI's front panel/user interface for a measured set of results obtained from a participant who performed a predetermined task at a fixed percentage values of their MVIC force, and (b) shows the VI's block diagram/graphical code used to display this force. This VI code used one of two while loops and a three-event sequence structure. The first events involves the initializing of the VI and allowing the participants to prepare themselves for the task. The second event is the data acquisition of the force trace, which was displayed for both the data collector and participant over a 2 second time window. Using the global variable of the maximum MVIC value found in section F–1, a predetermined task at a fixed percentage value was set. The corresponding force was displayed as a target value for the participant to aim for and hold for 10 seconds. Due to the participant not being able to maintain a steady force, the margin of error was set at ±5% of this target value, which was also displayed. The data collector during this task had control over setting a predetermined percentage value of MVIC after each 2-minute rest between MVIC forces. A timer was set for 2-minutes, after which a warning LED flashed to ensure that the MVIC value had been changed for the participant.

(a) Front panel

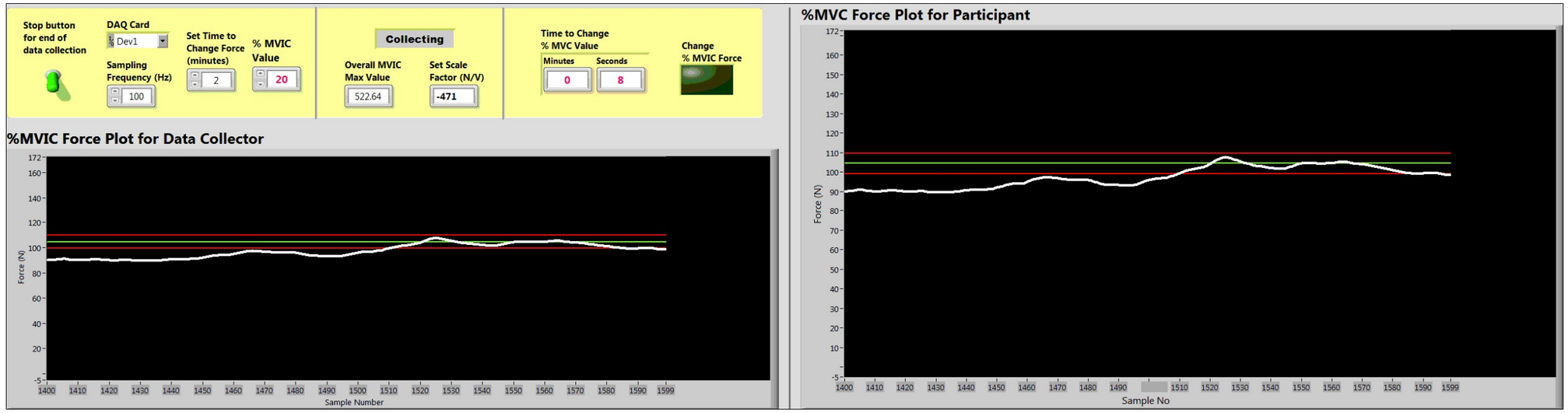

(b) Block diagram

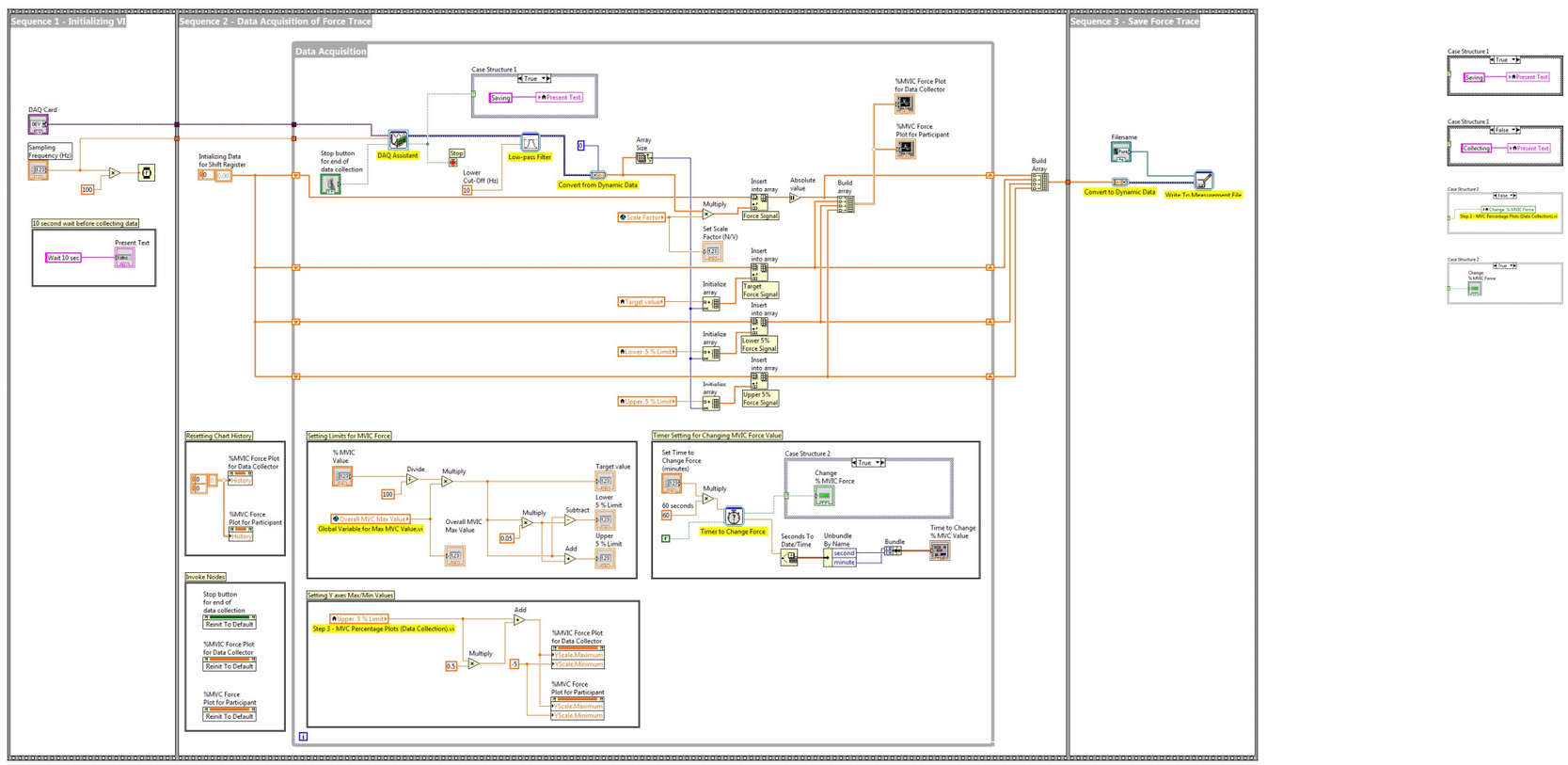

Figure F.2 Custom-built VI for participants performing predetermined tasks at fixed percentage values of their MVIC. (a) Front panel for the data collector and participant. (b) Block diagram.

Section F–3: Custom-built VI for Testing the Participant Performing Endurance (or Fatiguing) Task at 50% of Their MVIC Force

Figure F.3 (a) shows the VI's front panel/user interface for a measured set of results obtained from a participant who performed the endurance task at 50% of their MVIC and (b) shows the VI's block diagram/graphical code used to display this force. This VI is the same as in section F.2, the only difference is that the data collector cannot change the percentage of the MVIC force value and there is no timer.

(a) Front panel

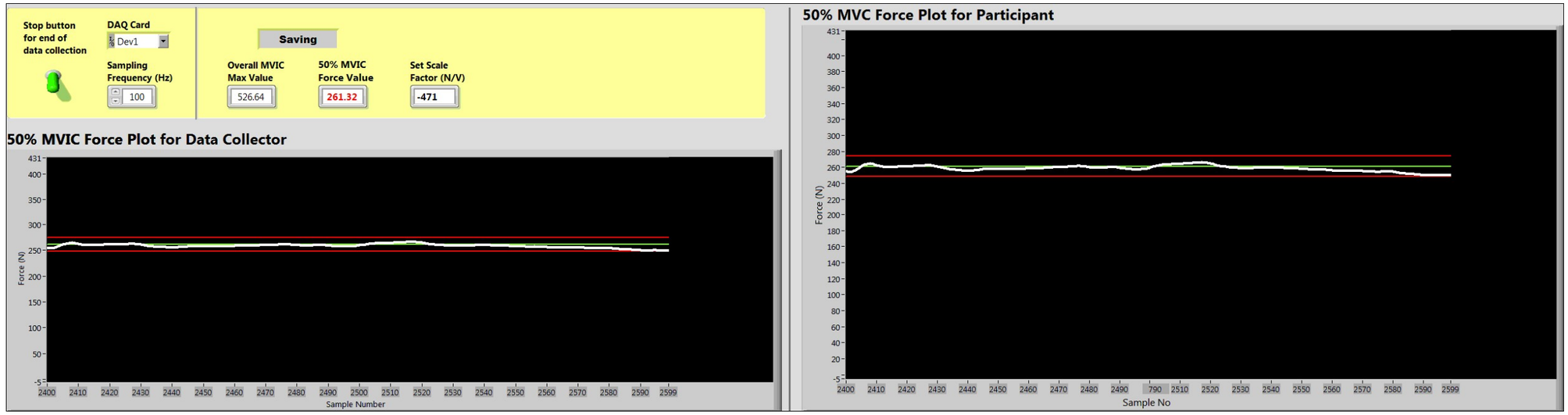

(b) Block diagram

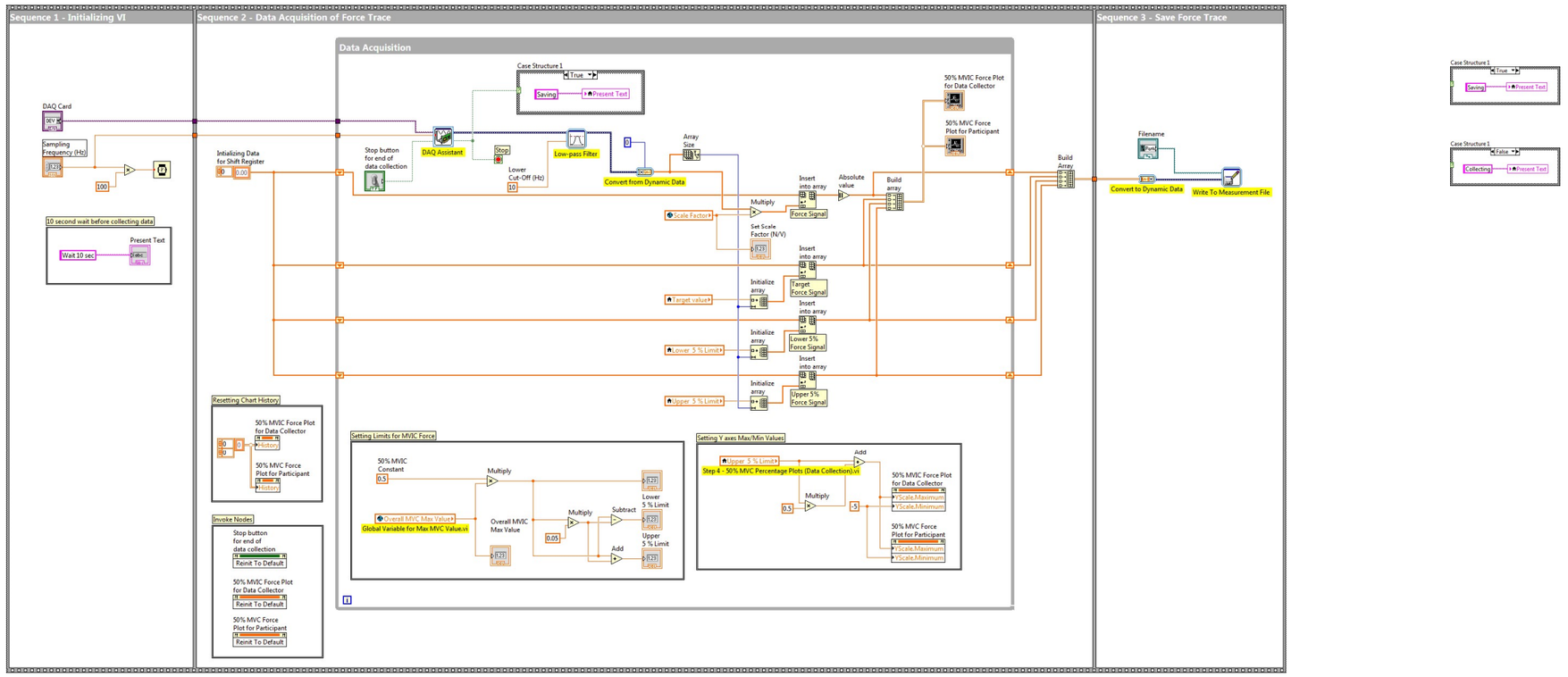

Figure F.3 Custom-built VI for endurance (or fatiguing) task. (a) Front panel for the data collector and participant. (b) Block diagram.

Appendix G: Data Acquisition VI for Principal Researcher

While each participant was performing the different tasks, the VI used by the principal researcher needed to perform the following tasks simultaneously:

1. Data acquisition
2. Display the data being acquired in real-time to the principal researcher
3. Store the data for later analysis

The large amount of data being collected was stored in the laptop hard drive for later signal processing. The signals being sampled at 10 kHz created a problem for collecting, displaying and storing the data while running the VI. Difficulties were initially experienced when developing a basic mode VI to display and store all the necessary information for the principal researcher – an *overwrite error* occurred after a few minutes of running the VI. This error indicated that information was being lost and that LabVIEW could not read the data from the PC buffer quickly enough.

A '*producer/consumer'* pattern was therefore used where the producer loop process performed data acquisition, and the consumer loop process took this data either to be displayed or stored without any loss [209]. This had a large enough communication *queue* (buffer) and minimized any data loss [138, 209].

Figure G.1 shows the VI's front panel/user interface viewed by the principal researcher. The waveforms collected from the data acquisition card on the left-hand side, shows the following:

1. The overall force trace produced by the participant.
2. Eleven separate 2 second windows of the monopolar signals.

The waveforms on the right-hand side show 2 second windows of the software generated for the linear array and Laplacian configurations from the monopolar signals.

Figure G.2 shows the block diagram used for acquiring a total of 12 channels of data: one from the load cell and 11 from the electrodes. The code shows there are three while loops, one producer loop and two consumer loops. The top while loop or producer loop in Figure G.2 is collecting the data and passing them on the two other while loops via a *notifier* or a queue. A notifier is a tool used for communicating between two independent parts of a

block diagram [138]. These two while loops are consumer loops: one for displaying a 2 second window and one for storing all the data collected.

The middle while loop uses notifiers to pass the data from the producer loop, so the data being collected is displayed on the front panel for the principal researcher to view. The bottom while loop uses queues to obtain data from the producer loop so the data can be stored on the laptop's hard drive. The advantage of using a queue is that the producer and consumer rates do not have to be identical [138].

The VI was successful as it was able to display and save data collected from the load cell, the electrodes and the generated signals for the linear array and Laplacian configurations. This was not possible when using conventional data acquisition techniques in LabVIEW due to the large amount of data being collected at a high sampling rate.

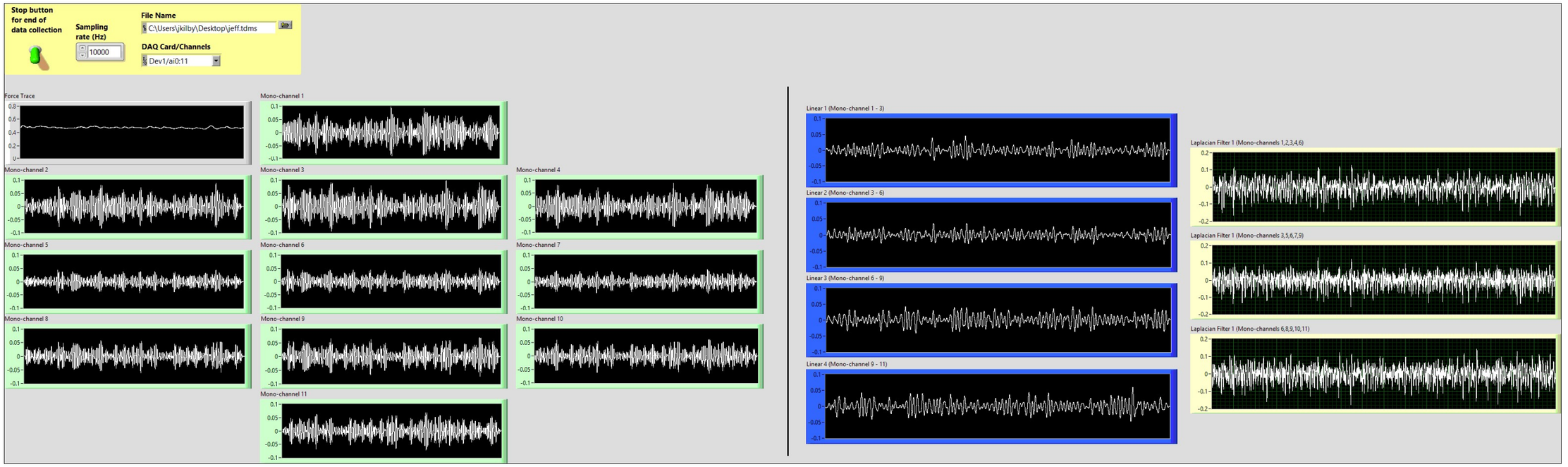

Figure G.1 Front panel of custom-built VI for data acquisition by the principal researcher.

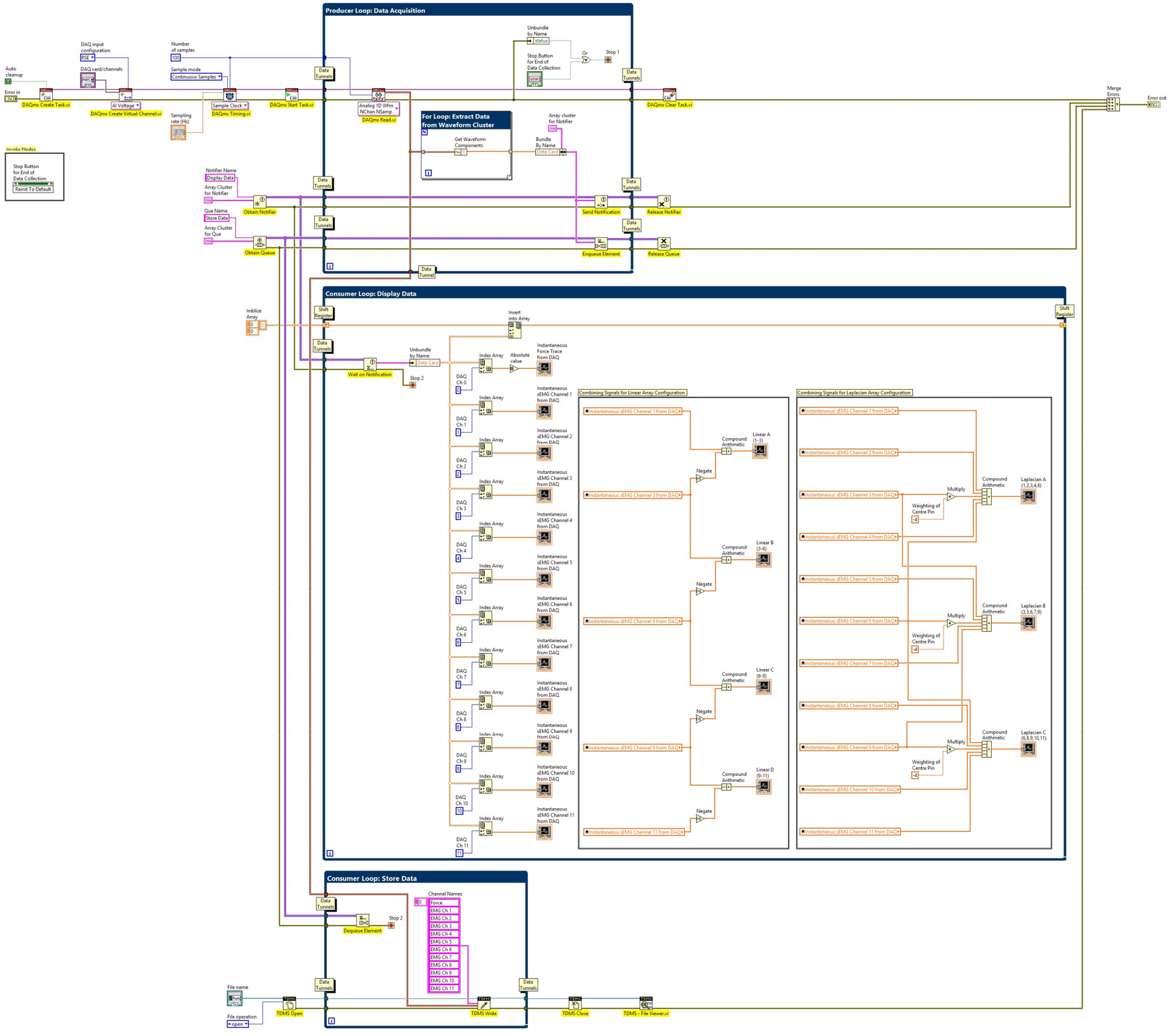

Figure G.2 Block diagram of custom-built VI front panel for the data acquisition by the principal researcher.

Appendix H: Sample of a Data Sheet for Measurement/Settings taken by Data Collector

Data Sheet – sEMG Signal Classification Study (Jeff Kilby)

Participant Details:

Information	
Name/participant number	
Date of Test	
Age	
Height	
Weight	
Skinfold thickness at muscle site	
UL Fat Width at muscle site	
Torque Length	
Dominant Leg	
Leg Tested	
Ethnicity	

Task 1: Maximum Voluntary Isometric Contraction (MVIC)

Test No	MVIC Value (N)
1	
2	
3	

Task No 2

(a) Percentage MVIC (10-90%)

Test No	Percentage MVIC Values
1	
2	
3	
4	
5	
6	
7	
8	
9	

(b) Endurance Test at 50% MVC

Estimated Time to Fatigue (secs)

Appendix I: Technical Specification Sheet for NI USB 6218 DAQ Card

NI USB-6218

M Series Data Acquisition: Isolated 32 AI, 2 AO, 8 DI, 8 DO
Bus-Powered USB

The following specifications are typical at 25 °C, unless otherwise noted. For more information about the NI USB-6218, refer to the *NI USB-621x User Manual* available at *ni.com/manuals*.

Caution The input/output ports of this device are not protected for electromagnetic interference due to functional reasons. As a result, this device may experience reduced measurement accuracy or other temporary performance degradation when connected cables are routed in an environment with radiated or conducted radio frequency electromagnetic interference.

To ensure that this device functions within specifications in its operational electromagnetic environment and to limit radiated emissions, care should be taken in the selection, design, and installation of measurement probes and cables.

Analog Input

Number of channels	16 differential or 32 single ended
ADC resolution	16 bits
DNL	No missing codes guaranteed
INL	Refer to the *AI Absolute Accuracy* section
Sample rate	
Single channel maximum	250 kS/s
Multichannel maximum (aggregate)	250 kS/s
Minimum	0 S/s
Timing resolution	50 ns
Timing accuracy	50 ppm of sample rate
Input coupling	DC
Input range	±0.2 V, ±1 V, ±5 V, ±10 V

Maximum working voltage for analog inputs (signal + common mode)	±10.4 V of AI GND
CMRR (DC to 60 Hz)	100 dB
Input impedance	
Device on	
AI+ to AI GND	>10 GΩ in parallel with 100 pF
AI- to AI GND	>10 GΩ in parallel with 100 pF
Device off	
AI+ to AI GND	1,200 Ω
AI- to AI GND	1,200 Ω
Input bias current	±100 pA
Crosstalk (at 100 kHz)	
Adjacent channels	-75 dB
Non-adjacent channels	-90 dB
Small signal bandwidth (-3 dB)	450 kHz
Input FIFO size	4,095 samples
Scan list memory	4,095 entries
USB	USB Signal Stream, programmed I/O
Overvoltage protection for all analog input and sense channels	
Device on	±30 V for up to two AI pins
Device off	±20 V for up to two AI pins
Input current during overvoltage condition	±20 mA maximum/AI pin

Settling Time for Multichannel Measurements

Accuracy, full-scale step, all ranges	
±90 ppm of step (±6 LSB)	4 µs convert interval
±30 ppm of step (±2 LSB)	5 µs convert interval
±15 ppm of step (±1 LSB)	7 µs convert interval

Appendix J: New Sliding Data Window Algorithm VI to Obtain MDF, MNF, RMS and MFCV Values from sEMG Signals

Figure J.1 shows the VI's front panel/user interface and Figure J.2 shows the VI's block diagram/graphical code for the new algorithm for determining the following values:

- Median frequency (MDF)
- Mean frequency (MNF)
- Root mean square (RMS)
- Muscle fibre conduction velocity (MFCV)

for a data window, which is passed through each of the three Laplacian sEMG signals.

The data file containing the force trace and the three signals was read into the code outside the main *while loop*, which contains a *for loop*. This was to allow all four signals from the data collected from the participant performing the endurance task to be displayed before analysis, as shown on the left-hand side of Figure J.1. The force value, where converted to torque, is given by:

$$\tau = F \times d \tag{J.1}$$

where F is force measured in Newtons (N), d is the participant's measured leg length (or is also called torque length), in metres (m) as explained in Chapter 4, and τ is torque measured in Newton metres (Nm).

On the torque trace in Figure J.1, the solid green horizontal line represents the target torque value for 50% MVIC and the red horizontal lines are ±5% of this target value. The yellow-dotted vertical lines are cursor 1 and cursor 2, which can be moved through the torque trace, to ensure they lie within the boundary of ±5% of the torque trace values. Cursor 1 is placed at the beginning and cursor 2 at the end of the torque trace, which is the time period where the participant is performing the endurance task. This time period value fixes the analysis period for the sliding window to be passed through the sEMG signals to find the MDF, MNF, RMS and MFCV values.

When cursors 1 and 2 have been positioned, these time period values (sample number) are then passed through to the *while loop* for the data analysis sliding window to set in terms of width and overlap. In the *while loop*, the three signals in Channel 1, 2 and 3 taken between cursor 1 and 2 are displayed on the right-hand side of Figure J.1. Once the window length and overlap period have been set, the number of data windows is calculated before the analysis is carried out in the *for loop*. The *for loop* takes a data window one at a time and finds the MDF and MNF frequency values from the power spectrum, as explained in Chapter 5 using a new subVI shown in Figure J.3. The RMS of the signals is found by using the standard function node in LabVIEW, and the MFCV is calculated using the cross-correlation technique as explained in Chapter 5.

The new subVI for finding the MDF and MNF values takes the signal and creates a power spectrum. The MDF is the corresponding frequency value that is found by the integration of the power spectrum, which is calculating the area under the power spectrum and dividing the area into two equal parts. The MNF is the corresponding frequency value that is found by taking the average of the frequency components in the power spectrum. Once the *for loop* has passed all the data windows through all three Laplacian sEMG signals, all the values are stored in a data file for further analysis at a later date.

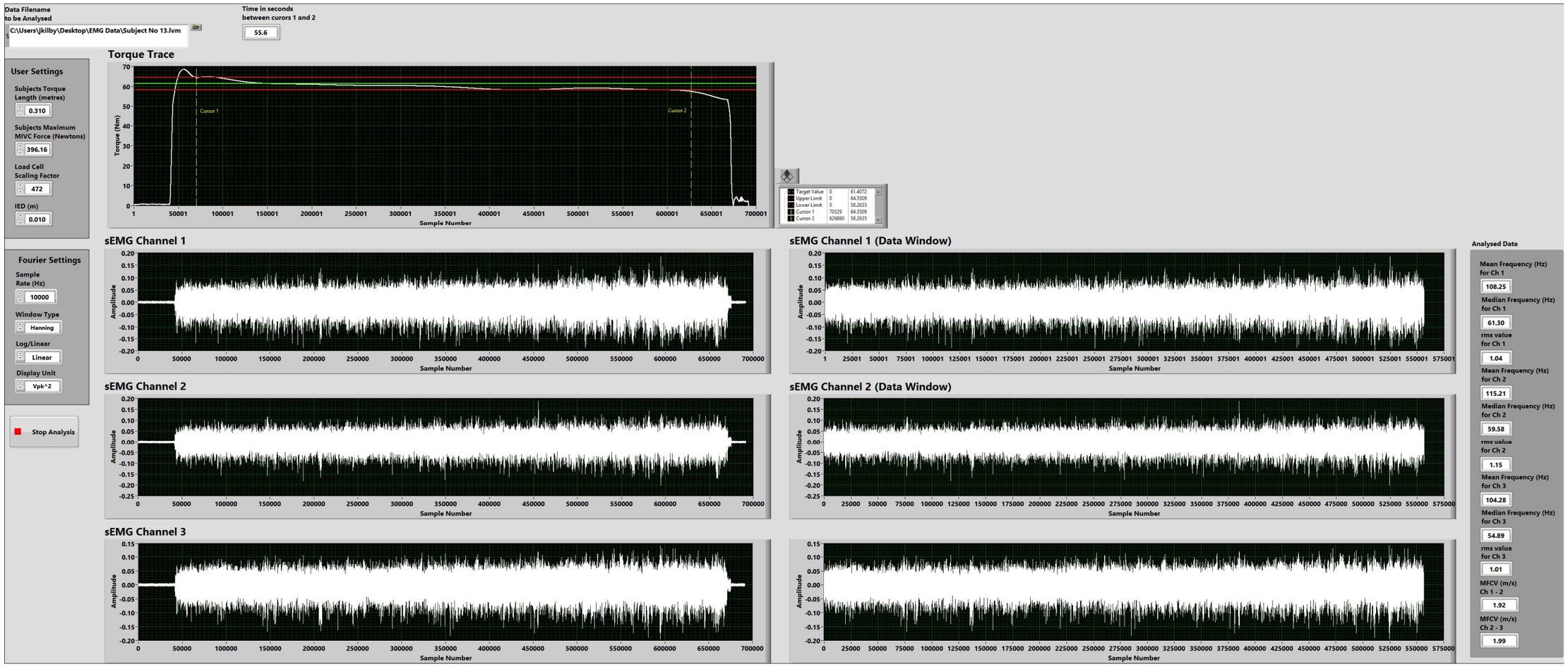

Figure J.1 The front panel of the custom-built VI for the new sliding data window algorithm to obtain MDF, MNF, RMS and MFCV values from sEMG signals.

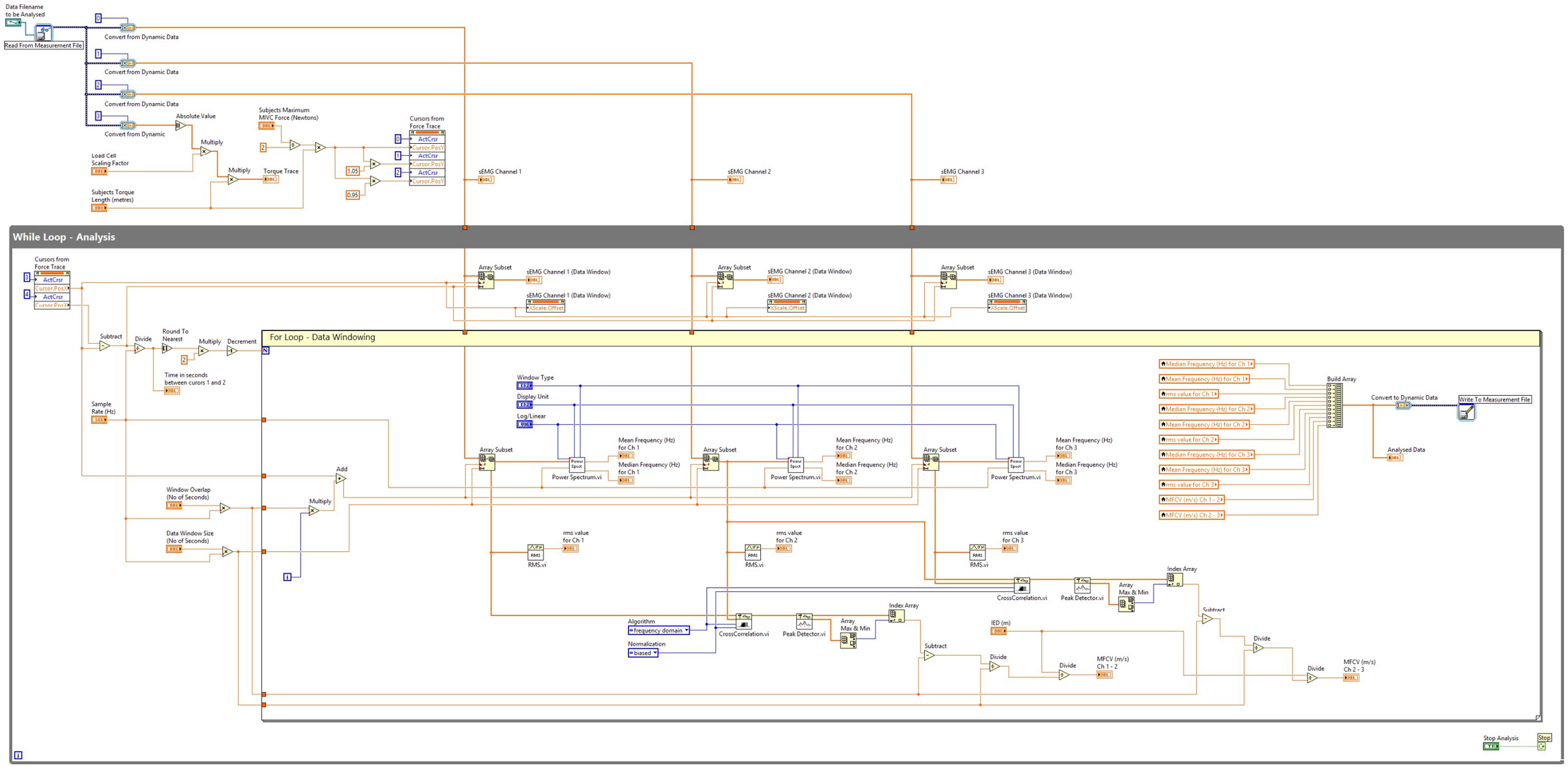

Figure J.2 The block diagram of the custom-built VI for the new sliding data window algorithm to obtain MDF, MNF, RMS and MFCV values from sEMG signals.

(c) Front panel

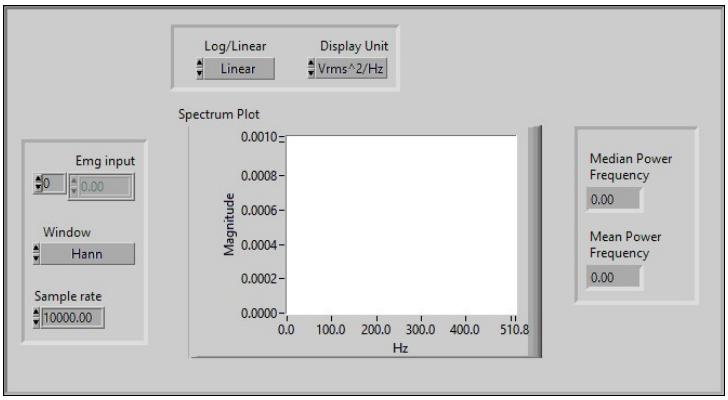

(d) Block diagram

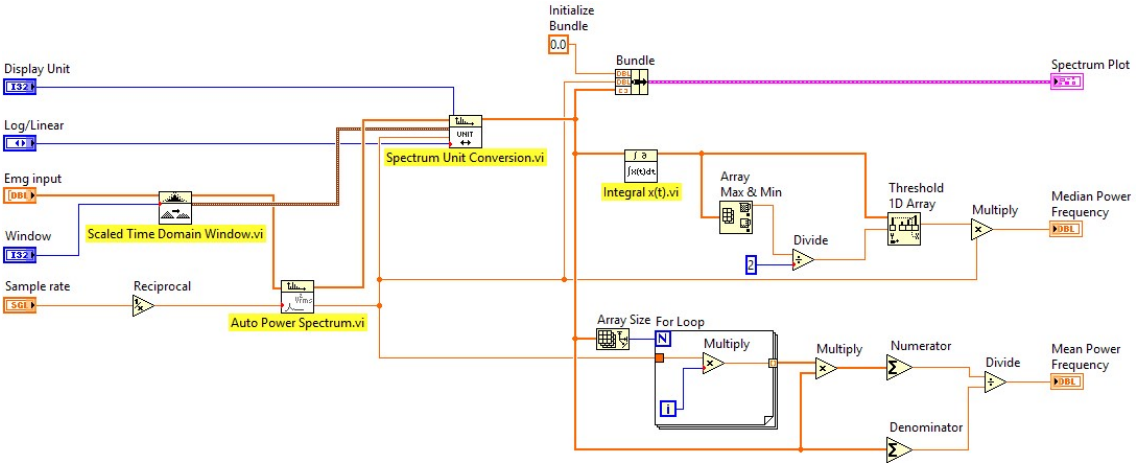

Figure J.3 Customized power spectrum subVI, (a) front panel and (b) block diagram

Appendix K: Participants Physiological Measurements

Participant number	Gender Female (F) Male (M)	Dominant leg Left (L) Right (R)	Age (years)	Weight kilogrammes (kg)	Height metres (m)	Skinfold thickness using calipers millimetres (mm)	Skinfold thickness using ultrasound millimetres (mm)	Torque length metres (m)
1	F	R	22	66.8	1.69	22	5.27	0.325
2	F	R	23	56.5	1.59	14	5.58	0.290
3	F	L	22	65.6	1.60	10	5.01	0.270
4	M	L	22	72.9	1.74	12	3.54	0.285
5	M	R	23	74.5	1.78	13	3.66	0.275
6	M	R	23	76.1	1.78	13	3.54	0.280
7	M	L	22	78.4	1.77	12	4.62	0.270
8	F	R	22	66.2	1.70	25	5.38	0.310
9	F	R	21	66.7	1.69	23	5.46	0.305
10	F	R	23	51.5	1.59	19	7.18	0.280
11	M	R	22	78.2	1.76	9	5.34	0.330
12	M	L	21	78.8	1.75	11	5.38	0.300
13	F	R	25	71.5	1.65	12	5.17	0.310
14	M	R	21	72.1	1.86	6	3.25	0.320
15	M	R	22	73	1.83	6	2.97	0.325
16	M	R	23	89.4	1.75	18	5.8	0.300
17	M	R	23	81	1.71	19	6.01	0.295
18	M	R	22	58.9	1.63	9	2.78	0.335
19	M	R	22	61.5	1.64	23	2.99	0.295
20	M	L	23	77.5	1.77	7	1.95	0.335
21	M	R	23	74.2	1.78	9	2.11	0.340
22	M	R	22	71	1.81	12	4.27	0.330
23	M	R	22	72.5	1.75	12	5.49	0.325
24	M	R	21	112.3	1.82	9	4.86	0.325
25	M	R	22	89.5	1.79	10	4.62	0.330
26	F	R	20	55	1.65	17	7.51	0.310
27	F	R	21	68.2	1.68	18	6.75	0.325
28	F	R	20	60.3	1.49	20	5.34	0.305
29	M	R	21	65.3	1.67	16	4.38	0.330
30	M	L	22	104.7	1.88	15	5.14	0.325
31	M	R	22	96.5	1.83	16	5.03	0.315
32	M	R	21	76.9	1.78	7	3.54	0.310
33	M	R	21	81.2	1.78	9	3.25	0.300
34	M	R	23	89.9	1.76	20	5.5	0.295
35	M	R	21	84.6	1.75	18	4.89	0.305
36	F	R	22	69.1	1.65	22	7.89	0.320
37	F	R	20	65.8	1.63	22	6.9	0.305
38	M	R	21	73.6	1.81	6	2.76	0.250
39	M	R	21	76.8	1.81	12	2.89	0.305
40	F	R	23	53.3	1.64	22	5.52	0.250

Appendix L: Fatigue Times and Torque Values at 50% MVIC Force

Participant number	Gender Female (F) Male (M)	Max MVIC value (a) Newtons (N)	50% MVIC value (b) = (a) × 0.5 Newtons (N)	Torque length (c) metres (m)	Torque values at 50% MVIC (c) = (a) × (b) Newton metres (Nm)	Time to fatigue seconds (s)
1	F	288.08	144.04	0.325	46.81	61.6
2	F	744.28	372.14	0.290	107.92	72.2
3	F	492.41	246.21	0.270	66.48	57.1
4	M	640.00	320.00	0.285	91.20	60.2
5	M	577.46	288.73	0.275	79.40	58.1
6	M	610.00	305.00	0.280	85.40	65.7
7	M	620.11	310.06	0.270	83.71	43.7
8	F	475.21	237.61	0.310	73.66	47.9
9	F	573.56	286.78	0.305	87.47	72.7
10	F	349.29	174.65	0.280	48.90	58.7
11	M	834.88	417.44	0.330	137.76	62.2
12	M	767.94	383.97	0.300	115.19	48.7
13	F	396.16	199.08	0.310	61.40	55.6
14	M	441.00	220.50	0.320	70.56	47.7
15	M	413.31	206.66	0.325	67.16	43.4
16	M	682.69	341.35	0.300	102.40	71.0
17	M	755.18	377.59	0.295	111.39	78.8
18	M	617.46	308.73	0.335	103.42	51.7
19	M	295.00	147.50	0.295	43.51	54.2
20	M	653.98	326.99	0.335	109.54	51.6
21	M	715.47	357.74	0.340	121.63	64.7
22	M	533.80	266.90	0.330	88.08	54.2
23	M	546.36	273.18	0.325	88.78	43.3
24	M	749.31	374.66	0.325	121.76	58.4
25	M	728.71	364.36	0.330	120.24	45.8
26	F	371.59	185.80	0.310	57.60	63.6
27	F	291.35	145.68	0.325	47.34	77.1
28	F	208.10	104.05	0.305	31.74	61.8
29	M	575.00	287.50	0.330	94.88	58.8
30	M	615.10	307.55	0.325	99.95	65.1
31	M	621.50	310.75	0.315	97.89	42.6
32	M	839.00	419.50	0.310	130.05	55.1
33	M	667.90	333.95	0.300	100.19	57.3
34	M	751.00	375.50	0.295	110.77	74.0
35	M	720.30	360.15	0.305	109.85	72.3
36	F	415.10	207.55	0.320	66.42	56.3
37	F	510.40	255.20	0.305	77.84	62.9
38	M	687.49	343.75	0.250	85.94	74.6
39	M	615.00	307.50	0.305	93.79	62.8
40	F	460.60	230.30	0.250	57.58	41.6

Appendix M: Analysis of MNF and MFCV Mean Trend Lines for 40 Participants

Section M-1: MNF and MFCV Mean Trend Line Analysis for the Lower Quartile Range of the Fatigue Times

Section M-2: MNF and MFCV Mean Trend Line Analysis for the Interquartile Range of the Fatigue Times

Section M-3: MNF and MFCV Mean Trend Line Analysis for the Upper Quartile Range of the Fatigue Times

Section M-1: MNF and MFCV Mean Trend Line Analysis for the Lower Quartile Range of the Fatigue Times

This section presents the results for both the MNF and MFCV features for the lower quartile range of the fatigue times, which were carried out by Participant Nos. 40, 31, 23, 15, 7, 25, 14, 8, 12 and 20. Participants are ordered in terms of shortest to longest times.

Table M.1 shows plots (a) – (j) for each participant and an explanation of the MNF feature over the period of the endurance (or fatiguing) task. Figure M.1 shows all the plots from Table M.1 on one plot for comparison purposes. Figure M.2 shows the normalized MNF plots of Figure M.1, equating the maximum values to a value of 1 to give a true comparison of the trend lines.

Table M.2 shows plots (a) – (j) for each participant, and an explanation of the MFCV feature over the period of the endurance (or fatiguing) task. Figure M.3 shows all the plots from Table M.2 on one plot for comparison purposes. Figure M.4 shows the normalized MFCV plots of Figure M.3, equating the maximum values to a value of 1 to give a true comparison of the trend lines.

Table M.1 Data analysis of the MNF mean trend lines for the lower quartile range of fatigue times

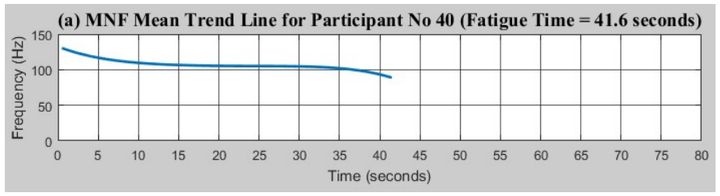 The trend line shows the initial MNF value dropped by 21% during the first 45% of muscle contraction, and then remained steady until the last 20% of muscle contraction where the MNF then dropped by 11%.	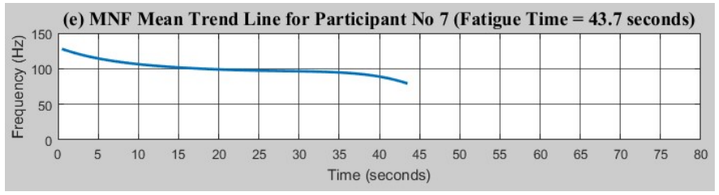 The trend line shows the initial MNF value dropped by 21% during the first 45% of muscle contraction, and then remained steady until the last 20% of muscle contraction where the MNF then dropped by 11%.	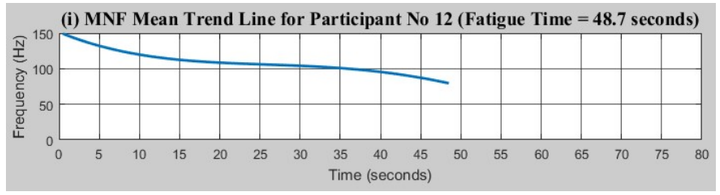 The trend line shows the initial MNF value dropped by 27% during the first 40% of muscle contraction, and then remained relatively steady until the last 28% of muscle contraction where the MNF then dropped by 13%.
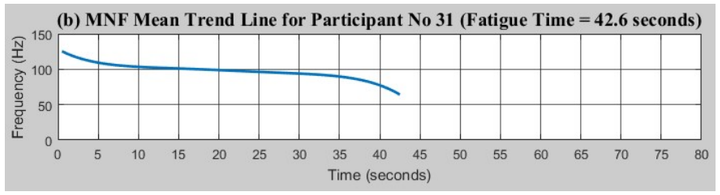 The trend line shows the initial MNF value dropped by 17% during the first 23% of muscle contraction, and then remained relatively steady until the last 19% of muscle contraction where the MNF then dropped by 20%.	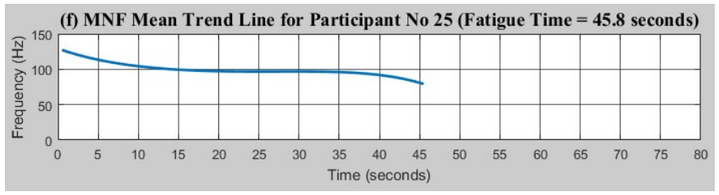 The trend line shows the initial MNF value dropped by 23% during the first 43% of muscle contraction, and then remained relatively steady until the last 24% of muscle contraction where the MNF then dropped by 13%.	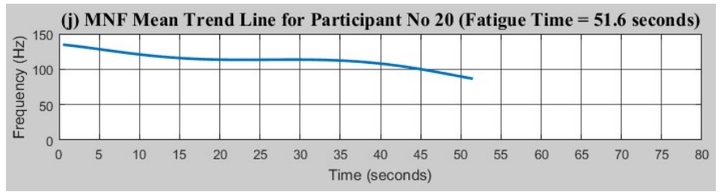 The trend line shows the initial MNF value dropped by 14% during the first 29% of muscle contraction, and then remained steady until the last 32% of muscle contraction where the MNF then dropped by 9%.
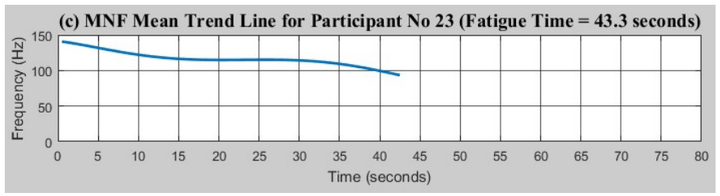 The trend line shows the initial MNF value dropped by 18% during first the 34% of muscle contraction, and then remained steady until the last 30% of muscle contraction where the MNF then dropped by 16%.	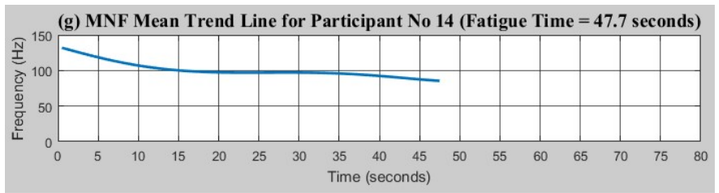 The trend line shows the initial MNF value dropped by 27% during the first 41% of muscle contraction, and then remained steady until the last 38% of muscle contraction where the MNF then dropped by 10%.	
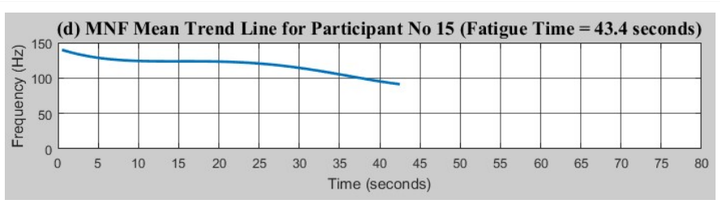 The trend line shows the initial MNF value dropped by 11% during the first 23% of muscle contraction, and then remained steady until the last 53% of muscle contraction where the MNF then dropped by 24%.	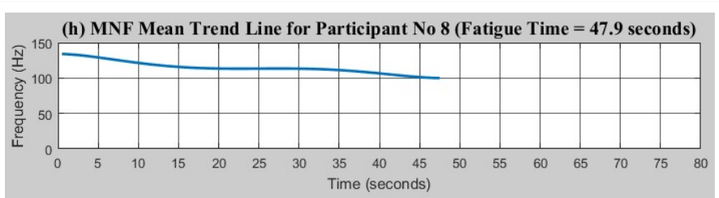 The trend line shows the initial MNF value dropped by 15% during the first 40% of muscle contraction, and then remained steady until the last 35% of muscle contraction where the MNF then dropped by 9%.	

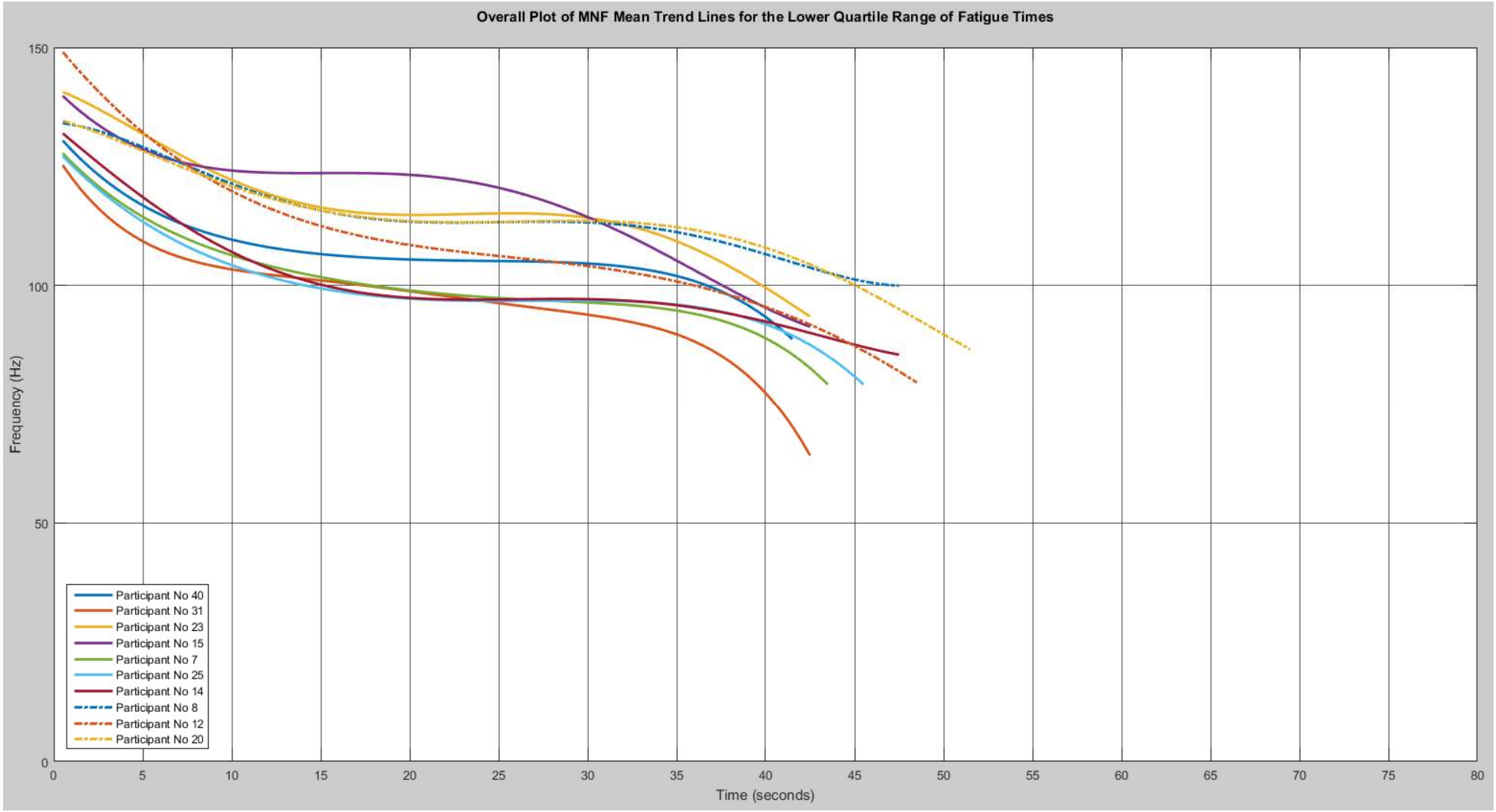

Figure M.1 Overall plot of MNF mean trend lines for the lower quartile range of fatigue times.

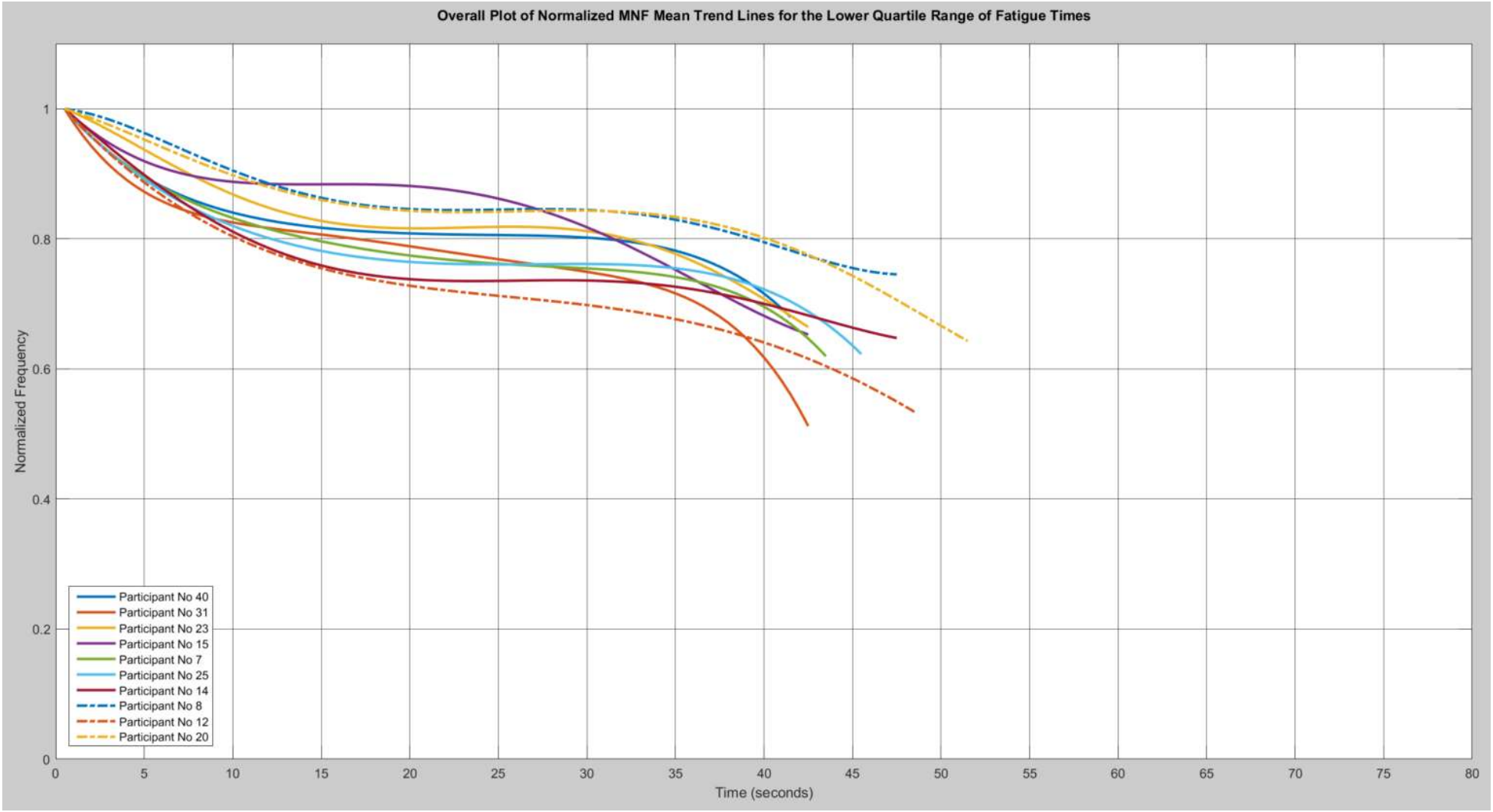

Figure M.2 Overall plot of normalized MNF mean trend lines for the lower quartile range of fatigue times.

Table M.2 Data analysis of the MFCV mean trend lines for the lower quartile range of fatigue times

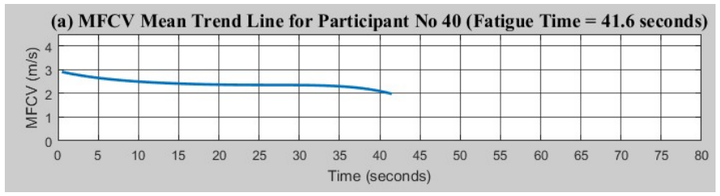 The trend line shows the initial MFCV dropped by 17% during the first 48% of muscle contraction, and then remained steady until the last 21% of muscle contraction where the MFCV then dropped by 13%.	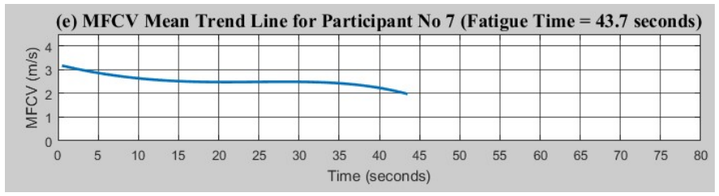 The trend line shows the initial MFCV dropped by 19% during the first 34% of muscle contraction, and then remained steady until the last 32% of muscle contraction where the MFCV then dropped by 16%.	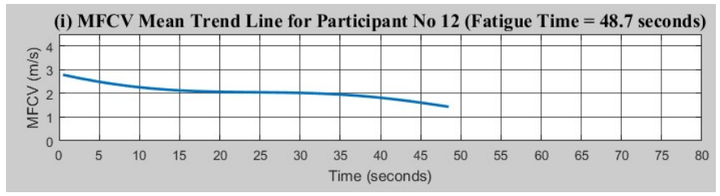 The trend line shows the initial MFCV dropped by 25% during the first 35% of muscle contraction, and then remained steady until the last 38% of muscle contraction where the MFCV then dropped by 26%.
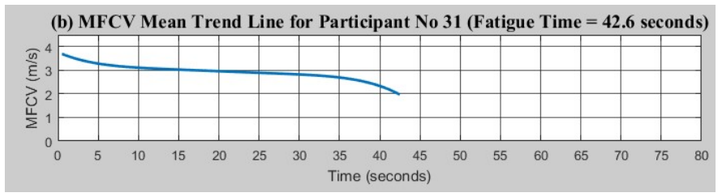 The trend line shows the initial MFCV dropped by 16% during the first 23% of muscle contraction, and then drops 10% until the last 23% of muscle contraction where the MFCV then drops 18%.	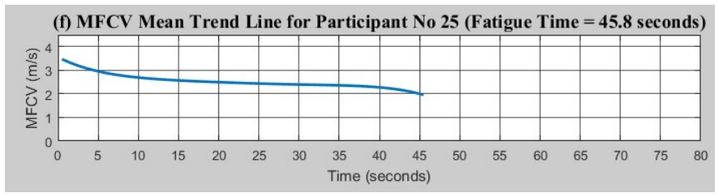 The trend line shows the initial MFCV dropped by 23% during the first 28% of muscle contraction, and then drops 7% until the last 21% of muscle contraction where the MFCV then drops 7%.	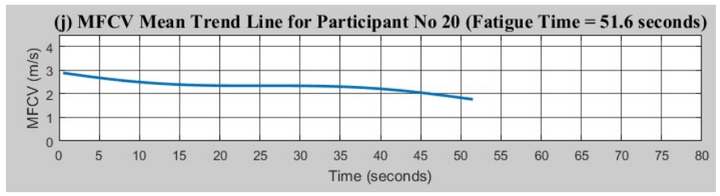 The trend line shows the initial MFCV dropped by 20% during the first 29% of muscle contraction, and then remained steady until the last 36% of muscle contraction where the MFCV then dropped by 17%.
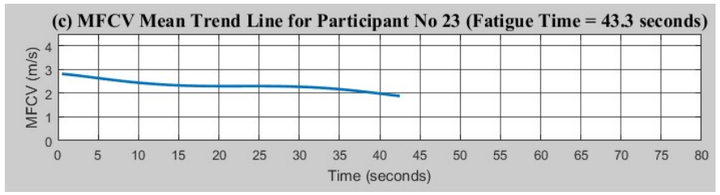 The trend line shows the initial MFCV dropped by 18% during the first 35% of muscle contraction, and then remained steady until the last 30% of muscle contraction where the MFCV then dropped by 14%.	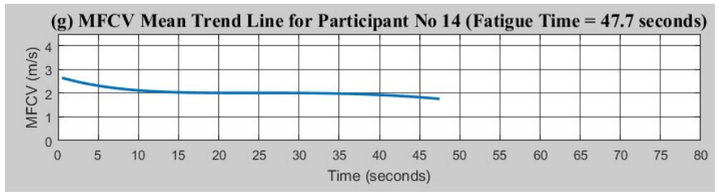 The trend line shows the initial MFCV dropped by 24% during the first 31% of muscle contraction, and then remained steady until the last 27% of muscle contraction where the MFCV then dropped by 9%.	
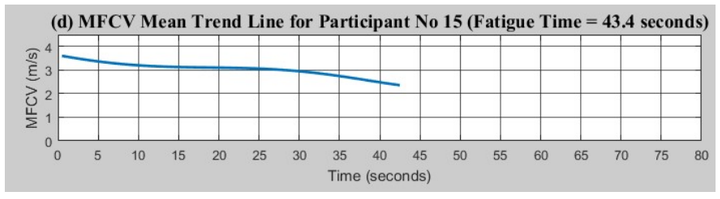 The trend line shows the initial MFCV dropped by 13% during the first 35% of muscle contraction, and then remained steady until the last 41% of muscle contraction where the MFCV then dropped by 19%.	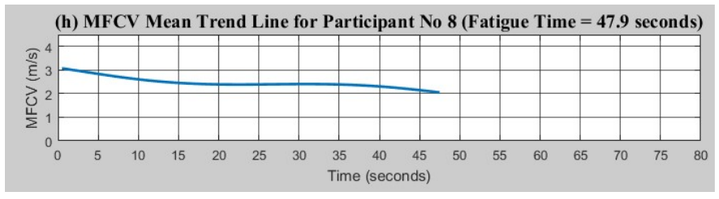 The trend line shows the initial MFCV dropped by 22% during the first 30% of muscle contraction, and then remained steady until the last 27% of muscle contraction where the MFCV then dropped by 13%.	

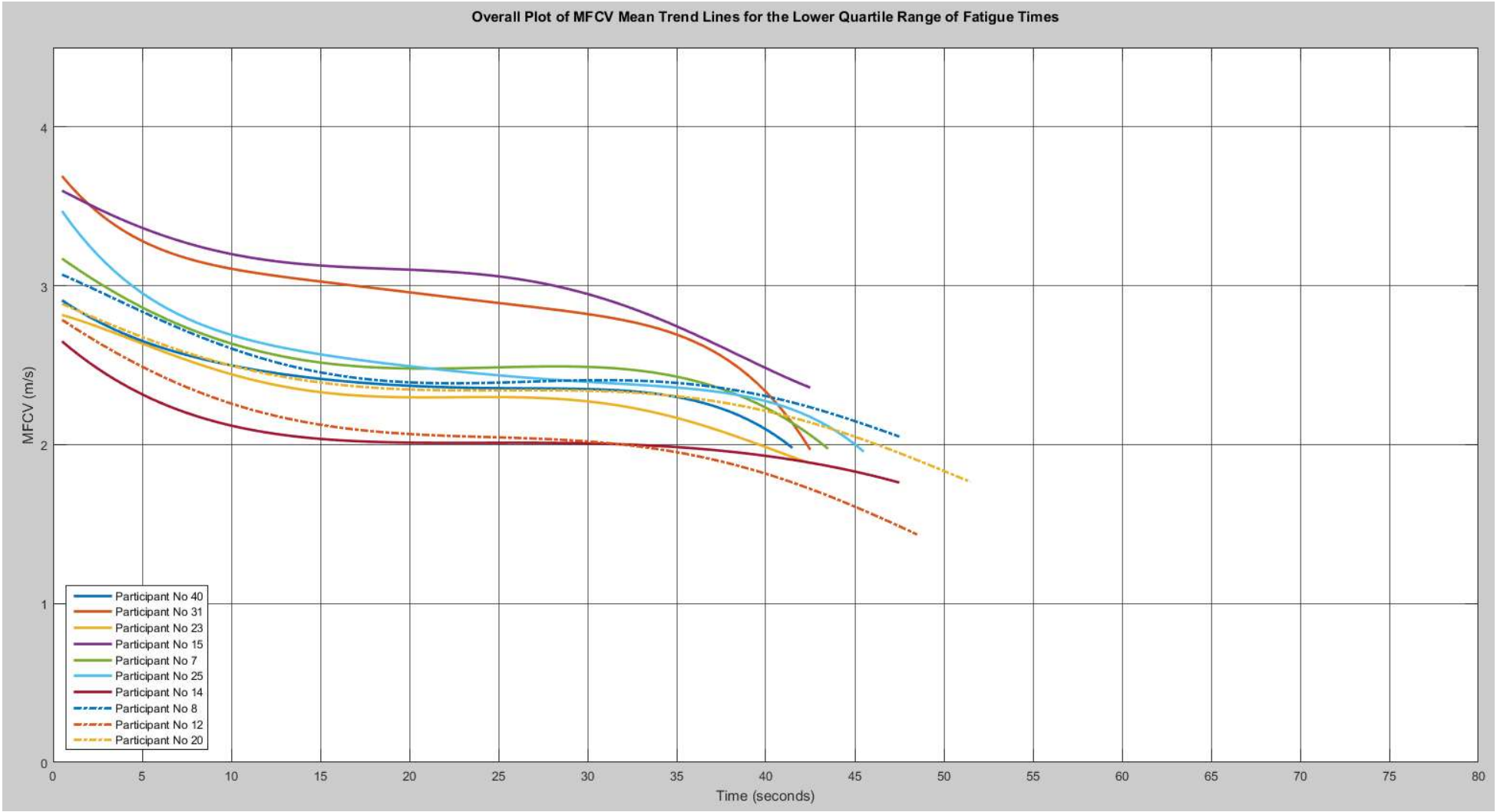

Figure M.3 Overall plot of MFCV mean trend lines for the lower quartile range of fatigue times.

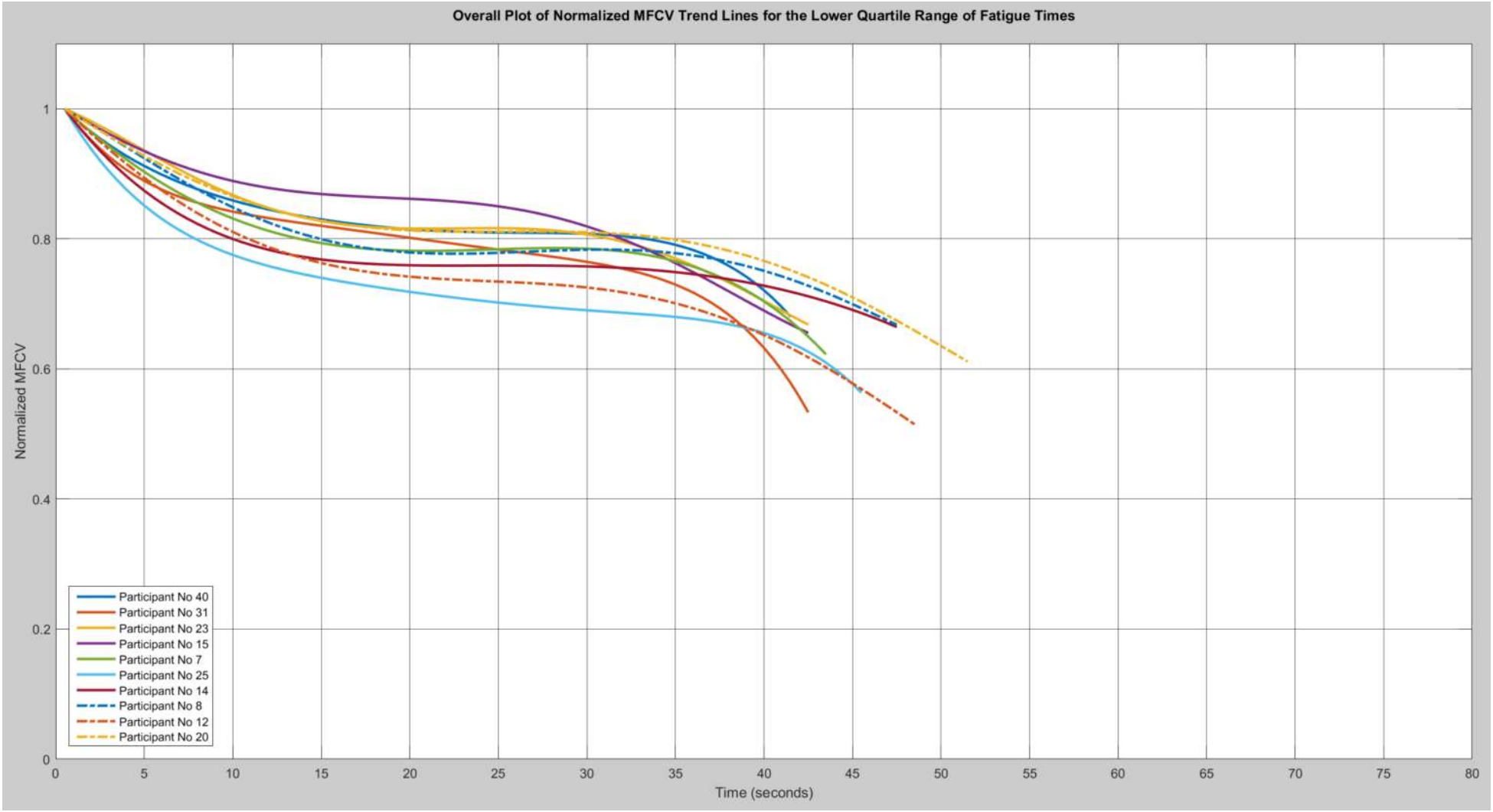

Figure M.4 Overall plot of normalized MFCV mean trend lines for the lower quartile range of fatigue times.

Section M-2: MNF and MFCV Mean Trend Line Analysis for the Interquartile Range of the Fatigue Times

This section presents the results for both the MNF and MFCV features for the interquartile range of the fatigue times, which were carried out by Participant Nos. 18, 19, 22, 32, 13, 36, 3, 33, 5, 24, 10, 29, 4, 1, 28, 11, 39, 37, 26 and 21. Participants are ordered in terms of shortest to longest times.

Table M.3 shows plots (a) – (t) for each participant and an explanation of the MNF feature over the period of the endurance (or fatiguing) task. Figure M.5 shows all the plots from Table M.3 on one plot for comparison purposes. Figure M.6 shows the normalized MNF plots of Figure M.5, equating the maximum values to a value of 1 to give a true comparison of the trend lines.

Table M.4 shows plots (a) – (t) for each participant and an explanation of the MFCV feature over the period of the endurance (or fatiguing) task. Figure M.7 shows all the plots from table M.4 on one plot for comparison purposes. Figure M.8 shows the normalized MFCV plots of Figure M.7, equating the maximum value to a value of 1 to give a true comparison of the trend lines.

Table M.3 Data analysis of the MNF mean trend lines for the interquartile range of fatigue times

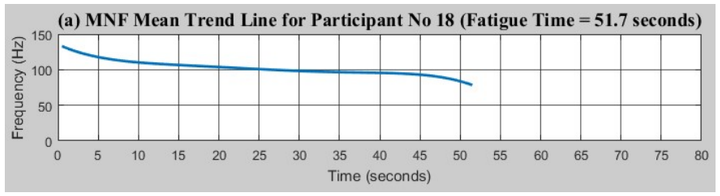 The trend line shows the initial MNF value dropped by 14% during the first 38% of muscle contraction, and then remained relatively steady until the last 17% of muscle contraction where the MNF then dropped by 20%.	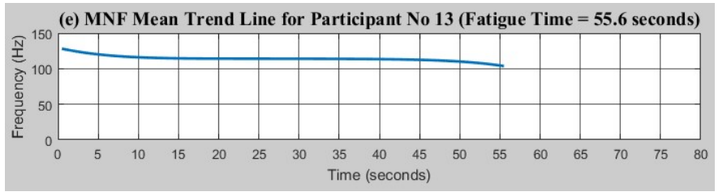 The trend line shows the initial MNF value dropped by 10% during the first 29% of muscle contraction, and then remained steady until the last 19% of muscle contraction where the MNF then dropped by 8%.	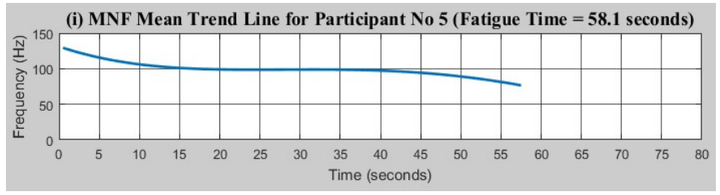 The trend line shows the initial MNF value dropped by 22% during the first 27% of muscle contraction, and then remained steady until the last 32% of muscle contraction where the MNF then dropped by 18%.
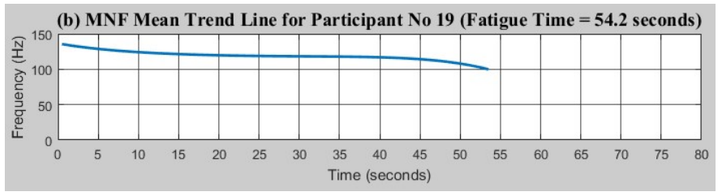 The trend line shows the initial MNF value dropped by 11% during the first 33% of muscle contraction, and then remained steady until the last 22% of muscle contraction where the MNF then dropped by 16%.	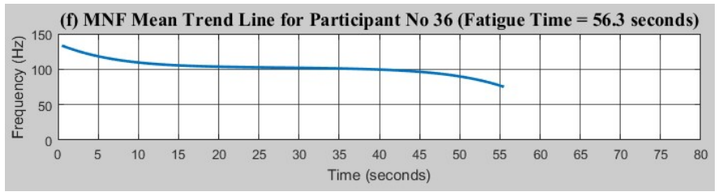 The trend line shows the initial MNF value dropped by 21% during the first 32% of muscle contraction, and then remained steady until the last 21% of muscle contraction where the MNF then dropped by 27%.	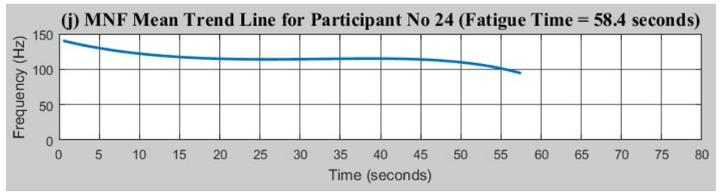 The trend line shows the initial MNF value dropped by 17% during the first 29% of muscle contraction, and then remained steady until the last 20% of muscle contraction where the MNF then dropped by 16%.
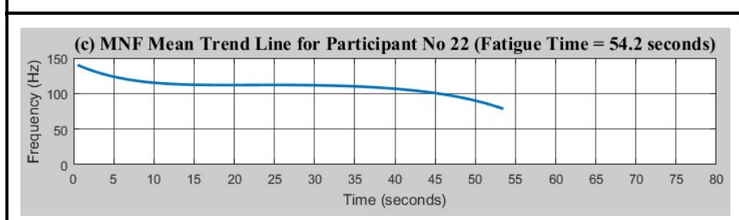 The trend line shows the initial MNF value dropped by 20% during the first 28% of muscle contraction, and then remained steady until the last 27% of muscle contraction where the MNF then dropped by 23%.	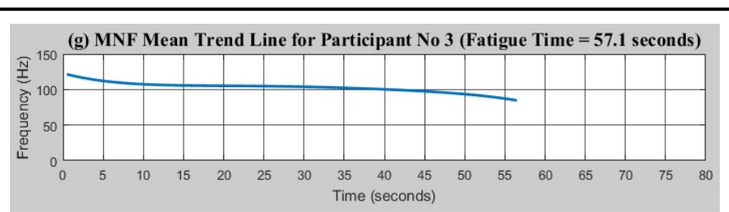 The trend line shows the initial MNF value dropped by 13% during the first 23% of muscle contraction, and then relatively remained steady until the last 12% of muscle contraction where the MNF then dropped by 17%.	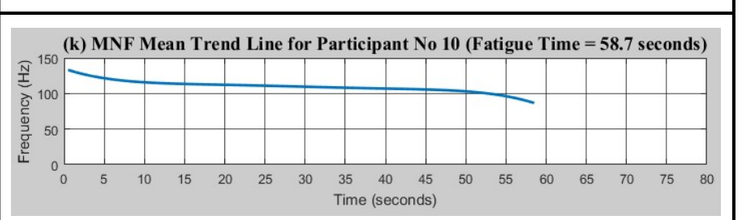 The trend line shows the initial MNF value dropped by 14% during the first 25% of muscle contraction, and then remained relatively steady until the last 18% of muscle contraction where the MNF then dropped by 20%.
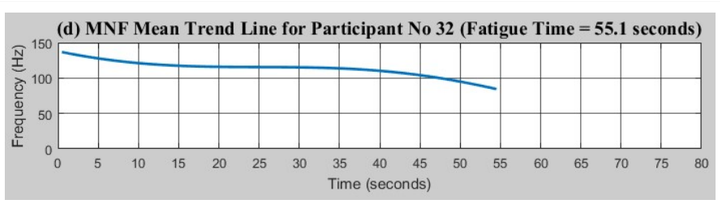 The trend line shows the initial MNF value dropped by 15% during the first 29% of muscle contraction, and then remained steady until the last 32% of muscle contraction where the MNF then dropped by 22%.	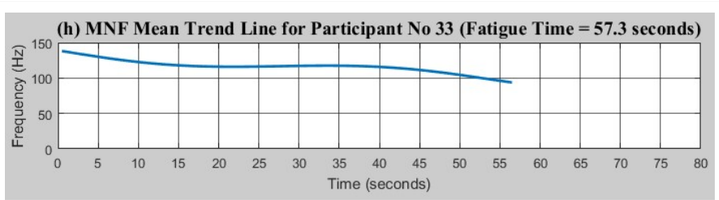 The trend line shows the initial MNF value dropped by 14% during the first 26% of muscle contraction, and then remained steady until the last 22% of muscle contraction where the MNF then dropped by 18%.	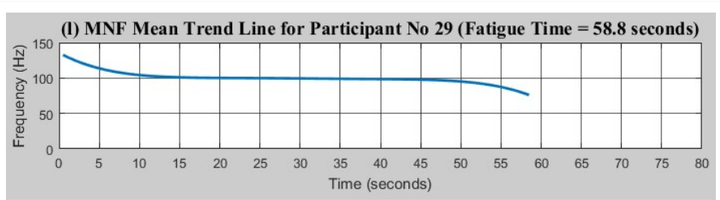 The trend line shows the initial MNF value dropped by 23% during the first 22% of muscle contraction, and then remained steady until the last 15% of muscle contraction where the MNF then dropped by 19%.

Table M.3 (continued)

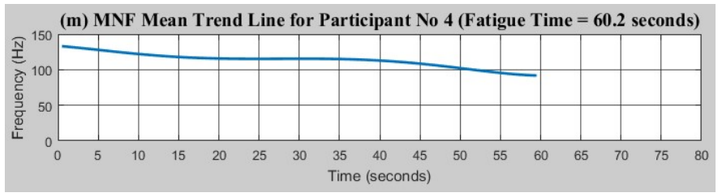	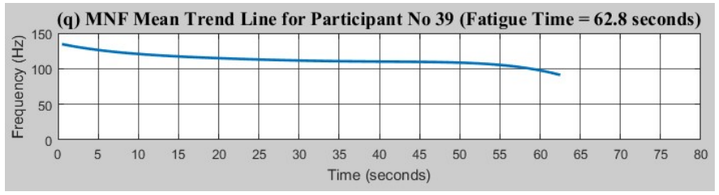
The trend line shows the initial MNF value dropped by 13% during the first 30% of muscle contraction, and then remained steady until the last 36% of muscle contraction where the MNF then dropped by 18%.	The trend line shows the initial MNF value dropped by 14% during the first 30% of muscle contraction, and then remained steady until the last 23% of muscle contraction where the MNF then dropped by 18%.
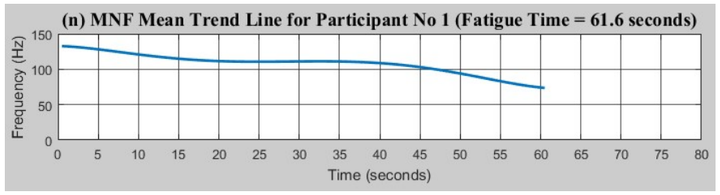	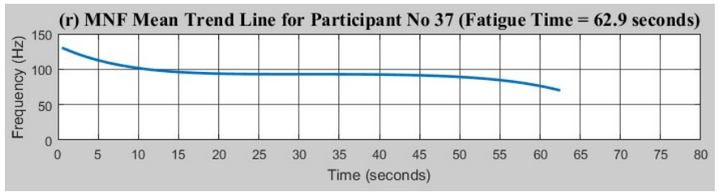
The trend line shows the initial MNF value dropped by 31% during the first 15% of muscle contraction, and then remained steady until the last 36% of muscle contraction where the MNF then dropped by 28%.	The trend line shows the initial MNF value dropped by 28% during the first 29% of muscle contraction, and remained steady until the last 23% of muscle contraction where the MNF then dropped by 18%.
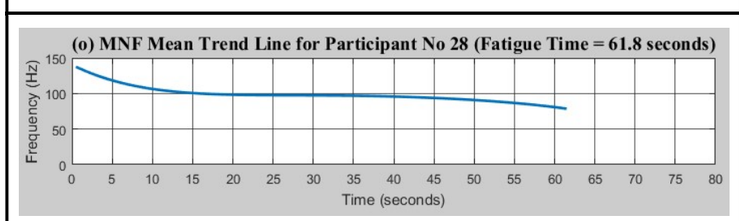	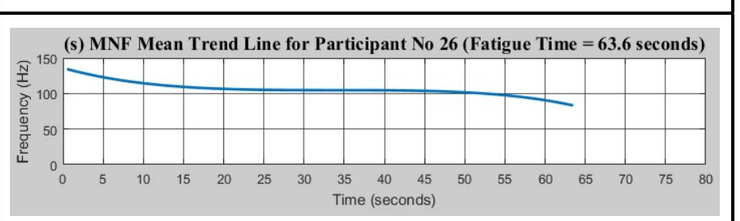
The trend line shows the initial MNF value dropped by 27% during the first 24% during the muscle contraction, and then remained relatively steady until the last 34% of muscle contraction where the MNF then dropped by 16%.	The trend line shows the initial MNF value dropped by 21% during the first 31% of muscle contraction, and then remained steady until the last 28% of muscle contraction where the MNF then dropped by 17%.
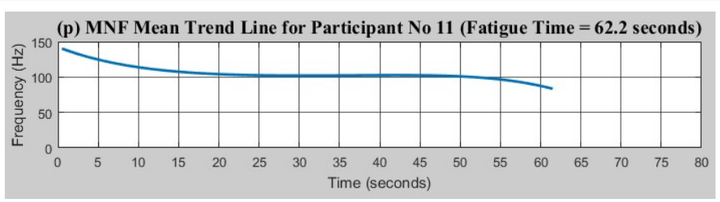	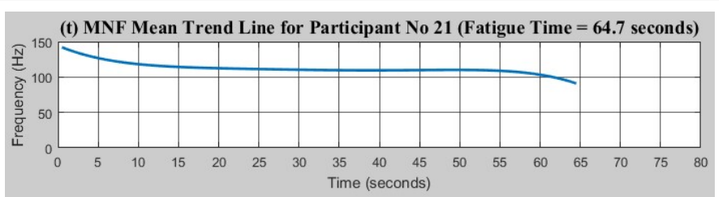
The trend line shows the initial MNF value dropped by 26% during the first 38% of muscle contraction, and then remained steady until the last 19% of muscle contraction where the MNF then dropped by 14%.	The trend line shows the initial MNF value dropped by 20% during the first 24% of muscle contraction, and then remained steady until the last 17% of muscle contraction where the MNF then dropped by 16%.

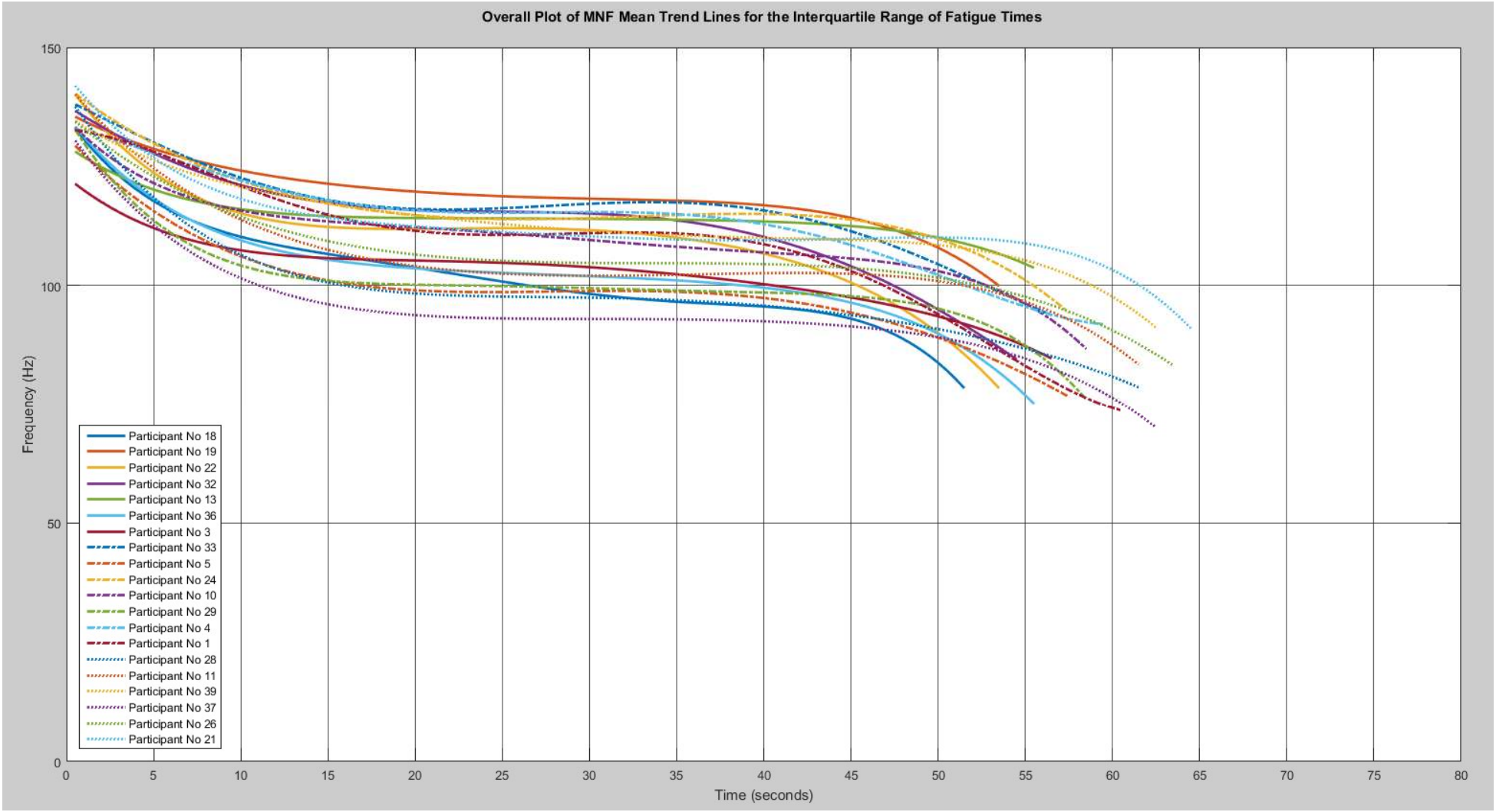

Figure M.5 Overall plot of MNF mean trend lines for the interquartile range of fatigue times.

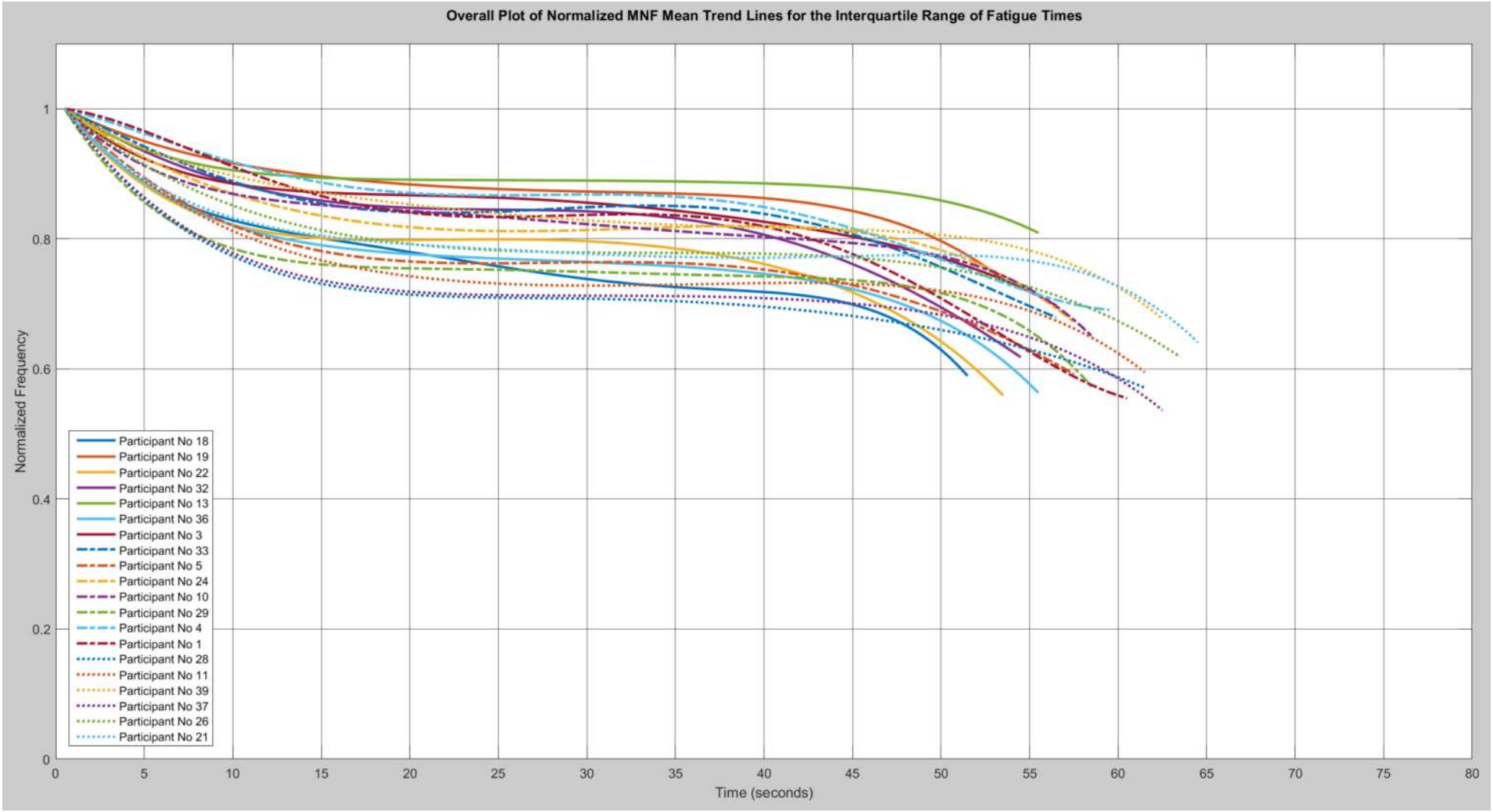

Figure M.6 Overall plot of normalized MNF mean trend lines for the interquartile range of fatigue times.

Table M.4 Data analysis of the MFCV mean trend lines for the interquartile range of fatigue times

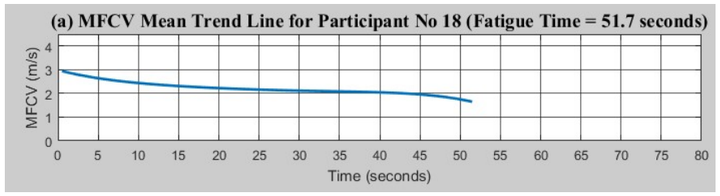 The trend line shows the initial MFCV dropped by 24% during the first 38% of muscle contraction, and then remained relatively steady until the last 21% of muscle contraction where the MFCV then dropped by 20%.	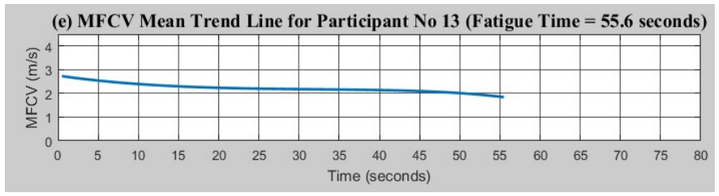 The trend line shows the initial MFCV dropped by 15% during the first 30% of muscle contraction, and then remained relatively steady until the last 23% of muscle contraction where the MFCV then dropped by 19%.	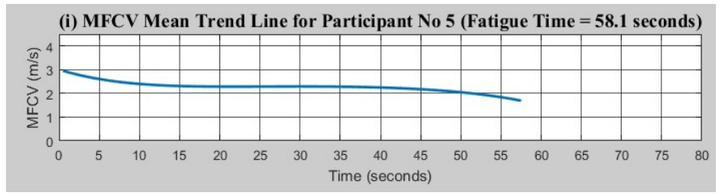 The trend line shows the initial MFCV dropped by 23% during the first 25% of muscle contraction, and then remained steady until the last 33% of muscle contraction where the MFCV then dropped by 20%.
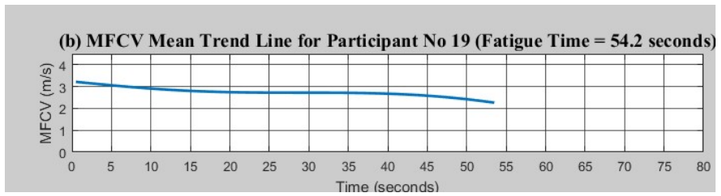 The trend line shows the initial MFCV dropped by 16% during the first 37% of muscle contraction, and then remained steady until the last 22% of muscle contraction where the MFCV then drops 16%.	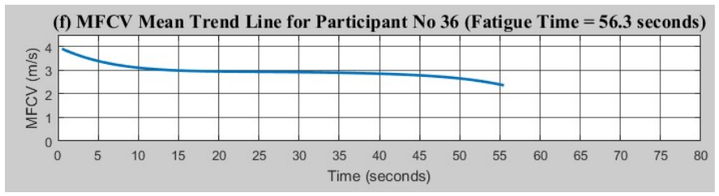 The trend line shows the initial MFCV dropped by 23% during the first 25% of muscle contraction, and then remained steady until the last 21% of muscle contraction where the MFCV then drops 25%.	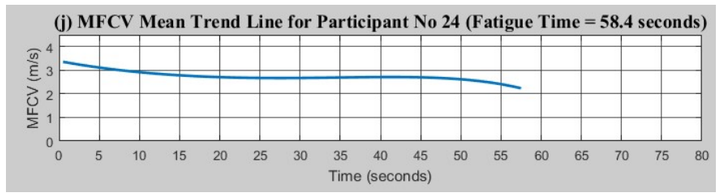 The trend line shows the initial MFCV dropped by 18% during the first 31% of muscle contraction, and then remained steady until the last 18% of muscle contraction where the MFCV then dropped by 13%.
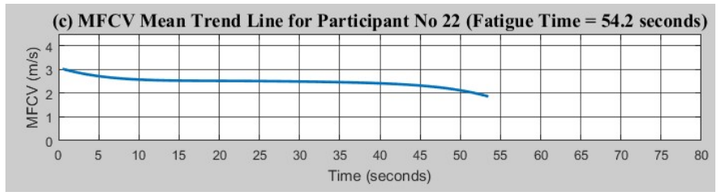 The trend line shows the initial MFCV dropped by 16% during the first 22% of muscle contraction, and then remained steady until the last 24% of muscle contraction where the MFCV then dropped by 23%.	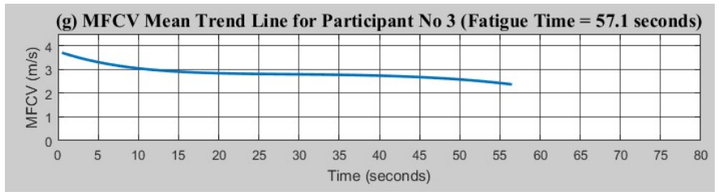 The trend line shows the initial MFCV dropped by 24% during the first 31% of muscle contraction, and then remained steady until the last 26% of muscle contraction where the MFCV then dropped by 11%.	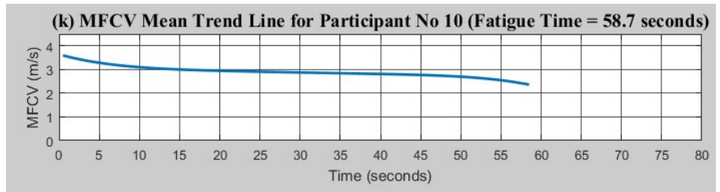 The trend line shows the initial MFCV dropped by 17% during the first 28% of muscle contraction, and then remained relatively steady until the last 33% of muscle contraction where the MFCV then dropped by 17%.
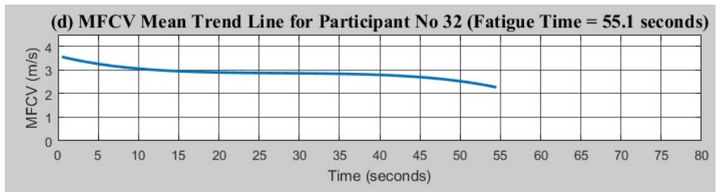 The trend line shows the initial MFCV dropped by 21% during the first 14% of muscle contraction, and then remained steady until the last 25% of muscle contraction where the MFCV then dropped by 22%.	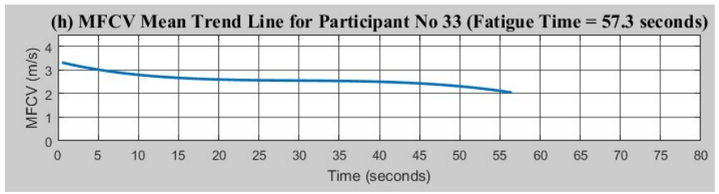 The trend line shows the initial MFCV dropped by 21% during the first 30% of muscle contraction, and then remained steady until the last 24% of muscle contraction where the MFCV then dropped by 18%.	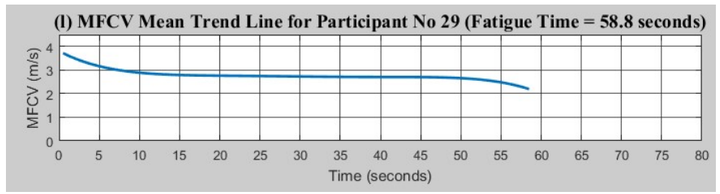 The trend line shows the initial MFCV dropped by 24% during the first 24% of muscle contraction, and then remained steady until the last 13% of muscle contraction where the MFCV then dropped by 16%.

Table M.4 (continued)

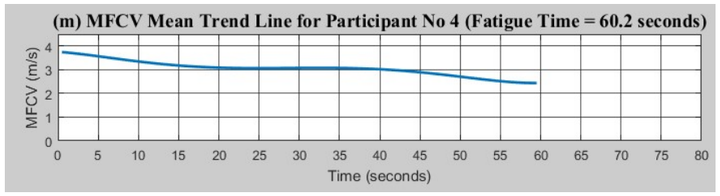	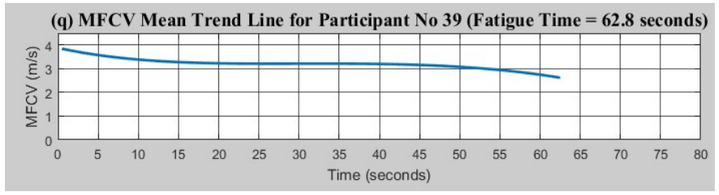
The trend line shows the initial MFCV dropped by 16% during the first 30% of muscle contraction, and then remained steady until the last 40% of muscle contraction where the MFCV then dropped by 18%.	The trend line shows the initial MFCV dropped by 16% during the first 25% of muscle contraction, and then remained steady until the last 19% of muscle contraction where the MFCV then dropped by 25%.
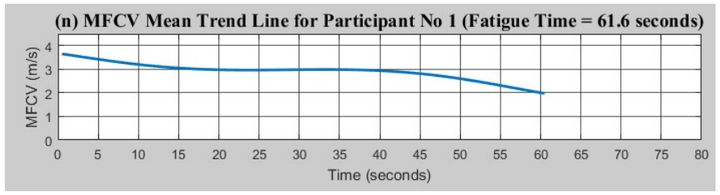	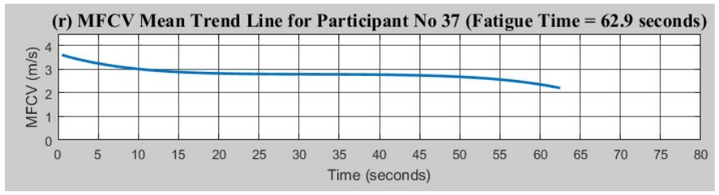
The trend line shows the initial MFCV dropped by 16% during the first 26% of muscle contraction, and then remained steady until the last 37% of muscle contraction where the MFCV then dropped by 30%.	The trend line shows the initial MFCV dropped by 19% during the first 20% of muscle contraction, and then remained steady until the last 16% of muscle contraction where the MFCV then dropped by 19%.
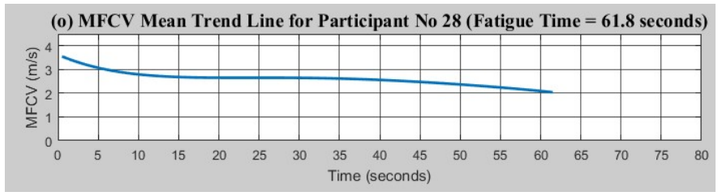	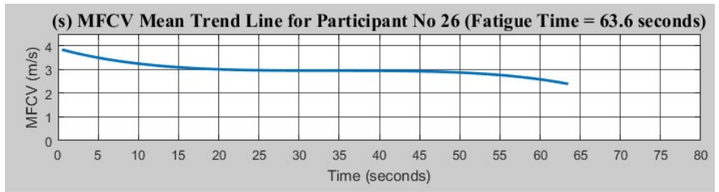
The trend line shows the initial MFCV dropped by 26% during the first 24% of muscle contraction, and then remained steady until the last 32% of muscle contraction where the MFCV then dropped by 17%.	The trend line shows the initial MFCV dropped by 21% during the first 28% of muscle contraction, and then remained steady until the last 25% of muscle contraction where the MFCV then dropped by 18%.
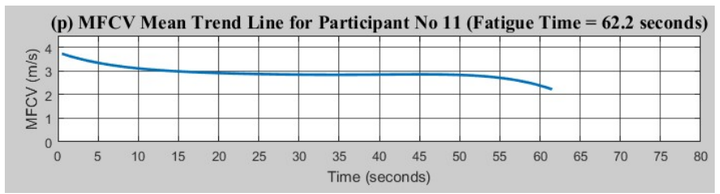	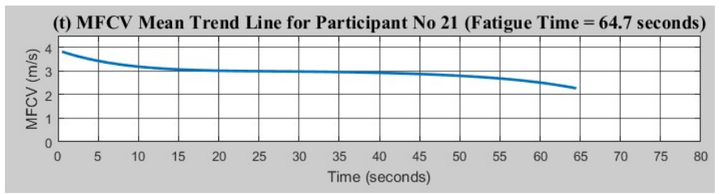
The trend line shows the initial MFCV dropped by 22% during the first 29% of muscle contraction, and then remained steady until the last 21% of muscle contraction where the MFCV then dropped by 18%.	The trend line shows the initial MFCV dropped by 21% during the first 30% of muscle contraction, and then remained steady until the last 35% of muscle contraction where the MFCV then dropped by 20%.

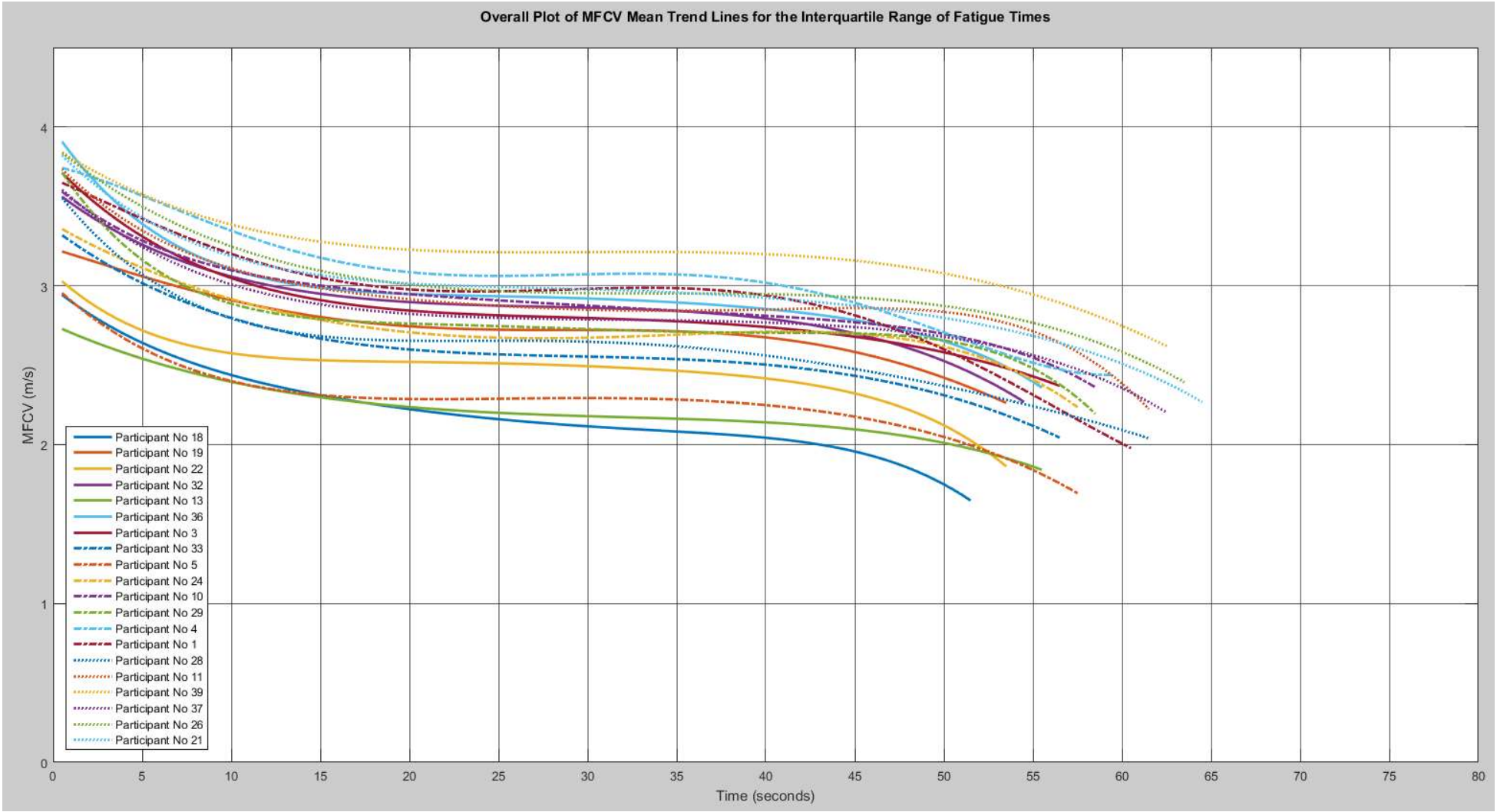

Figure M.7 Overall plot of MFCV mean trend lines for the interquartile range of fatigue times.

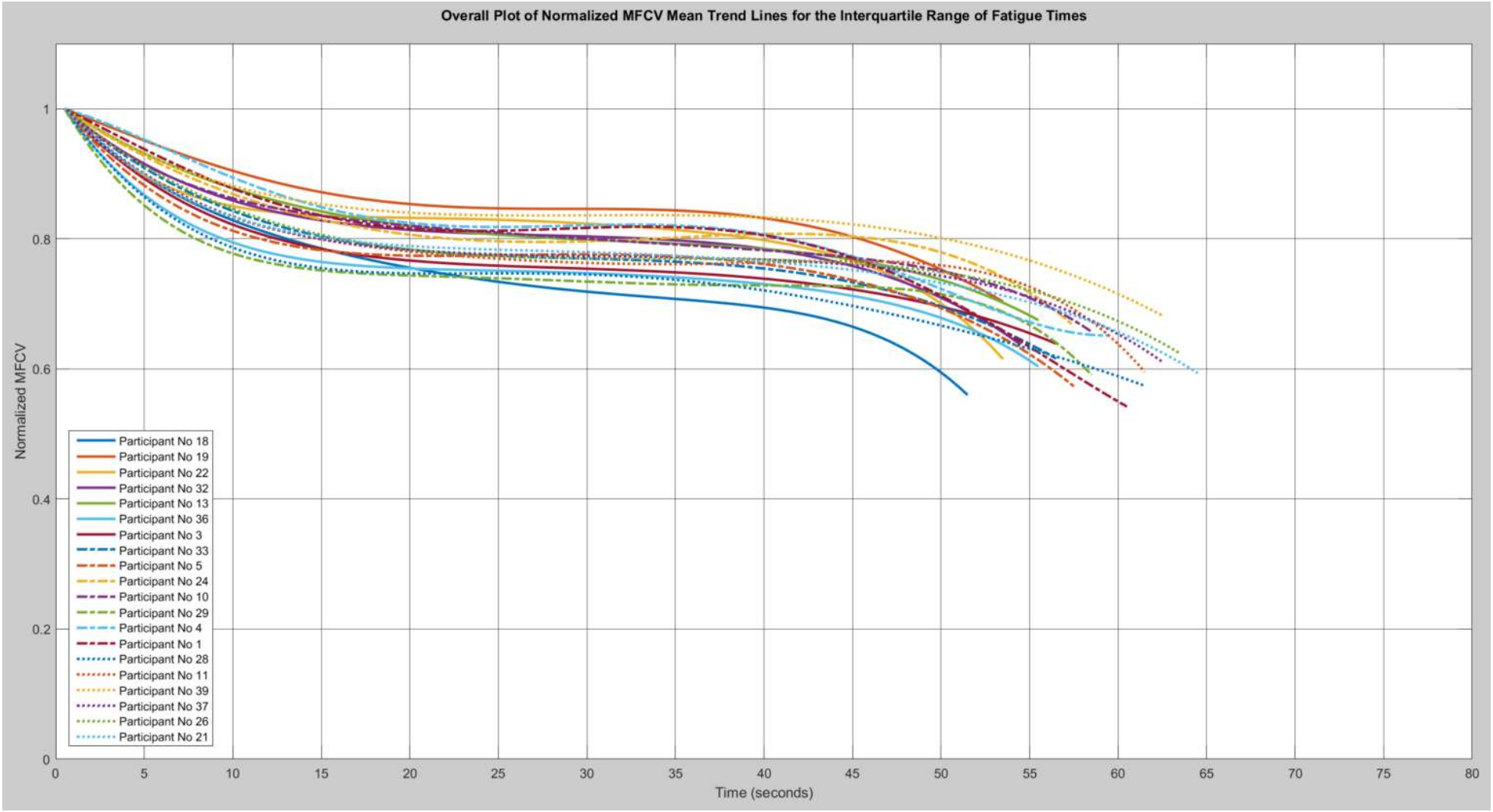

Figure M.8 Overall plot of normalized MFCV mean trend lines for the interquartile range of fatigue times.

Section M-3: MNF and MFCV Mean Trend Line Analysis for the Upper Quartile Range of the Fatigue Times

This section presents the results for both the MNF and MFCV features for the upper quartile range of the fatigue times, which were carried out by participants Nos. 30, 6, 16, 2, 35, 9, 34, 38, 27 and 17. Participants are ordered in terms of shortest to longest times.

Table M.5 shows plots (a) – (j) for each participant and an explanation of the MNF feature over the period of the endurance (or fatiguing) task. Figure M.9 shows all the plots from Table M.5 on one plot for comparison purposes. Figure M.10 shows the normalized MNF plots of Figure M.9, equating the maximum values to a value of 1 to give a true comparison of the trend lines.

Table M.6 shows plots (a) – (j) for each participant and an explanation of the MFCV feature over the period of the endurance (or fatiguing) task. Figure M.11 shows all the plots from Table M.6 on one plot for comparison purposes. Figure M.12 shows the normalized MFCV plots of Figure M.11, equating the maximum values to a value of 1 to give a true comparison of the trend lines.

Table M.5 Data analysis of the MNF mean trend lines for the upper quartile range of fatigue times

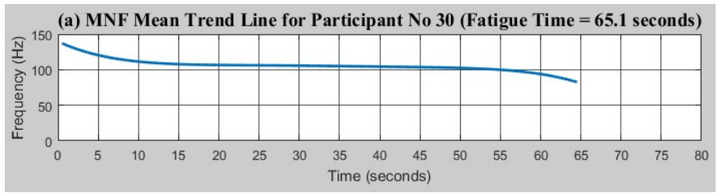 The trend line shows the initial MNF value dropped by 19% during the first 17% of muscle contraction, and then remained steady until the last 16% of muscle contraction where the MNF then dropped by 18%.	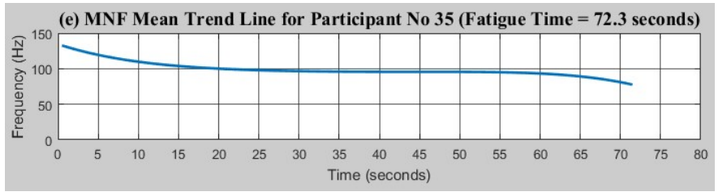 The trend line shows the initial MNF value dropped by 23% during the first 25% of muscle contraction, and then remained relatively steady until the last 23% of muscle contraction where the MNF then dropped by 18%.	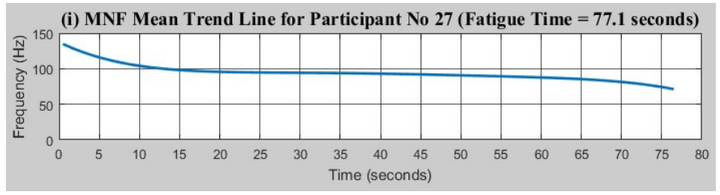 The trend line shows the initial MNF value dropped by 28% during the first 20% of muscle contraction, and then remained steady until the last 24% of muscle contraction where the MNF then dropped by 19%.
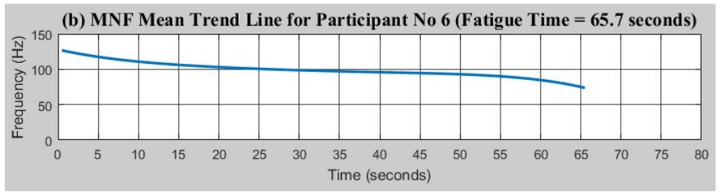 The trend line shows the initial MNF value dropped by 20% during the first 36% of muscle contraction, and then remained relatively steady until the last 21% of muscle contraction where the MNF then dropped by 14%.	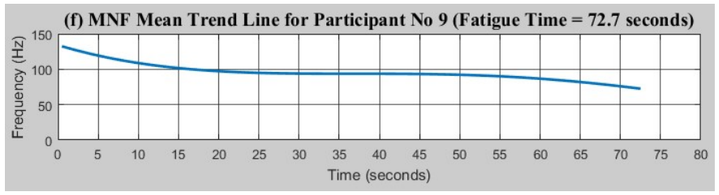 The trend line shows the initial MNF value dropped by 28% during the first 32% of muscle contraction, and then remained steady until the last 28% of muscle contraction where the MNF then dropped by 17%.	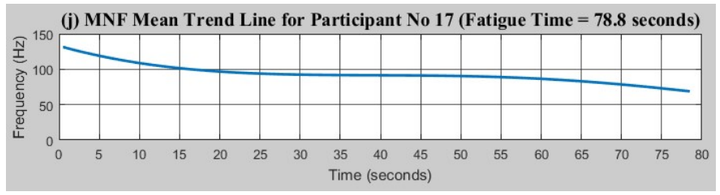 The trend line shows the initial MNF value dropped by 27% during the first 28% of muscle contraction, and then remained steady until the last 30% of muscle contraction where the MNF then dropped by 19%.
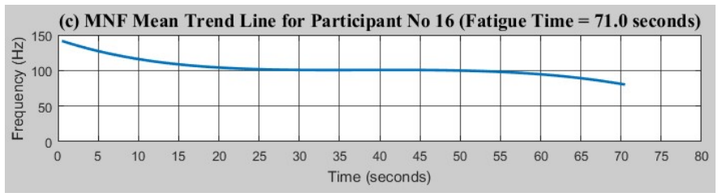 The trend line shows the initial MNF value dropped by 28% during the first 33% of muscle contraction, and then remained steady until the last 24% of muscle contraction where the MNF then dropped by 15%.	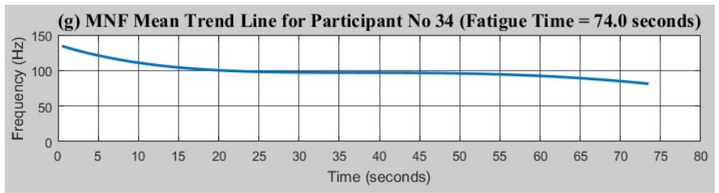 The trend line shows the initial MNF value dropped by 24% during the first 20% of muscle contraction, and then remained steady until the last 18% of muscle contraction where the MNF then dropped by 16%.	
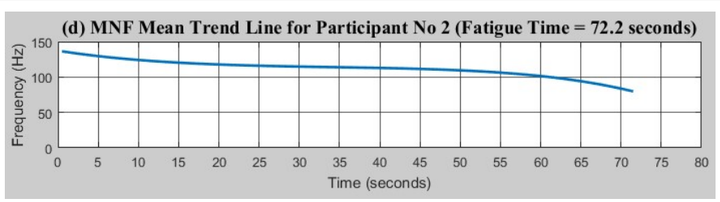 The trend line shows the initial MNF value dropped by 14% during the first 28% during the muscle contraction, and then remained relatively steady until the last 30% of muscle contraction where the MNF then dropped by 22%.	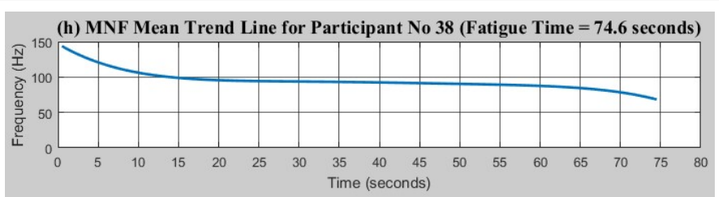 The trend line shows the initial MNF value dropped by 33% during the first 28% of muscle contraction, and then remained steady until the last 22% of muscle contraction where the MNF then dropped by 20%.	

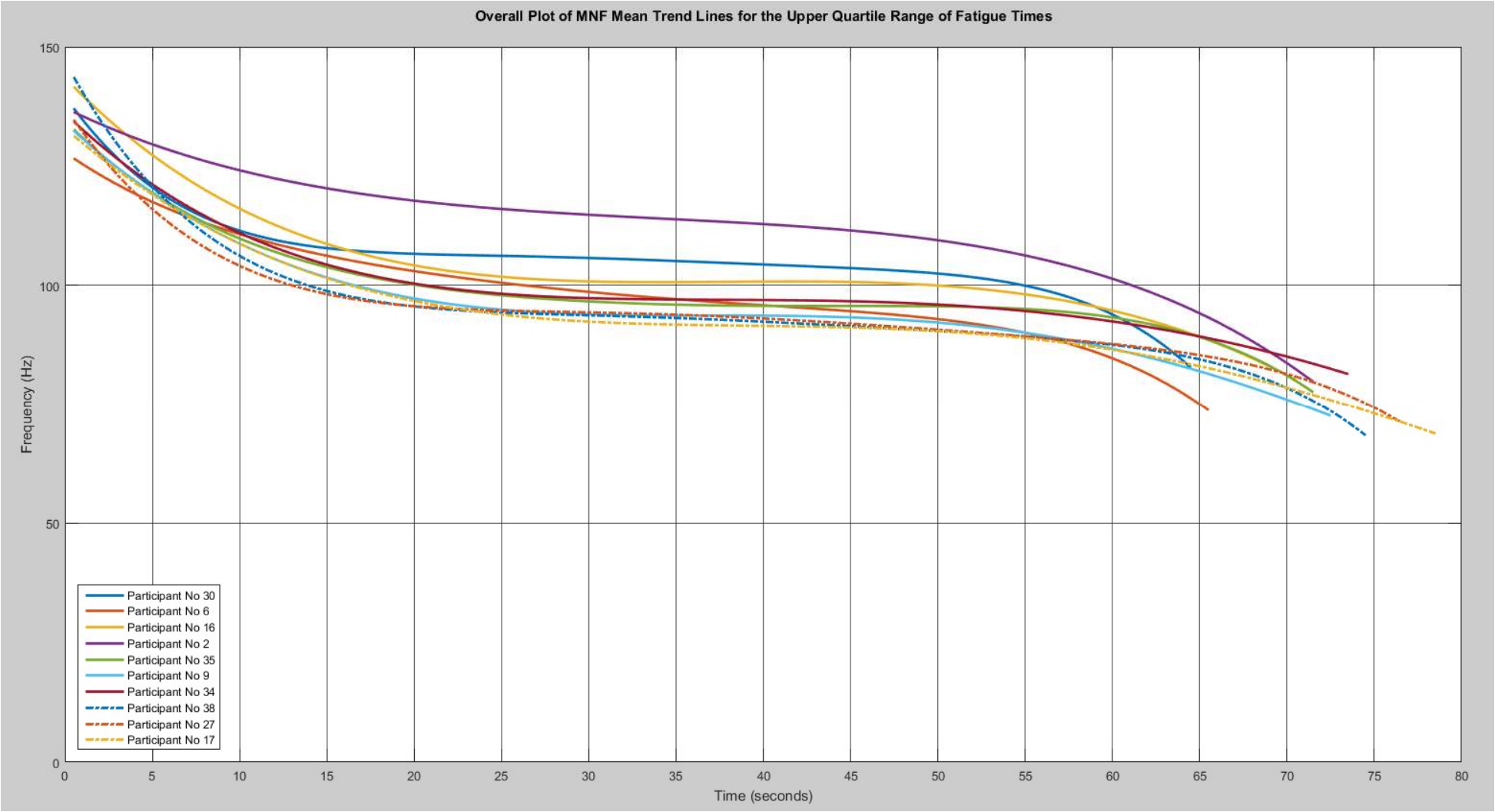

Figure M.9 Overall plot of MNF mean trend lines for the upper quartile range of fatigue times.

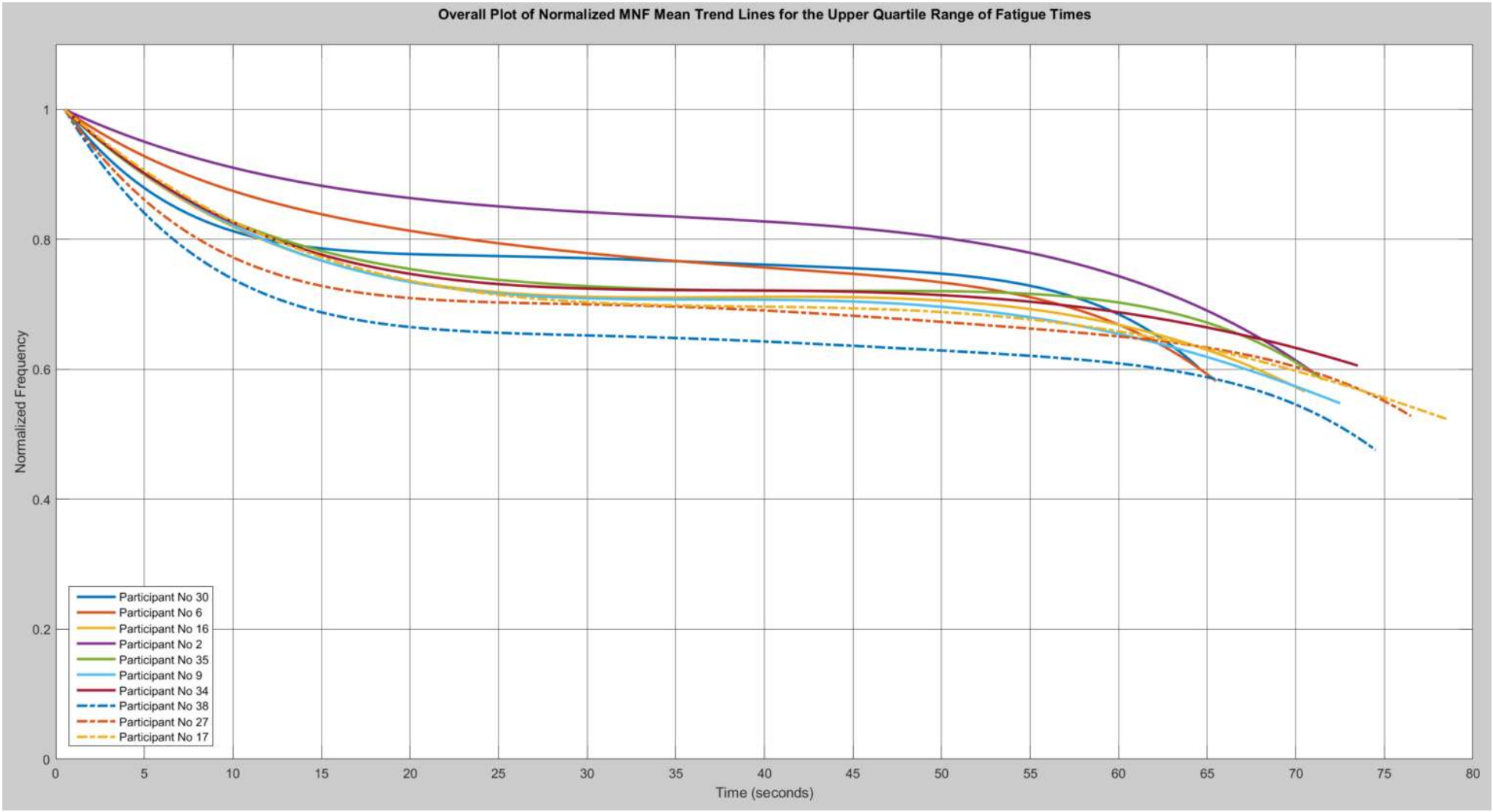

Figure M.10 Overall plot of normalized MNF mean trend lines for the upper quartile range of fatigue times.

Table M.6 Data analysis of the MFCV trend Lines for the upper quartile range of fatigue times

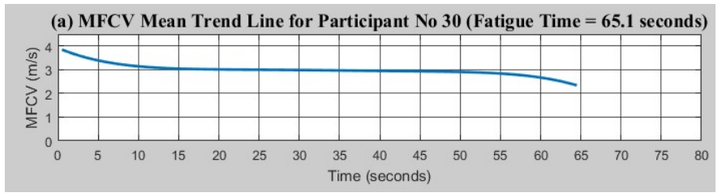 The trend line shows the initial MFCV dropped by 19% during the first 25% of muscle contraction, and then remained steady until the last 21% of muscle contraction where the MFCV then dropped by 18%.	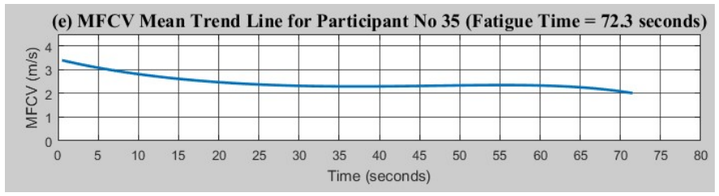 The trend line shows the initial MFCV dropped by 29% during the first 27% of muscle contraction, and then remained relatively steady until the last 14% of muscle contraction where the MFCV then dropped by 12%.	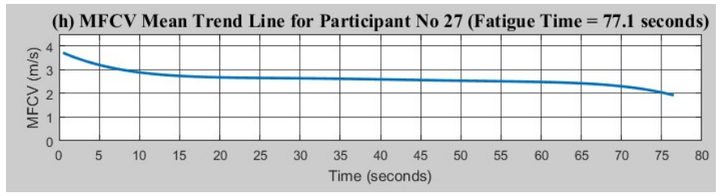 The trend line shows the initial MFCV dropped by 27% during the first 21% of muscle contraction, and then remained steady until the last 14% of muscle contraction where the MFCV then dropped by 22%.
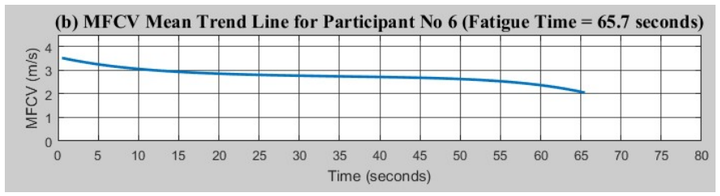 The trend line shows the initial MFCV dropped by 17% during the first 22% of muscle contraction, and then remained relatively steady until the last 28% of muscle contraction where the MFCV then dropped by 22%.	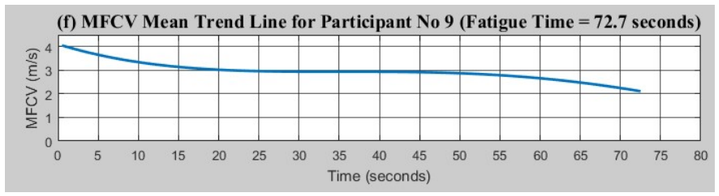 The trend line shows the initial MFCV dropped by 25% during the first 27% of muscle contraction, and then remained steady until the last 31% of muscle contraction where the MFCV then dropped by 23%.	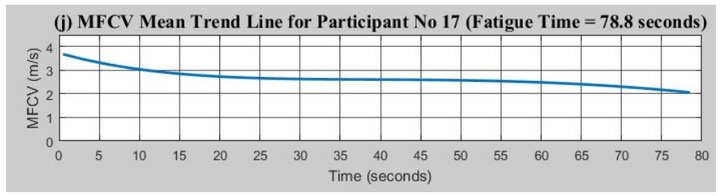 The trend line shows the initial MFCV dropped by 25% during the first 25% of muscle contraction, and then remained steady until the last 30% of muscle contraction where the MFCV then dropped by 18%.
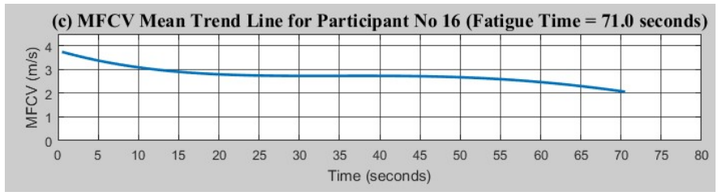 The trend line shows the initial MFCV dropped by 26% during the first 33% of muscle contraction, and then remained steady until the last 27% of muscle contraction where the MFCV then dropped by 18%.	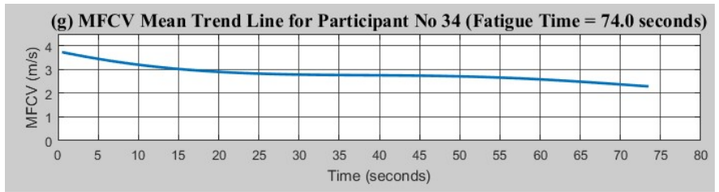 The trend line shows the initial MFCV dropped by 22% during the first 25% of muscle contraction, and then remained steady until the last 18% of muscle contraction where the MFCV then dropped by 19%.	
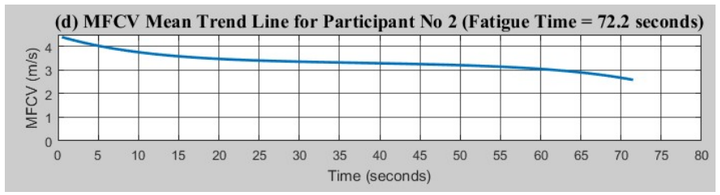 The trend line shows the initial MFCV dropped by 20% during the first 25% of muscle contraction, and then remained relatively steady until the last 24% of muscle contraction where the MFCV then dropped by 14%.	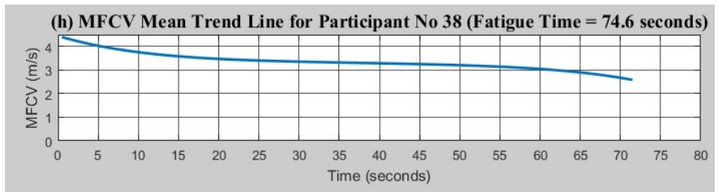 The trend line shows the initial MFCV dropped by 28% during the first 30% of muscle contraction, and then remained steady until the last 25% of muscle contraction where the MFCV then dropped by 19%.	

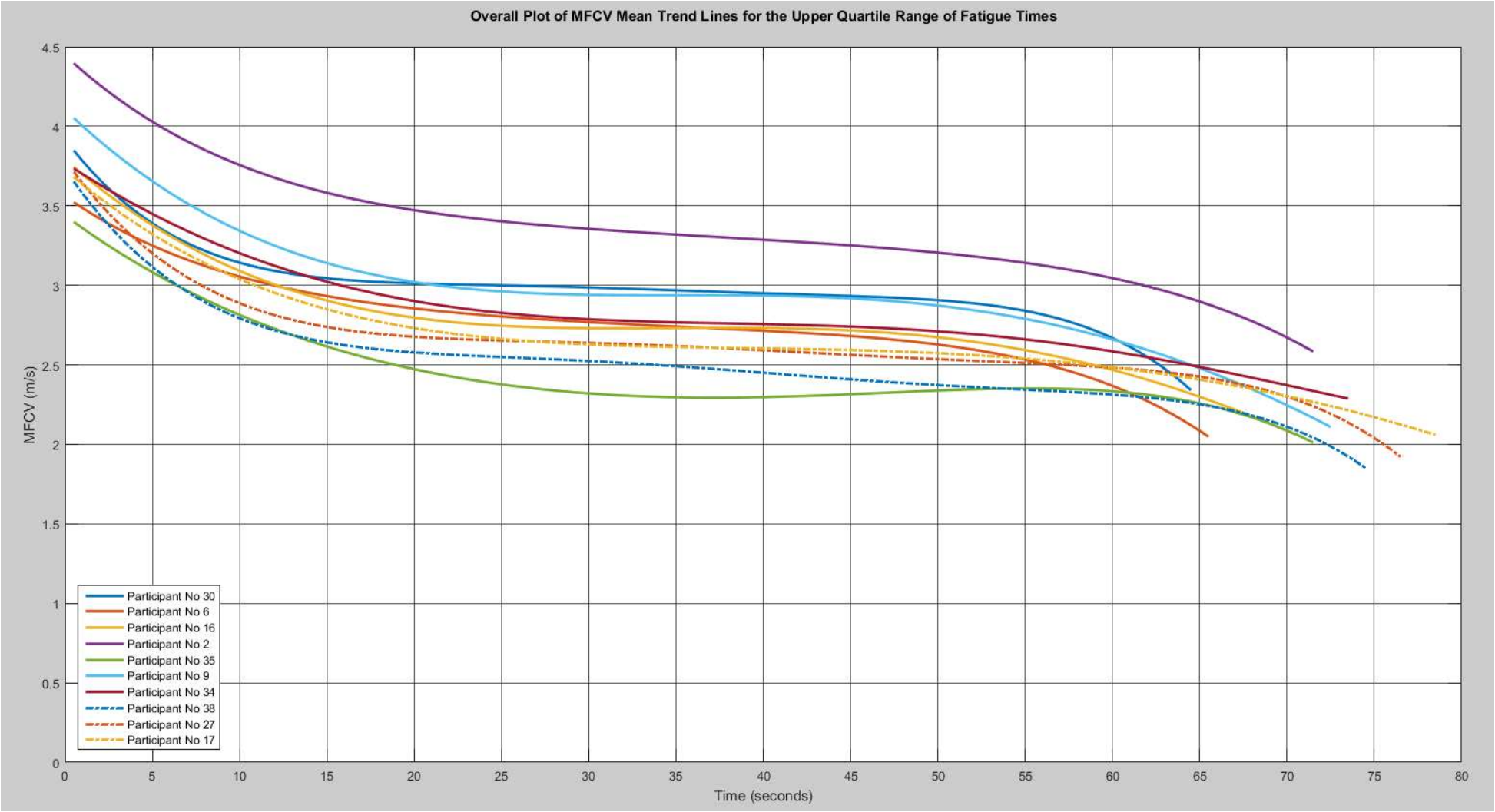

Figure M.11 Overall plot of MFCV mean trend lines for the upper quartile range of fatigue times.

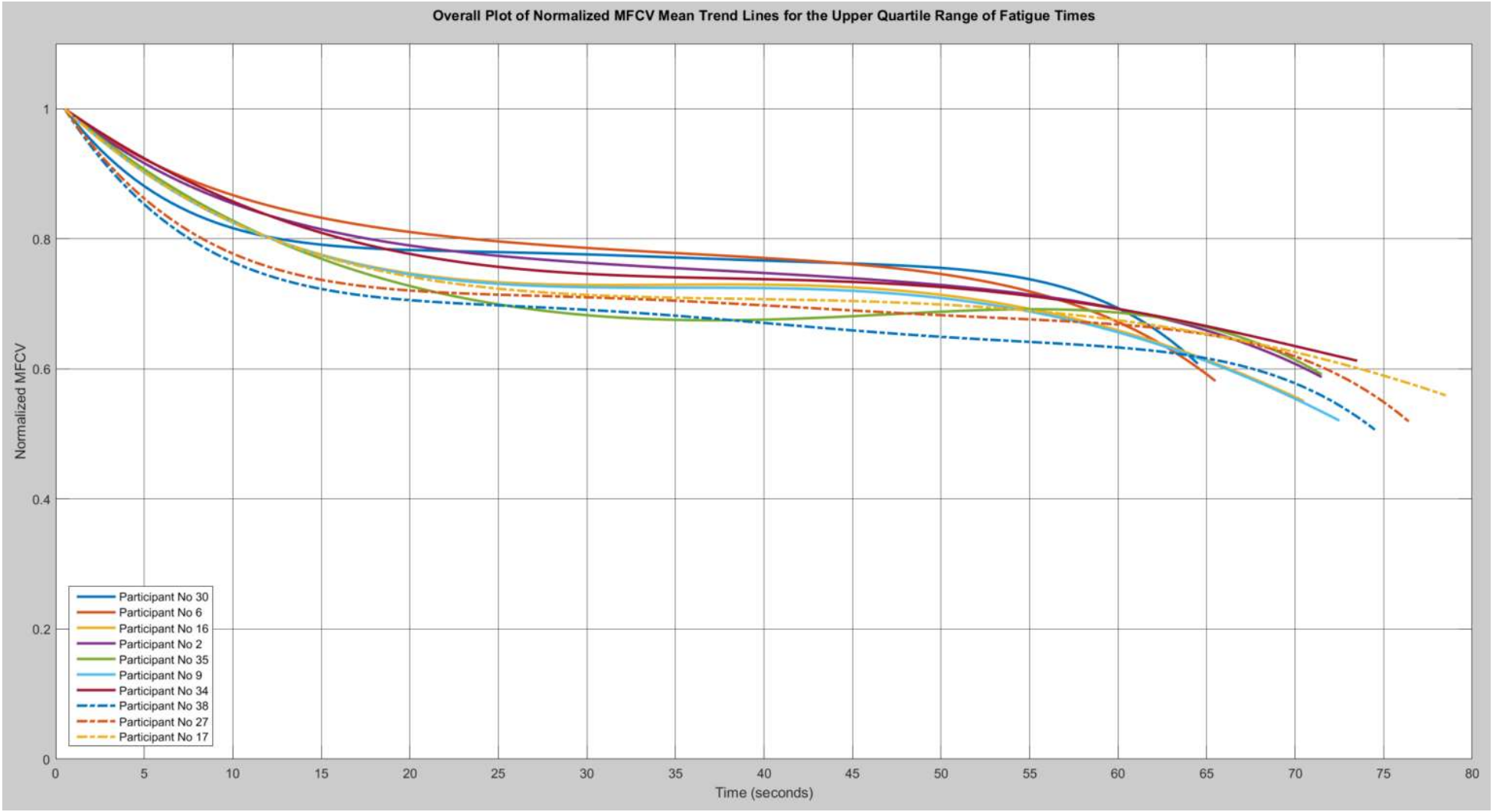

Figure M.12 Overall plot of normalized MFCV mean trend lines for the upper quartile range of fatigue times.

Appendix N: Statistical Analysis of MNF and MFCV Mean Trend Lines

		MNF Trend Lines Values			
		Start of Contraction		End of Contraction	
	Participant No	Drop (%)	Period (%)	Drop (%)	Period (%)
Lower Quartile Range	40	21	45	11	20
	31	17	23	20	19
	23	18	34	16	30
	15	11	23	24	53
	7	21	45	11	20
	25	23	43	13	24
	14	27	41	10	38
	8	15	40	9	35
	12	27	40	13	28
	20	14	29	9	32
Interquartile Range	18	14	38	20	17
	19	11	33	16	22
	22	20	28	23	27
	32	15	29	22	32
	13	10	29	8	19
	36	21	32	27	21
	3	13	23	17	12
	33	14	26	18	22
	5	22	27	18	32
	24	17	29	16	20
	10	14	25	20	18
	29	23	22	19	15
	4	13	30	18	36
	1	31	15	28	16
	28	27	24	16	34
	11	26	38	14	19
	39	14	30	18	23
	37	28	29	18	23
	26	21	31	17	28
	21	20	24	16	17
Upper Quartile Range	30	19	17	18	16
	6	20	36	14	21
	16	28	33	15	24
	2	14	28	22	30
	35	23	25	18	23
	9	28	32	17	28
	34	24	20	16	18
	38	33	28	20	22
	27	28	20	19	24
	17	27	28	30	30
	Mean Value	20.3	29.8	17.4	24.7
	Maximum Value	33	45	30	53
	Minimum Value	10	15	8	12

		MFCV Trend Lines Values			
		Start of Contraction		End of Contraction	
	Participant No	Drop (%)	Period (%)	Drop (%)	Period (%)
Lower Quartile Range	40	17	48	13	21
	31	16	23	18	23
	23	18	35	14	30
	15	13	35	19	41
	7	19	34	16	32
	25	23	28	7	21
	14	24	31	9	27
	8	22	30	13	27
	12	25	35	26	38
	20	20	29	17	36
Interquartile Range	18	24	38	20	21
	19	16	37	16	22
	22	16	22	23	24
	32	21	14	22	25
	13	15	30	19	23
	36	23	25	25	21
	3	24	31	11	26
	33	21	30	18	24
	5	23	25	20	33
	24	18	31	13	18
	10	17	28	17	33
	29	24	24	16	13
	4	16	30	18	40
	1	16	26	30	37
	28	26	24	17	32
	11	22	29	18	21
	39	16	25	25	19
	37	19	20	19	16
	26	21	28	18	25
	21	21	30	20	35
Upper Quartile Range	30	19	25	18	21
	6	17	22	22	28
	16	26	26	18	27
	2	20	25	14	24
	35	29	27	12	14
	9	25	27	23	31
	34	22	25	19	18
	38	28	30	19	25
	27	27	21	22	14
	17	25	25	18	30
	Mean Value	20.9	28.2	18.1	25.9
	Maximum Value	29	48	30	41
	Minimum Value	13	14	7	13

Appendix O: Published Papers

Paper 1. J. Kilby and K. Prasad, "Continuous Wavelet Analysis and Classification of Surface Electromyography Signals", *International Journal of Computer and Electrical Engineering,* vol. 5, pp. 30-35, 2013.

Paper 2. J. Kilby and K. Prasad, "Analysis of Surface Electromyography Signals using Discrete Fourier Transform Sliding Window Technique", *International Journal of Computer Theory and Engineering,* vol. 5, pp. 321-325, 2013.

Paper 3. J. Kilby and K. Prasad, "Extracting Temporal and Spectral Parameters from Surface Electromyography Signals During a Fatigue Contraction", *International Journal of Signal Processing Systems,* vol. 1, pp. 278-283, 2013.

Paper 4. J. Kilby and K. Prasad, "A Comparison of Surface Electromyography Signals Temporal and Spectral Parameters during a Sustained Fatigue Contraction", *Advanced Science, Engineering and Medicine,* vol. 6, pp. 56-61, 2014.

Paper 5. J. Kilby, K. Prasad, and G. Mawston, "Multi-channel Surface Electromyography Electrodes: A Review", *IEEE Sensors Journal*, vol. 16, pp. 5510-5519, 2016.

Paper 6. J. Kilby, K. Prasad, and G. Mawston, "Design of New Multi-channel Electrodes for Surface Electromyography Signals for Signal-Processing", *in Proceedings of the 38th Annual International Conference of the IEEE Engineering in Medicine and Biology Society (EMBC),* 2016, pp. 4853-4856.

Paper 1

International Journal of Computer and Electrical Engineering, Vol. 5, No. 1, February 2013

Continuous Wavelet Analysis and Classification of Surface Electromyography Signals

J. Kilby and K. Prasad

***Abstract*—The purpose of this research is to classify Surface Electromyography (SEMG) signals for normal muscle activity. The aim is to use different extracted features from Continuous Wavelet Transform (CWT) to build and train an Artificial Neural Network (ANN). The extracted features of the SEMG signals used in this research are the mean frequency and the median frequency of the Fourier Power Spectrum along with the RMS values of the signal. These features will be extracted at the selected scales of 8, 16, 32, 64 and 128 of the CWT. The SEMG were collected from normal vastus lateralis and vastus medialis muscles of both legs from 45 male subjects at 25%, 50%, and 75% of their Maximum Voluntary Isometric Contraction (MVIC) force of the quadriceps. Using CWT for extracting features in order to analyse and classify SEMG signals by an ANN has shown to be sound and successful for the basis implementation for developing an intelligent SEMG signal classifier.**

***Index Terms*—Component, electromyography, wavelet, fourier, neural network.**

I. Introduction

Feature extraction and pattern recognition is the key in processing and analysing bio-medical signals. The use of the signal analysis is apparent in the field of clinical health for diagnosing health related problems and rehabilitation using bio-medical signals such as Electromyography (EMG) signals. The EMG signals, also commonly known as myoelectric signals, are obtained by means of recording the activity of striated muscle using sensors or electrodes.

An accurate and computationally efficient means of classifying myoelectric signal patterns has been the subject of considerable research effort in recent years where having effective feature extraction is crucial for reliable classification [1]. Numerous research and studies concentrated on feature extraction and pattern recognition in the bio-medical signal or bio-signal processing have achieved tremendous contribution to the facilities developed and available for the signal analysis in the clinical field today.

In signal processing, determining the frequency content of a signal by Fourier transform is one of the main aspects in feature extraction and understanding the characteristics of a signal. However, obtaining the frequency content alone is not sufficient for analysing bio-medical signals due to it being non-stationary in nature [2], [3]. Fourier transform loses the time information after transforming time-based signal to frequency-based signal.

The Fourier transform of input signal $x(t)$ is defined as the following notation as in (1) where ω is the angular frequency and $\omega = 2\pi f$ with f is the input frequency. $x(t)$ is the time domain signal and $F(\omega)$ is its Fourier transform represented in frequency domain

$$F(\omega) = \int_{-\infty}^{\infty} x(t) e^{-j\omega t} dt \tag{1}$$

which is the sum over all time of the signal $x(t)$ multiplied by complex exponential [4].

Since a digital computer only works with discrete data, a technique called Discrete Fourier Transform (DFT) is used [5]. FFT is the practical application name used for the DFT that maps discrete-time sequences into discrete-frequency representation as in (2) where $x[n]$ is the input sequence, $F(k)$ is the DFT, $2\pi k$ is the angular frequency of input sequence frequency k and N is the number of samples in both discrete-time and the discrete-frequency domains.

$$F(k) = \sum_{n=0}^{N-1} x[n] e^{-j2\pi kt/N} \tag{2}$$

The mean frequency (MDF) is the average of all frequencies from the power spectrum and can be expressed as in (3) where $P(\omega)$ is the power spectrum of the signal.

$$\int_{0}^{MDF} P(\omega)\, d\omega = \int_{MDF}^{\infty} P(\omega)\, d\omega \tag{3}$$

The median frequency (MNF) is that frequency having 50% of the distribution on each side from the power spectrum and is given in (4).

$$MNF = \frac{\int_{0}^{\infty} \omega P(\omega)\, d\omega}{\int_{0}^{\infty} P(\omega)\, d\omega} \tag{4}$$

The collection of the SEMG signals from the surface of the skin to the data being stored involves a number of different stages, starting from a continuous analogue signal and ending with a discrete or digital signal [6]. These stages include amplification, analogue-to-digital conversion and signal conditioning.

It is essential and in the interest of analysing bio-signal to obtain 'time-based' information of when a particular frequency content occurs [3], [7]. Wavelet transform is a method capable of achieving this which is so called the time-frequency content or the time-frequency based representation.

The mathematical expression of a wavelet family which consists of members or daughter wavelets, $\psi_{a,\tau}$ is obtained by

Manuscript received October 14, 2012; revised November 18, 2012.

The authors are with the School of Engineering at AUT University, Auckland, New Zealand (e-mail: jkilby@ aut.ac.nz; kprasad@laut.ac.nz).

DOI: 10.7763/IJCEE.2013.V5.656

scaling and time shifting of the mother wavelet $\psi(t)$ defined as in (5) where $a \in \Re^+$ represents scale parameter and $\tau \in \Re$ represent the translation parameter. When a becomes large, the basis function $\psi_{a,\tau}$ becomes a stretched version of the prototype, which emphasises the low-frequency components. A small a contracts the basis function $\psi_{a,\tau}$ and stresses the high-frequency components. However, the shape of the basis function will always remain unchanged [8].

$$\psi_{a,\tau}(t) = \frac{1}{\sqrt{a}} \psi\left(\frac{t-\tau}{a}\right) \quad (5)$$

Since $\psi(t)$ can be implemented as a band pass filter whose centre frequency can change, at a given scale, the filter yields wider or narrower frequency-response changes depending on the centre's frequency. This time-scale expression has an equivalent time-frequency expression. Since wavelets are well localised around a non-zero frequency f_0, at a scale a=1 (i.e. the mother wavelet), there is an inversely proportional relationship between scale and frequency, given by $a = f_0 / f$. Note that the factor $1/\sqrt{a}$ in (2) is introduced to guarantee energy preservation, that is to normalise the wavelet so that it has unit energy [8].

Other aspects of a signal such as the mean and median frequency of the power spectrum and the (RMS) value of signal's electrical potential also play an important role to the whole task of features extraction for signal characterisation. The ultimate aim of this exercise is to develop a system with the ability for signal classification by features, a powerful and promising tool for diagnosing problems.

The application of wavelet transform in analysing biological signals has only become increasingly developed in the last fifteen years [3], [9]. The wavelet theory is a relatively recent mathematical development where its application is a potentially promising and exciting area of research. Its application to the analysis of EMG signals is even more recent [3].

SEMG uses surface electrodes placed on the skin overlying the muscle observed. The other common EMG uses needle electrodes penetrated into the muscle, thus signals obtained are focused on a particular muscle motor unit. Needle EMG is an invasive method which can cause stress to the patient involved [10], hence SEMG is a preferable method of gathering signals. Furthermore, SEMG obtains signals sourced from a group of muscle rather than one single muscle unit.

This research designed and developed appropriate practice-oriented methodology and descriptive procedures for SEMG signal acquisitions, feature extraction, classification and validation by Artificial Neural Network (ANN).

This research explored and demonstrated the ability and potential in achieving reliable means for the diagnostic equipment development of a SEMG signal analyser using comparative database.

Traditionally, practical methodologies for pattern classification are the statistical and the syntactic approaches [8], [11]-[13]. Much early research on EMG signals classification found many difficulties associated with the statistical method of instrumenting many channels of the signal. The learning or neural approach in ANN is the most recent established type of pattern classifier which is a matured form of adaptive linear elements in learning algorithms [8], [14]-[16]. The first ANN began to appear in the mid 1980s where it could be a powerful method for classifying EMG signals. *It is the feature set or* data itself that is crucial to the overall performance of the classifier [8], which comes down to the selecting of the signal features that produce the best performance in terms of accuracy and efficiency [17]. Hence, a substantial set of database with sufficient quantity and effective selected features, may improve the classification of the EMG signals. ANN's potential ability as a powerful tool is yet required to be investigated for the classification purposes in this research. Research by Englehart et al [17] showed an effective representation for classification using ANN.

II. Methodology

A. Subjects

Forty five healthy volunteers with no previous history of knee or severe musculoskeletal injury (35 males and 10 females, age 18-35 years) participated in this study. This study was approved by the Auckland University of Technology Ethics Committee (AUTEC) and was performed after each subject had given written consent.

B. SEMG Electrode Placement

The SEMG signals were obtained from the vastus lateralis and vastus medialis muscles of both legs. Before the data collection, the subject's legs were shaved around the area of the muscles being tested. It was gently abraded with skin preparation cleanser, then cleansed with a 70% alcoholic swab and left to dry before attaching adhesive Ag (99.9%) electrodes Norotrode 20^{TM} bipolar silver/silver chloride electrodes (Myotronics, UK) with 20 mm inter-electrode spacing. The electrode was placed according to the set of recommendations published by Surface Electromyography for Non-invasive Assessment of Muscle (SENIAM) [18] as seen in Fig. 1. The reference electrode 3M^{tm} Red Dot silver/silver chloride monitoring electrode (3M, USA) was attached to an area with no muscle tissue below the knee.

C. Experimental Setup

After the completion of a general warm-up, the subject was seated on a Biodex System 3 Pro dynamometer (Biodex Medical, Shirley, USA) with the upright chair set at 110° and one knee bent to 90°. The load cell lever arm was attached to the chair that measured voluntary isometric force of the quadriceps.

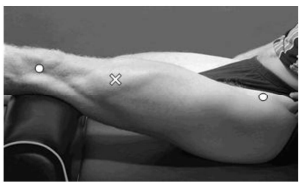

Fig. 1. Placement of electrode on the vastus lateralis muscle marked as a white cross between the two reference points marked as white dots.

Following the maximal strength tests, the subject performed a sustained force production test. This test was

executed by having the subject push the load cell lever with 50% of MVIC force. The subject was required to perform and sustain the isometric contraction of the quadriceps at the given force level for a period of 10 seconds.

D. Conventional Data Acquisition of SEMG Signals

Signals from the SEMG electrodes were amplified at a gain of 100 and bandwidth filtered between 1 Hz and 3 kHz using a Grass model P511 amplifier (Grass Instruments Company, USA). The analogue signals were acquired by a multifunction data acquisition board NI PCI-6024E (National Instruments Corporation, USA) with LabVIEW 2010 software (National Instruments Corporation, USA) for raw data acquisition on a host desktop computer. The signals were analogue-to-digital converted with 16 bit resolution in the ± 5 V range and sampled at 2048 Hz.

E. Signal Processing

The recorded SEMG signals were subsequently analysed off-line using a newly developed virtual instrument (VI) within the software processing programme LabVIEW shown in Fig. 2. Any direct current (DC) component that may exist in the signals was removed before the analysis. The signals were subsequently digitally filtered using a 4th order Butterworth band-pass filter with a pass-band from 5 to 500 Hz.

For the feature extraction process, a section of the raw SEMG was selected. The selected region is an interval after the first peak activation as shown in Fig. 3. The selected first two seconds section (A) in Fig. 3 was not used for analysis. This region was to allow for changes in muscle tension at the beginning of the muscle contraction. The next two seconds section (B) in Fig.3 was the region to be used for analysis.

This region was where no muscle fatigue present and assumed to be quasi-stationary that is the stationary during short time intervals. Under this assumption spectral analysis for feature extraction can be applied [19, 20].

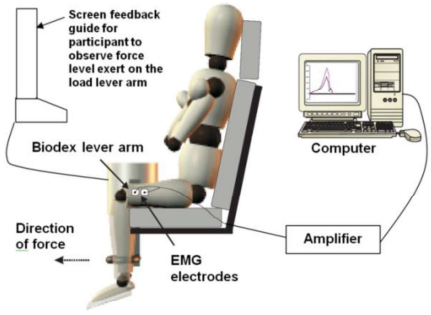

Fig. 2. Schematic diagram of equipment setup for signal acquisition.

Within this 2-second region, the initial scalogram was produced shown in middle plot in Fig. 4. The scalogram shows lower scale numbers as for the narrow version of the wavelet window which represent high frequencies, and the higher scale numbers for the wider windows represent as low frequencies. The conversion of scale index numbers to frequencies or pseudo frequencies were then carried out using the centre frequency F_c of the mother wavelet, which in this case was the Morlet (F_c = 0.8125 Hz). A frequency-time based spectrum was plotted as a result of this conversion shown in the bottom plot of Fig. 4. A range of dominant frequencies could also be viewed from the frequency-time spectrum.

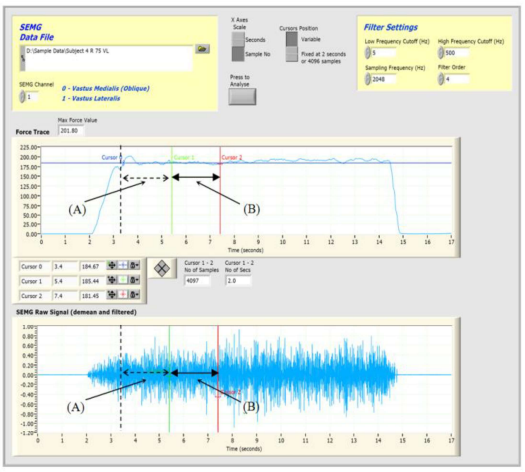

Fig. 3. Showing graph of force trace and raw SEMG signal displayed on a new developed LabVIEW VI. Part (A) first two second period to be ignored after first peak activation and Part (B) two period of muscle contraction to be analysed for feature extraction.

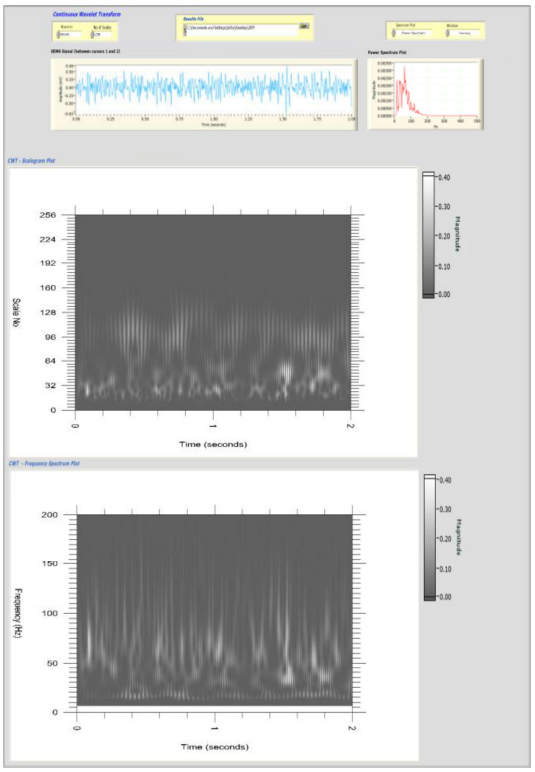

Fig. 4. The top plot shows the extracted two second period of the SEMG signal taken from the VI shown in Fig. 3. The middle plot shows CWT scalogram plot of scales against time. The bottom plot is corresponding CWT pseudo scalogram showing frequency against time.

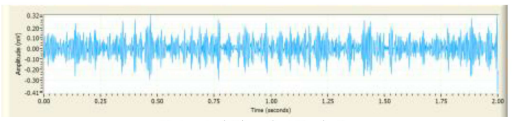
Extracted Signal at Scale 8

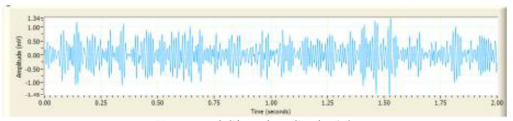
Extracted Signal at Scale 16

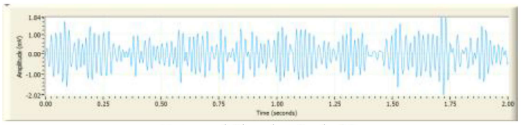
Extracted Signal at Scale 32

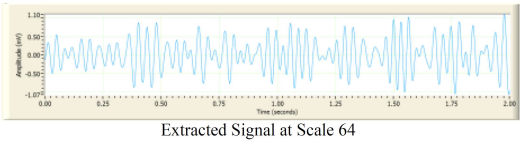
Extracted Signal at Scale 64

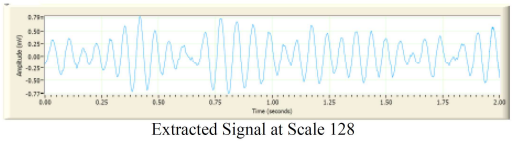
Extracted Signal at Scale 128

Fig. 5. Extracted signals at scales (a) 8, (b) 16, (c) 32, (d) 64 and (e) 128 from the scalogram plot shown in Fig. 4.

From the scalogram in Fig. 4, the scales selected were 8, 16, 32, 64 and 128. At each scale the transform wave was plotted in LabVIEW. These will then be analysed to extract the following features of MDF, MNF and RMS. These features are to be used to train and validate an ANN shown in Fig. 5.

F. Artificial Neural Network

The neural network architecture was built using MATLAB 2010 (MathWorks, USA) for this research and is illustrated in the Fig. 6. Fifteen input features from 35 subjects in the input layer were trained for 3 targets of 25%, 50% and 75% MVIC in the output layer. In the hidden layer, the neuron numbers tested are from 3 to 10 to start with. The lower the number of neurons selected for the iterations, the faster the processing is.

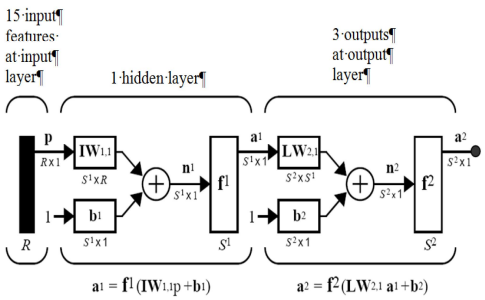

Fig. 6. Neural Network Architecture build using MATLAB used for this research.

TABLE I: EXTRACTED FEATURES FROM THE RIGHT LEG'S VASTUS LATERALIS OF SUBJECT PERFORMING 75% OF MVIC (SUBJECT NO.4).

Scales	Mean frequencies (Hz)	Median frequencies (Hz)	RMS (mV)
8	168.83	167.12	0.0839
16	95.47	94.21	0.3886
32	51.70	50.59	0.6281
64	26.77	26.25	0.4095
128	14.93	13.89	0.3265

With both transfer functions, tan-sigmoid and log-sigmoid, parameters were set as follows:

1) Training algorithm: Levenberg-Marquardt
2) No. of epochs or iterations: 1000
3) Performance goal: 0.001 or 0.1% error
4) Maximum performance gradient: 1×10^{-10}

Using the two transfer functions, tan-sigmoid and log-sigmoid, and the neuron numbers in the hidden layer were set between 3 and 10, hence there were 16 different ANNs to be trained. After the training, the 16 ANNs went through the validation process using the untrained data from the rest of the ten subjects. The performance goal or the error results between the 16 ANNs were then compared.

III. RESULTS

Table I shows a sample of extracted features from a subject who exerted 75% of the MVIC from his right leg's vastus lateralis at selected scales for scalogram.

After training the 35 sets of data and validating with the remaining set of ten data, the transfer function which met the network target vector was the tan-sigmoid transfer function with neuron numbers 4, 5, 6 and 7 in the hidden layer. None of the log-sigmoid transfer function networks met the target after validation. The tan-sigmoid ANNs with the mentioned neuron numbers produced more comparable results in terms of meeting the performance goal. ANNs with neuron numbers 3, 8, 9 and 10 did not meet the target with some number of epochs or iterations being too great compared to the ANNs with neuron numbers 4, 5, 6 and 7.

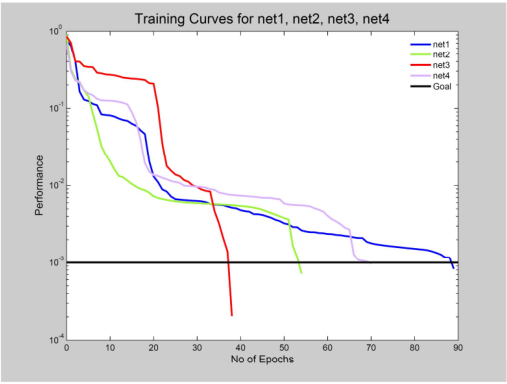

Fig. 7. The training of ANN net1, net 2, net3 and net 4 showing efficiency in reaching the performance goal of 0.001 or 0.1% error.

TABLE II: SUMMARY OF RESULTS OF TRAINING AND VALIDATING NEURAL NETWORKS USING TAN-SIGMOID TRANSFER FUNCTION

Network name	Neuron number at Hidden layer	Error	Error Percentages
net1	4	6/30	20
net2	5	2/30	6.67
net3	6	1/30	3.33
net4	7	7/30	23.33

The network with neuron number 4 in the hidden layer is named as 'net1', the one with neuron number 5 is 'net2' and so on. Ten sets of untrained data from 10 subjects were validated, 15 input features were tested for three targets from each subject. With ten subjects, 10 validations with Boolean notation results were produced for each of the three output targets, which are 25%, 50% and 75% MVIC, totalling 30 validation results.

Fig. 7 shows the comparison between training curves of the different neuron numbers in the hidden layer with efficiency in reaching the performance goal. The summary of results of the ANNs which met the target is listed in Table II.

IV. DISCUSSION AND CONCLUSION

Extracting feature from the whole 10-second signal would be an ideal as it may show more variants of the signal characteristics. Processing the whole duration at one time would require a vast amount of power from the computer and disk-space to run. Such facilities are not available at this stage. Breaking the signals into short time durations would be more achievable for feature extraction, but a laborious task. At this stage, processing the 2-second region is sufficient to represent the signal characterisation. Researching into extracting the features from the whole signal duration could be expanded for the future work in this research.

After applying the CWT analysis to this 2-second quasi-stationary region, a scalogram was formed presenting the scale and time-based plot. This plot showed which scale at particular time was dominant indicated by the amplitude. The technique of scales to frequencies conversion is relatively new and found to be a powerful way of portraying scales. Scales are less familiar parameters, converting them to frequencies are making them a more common and meaningful parameters. This technique leads to the selection of the scale which would largely impact the whole signal characterisation.

Selecting the scale index numbers was carried out by visually viewing the scalogram and the frequency-time based spectrum plot. The dominant regions were noted with the corresponding scale numbers which were chosen. This technique required sound judgement and accuracy as it was done manually. Hence, the results can still be subjected by human error. Although, whichever index scale number is chosen, as long as the same ones are being used throughout the rest of the research process, the end results should give the same consistency. This is due to the nature of the values from any parameter being relative rather than absolute. Future work to develop an extension programming code for selecting dominant scale index numbers can be done to eliminate or minimise error.

So far, the ANN stage has produced satisfactory results with minimal error in terms of classifying an untrained normal muscle data as 'normal'. This showed that the basic procedure developed using ANN can be further utilised and refined for future work by collecting more data and investigating into setting features in different units. This technique is concluded to be a strong base method for further study in this research of developing muscle signal classifier.

Future work of data collection from abnormal muscles can be carried out where they can be used to test and validate the existing classifier which was built to classify for normal muscle. This technique can be executed for validating various classifiers that can be built for different muscles condition. It will need a vast amount of database of muscle signal for building this type of muscle condition diagnostic tool.

In summary, this research has investigated aspects involved in the digital signal processing using Continuous wavelet and Fourier analysis for extracting features of SEMG signals from 45 subjects with normal leg muscles. Then the use of ANN for developing a signal classifier was also explored. As an early stage in this area of research, various aspects were developed more in an outlined manner rather than a strong focus in one area using techniques from the literature review. More focus work on a particular area can be done in future work of this research.

ACKNOWLEDGMENT

This work was supported in part by the AUT University School of Engineering Research Grant with AUT Ethics Approval.

REFERENCES

[1] K. Englehart *et al.*, "Classification of the Myoelectric Signal using Time-Frequency Based Representations," *Medical Engineering & Physics,* pp. 431-438, 1999.
[2] R. Constable and R. J. Thornhill, "Using the Discrete Wavelet Transform For Time-Frequency Analysis of the Surface EMG Signal," *ISA,* vol. 16, pp. 121-127, 1993.
[3] P. J. Sparto *et al.*, "Wavelet Analysis of Electromyography for Back Muscle Fatigue Detection During Dynamic Constant-Torque Exertions," *ISA,* vol. 33, pp. 82-87, 1997.
[4] M. Misiti *et al.*, *Wavelet Toolbox For Use with MATLAB*. Natick, MA: The MathWorks Inc., 2000.
[5] J. V. d. Vegte, *Fundamentals of Digital Signal Processing*: Prentice Hall, 2002.
[6] M. T. Young *et al.*, "Biosignal Processing," in *Introduction to Biomedical Engineering*, J. D. Enderle, *et al.*, Eds., ed San Diego, CA: Academic Press, 2000, pp. 233-278.
[7] J. A. Crowe *et al.*, "Wavelet Transforms as a Potential Tool for ECG Analysis and Compression," *J Biomed Eng,* vol. 14, pp. 268-272, 1992.
[8] R. Merletti and P. A. Parker, "Electromyography," *Hoboken, New Jersey: John Wiley & Sons*, 2004.
[9] B. Kieft. (2005, 2 March). A Brief History of Wavelets. [Online]. Available: http://www.gvsu.edu/math/student_work/Kieft/Wavelets%20-%20Main%20Main%20Page.html
[10] G. Drost *et al.*, "Motor Unit Characteristics in Healthy Subjects and Those with Postpoliomyelitis Syndrome: A High Density Surface EMG Study," *Muscle Nerve,* vol. 30, pp. 269-276, September 2004.
[11] R. O. Duda and P. E. Hart, *Pattern Classification and Scene Analysis*, New York: Wiley, 1973.
[12] J. T. Tou and R. C. Gonzalez, *Pattern Recognition Principles*. Reading, MA: Addison-Wesley, 1974.
[13] K. S. Fu, *Syntactic Pattern Recognition and Applications*, Englewood Cliffs, NJ: Prentice-Hall, 1982.

[14] F. Rosenblatt, "The perceptron: A probabilistic model for information storage and organization in the brain," *Psycho Rev,* vol. 65, pp. 386-408, 1958.
[15] B. Widrow and M. A. Lehr, "30 years of adaptive neural networks: Perceptron, madaline and backpropagation," in *Proc. IEEE,* vol. 78, pp. 1415-1442, 1990.
[16] D. R. Hush and B. G. Horne, "Progress in supervised neural networks: What's new since Lippmann," *IEEE Sig Process Mag*. 8-39, 1993.
[17] K. Englehart *et al.*, "Classification of the Myoelectric Signal using Time-Frequency Based Representations," *Medical Engineering & Physics,* 1999.
[18] Surface Electromyography for Noninvasive Assessment of Muscle (SENIAM). (2005). Recommendations for sensor locations in hip or upper leg muscles - vastus medialis. [Online]. Available: http://www.seniam.org/quadricepsfemorisvastusmedialis.html.
[19] R. Merletti and L. R. Lo Conte, "Surface EMG Signal Processing During Isometric Contractions," *J Electromyogr Kinesiol,* vol. 7, pp. 241-250, 1997.
[20] A. Luttmann *et al.*, "Electromyographical study on surgeons in urology - II. Determination of muscular fatigue," *Ergonomics,* vol. 39, pp. 298-313, 1996.

Jeff Kilby was born Edmonton, Alberta, Canada, has a MEng (Hons) in Signal Processing from the AUT University, Auckland New Zealand. Senior Lecturer in Electronics and Computing in the School of Engineering at AUT University.Main research topic is in the field of Biomedical Signal Processing and Devices with other research interests are LabVIEW Applications Micro-controller Applications and Wireless Sensor Network Applications

Krishnamachar Prasad has Ph.D. (University of Western Australia), M.Tech. (IIT Madras, India) and BE (Bangalore University, India) degrees, all in Electrical Engineering. Professor in the School of Engineering ay AUT University. His research focuses on the development and reliability studies of novel interconnects in conventional and three-dimensional integrated circuits.

Paper 2

International Journal of Computer Theory and Engineering, Vol. 5, No. 2, April 2013

Analysis of Surface Electromyography Signals Using Discrete Fourier Transform Sliding Window Technique

J. Kilby and K. Prasad

***Abstract*—An optimum frequency resolution is useful for extracting features of any signals for further analysis. The purpose of this research was to determine the best frequency resolution of Surface Electromyography (sEMG) signals by using a sliding window with Discrete Fourier Transform to produce spectrogram plots. The process was carried out in two stages of investigations.**

The first investigation was to hold the sampling frequency constant at 8192 Hz and to use a new algorithm with sliding window sizes ranging from 16 to 512 samples through the signal. The results showed that the spectrogram that produced the best visual frequency resolution was with a window size of 64 samples. The calculated time period of sampling frequency of 8192 Hz with window size of 64 samples is hence 1/128 seconds.

The second investigation was to use the time period of 1/128 seconds found in the investigation one. This time period of 1/128 second is held constant in order to determine window sizes that passed through different sampling frequencies which were set at 1024 Hz, 2048 Hz and 4096 Hz. Hence the calculated window sizes sample values are 8, 16 and 32 respectively. The spectrogram was plotted for each window sizes and it was found that a window size of 32 samples with the sampling frequency at 2048 Hz gave the best visual frequency resolution for the analysis of sEMG signals.

***Index Terms*—Fourier, spectrogram, electromyography, signal Processing.**

I. Introduction

Surface electromyography (sEMG) signals is the study of muscle activity obtained in the form of electrical signals [1]. The sEMG signals obtained by electrodes placed on the skin surface overlying the muscle are then sent to a computer. The sEMG signals are collected in data files for subsequent processing and analysed using relevant mathematical procedures to determine mean and median frequencies.

The amplitude characteristics of sEMG signals have a random or stochastic behaviour with no periodic form [2]. The amplitudes of these signals can range from 0 to 10 mV (peak to peak) or 0 to 1.5 mV (RMS) [2]. The useable frequency range of the signal is from 0 to 500 Hz, with dominance being in the 50 to 150 Hz range [2]. Signals at frequencies above 500 Hz are considered noise, and have little information, so they need to be filtered out by a low pass filter [2].

An accurate and computationally efficient means of classifying surface electromyography signal patterns have been the subject of considerable research efforts in recent years where having effective signal features extraction is crucial for reliable classification [3]. Numerous research and studies have concentrated on feature extraction and pattern recognition in the field of bio-medical signal or bio-signal processing and achieved tremendous contribution to the facilities developed for the signal analysis in the clinical field today [2].

With computers and software becoming more and more powerful tools which are able to process complex algorithms on numerous data at high speed, the advancement in digital signal processing applied to bio-signals is an inevitable one and ongoing. Software such as MATLAB and LabVIEW are well known for their use in mathematical processing and virtual instrumentation for laboratory requirements. They are commercially available where both have built-in functions or tools for signal processing.

The Fourier Transform (FT) of input signal $x(t)$ is defined as the following notation in equation (1), where ω is the angular frequency and $\omega = 2\pi f$ with f as the input frequency, $x(t)$ is the time domain signal. Then $F(\omega)$ is its FT represented in frequency domain, which is the sum over all time of the signal $x(t)$ multiplied by complex exponential [4].

$$F(\omega) = \int_{-\infty}^{\infty} x(t) e^{-j\omega t} dt \tag{1}$$

FT allows the frequencies within the sEMG signal to be broken down. These extracted frequencies can be used to relate to force production, muscle fatigue and deficits in the musculoskeletal system [2].

Since a digital computer only works with discrete data, a technique called Discrete Fourier Transform (DFT) is used [5]. Fast Fourier Transform (FFT) is the practical application name used for the DFT that maps discrete-time sequences into discrete-frequency representation as in equation (2), where $x[n]$ is the input sequence, $F(k)$ is the DFT, $2\pi k$ is the angular frequency of input sequence frequency k and N is the number of samples in both discrete-time and the discrete-frequency domains.

$$F(k) = \sum_{n=0}^{N-1} x[n] e^{-j2\pi kt/N} \tag{2}$$

In signal processing, determining the frequency content of a signal by DFT is one of the main aspects in feature extraction and understanding the characteristics of a signal. However, obtaining the frequency of the overall signal content alone is not sufficient for analyzing bio- the time information after transforming time-based signal to

Manuscript received October 14, 2012; revised November 21, 2012.

This work was supported in part by the AUT University School of Engineering Research Grant with AUT Ethics Approval.

J. Kilby and K. Prasad are with the School of Engineering at AUT University, Auckland, New Zealand (e-mail: jkilby@ aut.ac.nz, kprasad@laut.ac.nz).

DOI: 10.7763/IJCTE.2013.V5.702

frequency-based signal. By using *Sliding Window Technique* in DFT, time information is regained and therefore frequency resolutions can be seen through its spectrogram plot [4].

II. Methodology

A. Subjects

Thirty healthy volunteers with no previous history of knee or severe musculoskeletal injury (18 males and 12 females, age 18-35 years) participated in this study. This study was approved by the Auckland University of Technology Ethics Committee (AUTEC) and was performed after each subject had given written consent.

B. Experimental Setup

After the completion of a general warm-up, the subject was seated on a Biodex System 3 Pro dynamometer (Biodex Medical, Shirley, USA) with the upright chair set at 110° and one knee bent to 90°. The load cell lever arm was attached to the chair that measured voluntary isometric force of the quadriceps as shown in Fig. 1.

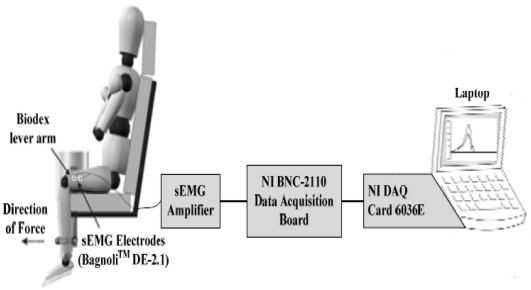

Fig. 1. Schematic of the components used for data acquisition of sEMG signals from a subject performing set value of their MVIC

The subject then performed a specific warm-up and familiarisation of the experimental setup. The subject was then rested for 3 minutes before performing the maximal strength test to obtain Maximum Voluntary Isometric Contraction (MVIC) of the quadriceps. The MVIC force (100% maximal force) of the leg quadriceps was executed by the subject pushing against the load cell lever in the direction shown by the arrow in Fig. 1. Three MVICs were measured and recorded for a 10 second period. There was a two-minute rest period between each MVIC test and the highest MVIC was selected for analysis.

Following the maximal strength tests, the subject performed a sustained force production test. This test was executed by having the subject push against the load cell lever with 10%, 20%, 30%, 40% and 50% of MVIC force. The subject was required to perform and sustain the isometric contraction of the quadriceps at the given force levels for a period of 10 seconds.

C. sEMG Electrode Placement

The sEMG signal was obtained from the vastus lateralis muscle of the leg. Before the data collection, the subject's leg was shaved around the area of the muscles being tested. It was gently abraded with skin preparation cleanser, then cleansed with a 70% alcoholic swab and left to dry before attaching adhesive Ag (99.9%) electrodes Bagnoli™ DE-2.1 (Delsys Inc., USA) with 10 mm inter-electrode spacing. sEMG signals were recorded by a single differential amplifier with a CMRR > 92 dB, input noise < 1.2 μV (RMS). The electrode was placed according to the set of recommendations published by Surface Electromyography for Non-invasive Assessment of Muscle (SENIAM) [6] see Fig. 2 for details. The reference electrode was attached to an area with no muscle tissue below the knee.

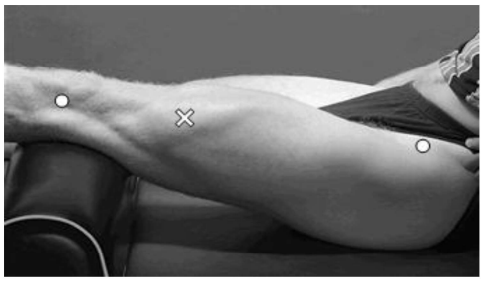

Fig. 2. Placement of electrode on the vastus lateralis muscle marked as a white cross between the two reference points marked as white dots.

D. Data Acquisition of sEMG Signals

Signals from the sEMG amplifier were acquired by a multifunction data acquisition board NI BNC-2110 plus NI DAQCard_6036E (National Instruments Corporation, USA) with LabVIEW 2011 software (National Instruments Corporation, USA) for raw data acquisition on a host laptop computer. The signals were analogue-to-digital converted with 16 bit resolution in the ± 5 V range and sampled using different sampling frequencies. Before sampling, the raw signals were amplified with a gain of 1000.

E. Signal Processing of sEMG Signals

Knowing the minimum acceptable sampling frequency is of critical importance in order to correctly reproduce the original analogue information. The rule for this is known as Nyquist Theorem where sampling frequency has to be at no less than twice the frequency of the original sampled signal. When sampling frequency is too low, the Nyquist Theorem is violated. This leads to an incorrect reconstruction of the signal, typically referred to as aliasing. Aliasing occurs when the original signal is under sampled as not enough points have been gathered to capture all the information correctly. As the usable frequency range of sEMG signals between 0 to 500 Hz, hence the minimum sampling frequency used to collect the sEMG signals was set at 1024 Hz. The other sampling frequencies used were 2048 Hz, 4096 Hz and 8192 Hz.

The recorded sEMG signals were subsequently analysed off-line using a newly developed code for performing signal processing analysis of the sEMG signals using MATLAB 2010 (MathWorks Inc, USA). Any direct current (DC) component that may exist in the signals was removed before the analysis. The signals were subsequently digitally filtered using a 4^{th} order Butterworth band-pass filter with a pass-band from 5 to 500 Hz.

A new algorithm was written in MATLAB to produce a spectrogram by sliding a window through the sEMG signal over a 1 second period at a known percentage value of MVIC as shown in Fig. 3.

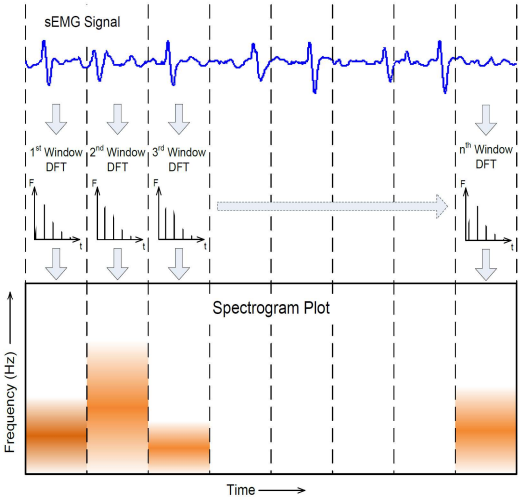

Fig. 3. The top plot shows a 1 second period of a sEMG signal to be analysed using the sliding window technique using DFT. The bottom plot shows a Spectrogram Plot produced by sliding a known fixed window length through the signal. DFT analysis was performed at each window shown graphically in the figure between the sEMG signal and the Spectrogram plot.

A window value was first set in terms of sample values of the signal and passing it through the signal. The algorithm takes the first sliding window of the signal and performing a DFT spectrum of the signal and stores the values in a matrix. This is continued until the final n^{th} window. Once the values of signal data was analyzed a spectrogram plot is produced showing the frequency content of each window against time. A Hanning window was used in the processing of the DFT frequency spectrum to obtain smoothness of the output frequency spectrum avoiding spectral leakages and outliers.

To find the optimum window size along with the sampling frequency for analysis of sEMG signals, two stages of investigations were carried out.

The first investigation was to use a fixed sampling frequency and then altering the window size through the same signal. This required only one signal to be collected at the highest sampling frequency of 8192 Hz and analyzing with different window sizes of using sample values of 16, 32, 64, 128, 256 and 512.

The second investigation was to use the window size from the first investigation that gave the best frequency resolution extracted from the signal. Using this window size, time period was determined and used to further calculate the sample values of window sizes over a range of different sampling frequencies. These selected sampling frequencies are 1024 Hz, 2048 Hz, 4096 Hz and 8192 Hz. Therefore there are more than one signal was collected at different sampling frequencies.

III. Results and Discussion

The results of the first investigation in determining a suitable window size analysis using single sEMG sampled at 8192 Hz and altering the sliding window sizes of DFT spectrum analysis is shown in Fig. 4.

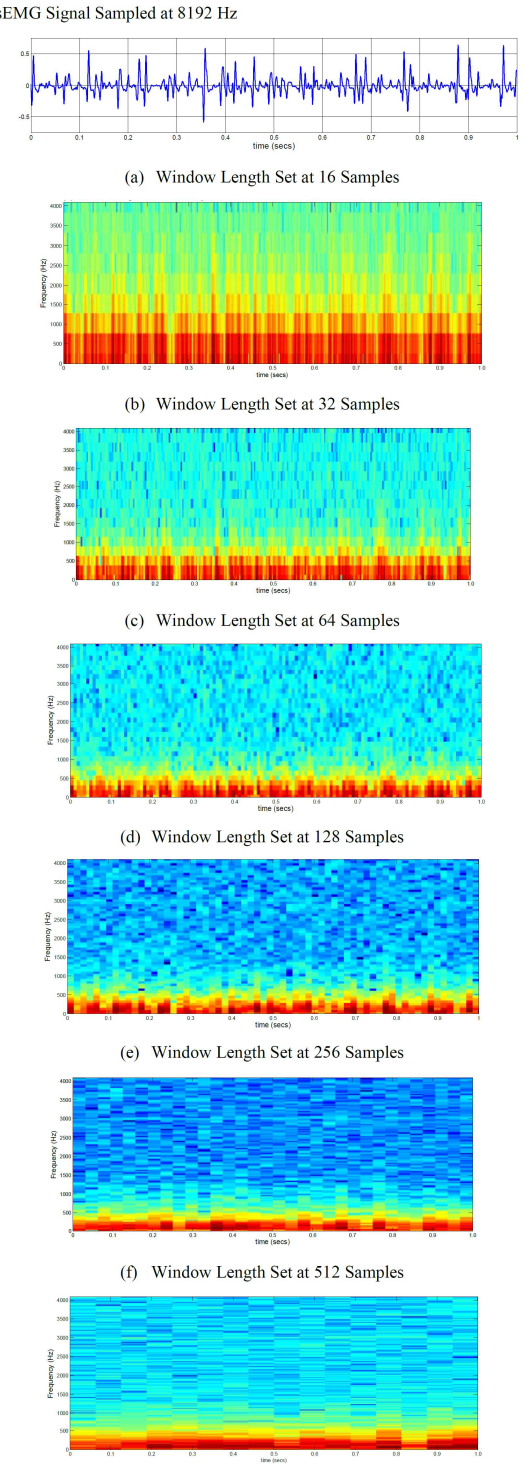

Fig. 4. The top plot shows a 1 second period of a sEMG signal sampled at 8192 Hz over that was used to produce the following Spectrogram plots. Plot (a) window length of 16 samples, plot (b) window length of 32 samples, plot (c) window length of 64 samples, plot (d) window length of 128 samples, plot (e) window length of 256 samples, and plot (f) window length of 512 samples.

The top plot shows a 1 second period of a sEMG signal that was collected at 20% MVIC from the vastus lateralis muscle of the quadriceps used for this investigation. The following plots below from (a) to (f) are the spectrograms plotted at various window sizes from 16 to 512 samples.

By increasing the window size from 16 to 512 samples, the best resolution is seen to be produced in plot (c) of Fig. 4 which was achieved at 64 samples. The frequency resolution in plot (c) is more refined than any of the other plots. The 'hard threshold' of the frequencies is just above the 500 Hz value at approximately 650 Hz. This frequency may vary due the level of contraction of the muscle and is due to the physiology of the muscle fibres [2].

The second investigation was to use the window size of 64 samples with sampling rate at 8192 Hz from the first investigation which yields the time period of 1/128 seconds.

This time period was kept constant for subsequent selected different sampling frequencies and hence a new window sample size was determined for each of the different sampling frequencies as shown in Table 1.

TABLE I: WINDOW SIZES AT VARIOUS SAMPLING FREQUENCIES

Sampling Frequency	Window Size
8192 Hz	64 samples (=time period 1/128 seconds)
4096 Hz	32 samples (=time period 1/128 seconds)
2048 Hz	16 samples (=time period 1/128 seconds)
1024 Hz	8 samples (=time period 1/128 seconds)

The spectrograms for each window size determined in Table I along with the corresponding sampling frequencies have a maximum frequency value of half of the sampling frequency which is due to the Nyquist Theorem. By examining the spectrogram plots, it can be seen visually that a sampling frequency of 4096 Hz and window size of 32 samples in plot (b) shown in Fig. 5 produced the best frequency resolution.

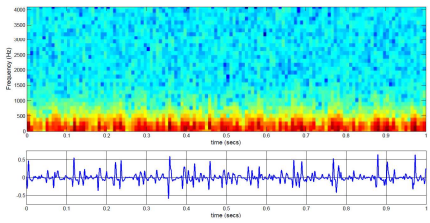

(a) Window Length set at 64 Samples and sEMG Signal Sampled at 8192 Hz

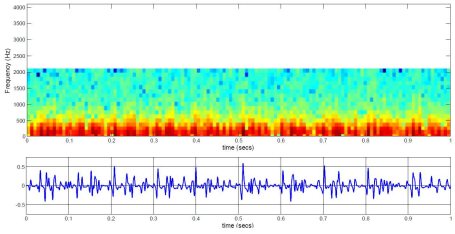

(b) Window Length set at 32 Samples and sEMG Signal Sampled at 4096 Hz

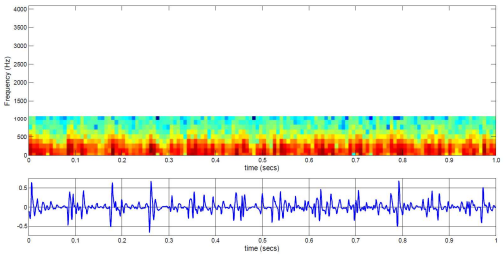

(c) Window Length set at 16 Samples and sEMG Signal Sampled at 2048 Hz

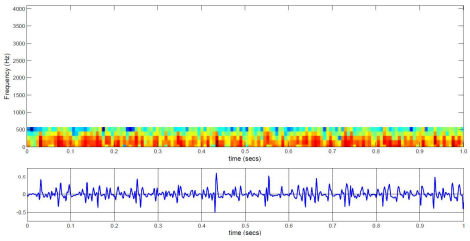

(d) Window Length set at 8 Samples and sEMG Signal Sampled at 1024 Hz

Fig.5. Spectrogram plots and sEMG Signals from the second investigation. Plot (a) window length set at 64 samples and sEMG signal sampled at 8192 Hz. Plot (b) window length set at 32 samples and sEMG signal sampled at 4096 Hz. Plot (c) window length of set at 16 samples and sEMG signal sampled at 2048 Hz. Plot (d) window length set at 8 samples and SEMG signal at 1024 Hz.

IV. CONCLUSION

The results of both investigations showed that performing a sliding window technique along with DFT and producing a spectrogram plot is a useful way for analysing sEMG signals which have no periodic form.

Overall, the results show that for a constant sampling frequency in the first investigation, having a wide window size of 512 samples gave a poor frequency resolution. This improved when the window size was made narrower to a size of 64 samples.

The second investigation showed that by using the best window size from the first investigation, time period can be determined and fixed for finding window sizes of different sampling frequencies. In this case, the best frequency resolution seen from the spectrogram was the one with a sampling frequency of 4096 Hz and a window size of 32 samples.

From this research the next step is to look at the other levels of MVIC and see if the above values of sampling frequency and window size give similar results in terms of frequency resolution. Once this has been determined, the next step will be to extract typical features such the mean and median frequency values from each of the DFT windows along with the RMS value for classification purposes.

REFERENCES

[1] J. V. Basmajian and C. J. De Luca, "Muscles alive: their functions revealed by electromyography," 5th ed. Baltimore: Williams and Wilkins, 1985.

[2] R. Merletti and P.A. Parker, "Electromyography: Physiology, Engineering and Noninvasive Applications," *IEEE Press and John Wiley & Sons*, Hoboken, 2004.
[3] S. Karlsson and B. Gerdle, "Mean frequency and signal amplitude of the surface EMG of the quadriceps muscles increase with increasing torque--a study using the continuous wavelet transform," *J Electromyogr Kinesiol*, vol. 11, pp. 131-40, Apr 2001.
[4] M. Misiti, et al., Wavelet Toolbox for Use with MATLAB. Natick, MA: The MathWorks Inc., 2000.
[5] J. V. d. Vegte, *Fundamentals of Digital Signal Processing*. Sydney: Prentice Hall, 2002.
[6] Surface Electromyography for Noninvasive Assessment of Muscle (SENIAM). 2005. Recommendations for sensor locations in hip or upper leg muscles - vastus medialis. Available: http://www.seniam.org/quadricepsfemorisvastusmedialis.html.

Jeff Kilby was born in Edmonton, Alberta, Canada, who holds a MEng (Hons) in Signal Processing from the AUT University, Auckland New Zealand. Main research topic is in the field of Biomedical Signal Processing and Devices with other research interests are LabVIEW Applications Micro-controller Applications and Wireless Sensor Network Applications

Krishnamachar Prasad holds Ph.D. (University of Western Australia), M.Tech. (IIT Madras, India) and BE (Bangalore University, India) degrees, all in Electrical Engineering. His research focuses on the development and reliability studies of novel interconnects in conventional and three-dimensional integrated circuits.

Paper 3

International Journal of Signal Processing Systems Vol. 1, No. 2 December 2013

Extracting Temporal and Spectral Parameters from Surface Electromyography Signals during a Fatigue Contraction

Jeff Kilby and Krishnamachar Prasad
AUT University/School of Engineering, Auckland, New Zealand
Email: jkilby@aut.ac.nz, kprasad@aut.ac.nz

***Abstract*—This paper presents findings from a study of five healthy subjects performing 50% maximum voluntary contraction until complete fatigue of the muscle. An overlapping window technique was used to find the values for mean frequency (MNF), median frequency (MDF) of the power spectrum, root mean square (RMS) and muscle fibre conduction velocity (MFCV). The surface electromyography signal (sEMG) was collected from the vastus lateralis muscle using a three channel Laplacian electrode. The results show the MNF and MDF values showed a consistent trend with each other where they remained at steady values between 20-30% and 75-80% of the signal after which they fell 15-30% of this value. The RMS showed a linear increase in value. The MFCV showed a similar trend to that found in the MNF and MDF values.**

***Index Terms*—MNF, MDF, RMS and MFCV**

I. Introduction

Fatigue is a factor that affects all individuals on a daily basis. Its definition is very complex, not unique and controversial. There are two basic types of fatigue (a) whole body physical fatigue and (b) localized muscle fatigue [1], [2]. If muscles are exercised strenuously for a long period of time, muscle fatigue occurs. A muscle is fatigued when it is unable to contract even though it is still being stimulated. Without rest, an active or working muscle begins to tire and contracts more weakly until it finally ceases to react and stops contracting [3].

Temporal and spectral parameters are used as feature extraction and pattern recognition in the processing and analysis of bio-medical signals [4], [5]. The use of the signal analysis is apparent in the field of research and clinical health for diagnosing health related problems and rehabilitation using bio-medical signals such as surface Electromyography (sEMG) signals. sEMG signals is the study of striated muscle activity obtained in the form of electrical signals [1]. The sEMG signals are obtained by electrodes placed on the skin surface overlying the muscle which are then sent to a computer.

In signal processing, determining the frequency content of a signal by Fourier transform is one of the main aspects in feature extraction and understanding the characteristics of a signal.

The Fourier transform $F(\omega)$ of a time domain input signal $x(t)$ represented in the frequency domain is the sum of the signal $x(t)$ multiplied by a complex exponential as given in equation (1), where ω is the angular frequency and $\omega = 2\pi f$ with f is the input frequency [6], [7].

$$F(\omega) = \int_{-\infty}^{\infty} x(t) e^{-j\omega t} dt \tag{1}$$

Since a digital computer only works with discrete data, a technique called Discrete Fourier Transform (DFT) is used [6]. Fast Fourier Transform (FFT) is the practical application name used for the DFT that maps discrete-time sequences into discrete-frequency representation as given in equation (2) where $x[n]$ is the input sequence, $F(k)$ is the DFT, $2\pi k$ is the angular frequency of input sequence frequency k and N is the number of samples in both discrete-time and the discrete-frequency domains [6, 7].

$$F(k) = \sum_{n=0}^{N-1} x[n] e^{-j2\pi kt/N} \tag{2}$$

A common technique in signal processing of sEMG signals is to consider the squared of the values of the FFT coefficients as given in equation (3) producing a resultant plot that is referred to as a power spectrum [7].

$$P(\omega) = |F(\omega)|^2 = \left| \int_{-\infty}^{\infty} x(t) e^{-j\omega t} dt \right|^2 \tag{3}$$

Aspects of a signal such as the mean and the median frequency of the power spectrum and the root mean square (RMS) value of signal's electrical potential also play important roles in the whole task of features extraction for signal characterization. The ultimate aim of this exercise is to develop a system with the ability for signal classification by features, which is a powerful and promising tool for diagnosing problems.

The mean frequency (MNF) is the average of all frequencies of the power spectrum and can be expressed as given in equation (4) where $P(\omega)$ is the power spectrum of the signal [4].

Manuscript received August 28, 2013; revised November 20, 2013

doi: 10.12720/ijsps.1.2.278-283

$$MNF = \frac{\int_0^{\infty} \omega P(\omega)\, d\omega}{\int_0^{\infty} P(\omega)\, d\omega} \quad (4)$$

The median frequency (MDF) is the frequency having 50% of the distribution on each side of the power spectrum as given in equation (5) [4].

$$\int_0^{MDF} P(\omega)\, d\omega = \int_{MDF}^{\infty} P(\omega)\, d\omega \quad (5)$$

The RMS value of a signal $x(t)$ over a time interval 0-T is determined by computing the equation as given in (6) [4].

$$RMS = \sqrt{\frac{1}{T}\int_0^T x^2(t)dt} \quad (6)$$

The collection of the sEMG signals from the surface of the skin to the data being stored involves a number of different stages, starting from a continuous analogue signal and ending with a discrete or digital signal [8]. These stages include amplification, analogue-to-digital conversion and signal conditioning.

Laplacian surface electrodes use spatial filters in sEMG recording and are represented by the Laplace filters. This is a class of high-pass spatial filters which approximate the second spatial derivative of the surface potential. Longitudinal and transversal Laplace filters can be combined to become the normal double differential (NDD) filter, which is a very selective spatial filter that enhances single motor unit (MU) activity from the interference signals, even at maximal contraction levels. The weights of the NDD filter, its filter mask can be written as in (7) [9, 10].

$$A_i = \begin{bmatrix} 0 & 1 & 0 \\ 1 & -4 & 1 \\ 0 & 1 & 0 \end{bmatrix} \quad (7)$$

The NDD configuration can be obtained by means of five cross-wised electrodes and is frequently used for two-dimensional sEMG recordings. This and other two-dimensional spatial filter configurations have been applied to extract single MU information from surface recordings [10-13].

The muscle fibre conduction velocity (MFVC) was obtained by performing a cross-correlation between two corresponding sEMG signals [14]. The cross-correlation is performed using the recorded data offline and was via the Fourier transform. The resulting cross-correlation function $R_{xy}(\tau)$ as given by (8).

$$R_{xy}(\tau) = \frac{x(t-\tau)y(t)dt}{k} \quad (8)$$

where $x(t)$ and $y(t)$ are two different sEMG signals, with τ is the time difference between them and k a constant to normalise the cross-correlation plot between -1 and +1. The peak in the cross-correlation plot was displaced by time ΔT from time zero, which was used to calculate the MFCV as given in (9).

$$MFCV = \frac{d}{\Delta T} \quad (9)$$

where d is the inter-electrode distance between the two sEMG signals.

II. Methodology

A. Subjects

Five healthy volunteers with no previous history of knee or severe musculoskeletal injuries (5 males, age 18-35 years) participated in this study. This study was approved by the Auckland University of Technology Ethics Committee (AUTEC) and was performed after each subject had given written consent.

B. Experimental Setup

Subjects were seated in a purpose built upright chair set at 110° with their knee flexed to 90° see Fig. 1. The chair was adjusted to ensure that the back of the knee rested comfortably against the edge of the seat. Once comfortable, the subject was secured to the chair using a lap and chest strap. The lower leg, minus socks or other clothing, was strapped to a metal attachment in series with a strain gauge at the ankle level, just proximal to the lateral malleolus. Comfort was ensured by using a heat-moulded thermoplastic brace to secure the leg. This experimental setup was similar to that used by Maïsetti, O., *et al* [15].

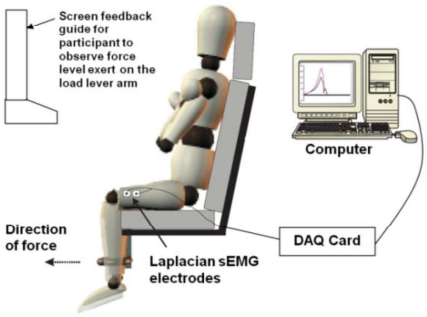

Figure 1. Schematic diagram showing the equipment setup for data acquisition of sEMG signals.

Force measurements: a PST model, 250 kg-maximum strain gauge (Precision Transducers Ltd, New Zealand) was used to measure the maximum voluntary contraction (MVC), and to provide a measurement of 50 % of MVC during endurance test. Force readings were in Newtons (N), and were collected from the strain gauge via a custom made amplifier by an Apple G4 personal computer sampling at 2 kHz. A real-time force trace was displayed on a computer monitor using a customized software program (Superscope LL 5.0 GW Instruments, USA). This provided visual feedback of the force being generated by the subjects.

C. sEMG Electrode Placement

Skin preparation: The procedure recommended by De Luca [16] was followed to ensure skin impedance was below 10kΩ. First, the electrode sites were shaved. The shaved area was then rubbed with an abrasive paste (Omni-Prep®, D.O. Weaver & Co., USA) and the skin was then cleansed with 70% alcohol wipes and left to dry before attaching the electrodes. Finally, a small amount of conductive gel was wiped onto the shaved area. This was shown during testing to improve the quality of the signal from the Laplacian electrode. Electrodes used are (a) mono-polar silver/silver-chloride (Ag/AgCl) passive electrodes (Red Dot, 3M Health Care, USA) for grounding purposes and (b) for data collection of sEMG signals was via an eleven-pin (4 mm diameter) two-dimensional high-spatial resolution three channels Laplacian electrode (Université de Technologie, Compiegne, France) with an inter-electrode distance of 10 mm see Fig. 2.

D. Data Acquisition of sEMG Signals

Signals were collected and filtered by NND using the mask as given in equation (7) for each channel by the Laplacian sEMG electrodes with a gain of 100. Each sEMG channel was then further amplified with a gain of 1000 and filtered using a band-pass filter between 3 Hz and 1 kHz Grass model P511 amplifier (Grass Instruments Company, USA). The analogue signals were acquired by a multifunction data acquisition board NI PCI-6024E (National Instruments Corporation, USA) with LabVIEW 2010 software (National Instruments Corporation, USA) for raw data acquisition on a host desktop computer. The signals were analogue-to-digital converted with 16 bit resolution in the ± 5 V range and sampled at 10 kHz.

Figure 2. Three channel Laplacian electrode (right) and amplifier (left) used for data collection of sEMG signals from the vastus medialis muscle of the quadriceps. Supplied by Université de Technologie, Compiegne, France.

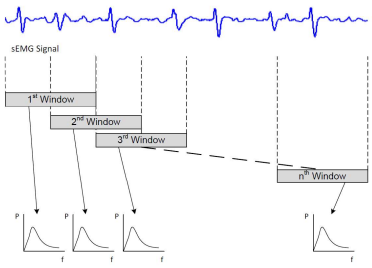

Figure 3. The top plot shows a single channel sEMG signal to be analysed using a 1 second window size with a 0.5 second overlap. Power Spectrum is used to calculate the MNF and MDF plus the RMS value of the windowed signal.

E. Signal Processing of sEMG Signals

Each of the three separate channel sEMG signals recorded were subsequently analysed off-line using a newly developed code for performing signal processing analysis of the sEMG signals using MATLAB 2010 (MathWorks Inc, USA). The sEMG signals were demeaned removing any direct current (DC) component that may exist in the signals before the analysis. The signals were subsequently digitally filtered using a 4th order Butterworth band-pass filter with a pass-band from 5 to 500 Hz.

A new algorithm was written in MATLAB to allow for each channel to be analysed at the same time see Fig 3 [6], [17]. The algorithm takes a 1 second window size of data from which a power spectrum was produced and analysed to calculate the MDF, and MNF values along with the RMS value. By taking a 1 second window size it is assumed to be quasi-stationary that is stationary during short time intervals. Under this assumption spectral analysis for feature extraction can be applied [18], [19].

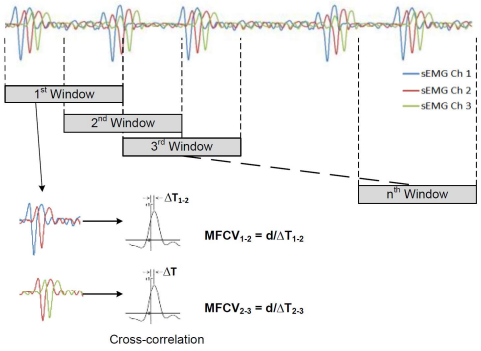

Figure 4. The top plot shows all 3 sEMG signals to be analysed using a 1 second window size with a 0.5 second overlap. Cross-correlation is used to obtain the MFCV between to channels 1-2 and channels 2-3.

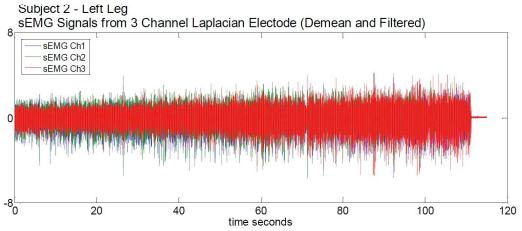

Figure 5. Demean and filtered sEMG signals collected from the three channel Laplacian electrode.

A Hanning window was used for the power spectrum to obtain smoothness of the output frequency spectrum avoiding spectral leakages and outliers. Each window size extracted was overlapped by 0.5 seconds to give a more detailed view of how the MNF, MDF and RMS vary over time through the sEMG signal. The values for MNF, MDF, and RMS were stored in a matrix; this was continued until the final nth window. Once all three signals were analysed, a separate plot for each value against time was produced.

The MFCV was calculated separately from a new algorithm using the cross-correlation function available in MATLAB see Fig. 4. This required taking channels 1 and 2 of the sEMG data to find the MCVF for a 1 second window and then proceeding to overlap each window by 0.5 seconds. The same method was performed using channels 2 and 3. The values for MFCV for each window were stored in a separate matrix, until the final n^{th} window. Once all the signals were analysed a separate plot for each value against time was produced.

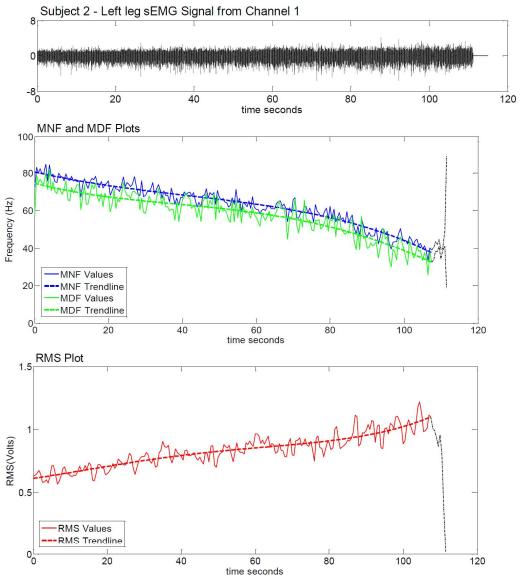

Figure 6. Show the sEMG signal for channel 1 (top plot) with the combined values for MNF, MDF (middle plot) and RMS values (bottom plot).

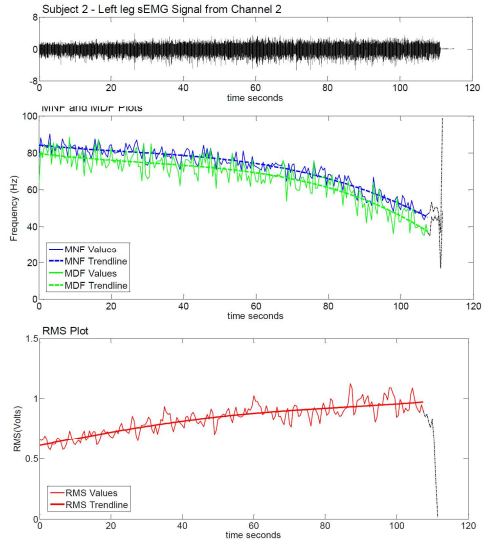

Figure 7. Shows the sEMG signal for channel 2 (top plot) with the combined values for MNF, MDF (middle plot) and RMS values (bottom plot).

III. Results and Discussions

Fig. 5 shows all three sEMG s collected from the left leg of subject 2 from this study of five subjects. These signals have been demeaned to remove any dc voltage component that may exist in the signals and further digitally filtered using a 4^{th} order Butterworth band pass filter between 5 Hz and 1 kHz.

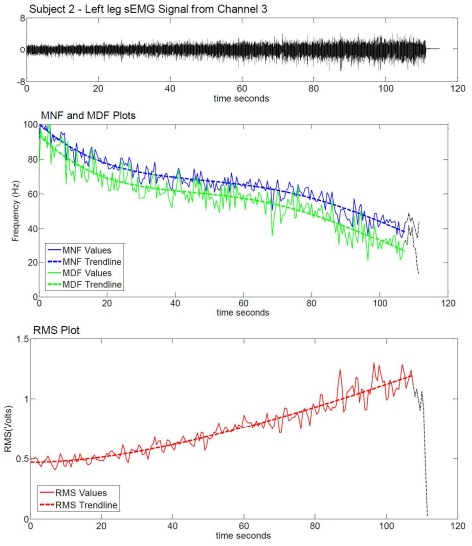

Figure 8. Shows the sEMG signal for channel 3 (top plot) with the combined values for MNF, MDF (middle plot) and RMS values (bottom plot).

The new algorithm using Fourier Power spectrum in Fig. 3 was used to find the MNF, MDF and RMS values for a set overlapping window size of 0.5 seconds was passed through each signal from the beginning until the end of the fatiguing. The results for each separate signal were plotted and are shown in Figs 6-8.

For analysis purposes, the last 4 seconds of the sEMG signal just before the subject completely fatigued were ignored in the overall analysis of the results. This is shown by the dotted black lines in Figs 6-8 for the MNF, MDF and RMS values. It clearly shows that the last 4 seconds are meaningless to the overall picture of the data presented.

Trendlines were added to the MNF, MDF and RMS plots using the *'polyval'* function in MatLAB. The 4^{th} order polynomial gave the best trendline in order to determine visually what was happening to these values throughout the signal.

By examining the results in Figs 6-8 the trendlines for MNF and MDF values follow same the trend, with MDF lower in value than the MNF. This indicates that the power spectrum for each window is skewed to the left i.e. the lower frequencies are dominant in the signal. Looking at the values for MNF and MDF frequencies it can be seen that all three signals have different trends during the first 20 seconds after which they follow a similar pattern. The values remain steady from 20 to

70 seconds after which they drop to about 20% in value until complete fatigue in the subject. The RMS values obtained show a doubling in a linear fashion throughout the signal for all three signals.

Once the analysis to find the MNF, MDF and RMS values were completed, a new algorithm was used to determine MFCV, see Fig. 4. To determine the MFCV, signals from channel 1 and channel 2 with the inter-electrode distance of 10 mm are required. The same was done to find the MFCV between channel 2 and channel 3. The results were plotted as a combined plot shown in Fig. 9.

For analysis purposes of MFCV, the last 2 seconds of the sEMG signal just before the subject completely fatigued was ignored in the overall analysis of the results. This is shown in as a black dotted line in in Fig. 9. It clearly shows that the last 2 seconds are meaningless to the overall picture of the data presented.

The MFCV results presented show the first values between channel 1 and 2 are greater than that for channel 2 and 3, but after about 20 seconds they follow the same trend. The MFCV remains at steady value between 20 seconds until 70 seconds after which it drops by 20-25% in value where after that complete fatigue occurred in the subject.

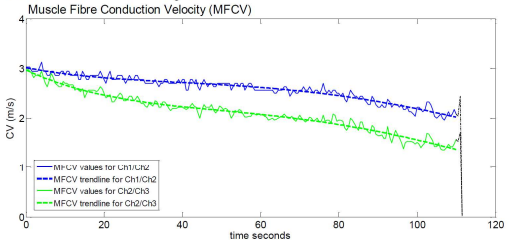

Figure 9. Shows a combined plot for MFCV values and trendlines between Ch1/Ch2 and Ch2/Ch3.

IV. Conclusion

All results using the first algorithm obtained for all subjects in this study have given similar results. That is for MNF and MDF values all follow the same trend throughout the sEMG signal. Therefore only one of these features need be selected for analysis purposes. The most beneficial one to use would be the MDF values as this shows a frequency value where the power spectrum splits the distribution in half. By visually examining the MNF and MDF trendlines, there was always a levelling off in these values between the 20-30% to the 75-80% of the muscle contraction. After this point these values dropped anywhere between 15-30% until the subject fatigues completely.

The RMS values in all cases showed a linear increase from the start of the muscle when it contracts until the subjects fatigued. However there was no other noticeable trend in the RMS values obtained from the analysis carried out.

The MFCV values in all cases showed a similar trend to that found in the MNF and MDF values. This indicates that these features are linked together in terms of the muscle behaviour through the contraction from start to finish. This can potentially be done as further investigation in terms of linking these features together.

References

[1] J. V. Basmajian and C. J. De Luca, *Muscles Alive: Their Functions Revealed by Electromyography*, 5th ed. Baltimore: Williams and Wilkins, 1985.

[2] D. B. Chaffin, "Localized muscle fatigue - Definition and measurement," *Journal of Occupational Medicine Article author,* vol. 15, pp. 346-354, 1973.

[3] E. N. Marieb, *Essentials of Human Anatomy & Physiology*, 8th ed. Benjamin Cummings, San Francisco: Pearson Benjamin Cummings, 2006.

[4] R. Merletti and P. A. Parker, *Electromyography: Physiology, Engineering, and Noninvasive Applications*. Hoboken, New Jersey: John Wiley & Sons, 2004.

[5] K. Englehart, B. Hudgins, P. A. Parker, and M. Stevenson, "Classification of the myoelectric signal using time-frequency based representations," *Medical Engineering & Physics,* pp. 431-438, 1999.

[6] J. V. d. Vegte, *Fundamentals of Digital Signal Processing*. Sydney: Prentice Hall, 2002.

[7] S. V. Vaseghi, *Advanced Digital Signal Processing and Noise Reduction*, 4th ed. Singapore: John Wiley & Son, 2008.

[8] M. T. Young, C. L. Lucas, and S. M. Blanchard, "Biosignal processing," in *Introduction to Biomedical Engineering*, J. D. Enderle, S. M. Blanchard, and J. D. Bronzino, Eds. San Diego, CA: Academic Press, 2000, pp. 233-278.

[9] H. Reucher, G. Rau, and J. Silny,"Spatial filtering of noninvasive multielectrode EMG. II. Filter performances in theory and modeling," *IEEE Trans. Biomed. Eng.,* vol. 34, pp. 106-113, 1987..

[10] R. Merletti, A. Botter, A. Troiano, E. Merlo, and M. A. Minetto, "Technology and instrumentation for detection and conditioning of the surface electromyographic signal: State of the art," *Clinical Biomechanics,* vol. 24, pp. 122-134, 2009.

[11] C. Disselhorst-Klug, G. Rau, A. Schmeer, and J. Silny, "Non-invasive detection of the single motor unit action potential by averaging the spatial potential distribution triggered on a spatially filtered motor unit action potential," *J. Electromyogr. Kinesiol.,* vol. 9, pp. 67–72, 1999.

[12] C. Disselhorst-Klug, J. Silny, and G. Rau, "Improvement of spatial resolution in surface-EMG: A theoretical and experimental comparison of different spatial filters," *IEEE Trans Biomed Eng,* vol. 44, pp. 567 - 74, 1997.

[13] N. Ostlund, J. Yu, K. Roeleveld, and J. S. Karlsson, "Adaptive spatial filtering of multichannel surface electromyogram signals," *Medical and Biological Engineering and Computing,* vol. 42, pp. 825-831, 2004.

[14] D. Farina and R. Merletti, "Methods for estimating muscle fibre conduction velocity from surface electromyographic signals," *Medical and Biological Engineering and Computing,* vol. 42, pp. 432-445, July 1st 2004.

[15] O. Maïsetti, A. Guével, P. Legros, and J.-Y. Hogrel, "Prediction of endurance capacity of quadriceps muscles in humans using surface electromyogram spectrum analysis during submaximal voluntary isometric contractions," *European Journal of Applied Physiology,* vol. 87, pp. 509-519, 2002.

[16] C. J. De Luca, "The use of surface electromyography in biomechanics," *Journal of Applied Biomechanics,* vol. 13, pp. 135-163, 1997.

[17] M. I. Heron and F. J. R. Richmond, "In-series fiber architecture in long human muscles," *Journal of Morphology,* vol. 216, pp. 35-45, 1993.

[18] R. Merletti and L. R. Lo Conte, "Surface EMG signal processing during isometric contractions," *J Electromyogr Kinesiol,* vol. 7, pp. 241-250, 1997.

[19] A. Luttmann, M. Jager, J. Sokeland, and W. Laurig, "Electromyographical study on surgeons in urology-II. determination of muscular fatigue," *Ergonomics,* vol. 39, pp. 298-313, 1996.

Jeff Kilby, was born in Edmonton, Alberta, Canada, who holds a MEng (Hons) in Signal Processing from the AUT University, Auckland New Zealand. Main research topic is in the field of Biomedical Signal Processing and Devices with other research interests are LabVIEW Applications Micro-controller Applications and Wireless Sensor Network Applications.

Krishnamachar Prasad holds Ph.D. (University of Western Australia), M.Tech. (IIT Madras, India) and BE (Bangalore University, India) degrees, all in Electrical Engineering. His research focuses on the development and reliability studies of novel interconnects in conventional and three-dimensional integrated circuits.

Paper 4

AMERICAN SCIENTIFIC PUBLISHERS

Advanced Science, Engineering and Medicine
Vol. 6, pp. 1–6, 2014
(www.aspbs.com/asem)

A Comparison of Surface Electromyography Signals Temporal and Spectral Parameters During a Sustained Fatigue Contraction

J. Kilby* and K. Prasad

School of Engineering, AUT University, Private Bag 92006, Auckland, New Zealand

This study investigates the fatigue characteristics of surface electromyography signals collected from the vastus medialis muscle of the quadriceps using a three channel Laplacian surface electrode. This paper presents initial findings of the pilot study of five healthy subjects performing 50% maximum voluntary contraction until complete fatigue of the muscle. An overlapping window was used to find the mean frequency (MNF), median frequency (MDF) of the power spectrum and RMS values at the beginning, middle and end of the signal. The results show the MNF and MDF values remain constant through the signal until a subject experiencing an increase in fatigue where these values dropped between 10–15% after 100 seconds. The RMS values also remain constant until the same point of time where it then increased between 20–30% in value.

KEYWORDS: Electromyography, Laplacian, Fatigue.

1. INTRODUCTION

Fatigue is a factor that affects all individuals on a daily basis. Its definition is very complex, not unique and controversial. There are two basic types of fatigue (a) whole body physical fatigue and (b) localized muscle fatigue.[1, 2] If muscles are exercised strenuously for a long period of time, muscle fatigue occurs. A muscle is fatigued when it is unable to contract even though it is still being stimulated. Without rest, an active or working muscle begins to tire and contracts more weakly until it finally ceases to react and stops contracting.[3]

Temporal and spectral parameters are used as feature extraction and pattern recognition in the processing and analysis of bio-medical signals.[4, 5] The use of the signal analysis is apparent in the field of research and clinical health for diagnosing health related problems and rehabilitation using bio-medical signals such as Surface Electromyography (sEMG) signals. Surface electromyography (sEMG) signals is the study of striated muscle activity obtained in the form of electrical signals.[1] The sEMG signals are obtained by electrodes placed on the skin surface overlying the muscle are then sent to a computer.

In signal processing, determining the frequency content of a signal by Fourier transform is one of the main aspects in feature extraction and understanding the characteristics of a signal.

The Fourier transform $F(\omega)$ of a time domain input signal $x(t)$ represented in the frequency domain is the sum of the signal $x(t)$ multiplied by a complex exponential as given in Eq. (1), where ω is the angular frequency and $\omega = 2\pi f$ with f is the input frequency.[6, 7]

$$F(\omega) = \int_{-\infty}^{\infty} x(t)e^{-j\omega t}\,dt \tag{1}$$

Since a digital computer only works with discrete data, a technique called Discrete Fourier Transform (DFT) is used.[6] Fast Fourier Transform (FFT) is the practical application name used for the DFT that maps discrete-time sequences into discrete-frequency representation as given in Eq. (2) where $x[n]$ is the input sequence, $F(k)$ is the DFT, $2\pi k$ is the angular frequency of input sequence frequency k and N is the number of samples in both discrete-time and the discrete-frequency domains.[6, 7]

$$F(k) = \sum_{n=0}^{N-1} x[n]e^{-j2\pi kt/N} \tag{2}$$

A common technique in signal processing of sEMG signals is to consider the squared of the values of the FFT coefficients as given in Eq. (3) producing a resultant plot that is referred to as a power spectrum.[7]

$$P(\omega) = |F(\omega)|^2 = \left|\int_{-\infty}^{\infty} x(t)e^{-j\omega t}\,dt\right|^2 \tag{3}$$

*Author to whom correspondence should be addressed.
Email: jkilby@aut.ac.nz
Received: xx Xxxx xxxx
Accepted: xx Xxxx xxxx

ARTICLE

Aspects of a signal such as the mean and the median frequency of the power spectrum and the root mean square (RMS) value of signal's electrical potential also play important roles in the whole task of features extraction for signal characterization. The ultimate aim of this exercise is to develop a system with the ability for signal classification by features, which is a powerful and promising tool for diagnosing problems.

The mean frequency (MNF) is the average of all frequencies of the power spectrum and can be expressed as given in Eq. (4) where $P(\omega)$ is the power spectrum of the signal.[4]

$$MNF = \frac{\int_0^\infty \omega P(\omega)\, d\omega}{\int_0^\infty P(\omega)\, d\omega} \tag{4}$$

The median frequency (MDF) is that frequency having 50% of the distribution on each side of the power spectrum and as given in Eq. (5).[4]

$$\int_0^{MDF} P(\omega)\, d\omega = \int_{MDF}^\infty P(\omega)\, d\omega \tag{5}$$

The RMS value of a signal $x(t)$ over a time interval 0–T is determined by computing equation as given in Eq. (6).[4]

$$RMS = \sqrt{\frac{1}{T}\int_0^T x^2(t)\, dt} \tag{6}$$

The collection of the sEMG signals from the surface of the skin to the data being stored involves a number of different stages, starting from a continuous analogue signal and ending with a discrete or digital signal.[8] These stages include amplification, analogue-to-digital conversion and signal conditioning.

Laplacian surface electrodes use spatial filters in sEMG recording and are represented by the Laplace filters. This is a class of high-pass spatial filters which approximate the second spatial derivative of the surface potential. Longitudinal and transversal Laplace filters can be combined to become the normal double differential (NDD) filter, which is a very selective spatial filter that enhances single motor unit (MU) activity from the interference signals, even at maximal contraction levels. The weights of the NDD filter, its filter mask can be written as in (7).[9, 10]

$$A_i = \begin{bmatrix} 0 & 1 & 0 \\ 1 & -4 & 1 \\ 0 & 1 & 0 \end{bmatrix} \tag{7}$$

The NDD configuration can be obtained by means of five cross-wised electrodes and is frequently used for two-dimensional sEMG recordings. This and other two-dimensional spatial filter configurations have been applied to extract single MU information from surface recordings.[10–13]

2. METHODOLOGY

2.1. Subjects

Five healthy volunteers with no previous history of knee or severe musculoskeletal injuries (5 males, age 18–35 years) participated in this pilot study. This study was approved by the Auckland University of Technology Ethics Committee (AUTEC) and was performed after each subject had given written consent.

2.2. Experimental Setup

Subjects were seated in a purpose built upright chair set at 110° with their knee flexed to 90° see Figure 1. The chair was adjusted to ensure that the back of the knee rested comfortably against the edge of the seat. Once comfortable, the subject was secured to the chair using a lap and chest strap. The lower leg, minus socks or other clothing, was strapped to a metal attachment in series with a strain gauge at the ankle level, just proximal to the lateral malleolus. Comfort was ensured by using a heat-moulded thermoplastic brace to secure the leg. This experimental setup was similar to that used by Maisetti et al.[14] Force measurements: a PST model, 250 kg-maximum strain gauge (Precision Transducers Ltd., New Zealand) was used to measure the maximum voluntary contraction (MVC), and to provide a measurement of 50% of MVC during endurance test. Force readings were in Newtons (N), and were collected from the strain gauge via a custom made amplifier by an Apple G4 personal computer sampling at 2 kHz. A real-time force trace was displayed on a computer monitor using a customized software program (Superscope LL 5.0 GW Instruments, USA). This provided visual feedback of the force being generated by the subjects.

2.3. sEMG Electrode Placement

Skin preparation: The procedure recommended by De Luca[15] was followed to ensure skin impedance was below 10 kΩ. First, the electrode sites were shaved.

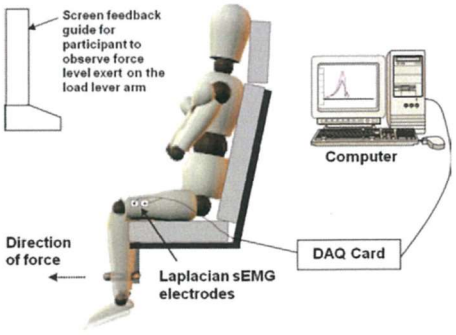

Fig. 1. Schematic diagram of equipment setup for signal acquisition.

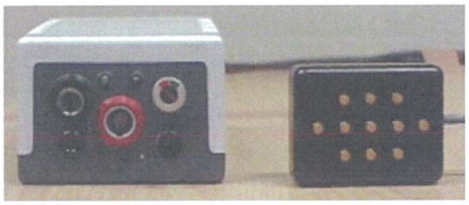

Fig. 2. Three-channel Laplacian electrode (right) and amplifier (left) used for data collection of sEMG signals from the vastus medialis muscle of the quadriceps.

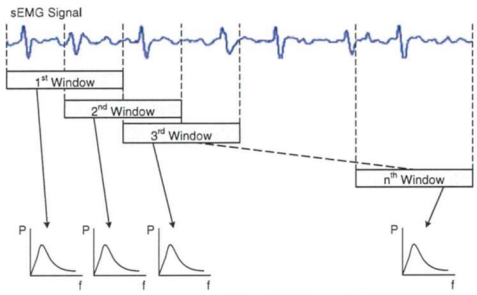

Fig. 3. The top plot shows a single channel sEMG signal to be analysed using a 2 second window size with a 0.01 second overlap. Power spectrum is used to calculate the MNF and MDF plus the RMS value of the signal.

The shaved area was then rubbed with an abrasive paste (Omni-Prep®, D.O. Weaver & Co., USA) and the skin was then cleansed with 70% alcohol wipes and left to dry before attaching the electrodes. Finally, a small amount of conductive gel was wiped onto the shaved area. This was shown during pilot testing to improve the quality of the signal from the Laplacian electrode. Electrodes used (a) mono-polar silver/silver-chloride (Ag/AgCl) passive electrodes (Red Dot, 3M Health Care, USA) was used for grounding purposes and (b) data collection of sEMG signals was via an eleven-pin (4 mm diameter) two-dimensional high-spatial resolution three channel Laplacian electrode (Université de Technologie, Compiegne, France) with an inter-electrode distance of 10 mm see Figure 2.

2.4. Data Acquisition of sEMG Signals

Signals were collected filtered by NND using the mask given in equation in (7) for each channel by the Laplacian sEMG electrodes with a gain of 100. Each sEMG channel was then further amplified with a gain 1000 and filtered using a band-pass filter between 3 Hz and 1 kHz Grass model P511 amplifier (Grass Instruments Company, USA). The analogue signals were acquired by a multifunction data acquisition board NI PCI-6024E (National Instruments Corporation, USA) with LabVIEW 2010 software (National Instruments Corporation, USA) for raw data acquisition on a host desktop computer. The signals were analogue-to-digital converted with 16 bit resolution in the ± 5 V range and sampled at 10 kHz.

2.5. Signal Processing of sEMG Signals

Each of the three separate channels sEMG signals recorded was subsequently analysed off-line using a newly developed code for performing signal processing analysis of the sEMG signals using MATLAB 2010 (MathWorks Inc., USA). The sEMG signals were demeaned removing any direct current (DC) component that may exist in the signals before the analysis. The signals were then digitally filtered using a 4th order Butterworth band-pass filter with a pass-band from 5 to 500 Hz.

A new algorithm was written in MATLAB to allow for each channel to be analysed at the same time. The algorithm takes a 2 second window size of data from which a power spectrum was produced and analysed to calculate the MDF and MNF values along with the RMS value. By taking a 2 second window size it is assumed to be quasi-stationary, that is stationary during short time

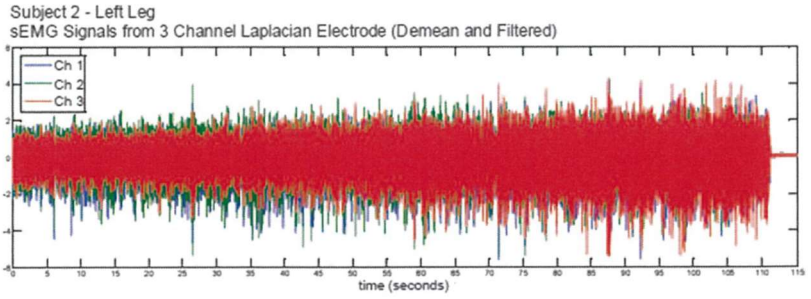

Fig. 4. Subject 2: sEMG signals collected from Laplacian electrode.

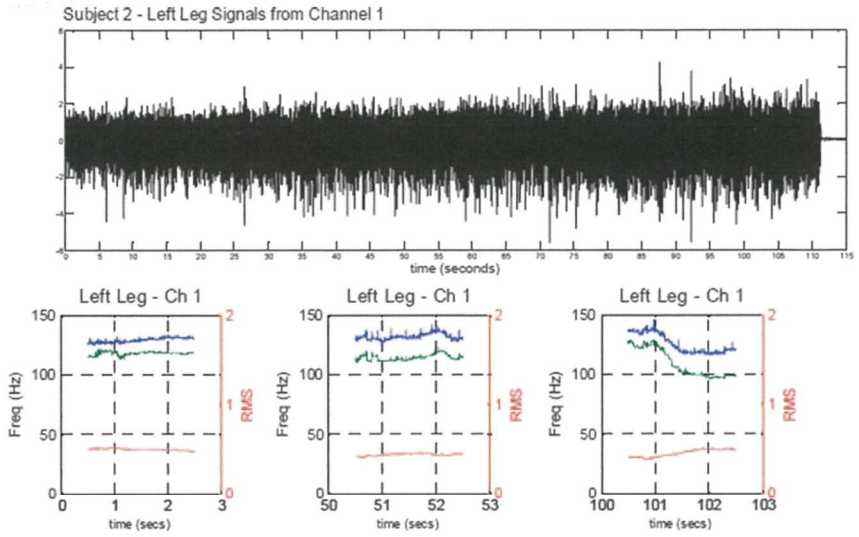

Fig. 5. sEMG signal plot for channel 1 (top) with combined corresponding plots (bottom plots) showing MNF (top blue line), MDF (middle green line) and RMS (bottom red line) for time periods (a) 0–3 seconds (bottom left) (b) 50–53 seconds (bottom middle) and (c) 100–103 seconds (bottom right).

intervals. Under this assumption spectral analysis for feature extraction can be applied.[16, 17] A Hanning window was used for the power spectrum to obtain smoothness of the output frequency spectrum avoiding spectral leakages and outliers. Each window size extracted was overlapped by 0.01 seconds to give a more detailed view of how the MNF, MDF and RMS vary over time through the sEMG signal.

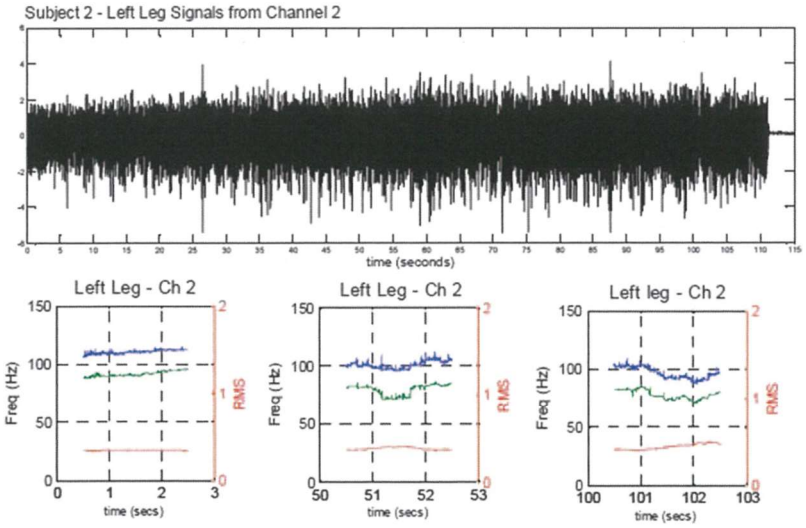

Fig. 6. sEMG signal plot for channel 2 (top) with combined corresponding plots (bottom plots) showing MNF (top blue line), MDF (middle green line) and RMS (bottom red line) for time periods (a) 0–3 seconds (bottom left) (b) 50–53 seconds (bottom middle) and (c) 100–103 seconds (bottom right).

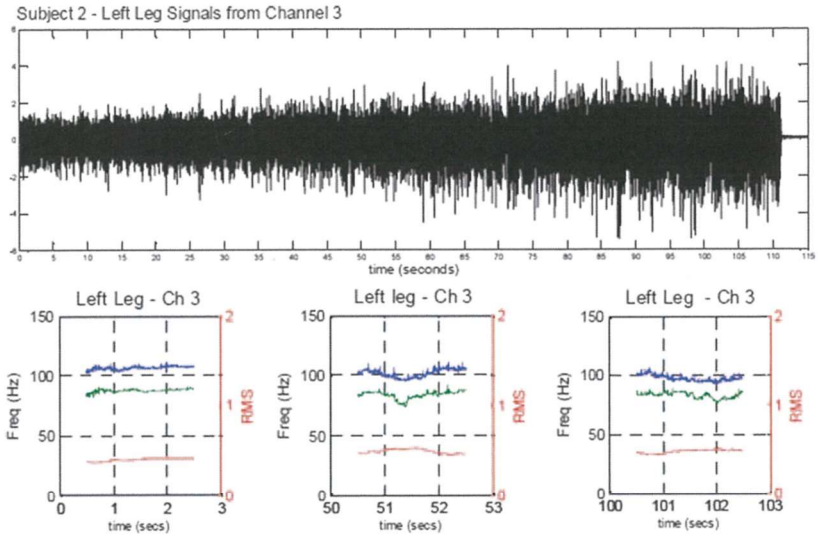

Fig. 7. sEMG signal plot for channel 3 (top) with combined corresponding plots (bottom plots) showing MNF (top blue line), MDF (middle green line) and RMS (bottom red line) for time periods (a) 0–3 seconds (bottom left) (b) 50–53 seconds (bottom middle) and (c) 100–103 seconds (bottom right).

The values for MNF, MDF and RMS, were stored in a matrix. This is continued until the final *n*th window. Once the values of signal data were analysed a separate plot for each value against time was produced.

3. RESULTS AND DISCUSSION

The initial results of this research for all 5 subjects has shown that there is a time in the sEMG where the MNF and MDF frequencies do decrease approximately 10–15% along with an increase in RMS value of an approximately 20–30%.

Figure 4 shows all three sEMG signals collected from the left leg of subject 2 from initial pilot study of five subjects. This sEMG signal from the Laplacian electrode has been demeaned and digitally filtered using MATLAB. The algorithm for the power spectrum analysis to determine the MNF, MDF frequencies and the RMS value require an extensive amount of time in computer processing. Hence for this stage of research, three portions of the signal were selected at the (a) beginning 0–3 seconds, (b) middle 50–53 seconds and (c) end 100–103 seconds.

Each sEMG signal for channels 1, 2 and 3 are shown in Figures 5–7 along with the corresponding combined plots for MNF (blue line), MDF (green line) and RMS (red line) for time periods (a), (b) and (c).

By examining the results displayed in Figures 5–7, the trends in MNF and MDF follow the same pattern with the MDF values lower than MNF values. This indicates that the power spectrum is skewed to the left i.e., the lower frequencies of the power spectrum. It can be seen from the combined plots of all three channels that the MNF and MDF remain considerably at constant values until between 100–103 seconds where the values show a significant drop. The RMS value remains constant until the same point of time between 100–103 seconds where there is an increase in value. Channel 1 showed the most apparent reductions in MNF and MDF with an increase in RMS over the period where channel 3 showed the least change. These are due to different channels that were originated from different positions from the inter-electrodes distance.

4. CONCLUSION

Since the MNF and MDF frequencies follow the same trend throughout the fatiguing contraction, the MDF frequency will be the most suitable to use as this gives the frequency where the power spectrum has 50% split either side of this value, this helps speed up the computer processing time.

Further research by using the MDF and RMS values is hoped to be carried out to analyse the complete sEMG signal, not just the selected three periods of time. By looking at the values and changes of the sEMG, there should be a pattern and trend that can be formed for the time of total fatigue occurs. Hence future work is favourable for this method to be used in predicting the time of fatigue in order to prevent patients to experience it which could lead to discomfort and injury.

This paper has not discussed the muscle fibre conduction velocity (CV) which is also possible to be determined using the Laplacian electrodes.[18] This will be the next step for this on-going research. Using the CV along with the MDF and RMS values, it is hoped that this will give an improved method for predicting the time of fatigue only by performing a short period of muscle contraction.

References and Notes

1. J. V. Basmajian and C. J. De Luca, Muscles Alive: Their Functions Revealed by Electromyography, 5th edn., Williams and Wilkins, Baltimore **(1985)**.
2. D. B. Chaffin, *Journal of Occupational Medicine Article Author* 15, 346 **(1973)**.
3. E. N. Marieb, Essentials of Human Anatomy and Physiology, 8th edn., Benjamin Cummings, Pearson Benjamin Cummings, San Francisco **(2006)**.
4. R. Merletti and P. A. Parker, Electromyography: Physiology, Engineering, and Noninvasive Applications, John Wiley & Sons, Hoboken, New Jersey **(2004)**.
5. K. Englehart, B. Hudgins, P. A. Parker, and M. Stevenson, *Medical Engineering and Physics* 431 **(1999)**.
6. J. V. D. Vegte, Fundamentals of Digital Signal Processing, Prentice Hall, Sydney **(2002)**.
7. S. V. Vaseghi, Advanced Digital Signal Processing and Noise Reduction, 4th edn., John Wiley & Son, Singapore **(2008)**.
8. M. T. Young, C. L. Lucas, and S. M. Blanchard, Biosignal processing, Introduction to Biomedical Engineering, edited by J. D. Enderle, S. M. Blanchard, and J. D. Bronzino, Academic Press, San Diego, CA **(2000)**, pp. 233–278.
9. H. Reucher, G. Rau, and J. Silny, *IEEE Trans. Biomed. Eng.* 34, 106 **(1987b)**.
10. R. Merletti, A. Botter, A. Troiano, E. Merlo, and M. A. Minetto, *Clinical Biomechanics* 24, 122 **(2009)**.
11. C. Disselhorst-Klug, G. Rau, A. Schmeer, and J. Silny, *J. Electromyogr. Kinesiol.* 9, 67 **(1999)**.
12. C. Disselhorst-Klug, J. Silny, and G. Rau, *IEEE Trans. Biomed. Eng.* 44, 567 **(1997)**.
13. N. Ostlund, J. Yu, K. Roeleveld, and J. S. Karlsson, *Medical and Biological Engineering and Computing* 42, 825 **(2004)**.
14. O. Maïsetti, A. Guével, P. Legros, and J.-Y. Hogrel, *European Journal of Applied Physiology* 87, 509 **(2002)**.
15. C. J. De Luca, *Journal of Applied Biomechanics* 13, 135 **(1997)**.
16. R. Merletti and L. R. Lo Conte, *J. Electromyogr. Kinesiol.* 7, 241 **(1997)**.
17. A. Luttmann, M. Jager, J. Sokeland, and W. Laurig, *Ergonomics* 39, 298 **(1996)**.
18. M. Gazzoni, F. Camelia, and D. Farina, *Journal of Neurophysiology* 94, 387 **(2005)**.

Paper 5

Multi-Channel Surface Electromyography Electrodes: A Review

Jeff Kilby, *Member, IEEE*, Krishnamachar Prasad, *Senior Member, IEEE*, and Grant Mawston

***Abstract*— This paper is a review of multi-channel surface electromyography (sEMG) electrode used in the research for investigating the properties of muscles. Over 300 papers from five recognized journals were examined from the year 2000 to 2013 with only 64 stating the use of multi-channel electrodes in their research. The review determined that multi-channel electrodes can be classified as linear array or 2D array electrodes. The 2D array is the basis for developing the high-spatial-resolution sEMG (HSR-sEMG) or high density sEMG (HD-sEMG). The important factors considered in this review of the electrodes are: 1) the material used; 2) the inter-electrode distance; and 3) the configuration for the collection of the electromyography signals. The basic configurations of the sEMG electrodes are monopolar, bipolar, and double differential. It was found that the majority of the linear array electrodes were used to collect either bipolar or double differential signals. The 2D array electrodes were used to collect monopolar signals. The HSR-sEMG electrodes used a normal double differentiating filter, referred to as Laplacian configuration. The HD-sEMG has versatility being able to collect all types of signals, such as monopolar, bipolar, double differential, or signals filtered by Laplacian configuration.**

***Index Terms*— Electromyography, multi-channel, electrodes.**

I. Introduction

ELECTROMYOGRAPHY or EMG is the term used for the study of electrical signals that are obtained from muscle activities by means of sensory electrodes. The word 'electromyography' itself is a combination of three Greek words, '***electron***' which associates it with the use of electricity, '***myos***' for 'muscle' and '***graph***' for 'writing'. Electromyography means a method of recording and analysing electrical signals, when generated by the muscles performing muscular activities. The electrical signals sourced from any biological organism are referred to as 'bioelectrical' or 'biosignal'. These biosignals are processed and analysed for the purpose of classifications. Classifier based EMG characterization system has been widely used by researchers and clinicians as a valuable tool for investigating muscle conditions and an accurate diagnosis for neuromuscular disorders for further rehabilitations [1], [2].

In surface Electromyography (sEMG), bio-electrical signals are obtained by surface electrodes placed on the skin over the selected muscle. Methods of using surface electrodes are non-invasive. Another method of EMG uses needle or fine-wire electrodes penetrating into the muscle approximately 2.5 to 5 mm deep. This method obtains signals that can be focused on a single muscle motor unit and used for targeting small muscles. The advantages of needle or 'indwelling' EMG are its selectivity, and also it is still able to detect other distant muscle activities or 'crosstalk'. However, indwelling EMG is an invasive method, which can cause stress and pain to the subject involved.

sEMG recordings provide a safe, easy and non-invasive method that can give objective measurement of muscle activities. It is not always necessary to penetrate the skin and record from single motor units to obtain useful and meaningful information regarding muscles. The technique allows the observer to see the muscle energy at rest and the continuous change over the course of a movement. sEMG obtains signals generated from a group of muscles rather than one single motor unit. With the use of multiple sensor channels electrode and spatial filtering technique, it becomes possible to observe different aspects of activities from a group of muscle fibres or compounded motor unit action potential. This has become the focus of many researchers in terms of their studies in the development of new multi-channel electrode design, along with advanced signal-processing techniques.

II. Literature Review of Multi-Channel Surface Electromyography Electrodes

A detailed literature review of the use of multi-channel electromyography electrodes was carried out, by examining recognized international peer-reviewed journal papers with a high impact factor (IF) [3]–[5] for research-related field of electromyography signals or analysis, from the year 2000 until 2013. The five recognized international journals selected and intensively searched were (a) European Journal of Applied Physiology, (b) Journal of Biomechanics, (c) Journal of Electromyography and Kinesiology, (d) Journal of Ergonomics and (e) Muscle & Nerve.

Over 364 papers were found to exist for the studies and research on '***surface emg electrode***'. The main component

Manuscript received January 28, 2016; revised April 25, 2016; accepted May 9, 2016. Date of publication May 16, 2016; date of current version June 16, 2016. This work was supported by the School of Engineering at Auckland University of Technology through a Contestable Grant. The associate editor coordinating the review of this paper and approving it for publication was Dr. Pantelis Georgiou.

J. Kilby is with the Signal Signals and Control Research Group, Department of Electrical and Electronic Engineering, Auckland University of Technology, Auckland 1010, New Zealand (e-mail: jkilby@aut.ac.nz).

K. Prasad is with the Department of Electrical and Electronic Engineering, Auckland University of Technology, Auckland 1010, New Zealand (e-mail: kprasad@aut.ac.nz).

G. Mawston is with the Department of Health and Rehabilitation Research Institute, Auckland University of Technology, Auckland 1010, New Zealand (e-mail: gmawston@aut.ac.nz).

Digital Object Identifier 10.1109/JSEN.2016.2569072

TABLE I
YEARLY DISTRIBUTION FROM 2000 TO 2013 OF THE NUMBER OF PUBLISHED JOURNAL PAPERS RELEVANT TO THIS RESEARCH FOR MULTI-CHANNEL sEMG ELECTRODES

Journal Name	2000	2001	2---002	2003	2004	2005	2006	2007	2008	2009	2010	2011	2012	2013	Total
European Journal of Applied Physiology	-	-	2	-	-	3	1	1	2	-	2	1	1	1	14 out of 57
Journal of Biomechanics	-	-	-	-	-	-	-	-	-	-	-	-	-	-	0 out of 14
Journal of Electromyography and Kinesiology	2	-	-	3	-	-	4	3	5	3	-	2	-	2	24 out of 76
Journal of Ergonomics	-	-	-	-	-	-	-	-	-	-	-	1	-	-	1 out of 170
Muscle & Nerve	1	1	1	1	3	2	2	1	1	2	-	2	5	1	23 out of 47
Total	3	1	3	4	3	5	7	5	8	5	2	6	6	4	62 out of 364

of this research contained the requirement to determine the configuration of the new multi-channel electrodes. The multi-channel electrodes which were mentioned in the literature review used more than two channels, either as '***linear array***' or a '***2D-matrix***' of surface electrodes.

From the initial number of papers sourced from the journal databases, only 62 of those papers [6]–[67] met the criteria of relevance for the literature review of this research. Table I shows the yearly distribution of journal papers from 2000 to 2013 that were reviewed and classified as using '***multi-channel***' electrodes for the collection of '***surface EMG***' signals. Out of the 62 journal papers, five papers were published [6]–[10] covering the recent progress, application, benefits and limitations of multi-channel electrodes in the field of research or clinical analysis of sEMG signals.

From Table I, four out of five journals showed the use of multi-channel electrodes. The three journals, European Journal of Applied Physiology, Journal of Electromyography and Kinesiology and Muscle & Nerve were generally interested in how muscle functions to produce movement or force. Of the other two journals, the Journal of Ergonomics showed only one paper that used multi-channel electrodes and the Journal of Biomechanics showed no journal papers. The majority of papers published in these two journals used standard sEMG electrodes with the conventional two-channel electrodes in bipolar configuration for traditional data acquisition of sEMG signals. These journals were mainly concerned with the general function of a movement by parts of the body and not analysing the condition of a muscle, which this research will be focused on.

The literature review showed there were various types of multi-channel electrodes that had been used in the collection and analysis of sEMG signals, which can be categorized as the following:

Linear-array electrode which were used for motor unit parameters such as amplitude and conduction velocity [17], [20]–[24], [28], [29], [31]–[34], [40]–[42], [45], [50]–[53], [55], [56], [58]–[60], [63]–[66].

Two-Dimensional (2D) array electrode which were used for motor unit recognition [11], [12], [14], [19], [25], [57], [67].

High-Spatial-Resolution surface electrode (HSR-sEMG) are 2D array-based electrodes, which were used for improved selectivity of motor unit parameters [15], [47].

High-Density surface electrode (HD-sEMG) are 2D array-based electrodes, which were used for motor unit recognition or motor unit topology [13], [16], [18], [26], [27], [30], [35]–[39], [43], [44], [46], [48], [49], [54], [61], [62].

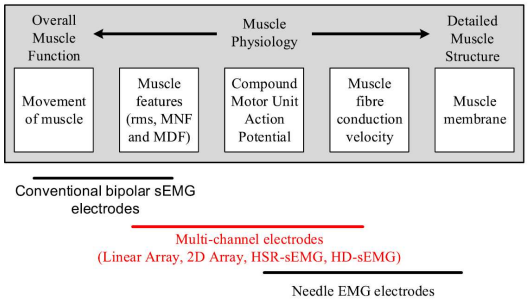

Fig. 1. Revised diagram showing what various EMG electrodes such as conventional *sEMG* electrodes, multi-channel *sEMG* electrodes (indicated in red) and needle EMG electrodes can measure in terms of muscle physiology [10].

Fig. 1 shows the overall picture of where the ***multi-channel electrodes*** sit, in terms of what can be measured in the muscle physiology using surface or needle electrodes.

From the literature review [11]–[67], the important aspects which were related to the multi-channel electrodes, focused on: ***electrode design and configuration, data acquisition, signal processing techniques used*** and ***testing of the subjects***.

Further specifications of each of these aspects are listed as follows:

A. Electrode Design and Configuration

Electrode material, shape and size
Inter-electrode distance (IED) of the electrodes
Gelled or dry electrodes
Electrode configuration
Filtering used and amplification of the signal

B. Data Acquisition of sEMG Signals

Sampling frequency
Bit-resolution of the data acquisition card

C. Signal Processing of sEMG Signals

Signal processing techniques used

D. Testing of the Subject

Muscles being investigated
Experimental set-up
Placement of the electrodes on the skin surface

III. Surface EMG Multi-Channel Electrodes

The basic sEMG includes the recommendations by the European project ***Surface EMG for Non-Invasive Assessment of Muscles (SENIAM)*** [68]–[75] in terms of materials used and the inter-electrode distances. The SENIAM recommendations is selected as it is an early and recognised association that substantially studied and researched in the area of sEMG. As with any type of electronic devices, sEMG electrodes have electrical properties and components which need to be considered. Hence the importance of noise filtering and amplification of the signals detected by the electrodes are also needed to be considered. All of these bases of building sEMG electrode are factors to consider for the development of new multi-channel electrode, which can be designed with configuration that enhance functions to extract more signal features and parameters of the muscle.

A. Surface EMG Electrodes Designs and Recommendations

sEMG electrodes which are placed over the skin surface act as sensors or transducers, detecting bioelectrical signals generated by the skeletal muscles during contractions. Surface electrodes can be classified, based on the materials and technologies implemented in their manufacturing. sEMG electrodes can be distinguished as dry and non-dry or wet electrodes. The dry electrodes available are such as pin or bar electrodes made of noble metals gold (Au), platinum (Pt) or silver (Ag), silver chloride (AgCl) or sintered silver chloride (Ag/AgCl). The wet electrodes (also called pre-gelled) consist of dry electrode components and a layer of conductive gel, hydrogel or sponge with an electrolyte solution, and they are often self-adhesive for ease of application. Fig. 2 shows examples of surface electrodes used for sEMG recordings.

A surface electrode's physical dimension, shape, technology and constituent materials may strongly influence the recorded

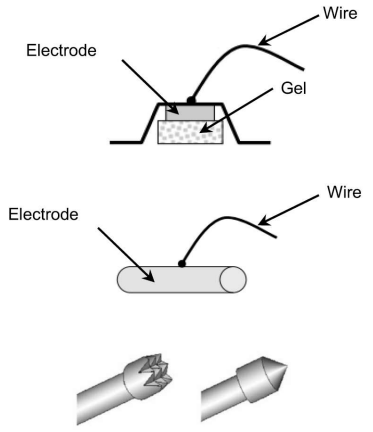

Fig. 2. Revised figure showing a range of common surface electrodes used, top: disposable electrode with sponge saturated with an electrolyte gel (wet), middle: solid metal bar electrode (dry) and bottom: pin electrodes (dry) [77].

sEMG signal [76], [77]. Hence, when choosing to use a sEMG sensor or electrode, the type, shape, size, inter-electrode distance, material and construction of the sensor have to be selected as well. The SENIAM wer developed by various researchers with recommendations on sensor design, material used, inter-electrode distance (IED), placement and signal processing.

The sensor type can be either monopolar or bipolar, which is a sensor consisting of two surface electrodes in either one or two-dimensional array. Since there were more reported publications using of the bipolar sensors in the sEMG inventory research, the SENIAM recommendations of sEMG sensors were restricted to the bipolar sensors only [76]. There is no information so far on the design recommendations for multi-channel sEMG electrodes, and there is a need for this information to be included as there were some research already carried out using multi-channel electrodes as mentioned previously [6]–[10]. For bipolar sensors, SENIAM developed recommendations for:

1) Electrode Shape and Size: The shape and size of the conductive area of sEMG electrodes can be either rectangular (square or bar) or circular (pin) electrodes are used, with not much difference in performance and pick-up area. SENIAM recommends that the maximum size of the electrode in the direction of the muscle fibres be circular with a diameter of 10 mm. Through literature review a wide variation of electrodes were found to be used, with either bar or pins with varying dimensions in terms of diameter and length as seen in Fig. 3.

2) Inter-Electrode Distance (IED): IED is the centre-to-centre distance between the conductive areas of two bipolar electrodes, as shown in Fig. 4.

The influence of the IED on the pick-up area and crosstalk is relevant, due to difference sizes of muscle. SENIAM recommends applying bipolar sEMG around the recommended sensor location with the IED of 20 mm.

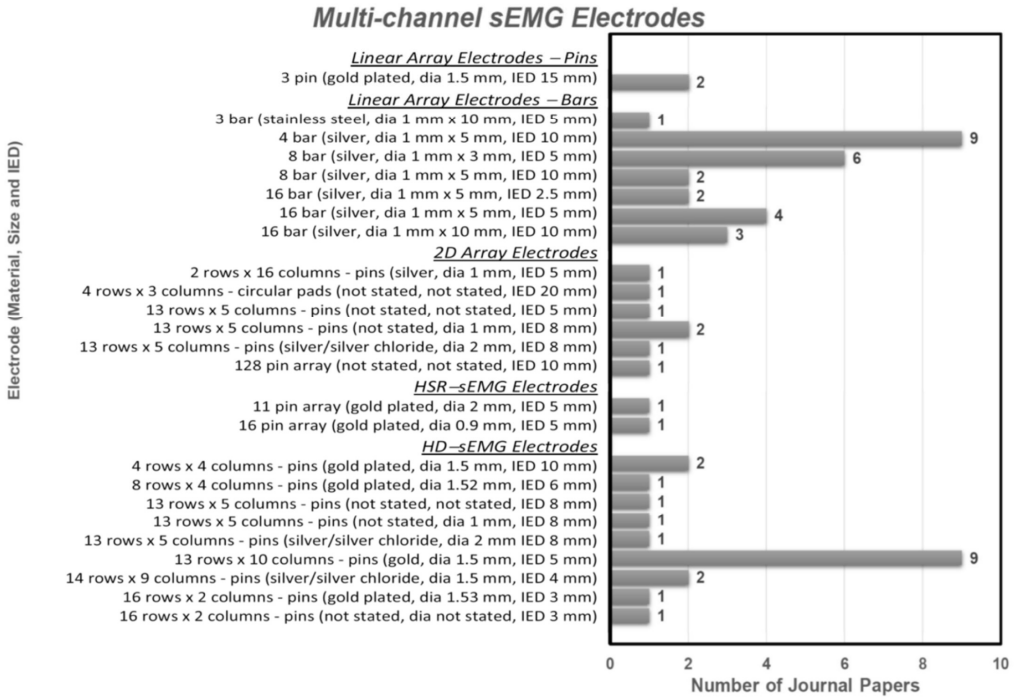

Fig. 3. Inventory of multi-channel sEMG electrodes where stated, shows the different configurations, electrode material, size and IED from the literature review.

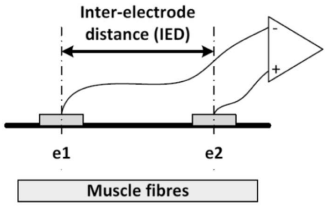

Fig. 4. The inter-electrode distance (IED) between two electrodes (e1 and e2) for a bipolar configuration.

When bipolar The IED shown in Fig.4 for this literature of multi-channel electrodes was determined by the distance between one electrode and the nearest electrode. These electrodes may be collecting monopolar signals from individual electrodes. There was a wide range of values, but the most common is either 5 mm or 10 mm.

3) Electrode Material: This forms the contact layer with the skin. The good electrode-skin contact exhibits a low electrode-skin impedance and a 'stable' behaviour in time, that is with respect to impedance and chemical reactions at the skin interface. Inventory research showed that varieties used were silver (Ag), silver chloride (AgCl), sintered Ag/AgCl, gold (Au), Au-plated and others. Electrodes are mostly combined with electrode gel [76], [77]. Electrode gel and paste are used to reduce the electrode-skin impedance. Electrode gel needs to be applied properly to a non-gelled electrode before use on a muscle, in order to obtain reliable sEMG recordings. SENIAM recommends using pre-gelled Ag/AgCl electrodes, as they were seen to provide stable transition with relatively low noise, and they are available commercially [76].

4) Sensor Construction: This is the mechanical construction used to integrate the electrodes, the cables and if applicable the pre-amplifier. SENIAM recommendations are to use a construction with fixed IED, built from lightweight material which should not directly affect sEMG characteristics. Cables need to be fixed, using tape or elastic band in such a manner as to avoid pulling or movement, especially in fast dynamic contractions. There was no specific information on the multi-channel sensor construction with various configurations, but generally the basic wiring stability is required as above.

5) Sensor Placement Procedure: Consists of a number of sequential steps to ensure location of the sensor in order to obtain reliable sEMG signals. SENIAM has set up a database showing how and where the electrode should be placed on the skin. The database was used in some previous research, with multi-channel electrodes for placing the sensor on the muscle of interest [78].

Another classification of the sEMG electrodes is based on their electro-chemical behaviour or their capacitive ability to

store charge, which is whether they are polarizable or non-polarizable [79], [80]. Polarizable electrodes have a strong capacitive behaviour, due to the double layer of charges at the metal-electrolyte interface. When a voltage is applied, there is no actual charge flow at the electrode-tissue interface, but a change of charge distribution associated to a displacement current occurred. Gold and platinum electrodes come closest to the ideal polarizable behaviour. A polarizable electrode is not suitable for sEMG recordings with dynamic muscle contractions, since a movement of the metal surface of the electrode with respect to the electrolyte solution or skin can induce a change in the surface potential [79], [80]. This is also called as 'movement artefact' which is typically lower than 20 Hz and partially overlaps with the low-frequency components of sEMG signal, causing loss of information. On the other hand, non-polarizable electrodes allow a free flow of charge across the interface, as it is characterized by mainly ohmic behaviour.

The currently most-preferred bipolar electrodes for sEMG application is the pre-gelled Ag/AgCl electrode as recommended by SENIAM. It fits the requirement of being non-polarizable as it has very low polarization property on current flow. It is also highly stable, since its junction with gel produces a lower noise level than other metallic electrodes [76], [79], [80]. When electrodes pre-gelled cannot be used, then the electrolyte has to be applied to the electrode metal shortly before the recording. However, further investigation on capacitive or polarizable electrodes is an ongoing research [76], [77] in order to build more effective electrodes which can be used to produce the least noise levels and to prevent loss of sEMG signal information. On the other hand, it is not always practical to have pre-gelled non-polarized electrodes when using a multi-channel system, as it consists an array of numerous pins [12]–[16], [18], [19], [25]–[27], [30], [35]–[39], [43], [44], [46]–[49], [54], [57], [61], [67]. A linear array electrode usually has pre-gelled electrodes [20], [21], [23], [24], [28], [29], [31], [33], [42], [45], [50]–[53], [55], [56], [58]–[60], [64], but HD-sEMG uses dry pins electrodes [12]–[14], [16], [18], [26], [27], [30], [35]–[39], [44], [46], [48], [54], [61].

B. Basic Configurations of sEMG Electrodes

When surface EMG signals are collected through an electrode placed on the surface of the skin, either during voluntary contraction of the muscle or at rest, the electrode acts as a passive electrical interface between the subject and the recording equipment. Electrode configuration for surface EMG refers to the number of electrodes for the recording site and their arrangement. The two most common configurations are 'monopolar (or unipolar)' and 'bipolar (or single differential)' configurations. In both cases there are usually two detection surfaces and a ground electrode. Any other electrode configurations are extensions of the bipolar configuration. For instance the bipolar configuration using a single differential amplifier can be expanded to a double differential configuration as shown in Fig. 5.

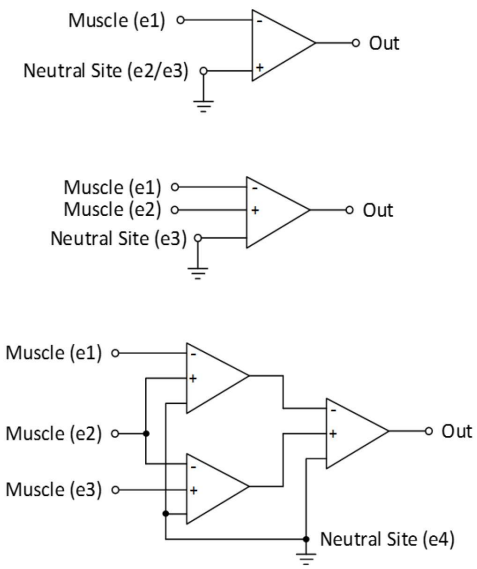

Fig. 5. The configurations for top: monopolar, middle: bipolar and bottom: double differential for the collection of sEMG signals.

1) Monopolar Configurations: Consists only one electrode (e1) as the active recording surface placed over the muscle, and the second electrode (e2) as the reference is placed on an electrically-neutral location such as the tendon to determine a potential difference. The third electrode (e3) as the ground is placed on a bony surface away from electrodes (e1 and e2). Usually the electrode (e2) is placed as the same location as the ground, and so only two electrodes are needed. Generally, monopolar signals produce lower frequency responses and less spatial selectivity than bipolar recordings. Monopolar configuration for surface electrodes is usually used during static contractions, or in clinical investigations using needle electrodes.

2) Bipolar Configuration: Has both active electrodes (e1 and e2) placed over the muscle, the other electrode (e3) acting as the ground is placed on a bony surface. Signals from the active electrodes are fed into a differential amplifier that records the electrical difference between the recording electrodes (e1 and e2). So any signal that is common to both inputs of the differential amplifier is greatly attenuated, and removed from the signal. This configuration is designed to minimize unwanted signals from surrounding environment such as radio frequency and electrical activity from power outlets, surrounds lights and so on [81], [82]. SENIAM recommendations on sEMG were based on bipolar configuration [76].

3) Double Differential Configuration: Consists of three active electrodes (e1, e2 and e3) in a row placed over the muscle, and one electrode (e4) for the reference or ground placed on a bony surface. This configuration gives an enhanced rejection of unwanted signals similar to that of the bipolar configuration [6], [81]–[84].

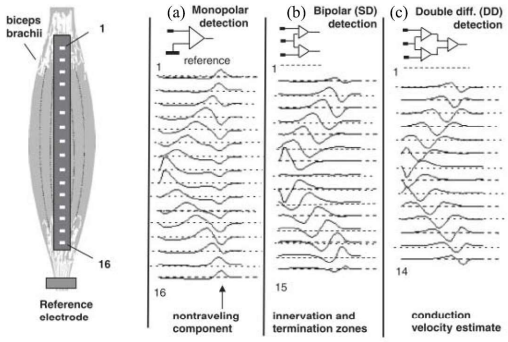

Fig. 6. Schematic diagram of the three configurations for the detection of surface EMG from linear arrays [85].

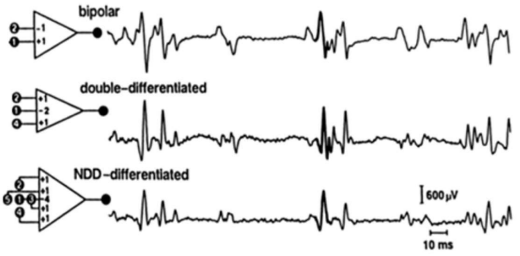

Fig. 7. Presentation of different EMG electrode configurations recorded from the musculus abductor pollicis brevis at maximum voluntary contraction. One excitation of a MU has been emphasized [87].

IV. Multi-Channel sEMG Electrode Configurations

By increasing the number of electrodes placed over the recording sites, the device is referred to as '***multi-channel electrode***'. The basic electrode configurations of monopolar, bipolar and double differential that are used in a multiple number with particular arrangements, form a multi-channel electrode. In this way a montage of information concerning the distribution of the EMG activity over a muscle or the timing relationships between different muscles becomes accessible. In principle, there is no hindrance to increasing the number of surface electrodes over the muscle, the number of channels, or arranging complex montages from different electrodes for each channel. The types of the multi-channel configurations are ***Linear array***, ***Two-Dimensional (2D) array, High-Spatial-Resolution sEMG (HSR-sEMG)*** and ***High-Density sEMG (HD-sEMG)***. This section covers these configurations in a greater detail, describing the various types of electrode arrangements done so far by other researchers. It also shows that different electrode arrangements can produce different form of signals, which can be further processed and analysed later.

A. Linear Array Electrodes

Connecting several recording electrodes placed in line results in a linear array recording, as shown in Fig. 6 [85]. The figure shows the three configurations, the first (a): monopolar detection which provides the maximum information available from the signal and includes the fibre end effects. The second (b): bipolar detection provides a clear picture of any innervation and tendon zones. The third (c): double differential detection is the most suitable for estimating the muscle fibre conduction velocity [85].

From the literature review, it was found that 24 of the 62 papers used linear array electrodes, either in the bipolar or double-differential configuration mode. The electrodes used in those researches were sourced from the same manufacturer LISiN-Spes Medica, Italy. They are semi-disposable pre-gel and the electrodes made from silver bars. The 2D Array and HD-sEMG electrodes were reusable and made from gold-plated pins.

B. 2D Array Electrodes

These sEMG electrodes form a grid or matrix which is covering a portion of the skin surface above one or more muscles [6]. Each of the electrodes collects a monopolar signal, which are further processed for analysis. The 2D array electrodes have been further developed to form the HSR-sEMG and HD-sEMG electrodes for specialized research and clinical uses of sEMG signals [6], [7], [86].

C. HSR-sEMG Electrodes

High-Spatial-Resolution sEMG (HSR-sEMG) is a class of high-pass spatial filters represented by Laplace filters which approximate the second spatial derivative of the surface potential. Fig. 7 shows the combination of activities of one electrode with one or several surrounding electrodes close to the muscle, which results in '*higher-order*' derivations [87]. The classic configuration of two electrodes used over the muscle result in a bipolar recording and double-differential recording as presented in Fig. 7 top and middle respectively. The effect is a '***spatial (high-pass) filtering***', producing a narrowing of the spatial view of the sEMG signal [87]–[95]. A more complex spatial filtering is '***normal double differentiating filter (NDD-filter)***' referred to as ***Laplacian configuration***, where a central electrode is connected with four surrounding electrodes [88], [89]. The weights of the NDD filter (its filter mask) are written as:

$$A = \begin{bmatrix} 0 & +1 & 0 \\ +1 & -4 & +1 \\ 0 & +1 & 0 \end{bmatrix}$$

where the '-4' is the weight of central electrode and '$+1$'s indicate the four surrounding filters. This NDD or Laplace configuration is shown in Fig. 7 bottom. The spatial Laplacian filtering is used with monopolar signals obtained from either the 2D-array or HDs-EMG electrodes [6], [77], [88], [89].

The exact montage to be used depends on the clinical or research question. It should be realized that the recording area

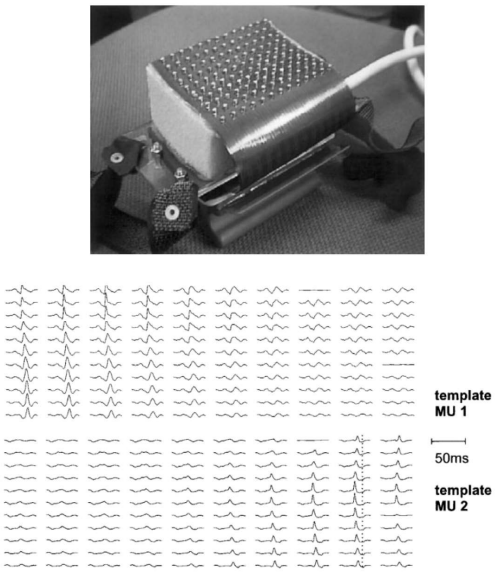

Fig. 8. Top: a 126-channel high-density electrode grid as it is developed for the study of the larger skeletal muscles. Three-dimensional surface MUP templates recorded from two MUs. Bottom: the signals are represented in monopolar montage [6].

of the electrodes becomes progressively smaller with higher-order derivations, but also with shorter IED. As a natural consequence, the amplitude of the signals usually decreases. An important and often intended consequence of bipolar and higher-order montages, and of a short IED, is the suppression of the far-field activity, originating during the start and extinction of the action potential [87]–[95].

The array which is applied along the muscle fibre direction, is also known to sample the propagating potential at different positions in the space. This can be used to estimate muscle fibre conduction velocity and to determine the location of innervation zones and tendons [8], [96], [97].

D. HD-sEMG Electrodes

High-Density sEMG (HD-sEMG) electrodes is a logical extension, consisting of a two-dimensional grid with an arbitrary number of electrodes and IEDs, shown in Fig. 8 (top). This configuration enables the localization and size estimation of motor units (MUs) as well as the determination of the position of the endplate zone. With a two-dimensional grid it is also possible to display the sEMG activity in an amplitude map, shown Fig. 8 (bottom) [6].

So it is recommended for all sEMG measurements, especially for HD-sEMG electrodes to record and store the signals of the individual electrodes in the array or grid, referenced to a remote electrode in a monopolar fashion. This approach allows versatility with respect to the desired montages such as bipolar, double differential or Laplacian configuration.

Some of the past research that used HD-sEMG electrodes, all of which collected monopolar signals [13], [16], [18], [26], [27], [30], [35]–[39], [43], [44], [46], [48], [49], [54], [61], [62]. There was a wide variation in number of pins used, some used a commercially available HD-sEMG electrode supplied by ActiveOne, BioSemi, Amsterdam, Netherlands with 126 gold-plated pins, shown in Fig. 8 [26], [27], [36]–[39], [46], [48], [54].

V. Conclusion

This paper has reviewed reported literature on multi-channel electrodes used for sensing EMG signals from the surface of the human skin. These signals represent the muscle activity or strength performing a specific task being researched. There are many types of multi-channel electrodes either using a linear array or 2D array configuration with various dimensions. None of the electrodes reported were commercially available or used with standard protocols.

Linear array electrodes ranged from 3 pin or bar to 16 bars. The material used for the electrodes either gold-plated or silver or silver/chloride with the IED varying from 2.5 to 15 mm, but is generally 10 mm. These electrodes were configured either as monopolar, bipolar or double differential. The most common configuration used was bipolar, which ensures any unwanted noise in the signals is greatly reduced.

The 2D array electrode configurations are the basis for developing the HSR-sEMG or HD-sEMG electrodes. The material used was mainly gold-plated pins with a diameter from 0.9 to 1.95 mm, but is generally is 1 mm. The IED ranged from 3 mm to 10 mm, but is generally 5 mm. The signals are generally collected as monopolar, but are then filtered using different montage masks, but the most widely used is the normal double differentiating filter mask referred to as Laplacian filtering.

This paper has shown that the multi-channel sEMG electrodes have been developed and used in the data collection and analysis of sEMG signals. Apart from the placement of electrodes on the skin surface, the configuration is also an important factor as well as the electrode material(s) and the IED when designing new electrodes. Other factors such as sampling frequency and the type(s) of filters are also of importance when using sEMG electrodes.

This review has provided a background information and understanding for the development of new multi-channel sEMG electrode. The new multi-channel electrode can be designed with configuration that enhance functions to extract more signal features and parameters of the muscle.

References

[1] J. Yousefi and A. Hamilton-Wright, "Characterizing EMG data using machine-learning tools," *Comput. Biol. Med.*, vol. 51, pp. 1–13, Aug. 2014.

[2] C. Disselhorst-Klug, "Non-invasive diagnosis of neuromuscular disorders by high-spatial-resolution-EMG," in *EMG Methods for Evaluating Muscle and Nerve Function*, M. Schwartz, Ed. Rijeka, Croatia: InTech, 2012, pp. 227–240.

[3] E. R. Smith, "The journal impact factor," *Can. J. Cardiol.*, vol. 22, pp. 787–788, 2006.

[4] E. Garfield, "Journal impact factor: A brief review," *CMAJ: Can. Med. Assoc. J.*, vol. 161, no. 8, pp. 979–980, 1999.

[5] L. A. Vucovich, J. B. Baker, and J. T. Smith, "Analyzing the impact of an author's publications," *J. Med. Library Assoc.*, vol. 96, no. 1, pp. 63–66, 2008.

[6] M. J. Zwarts and D. F. Stegeman, "Multichannel surface EMG: Basic aspects and clinical utility," *Muscle Nerve*, vol. 28, no. 1, pp. 1–17, 2003.

[7] M. J. Zwarts, G. Drost, and D. F. Stegeman, "Recent progress in the diagnostic use of surface EMG for neurological diseases," *J. Electromyogr. Kinesiol.*, vol. 10, no. 5, pp. 287–291, Oct. 2000.

[8] R. Merletti, D. Farina, and M. Gazzoni, "The linear electrode array: A useful tool with many applications," *J. Electromyogr. Kinesiol.*, vol. 13, no. 1, pp. 37–47, 2003.

[9] F. Felici, "Neuromuscular responses to exercise investigated through surface EMG," *J. Electromyogr. Kinesiol.*, vol. 16, pp. 578–585, Dec. 2006.

[10] G. Drost, D. F. Stegeman, B. G. M. van Engelen, and M. J. Zwarts, "Clinical applications of high-density surface EMG: A systematic review," *J. Electromyogr. Kinesiol.*, vol. 16, pp. 586–602, Dec. 2006.

[11] S. M. Wood, J. A. Jarratt, A. T. Barker, and B. H. Brown, "Surface electromyography using electrode arrays: A study of motor neuron disease," *Muscle Nerve*, vol. 24, no. 2, pp. 223–230, 2001.

[12] K. Watanabe *et al.*, "Motor unit firing pattern of vastus lateralis muscle in type 2 diabetes mellitus patients," *Muscle Nerve*, vol. 48, no. 5, pp. 806–813, 2013.

[13] M. C. P. Van Beekvelt, G. Drost, G. Rongen, D. F. Stegeman, B. G. M. Van Engelen, and M. J. Zwarts, "Na^+-K^+-ATPase is not involved in the warming-up phenomenon in generalized myotonia," *Muscle Nerve*, vol. 33, pp. 514–523, 2006.

[14] D. Staudenmann, I. Kingma, A. Daffertshofer, D. F. Stegeman, and J. H. van Dieën, "Heterogeneity of muscle activation in relation to force direction: A multi-channel surface electromyography study on the triceps surae muscle," *J. Electromyogr. Kinesiol.*, vol. 19, pp. 882–895, Oct. 2009.

[15] E. Schulte, O. Miltner, E. Junker, G. Rau, and C. Disselhorst-Klug, "Upper trapezius muscle conduction velocity during fatigue in subjects with and without work-related muscular disorders: A non-invasive high spatial resolution approach," *Eur. J. Appl. Physiol.*, vol. 96, pp. 194–202, Jan. 2006.

[16] J. P. J. Schmitz, J. P. van Dijk, P. A. J. Hilbers, K. Nicolay, J. A. L. Jeneson, and D. F. Stegeman, "Unchanged muscle fiber conduction velocity relates to mild acidosis during exhaustive bicycling," *Eur. J. Appl. Physiol.*, vol. 112, pp. 1593–1602, May 2012.

[17] P. Sbriccoli, V. Camomilla, A. Di Mario, F. Quinzi, F. Figura, and F. Felici, "Neuromuscular control adaptations in elite athletes: The case of top level karateka," *Eur. J. Appl. Physiol.*, vol. 108, no. 6, pp. 1269–1280, 2010.

[18] A. Samani, A. Holtermann, K. Søgaard, and P. Madeleine, "Active biofeedback changes the spatial distribution of upper trapezius muscle activity during computer work," *Eur. J. Appl. Physiol.*, vol. 110, pp. 415–423, Sep. 2010.

[19] J. Rodriguez-Falces, F. Negro, M. Gonzalez-Izal, and D. Farina, "Spatial distribution of surface action potentials generated by individual motor units in the human biceps brachii muscle," *J. Electromyogr. Kinesiol.*, vol. 23, pp. 766–777, Aug. 2013.

[20] A. Rainoldi, M. Nazzaro, R. Merletti, D. Farina, I. Caruso, and S. Gaudenti, "Geometrical factors in surface EMG of the vastus medialis and lateralis muscles," *J. Electromyogr. Kinesiol.*, vol. 10, no. 5, pp. 327–336, 2000.

[21] A. Rainoldi, M. Gazzoni, and R. Casale, "Surface EMG signal alterations in Carpal Tunnel syndrome: A pilot study," *Eur. J. Appl. Physiol.*, vol. 103, pp. 233–242, May 2008.

[22] A. Rainoldi, D. Falla, R. Mellor, K. Bennell, and P. Hodges, "Myoelectric manifestations of fatigue in vastus lateralis, medialis obliquus and medialis longus muscles," *J. Electromyogr. Kinesiol.*, vol. 18, no. 6, pp. 1032–1037, 2008.

[23] M. Pozzo, E. Merlo, D. Farina, G. Antonutto, R. Merletti, and P. E. D. Prampero, "Muscle-fiber conduction velocity estimated from surface EMG signals during explosive dynamic contractions," *Muscle Nerve*, vol. 29, no. 6, pp. 823–833, 2004.

[24] H. Piitulainen, A. Botter, R. Merletti, and J. Avela, "Muscle fiber conduction velocity is more affected after eccentric than concentric exercise," *Eur. J. Appl. Physiol.*, vol. 111, no. 2, pp. 261–273, Feb. 2011.

[25] H. Piitulainen, R. Bottas, V. Linnamo, P. Komi, and J. Avela, "Effect of electrode location on surface electromyography changes due to eccentric elbow flexor exercise," *Muscle Nerve*, vol. 40, no. 4, pp. 617–625, 2009.

[26] E. R. Mulder *et al.*, "Knee extensor fatigability after bedrest for 8 weeks with and without countermeasure," *Muscle Nerve*, vol. 36, no. 6, pp. 798–806, 2007.

[27] E. R. Mulder, K. H. L. Gerrits, J. Rittweger, D. Felsenberg, D. F. Stegeman, and A. de Haan, "Characteristics of fast voluntary and electrically evoked isometric knee extensions during 56 days of bed rest with and without exercise countermeasure," *Eur. J. Appl. Physiol.*, vol. 103, pp. 431–440, Jul. 2008.

[28] M. A. Minetto *et al.*, "Feasibility study of detecting surface electromyograms in severely obese patients," *J. Electromyogr. Kinesiol.*, vol. 23, no. 2, pp. 285–295, 2013.

[29] L. Mesin, C. Cescon, M. Gazzoni, R. Merletti, and A. Rainoldi, "A bi-dimensional index for the selective assessment of myoelectric manifestations of peripheral and central muscle fatigue," *J. Electromyogr. Kinesiol.*, vol. 19, no. 5, pp. 851–863, 2009.

[30] R. Merletti, A. Holobar, and D. Farina, "Analysis of motor units with high-density surface electromyography," *J. Electromyogr. Kinesiol.*, vol. 18, pp. 879–890, Dec. 2008.

[31] R. Merletti, D. Farina, M. Gazzoni, and M. P. Schieroni, "Effect of age on muscle functions investigated with surface electromyography," *Muscle Nerve*, vol. 25, no. 1, pp. 65–76, 2002.

[32] F. Menotti, I. Bazzucchi, F. Felici, A. Damiani, M. C. Gori, and A. Macaluso, "Neuromuscular function after muscle fatigue in Charcot–Marie–Tooth type 1A patients," *Muscle Nerve*, vol. 46, no. 3, pp. 434–439, 2012.

[33] G. Melchiorri and A. Rainoldi, "Muscle fatigue induced by two different resistances: Elastic tubing versus weight machines," *J. Electromyogr. Kinesiol.*, vol. 21, no. 6, pp. 954–959, 2011.

[34] K. C. D. McIntosh and D. A. Gabriel, "Reliability of a simple method for determining muscle fiber conduction velocity," *Muscle Nerve*, vol. 45, no. 2, pp. 257–265, 2012.

[35] E. M. Maathuis, J. Drenthen, J. P. van Dijk, G. H. Visser, and J. H. Blok, "Motor unit tracking with high-density surface EMG," *J. Electromyogr. Kinesiol.*, vol. 18, no. 6, pp. 920–930, 2008.

[36] B. U. Kleine, J. P. van Dijk, M. J. Zwarts, and D. F. Stegeman, "Inter-operator agreement in decomposition of motor unit firings from high-density surface EMG," *J. Electromyogr. Kinesiol.*, vol. 18, no. 4, pp. 652–661, 2008.

[37] B. U. Kleine, J. P. van Dijk, B. G. Lapatki, M. J. Zwarts, and D. F. Stegeman, "Using two-dimensional spatial information in decomposition of surface EMG signals," *J. Electromyogr. Kinesiol.*, vol. 17, no. 5, pp. 535–548, 2007.

[38] B. U. Kleine, D. F. Stegeman, G. Drost, and M. J. Zwarts, "Interspike interval analysis in a patient with peripheral nerve hyperexcitability and potassium channel antibodies," *Muscle Nerve*, vol. 37, no. 2, pp. 269–274, 2008.

[39] B. U. Kleine, J. H. Blok, R. Oostenveld, P. Praamstra, and D. F. Stegeman, "Magnetic stimulation-induced modulations of motor unit firings extracted from multi-channel surface EMG," *Muscle Nerve*, vol. 23, no. 7, pp. 1005–1015, 2000.

[40] E. G. Klaver-Król, J. J. Rasker, N. R. Henriquez, W. G. Verheijen, and M. J. Zwarts, "Muscle fiber velocity and electromyographic signs of fatigue in fibromyalgia," *Muscle Nerve*, vol. 46, no. 5, pp. 738–745, 2012.

[41] E. G. Klaver-Król, N. R. Henriquez, S. J. Oosterloo, P. Klaver, J. M. Bos, and M. J. Zwarts, "Distribution of motor unit potential velocities in short static and prolonged dynamic contractions at low forces: Use of the within-subject's skewness and standard deviation variables," *Eur. J. Appl. Physiol.*, vol. 101, pp. 647–658, Nov. 2007.

[42] L. A. C. Kallenberg, S. Preece, C. Nester, and H. J. Hermens, "Reproducibility of MUAP properties in array surface EMG recordings of the upper trapezius and sternocleidomastoid muscle," *J. Electromyogr. Kinesiol.*, vol. 19, no. 6, pp. e536–e542, 2009.

[43] L. A. C. Kallenberg and H. J. Hermens, "Motor unit properties of biceps brachii during dynamic contractions in chronic stroke patients," *Muscle Nerve*, vol. 43, no. 1, pp. 112–119, 2011.

[44] L. A. C. Kallenberg and H. J. Hermens, "Motor unit properties of biceps brachii in chronic stroke patients assessed with high-density surface EMG," *Muscle Nerve*, vol. 39, no. 2, pp. 177–185, 2009.

[45] A. Hummel, T. Läubli,, M. Pozzo, P. Schenk, S. Spillmann, and A. Klipstein, "Relationship between perceived exertion and mean power frequency of the EMG signal from the upper trapezius muscle during isometric shoulder elevation," *Eur. J. Appl. Physiol.*, vol. 95, pp. 321–326, Nov. 2005.

[46] A. Holtermann, K. Roeleveld, B. Vereijken, and G. Ettema, "Changes in agonist EMG activation level during MVC cannot explain early strength improvement," *Eur. J. Appl. Physiol.*, vol. 94, pp. 593–601, Aug. 2005.

[47] J.-Y. Hogrel, "Use of surface EMG for studying motor unit recruitment during isometric linear force ramp," *J. Electromyogr. Kinesiol.*, vol. 13, no. 5, pp. 417–423, Oct. 2003.

[48] B. Gerdle, N. Östlund, C. Grönlund, K. Roeleveld, and J. S. Karlsson, "Firing rate and conduction velocity of single motor units in the trapezius muscle in fibromyalgia patients and healthy controls," *J. Electromyogr. Kinesiol.*, vol. 18, pp. 707–716, Oct. 2008.

[49] A. Gallina, R. Merletti, and M. Gazzoni, "Uneven spatial distribution of surface EMG: What does it mean?" *Eur. J. Appl. Physiol.*, vol. 113, pp. 887–894, Apr. 2013.

[50] D. Farina, P. Madeleine, T. Graven-Nielsen, R. Merletti, and L. Arendt-Nielsen, "Standardising surface electromyogram recordings for assessment of activity and fatigue in the human upper trapezius muscle," *Eur. J. Appl. Physiol.*, vol. 86, pp. 469–478, 2002/04/01 2002.

[51] D. Farina, M. Gazzoni, and R. Merletti, "Assessment of low back muscle fatigue by surface EMG signal analysis: Methodological aspects," *J. Electromyogr. Kinesiol.*, vol. 13, pp. 319–332, Aug. 2003.

[52] D. Farina, R. A. Ferguson, A. Macaluso, and G. De Vito, "Correlation of average muscle fiber conduction velocity measured during cycling exercise with myosin heavy chain composition, lactate threshold, and VO_{2max}," *J. Electromyogr. Kinesiol.*, vol. 17, pp. 393–400, Aug. 2007.

[53] D. Falla, P. Dall'Alba, A. Rainoldi, R. Merletti, and G. Jull, "Repeatability of surface EMG variables in the sternocleidomastoid and anterior scalene muscles," *Eur. J. Appl. Physiol.*, vol. 87, pp. 542–549, Oct. 2002.

[54] G. Drost *et al.*, "Motor unit characteristics in healthy subjects and those with postpoliomyelitis syndrome: A high-density surface EMG study," *Muscle Nerve*, vol. 30, no. 3, pp. 269–276, 2004.

[55] C. Cescon, E. Sguazzi, R. Merletti, and D. Farina, "Non-invasive characterization of single motor unit electromyographic and mechanomyographic activities in the biceps brachii muscle," *J. Electromyogr. Kinesiol.*, vol. 16, pp. 17–24, Feb. 2006.

[56] T. Castroflorio *et al.*, "Reproducibility of surface EMG variables in isometric sub-maximal contractions of jaw elevator muscles," *J. Electromyogr. Kinesiol.*, vol. 16, pp. 498–505, Oct. 2006.

[57] I. Campanini, A. Merlo, P. Degola, R. Merletti, G. Vezzosi, and D. Farina, "Effect of electrode location on EMG signal envelope in leg muscles during gait," *J. Electromyogr. Kinesiol.*, vol. 17, pp. 515–526, Aug. 2007.

[58] K. Bouillard, J. Frère, F. Hug, and A. Guével, "Prediction of time-to-exhaustion in the first dorsal interosseous muscle from early changes in surface electromyography parameters," *Muscle Nerve*, vol. 45, no. 6, pp. 835–840, 2012.

[59] T. Bosch, S. E. Mathiassen, B. Visser, M. P. D. Looze, and J. H. van Dieën, "The effect of work pace on workload, motor variability and fatigue during simulated light assembly work," *Ergonomics*, vol. 54, pp. 154–168, Feb. 2011.

[60] R. Bonfiglioli, A. Botter, M. Calabrese, P. Mussoni, F. S. Violante, and R. Merletti, "Surface electromyography features in manual workers affected by carpal tunnel syndrome," *Muscle Nerve*, vol. 45, no. 6, pp. 873–882, 2012.

[61] J. H. Blok, J. P. van Dijk, M. J. Zwarts, and D. F. Stegeman, "Motor unit action potential topography and its use in motor unit number estimation," *Muscle Nerve*, vol. 32, no. 3, pp. 280–291, 2005.

[62] R. B. Beck, M. J. O'Malley, D. F. Stegeman, C. J. Houtman, S. Connolly, and M. J. Zwarts, "Tracking motor unit action potentials in the tibialis anterior during fatigue," *Muscle Nerve*, vol. 32, no. 4, pp. 506–514, 2005.

[63] I. Bazzucchi, P. Sbriccoli, G. Marzattinocci, and F. Felici, "Coactivation of the elbow antagonist muscles is not affected by the speed of movement in isokinetic exercise," *Muscle Nerve*, vol. 33, no. 2, pp. 191–199, 2006.

[64] I. Bazzucchi *et al.*, "Differences in the force/endurance relationship between young and older men," *Eur. J. Appl. Physiol.*, vol. 93, pp. 390–397, Jan. 2005.

[65] I. Bazzucchi, F. Felici, M. Montini, F. Figura, and M. Sacchetti, "Caffeine improves neuromuscular function during maximal dynamic exercise," *Muscle Nerve*, vol. 43, no. 6, pp. 839–844, 2011.

[66] I. Bazzucchi, F. Felici, A. Macaluso, and G. De Vito, "Differences between young and older women in maximal force, force fluctuations, and surface EMG during isometric knee extension and elbow flexion," *Muscle Nerve*, vol. 30, no. 5, pp. 626–635, 2004.

[67] M. Barbero, R. Gatti, L. Lo Conte, F. Macmillan, F. Coutts, and R. Merletti, "Reliability of surface EMG matrix in locating the innervation zone of upper trapezius muscle," *J. Electromyogr. Kinesiol.*, vol. 21, no. 5, pp. 827–833, 2011.

[68] H. J. Hermens and R. Merletti, "SENIAM 1: European activities on surface electromyography," in *Proc. 1st General SENIAM Workshop*, Turin, Italy, Sep. 1996, pp. 1–3.

[69] H. Hermens, G. Hägg, and B. Freriks, "SENIAM 2: European applications on surface electromyography," in *Proc. 2nd General SENIAM Workshop*, Stockholm, Sweden, 1997, pp. 75452–75490.

[70] H. J. Hermens, G. Rau, C. Disselhorst-Klug, and B. Freriks, "SENIAM 3: Surface electromyography application areas and parameters," in *Proc. 3rd General SENIAM (Surface EMG Non Invasive Assessment Muscles) Workshop*, May 1998, pp. 1–3.

[71] H. Hermens and B. Freriks, "SENIAM 4: Future applications of surface electromyography," Roessingh Res. Develop., Enschede, The Netherlands, Tech. Rep., 1999.

[72] H. Hermens and B. Freriks, "SENIAM 5: The state of the art on sensors and sensor placement procedures for surface electromyography: A proposal for sensor placement procedures," Roessingh Res. Develop., Enschede, The Netherlands, Tech. Rep., 1997.

[73] H. Hermens, D. Stegeman, J. Blok, and B. Freriks, "SENIAM 6: State of the art on modelling methods for surface electromyography," Roessingh Res. Develop., Enschede, The Netherlands, Tech. Rep., 1998.

[74] H. J. Hermens, R. Merletti, H. Rix, and B. Freriks, "SENIAM 7: The state of the art on signal processing methods for surface electromyography," Roessingh Res. Develop., Enschede, The Netherlands, Tech. Rep., 1999.

[75] H. J. Hermens *et al.*, "SENIAM 8: European recommendations for surface electromyography," Roessingh Res. Develop., Enschede, The Netherlands, Tech. Rep., 1999.

[76] H. J. Hermens, B. Freriks, C. Disselhorst-Klug, and G. Rau, "Development of recommendations for SEMG sensors and sensor placement procedures," *J. Electromyogr. Kinesiol.*, vol. 10, no. 5, pp. 361–374, 2000.

[77] R. Merletti, A. Botter, A. Troiano, E. Merlo, and M. A. Minetto, "Technology and instrumentation for detection and conditioning of the surface electromyographic signal: State of the art," *Clin. Biomech.*, vol. 24, pp. 122–134, 2009.

[78] B. Freriks and H. J. Hermens, "SENIAM 9: European recommedations for surface electromyography (CDROM)," Roessingh Res. Develop., Enschede, The Netherlands, Tech. Rep., 1999.

[79] J. D. Bronzino, *The Biomedical Engineering Handbook*. Boca Raton, FL, USA: CRC Press, 2006.

[80] J. G. Webster, *Medical Instrumentation: Application and Design*, 4th ed. New York, NY, USA: Wiley, 2009.

[81] E. Criswell, *Cram's Introduction To Surface Electromyography*, 2nd ed. Sudbury, MA, USA: Jones & Bartlett, 2011.

[82] G. Kamen and D. A. Gabriel, *Essentials of Electromyography*. Champaign, IL, USA: Human Kinetics, 2010.

[83] R. Merletti and P. A. Parker, *Electromyography: Physiology, Engineering, and Non-Invasive Applications*. Hoboken, NJ, USA: IEEE Press, 2004.

[84] D. G. E. Robertson, G. E. Caldwell, J. Hamill, G. Kamen, and S. Whittlesey, *Research Methods in Biomechanics*, 2nd ed. Champaign, IL, USA: Human Kinetics, 2014.

[85] R. Merletti, D. Farina, and A. Granata, "Non-invasive assessment of motor unit properties with linear electrode arrays," in *Clinical Neurophysiology: From Receptors to Perception*. Amsterdam, The Netherlands: Elsevier, 1999, pp. 293–300.

[86] R. Merletti, B. Afsharipour, and G. Piervirgili, "High density surface EMG technology," in *Converging Clinical and Engineering Research on Neurorehabilitation*, J. L. Pons, D. Torricelli, and M. Pajaro, Eds. Berlin, Germany: Springer-Verlag, 2013, pp. 1205–1209.

[87] G. Rau and C. Disselhorst-Klug, "Principles of high-spatial-resolution surface EMG (HSR-EMG): Single motor unit detection and application in the diagnosis of neuromuscular disorders," *J. Electromyogr. Kinesiol.*, vol. 7, pp. 233–239, Dec. 1997.

[88] H. Reucher, J. Silny, and G. Rau, "Spatial filtering of noninvasive multielectrode EMG: Part II—Filter performance in theory and modeling," *IEEE Trans. Biomed. Eng.*, vol. BME-34, no. 2, pp. 106–113, Feb. 1987.

[89] H. Reucher, G. Rau, and J. Silny, "Spatial filtering of noninvasive multielectrode EMG: Part I—Introduction to measuring technique and applications," *IEEE Trans. Biomed. Eng.*, vol. BME-34, no. 2, pp. 98–105, Feb. 1987.

[90] N. Östlund, J. Yu, K. Roeleveld, and J. S. Karlsson, "Adaptive spatial filtering of multichannel surface electromyogram signals," *Med. Biol. Eng. Comput.*, vol. 42, pp. 825–831, Nov. 2004.

[91] D. Farina, L. Mesin, S. Martina, and R. Merletti, "Comparison of spatial filter selectivity in surface myoelectric signal detection: Influence of the volume conductor model," *Med. Biol. Eng. Comput.*, vol. 42, pp. 114–120, Jan. 2004.
[92] J. Bahm, L. Meinecke, V. Brandenbusch, G. Rau, and C. Disselhorst-Klug, "High spatial resolution electromyography and video-assisted movement analysis in children with obstetric brachial plexus palsy," *Hand Clin.*, vol. 19, no. 3, pp. 393–399, 2003.
[93] C. Disselhorst-Klug, J. Silny, and G. Rau, "Improvement of spatial resolution in surface-EMG: A theoretical and experimental comparison of different spatial filters," *IEEE Trans. Biomed. Eng.*, vol. 44, no. 7, pp. 567–574, Jul. 1997.
[94] E. Schulte, D. Farina, G. Rau, R. Merletti, and C. Disselhorst-Klug, "Single motor unit analysis from spatially filtered surface electromyogram signals. Part 2: Conduction velocity estimation," *Med. Biol. Eng. Comput.*, vol. 41, pp. 338–345, May 2003.
[95] D. Farina, E. Schulte, R. Merletti, G. Rau, and C. Disselhorst-Klug, "Single motor unit analysis from spatially filtered surface electromyogram signals. Part I: Spatial selectivity," *Med. Biol. Eng. Comput.*, vol. 41, pp. 330–337, May 2003.
[96] D. Farina, E. Fortunato, and R. Merletti, "Noninvasive estimation of motor unit conduction velocity distribution using linear electrode arrays," *IEEE Trans. Biomed. Eng.*, vol. 47, no. 3, pp. 380–388, Mar. 2000.
[97] R. Merletti, A. Rainoldi, and D. Farina, "Surface electromyography for noninvasive characterization of muscle," *Exerc. Sport Sci. Rev.*, vol. 29, no. 1, pp. 20–25, 2001.

Jeff Kilby received the M.Eng. (Hons.) degree in signal processing from the Auckland University of Technology, New Zealand. He is currently a Senior Lecturer with the School of Engineering, Auckland University of Technology, New Zealand. Main research topic is in the field of biomedical signal processing and devices, other research interests are LabVIEW applications, micro-controller applications, and wireless sensor network applications.

Krishnamachar Prasad received the B.E. degree from Bangalore University, India, the M.Tech. degree from IIT Madras, India, and the Ph.D. degree from the University of Western Australia, all in electrical engineering. He is currently a Professor with the School of Engineering, Auckland University of Technology, New Zealand. His research interests are reliability studies of novel interconnects in conventional, 3D integrated circuits, solid state, and biomedical devices.

Grant Mawston is currently a Senior Lecturer with the Department of Physiotherapy and a Co-Director of the Health and Rehabilitation Research Institute, Auckland University of Technology, New Zealand. His research interests are in exercise-based rehabilitation and neuromuscular control of the lumbar spine.

Design of New Multi-channel Electrodes for Surface Electromyography Signals for Signal-Processing

J. Kilby, *Member, IEEE,* K. Prasad, *Senior Member, IEEE* and G. Mawston

***Abstract*—This paper covers the design aspects of a new multi-channel electrode for the acquisition of surface electromyography signals from a selected muscle. The new multi-channel electrode has 11 pins where the monopolar signals produced will be configured in a software either as *Linear* array or *Laplacian* configuration. The design specification of the pre-amplifier ideally was to have a voltage gain of 500 with bandpass filtering of 5 Hz - 1 kHz. The final design of the pre-amplifier circuit using an INA 118 instrumentation amplifier was built and tested to give values for voltage gain of 484 with bandpass filtering of 6.8 Hz - 1.02 kHz. The software configuration that gives clearer and more defined signals in terms of motor unit action potentials for future signal processing is the *Laplacian* rather than *Linear* array.**

I. Introduction

Surface electromyography or sEMG is the term used for the study of *'bio-electrical signals'* or *'bio-signals'* from muscle activities, by means of sensory electrodes being placed on the surface of the skin [1, 2].

sEMG recordings provide a safe, easy and non-invasive method that can give objective measurement of muscle activities. Another method of EMG uses needle or fine-wire electrodes penetrating into the muscle approximately 2.5 to 5 mm deep [3]. Those signals focus on a single muscle motor unit and they are used for targeting small muscles. The advantages of needle or 'indwelling' EMG are its selectivity and being still able to detect other distant muscle activities or 'crosstalk' [3]. However, indwelling EMG is an invasive method, which can cause stress and pain to the subject involved.

It is not always necessary to penetrate the skin and record from single motor units to obtain useful and meaningful information regarding muscles. With the use of multiple channel surface electrodes [4-10], it is possible to observe different aspects of activities from a group of muscle fibres or compounded motor unit action potential. That has become the focus of many researchers in terms of their studies in the development of new multi-channel electrode design, along with advanced signal-processing techniques.

By increasing the number of electrodes placed over the recording sites, the device is referred to as *'multi-channel electrodes'*. In this way, a montage of information concerning the distribution of the EMG activity over a muscle or the timing relationships between different muscles become accessible. In principle, there is no hindrance to increasing the number of surface electrodes over the muscle, the number of channels, or arranging complex montages from different electrodes for each channel. Both of the basic configurations of monopolar and bipolar, along with double differential which are used with a more complex electrode configurations, form a multi-channel electrode.

Typical types of the multi-channel configurations are: (a) Linear array, (b) High-spatial-resolution surface EMG (HSR-sEMG) and (c) High density-sEMG (HD-sEMG).

Connecting several recording electrodes placed in-line with each other results in a Linear array recording of sEMG signals [11]. The basic three configurations are: (a) monopolar detection (b) bipolar or single differential and (c) double differential [11].

HSR-sEMG and HD-sEMG electrodes are a logical extension of Linear array, consisting of a two-dimensional grid with an arbitrary number of electrodes [12, 13]. A combination of activities of one electrode with one or several surrounding electrodes close to the muscle, results in 'higher-order' derivatives [13]. The effect is a 'spatial (high-pass) filtering', producing a narrowing of the spatial view of the sEMG signal [4, 6-8, 13-17]. A more complex spatial filtering is normal double differentiating filter (NDD-filter) referred to as *'Laplacian configuration'*, where a central electrode is connected with four surrounding electrodes [7, 8].

II. Design of New Multi-Channel Electrodes

There are a number of aspects that need to be considered when designing electronic hardware of sEMG electrodes. The most important one is selecting the possible range of voltage and frequency values when detecting sEMG signals. Fig. 1 shows the range of frequencies of sEMG sits in terms of other bio-signals that can be found in the human body [18], where for sEMG, muscle signals sits between 5 Hz - 2 kHz.

The initial specification for each electrode was to have the sEMG signal pre-amplified to obtain a voltage gain of 500 or 53.97 dB (≈54 dB) with a band-pass filter of 5 Hz - 1 kHz [18].

There are standards and protocols for reporting the sEMG

This work was supported by a Contestable Grant from the School of Engineering and Ethics Approval at Auckland University of Technology.

J. Kilby is with the Signals and Control Research Group and the Department of Electrical and Electronic Engineering at Auckland University of Technology, Auckland, New Zealand (e-mail: jkilby@aut.ac.nz).

K. Prasad is with the Department of Electrical and Electronic Engineering at Auckland University of Technology, Auckland, New Zealand (e-mail: kprasad@aut.ac.nz).

G. Mawston is with the Health and Rehabilitation Research Institute at Auckland University of Technology, Auckland, New Zealand (e-mail: gmawston@aut.ac.nz).

978-1-4577-0220-4/16/$31.00 ©2016 IEEE

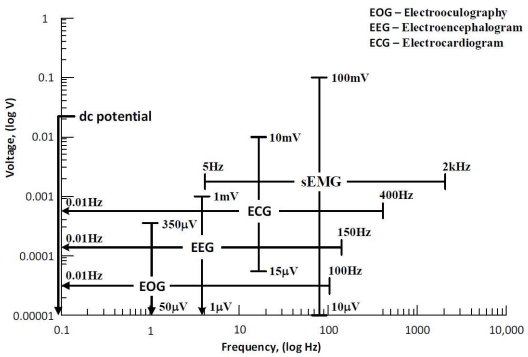

Figure 1. A revised graph showing the range of frequencies of different bio-signals found in human body [18].

data, which had been consolidated over the years by the Journal of Electromyography and Kinesiology [19] usually referred to as the *golden rule*. The essential factors involved for the hardware are the:

- Electrodes
- Amplification (or Gain)
- Filtering

A. Electrodes

The design of a new multi-channel electrodes presented in this paper consists of 11 electrode pins collecting monopolar sEMG signals from the vastus lateralis muscle performing isometric static contraction with detailed testing protocols. These signals will be further processed online for both the Linear and Laplacian configuration as shown in Fig. 2.

The selected electrode material has gold-plated pins with a diameter of 4.8 mm (3/16 inches) with an inter-electrode distance (IED) of 10 mm. Fig. 3 shows the general schematic circuit for the new preamplifier circuit for each of the 11 monopolar signals.

B. Amplification

The three possible instrumentation amplifiers (in-amps) considered for the design were the Texas Instruments INA118, INA128 and INA333, which are suitable for

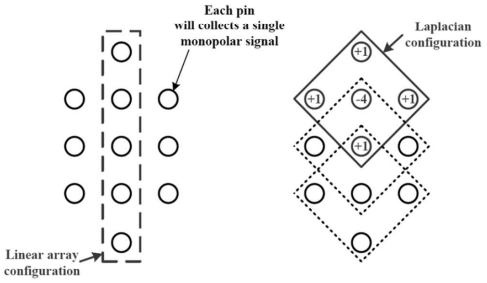

Figure 2. The configuration of the 11 electrode pins: left figure shows the five pins that will be used for a Linear array and the right figure shows the pins that make up the three channels of Laplacian configuration.

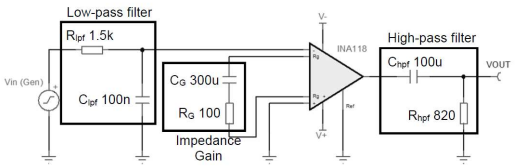

Figure 3. Passive components used to make a pre-amplifier circuit for one monopolar channel in the new multi-multichannel electrode.

biomedical devices. Each of the in-amps were simulated using TINA-TI™ (V9, DesignSoft Inc.) a SPICE-Based Analogue Simulation Program. From the simulated gain-frequency plots (without any filtering) with the voltage gain set to 500, the INA118 was found to be the most suitable out of the three possible in-amps investigated, due to following points:

- INA118 showed an upper cut-off frequency of 13.82 kHz at -3 dB, which covers the frequencies up to 1 kHz and hence met the requirements of the design specifications. INA128 also met the specification as it showed an upper cut-off frequency of 47.32 kHz, but INA333 did not meet the specifications, as it had an upper cut-off frequency of 770 Hz, which is less than the requirements of 1 kHz.
- INA118 has a low quiescent current and requires lower supply voltage than INA128, which is ideal for a stand-alone battery-powered operated device to limit any electrical noises from the mains and surroundings.

C. Filtering

To achieve the voltage impedance gain of 500 of the amplifier and signals bandpass filtered from of 5 Hz - 1 kHz, TINA-TI software were used in order to select components for the filters with the INA118 in-amp. The following steps taken were for this purpose:

- Setting the gain of the amplifier without any filtering. This was achieved by placing an initial resistor of 100 Ω giving a gain of 501 or 53.99 dB (≈54 dB). This was replaced with a 100 Ω resistor in series with a capacitance of 300 µF between gain setting pins of the amplifier. This is to ensure that the any DC component in the signal was not amplified and to prevent saturation of the output signal. The 300 µF capacitor and the 100 Ω resistor creates a high-pass filter with a cut-off frequency of 5.93 Hz.
- The low-pass filter in Fig. 3, is a passive *'first-order'* or *'one pole'* RC filter. The filter was placed before the amplifier with component values of 1.5 kΩ resistor and a 100 µF capacitor, which gives a cut-off frequency of 1.06 kHz. A small value for the capacitor ensures that the filter has little or no-loading effect on the amplifier.
- The passive high-pass filter was designed using component values of 820 Ω resistor and a capacitor of 100 µF giving a cut-off frequency of 1.94 Hz.

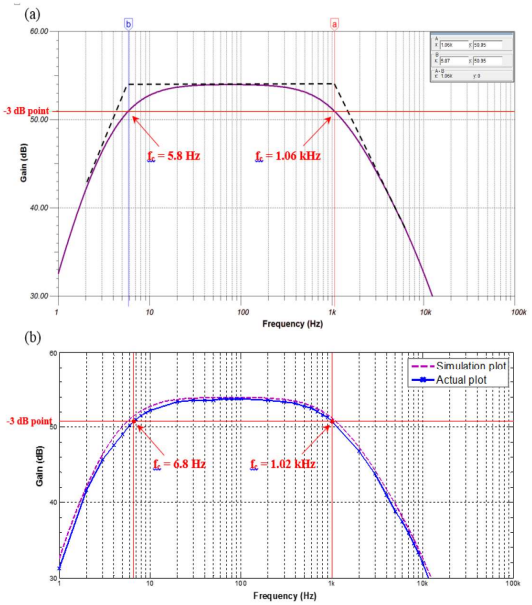

Figure 4. Plot (a) shows the simulation gain-frequency response curve for pre-amplifier circuit in Fig. 3, the gain is 498 (53.95 dB), lower cut-off frequency is 5.8 Hz and upper cut-off frequency is 1.06 kHz. Plot (b) shows gain-frequency response for both simulation and actual values. The actual values have a maximum gain of 484 (53.7 dB) with a lower cut-off frequency of 6.8 Hz and an upper cut-off frequency of 1.02 kHz.

Taking into account the high-pass filtering of the impedance gain the circuit's overall high-pass filter cut-off frequency is 5.8 Hz with a better roll-rate of +40 dB as shown in Fig. 4(a). Using a small value for the resistor ensures that the filter has little or no-loading effect on the data acquisition card.

III. Electrode Pre-amplifier Circuit

The frequency response (both simulated and actual) of the circuit in Fig. 3 is shown in Fig. 4. The actual values were found by using a recording a range of readings between 1 to 100 kHz using a Tektronix AFG3000 Arbitrary/Function Generator for the input signal and a Tektronix TDS2002 Dual Channel Digital Storage Oscilloscope for measuring both the input signal and output signals at known frequencies. These recorded measurements were used to work out the voltage gain and plotted against the simulated values, as shown in Fig. 4(b). The input signal was set to 10 mV peak-to-peak to ensure that the output would not be saturated.

Table 1 shows the simulation and actual values obtained from Fig. 4 for the gain, lower cut-off and upper cut-off for the circuit shown in Fig. 3. The values showed that they were close to each other, and that the new designed pre-amplifier circuit adequately met the specification set out for the circuit. The actual values were a gain of 484 (53.7 dB) and a band-pass filter from 6.8 Hz to 1.02 kHz.

The next step was to build the new 11-channel electrode

TABLE I. Simulation and Actual Values for Gain, Upper Cut-off and Lower Cut-off Frequencies for the Pre-amplifier Circuit Shown in Fig. 3

Value	Simulation	Actual
Gain	498 (53.98 dB)	484 (53.7 dB)
Low cut-off frequency	5.8 Hz	6.8 Hz
High cut-off frequency	1.06 kHz	1.02 kHz

using high precision passive components for each of the pre-amplifier circuit. The schematics and PCBs were designed using Altium Design 13 for the new multi-channel electrode and the battery power supply unit. The electrode casing and power supply cover were drawn in SolidWorks 2012 and produced by using the 3D printing. The completed electrode is shown in Fig. 5, where the dimensions of the electrode casing are 88.5 mm (length) by 42 mm (width) and 14.5 mm (height), and the inter-electrode distance is 10 mm.

The stand-alone battery power supply unit is designed to supply ± 6 V to each pre-amplifier circuit from two standard PP3 9 V batteries. The stand-alone battery supply unit eliminates any electrical noise and interference, which is more apparent when using a power supply from the mains.

The new multi-channel electrode was then tested by acquiring sEMG signals from the vastus lateralis muscle of the quadriceps from twenty healthy participants aged between 18 and 35 years old. This was carried out under ethics approval from Auckland University of Technology Ethics Committee. The protocols require the participant to be seated and secured on a testing chair, performing an isometric contraction of the leg at 50 % of their Maximum Voluntary Contraction (MVC).

IV. Results and Discussions

The signals collected were displayed in real time and stored on the computer for further analysis at a later date. The signals were displayed in National Instruments LabVIEW 2012, showing all the monopolar signals at the same time as the single Linear array and three channel Laplacian electrode signals that are configured in the software.

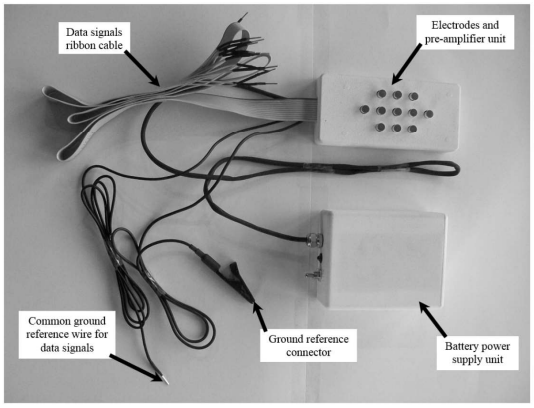

Figure 5. The new sEMG multi-channel electrode with separate battery power supply unit.

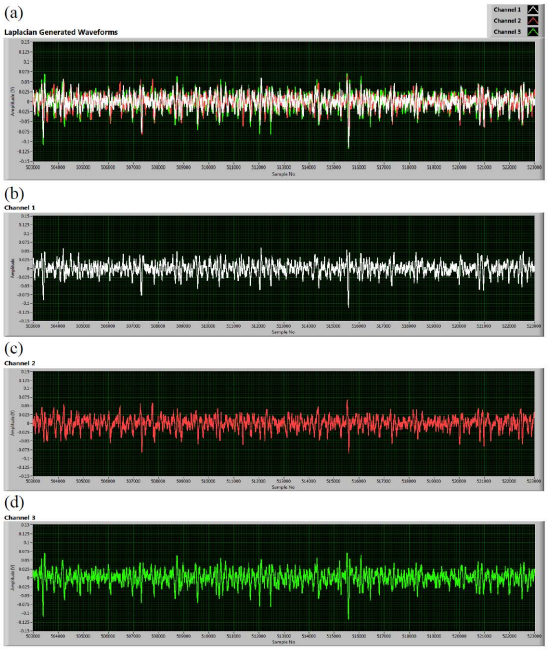

Figure 6 The software-generated waveforms for the Laplacian configuration from the monopolar signals for a 2 second period from a participant performing 50% of their MVC. Plot (a) shows all three channel signals. Plots (b) to (d) shows channel 1 to channel 3 plotted separately.

The sEMG signals generated from the monopolar signals to form the three-channel Laplacian configuration are shown in Fig. 6. These signals configured by the Laplacian were superior to the Linear array as they show better definitions which is similar to motor unit action potential of muscle fibres obtained by needle electrodes.

The next step for this research is to use signal-processing techniques to extract useful features for classification purposes of both the Linear array and Laplacian configurations generated signals. The standard signal processing techniques used will be the Fourier Transform and Short Time Fourier Transform with advanced ones such as Wavelet Transform, Independent and Principal Component Analysis.

V. Conclusion

A new design for a multi-channel electrode for sEMG is described to collect monopolar signals, which are then configured by a software as either Linear array or Laplacian configuration. The specification of the new multi-channel electrode had a voltage gain of 484 and a bandpass filtered 6.8 Hz - 1.02 kHz which was subsequently built and used to acquire sEMG signals from participants performing 50% MVC. Signals by Laplacian configurations showed better definitions than Linear Array. Further work is required to analyze these generated signals, using standard and advance signal processing techniques to extract meaningful features for classification purposes.

References

[1] E. Criswell, *Cram's Introduction to Surface Electromyography*, 2nd ed. Sudbury, Mass.: Jones and Bartlett, 2011.

[2] R. Merletti and P. A. Parker, *Electromyography: Physiology, Engineering, and Noninvasive Applications*. Hoboken, New Jersey: IEEE Press and John Wiley & Sons, 2004.

[3] J. D. Bronzino, *The Biomedical Engineering Handbook*. 6000 Broken Sound Parkway NW, Suite 300: CRC Press, 2006.

[4] D. Farina, E. Schulte, R. Merletti, G. Rau, and C. Disselhorst-Klug, "Single motor unit analysis from spatially filtered surface electromyogram signals. Part I: Spatial selectivity," *Medical and Biological Engineering and Computing,* vol. 41, pp. 330-337, 2003/05/01 2003.

[5] B. U. Kleine, J. P. van Dijk, B. G. Lapatki, M. J. Zwarts, and D. F. Stegeman, "Using two-dimensional spatial information in decomposition of surface EMG signals," *Journal of Electromyography and Kinesiology,* vol. 17, pp. 535-548, 2007.

[6] N. Östlund, J. Yu, K. Roeleveld, and J. S. Karlsson, "Adaptive spatial filtering of multichannel surface electromyogram signals," *Medical and Biological Engineering and Computing,* vol. 42, pp. 825-831, 2004/11/01 2004.

[7] H. Reucher, G. Rau, and J. Silny, "Spatial Filtering of Noninvasive Multielectrode EMG: Part I-Introduction to Measuring Technique and Applications," *Biomedical Engineering, IEEE Transactions on,* vol. BME-34, pp. 98-105, 1987.

[8] H. Reucher, J. Silny, and G. Rau, "Spatial Filtering of Noninvasive Multielectrode EMG: Part II-Filter Performance in Theory and Modeling," *Biomedical Engineering, IEEE Transactions on,* vol. BME-34, pp. 106-113, 1987.

[9] J. Rodriguez-Falces, F. Negro, M. Gonzalez-Izal, and D. Farina, "Spatial distribution of surface action potentials generated by individual motor units in the human biceps brachii muscle," *Journal of Electromyography and Kinesiology,* vol. 23, pp. 766-777, 8// 2013.

[10] K. Watanabe, M. Kouzaki, R. Merletti, M. Fujibayashi, and T. Moritani, "Spatial EMG potential distribution pattern of vastus lateralis muscle during isometric knee extension in young and elderly men," *Journal of Electromyography and Kinesiology,* vol. 22, pp. 74-79, 2012.

[11] R. Merletti, D. Farina, and M. Gazzoni, "The linear electrode array: a useful tool with many applications," *Journal of Electromyography and Kinesiology,* vol. 13, pp. 37-47, 2003.

[12] M. J. Zwarts and D. F. Stegeman, "Multichannel surface EMG: Basic aspects and clinical utility," *Muscle & Nerve,* vol. 28, pp. 1-17, 2003.

[13] G. Rau and C. Disselhorst-Klug, "Principles of high-spatial-resolution surface EMG (HSR-EMG): single motor unit detection and application in the diagnosis of neuromuscular disorders," *Journal of Electromyography and Kinesiology,* vol. 7, pp. 233-239, 12// 1997.

[14] D. Farina, L. Mesin, S. Martina, and R. Merletti, "Comparison of spatial filter selectivity in surface myoelectric signal detection: Influence of the volume conductor model," *Medical and Biological Engineering and Computing,* vol. 42, pp. 114-120, 2004/01/01 2004.

[15] J. Bahm, L. Meinecke, V. Brandenbusch, G. Rau, and C. Disselhorst-Klug, "High spatial resolution electromyography and video-assisted movement analysis in children with obstetric brachial plexus palsy," *Hand Clinics,* vol. 19, pp. 393-399, 2003.

[16] C. Disselhorst-Klug, J. Silny, and G. Rau, "Improvement of spatial resolution in surface-EMG: a theoretical and experimental comparison of different spatial filters," *Biomedical Engineering, IEEE Transactions on,* vol. 44, pp. 567-574, 1997.

[17] E. Schulte, D. Farina, G. Rau, R. Merletti, and C. Disselhorst-Klug, "Single motor unit analysis from spatially filtered surface electromyogram signals. Part 2: Conduction velocity estimation," *Medical and Biological Engineering and Computing,* vol. 41, pp. 338-345, 2003/05/01 2003.

[18] J. G. Webster, *Medical Instrumentation: Application and Design*, 4th ed. USA: Wiley, 2009.

[19] "Standards for Reporting EMG Data," *Journal of Electromyography and Kinesiology,* vol. 24, pp. I-II, February 2014.

References

1. Disselhorst-Klug, C., *Non-invasive Diagnosis of Neuromuscular Disorders by High-Spatial-Resolution-EMG*, in *EMG Methods for Evaluating Muscle and Nerve Function*, M. Schwartz, Editor. 2012, InTech: Rijeka, Croatia. p. 227-240.
2. Yousefi, J. and A. Hamilton-Wright, *Characterizing EMG data using machine-learning tools.* Computers in Biology and Medicine, 2014. **51**: p. 1-13.
3. Criswell, E., *Cram's Introduction to Surface Electromyography*. 2nd ed. 2011, Sudbury, Mass.: Jones and Bartlett.
4. Basmajian, J.V. and C.J. De Luca, *Muscles Alive: Their Functions Revealed by Electromyography*. 5th ed. 1985, Baltimore: Williams & Wilkins.
5. Borelli, G.A., *On the Movement of Animals ; translated by Paul Maquet*. 1989: Berlin ; New York : Springer-Verlag, c1989.
6. Piccolino, M. and M. Bresadola, *Drawing a spark from darkness: John Walsh and electric fish.* Trends in Neurosciences, 2002. **25**(1): p. 51-57.
7. Galvani, L. and t.b. Green, *Commentary on the Effect of Electricity of Muscular Motion*. 1953, Cambridge, MA.
8. Finger, S. and N.J. Wade, *The Neuroscience of Helmholtz and the Theories of Johannes Müller Part 1: Nerve Cell Structure, Vitalism, and the Nerve Impulse.* Journal of the History of the Neurosciences, 2002. **11**(2): p. 136-155.
9. Pratt, F., *The All or None Principle in Graded Response of Skeletal Muscle.* AM J Physiol, 1917. **44**: p. 517-542.
10. Perl, E., *The 1944 Nobel Prize to Erlanger and Gasser.* FASEB journal : official publication of the Federation of American Societies for Experimental Biology, 1994. **8**(10): p. 782.
11. Adrian, E.D. and D.W. Bronk, *The discharge of impulses in motor nerve fibres: Part II. The frequency of discharge in reflex and voluntary contractions.* The Journal of physiology, 1929. **67**(2): p. i3.
12. Basmajian, J. and R. Blumenstein, *Biofeedback Principles and Practice for Clinicians*. 3rd ed. 1989, Baltimore, MD: Williams & Wilkins.
13. Green, E., et al., *Feedback Techniques for Deep Relaxation.* Psychophysiology, 1969. **6**: p. 371-377.
14. Budzynski, T., et al., *EMG biofeedback and tension study.* Psychosomatic Med, 1973. **35**: p. 484-496.
15. Hardyck, C., L. Petrincovich, and D. Ellsworth, *Feedback of speech muscle activity during silent reading: rapid extension.* Science, 1966. **154**: p. 1467-1468.
16. Booker, H., R. Rubow, and P. Coleman, *Simplified feedback in neuromuscular retraining: an automated approach using EMG signals.* Arch Phys Med, 1969. **50**: p. 621-625.
17. Johnson, H. and W. Garton, *Muscle re-education in hemiplegia by use of electromyographic device.* Arch Phys Med, 1973. **54**: p. 320-332.
18. Wolf, S. and J. Basmajian, *Assessment of Paraspinal Electromyographic Activity in Normal Subjects and Chronic Back Pain Patients Using a Muscle Biofeedback*

Device. International Series on Biomechanics, ed. E. Asmussen and K. Jorgensen. 1978, Baltimore, MD: University Press.

19. Wolf, S.L., M. Nacht, and J.L. Kelly, *EMG feedback training during dynamic movement for low back pain patients.* Behavior Therapy, 1982. **13**(4): p. 395-406.
20. De Luca, C.J., *Myoelectric Manifestations of Localized Muscular Fatigue in Humans.* CRC Crit Rev Biomed Eng, 1984. **11**: p. 251.
21. Davis, J.F. and U. McGill, *Manual of Surface Electromyography*. WADC technical report59-145. 1959, Wright-Patterson Air Force Base, Ohio: Aerospace Medical Laboratory, Wright Air Development Center, Air Research and Development Command, U.S. Air Force. viii, 122 p.
22. Basmajian, J.V.B.R., *Electrode placement in EMG biofeedback*, ed. R. Blumenstein. 1980, Baltimore: Williams & Wilkins.
23. Hermens, H.J., et al., *Development of recommendations for SEMG sensors and sensor placement procedures.* Journal of Electromyography and Kinesiology, 2000. **10**(5): p. 361-374.
24. Barbero, M., R. Merletti, and A. Rainoldi, *Atlas of Muscle Innervation Zones: Understanding Surface Electromyography and Its Applications*. 2012, Italy: Springer.
25. Merletti, R. and P.A. Parker, *Electromyography: Physiology, Engineering, and Noninvasive Applications*. 2004, Hoboken, New Jersey: IEEE Press and John Wiley & Sons. 259-304.
26. Merletti, R., et al., *Technology and instrumentation for detection and conditioning of the surface electromyographic signal: State of the art.* Clinical Biomechanics, 2009. **24**(2): p. 122-134.
27. Blok, J.H., et al., *A high-density multichannel surface electromyography system for the characterization of single motor units.* Review of Scientific Instruments, 2002. **73**(4): p. 1887-1897.
28. Disselhorst-Klug, C., et al., *Non-invasive detection of the single motor unit action potential by averaging the spatial potential distribution triggered on a spatially filtered motor unit action potential.* Journal of Electromyography and Kinesiology, 1999. **9**(1): p. 67-72.
29. Disselhorst-Klug, C., J. Silny, and G. Rau, *Improvement of spatial resolution in surface-EMG: a theoretical and experimental comparison of different spatial filters.* Biomedical Engineering, IEEE Transactions on, 1997. **44**(7): p. 567-574.
30. Metting van Rijn, A.C., A. Peper, and C.A. Grimbergen, *High-quality recording of bioelectric events. Part 1. Interference reduction, theory and practice.* Med Biol Eng Comput, 1990. **28**(5): p. 389-97.
31. Metting van Rijn, A.C., A. Peper, and C.A. Grimbergen, *High-quality recording of bioelectric events. Part 2. Low-noise, low-power multichannel amplifier design.* Med Biol Eng Comput, 1991. **29**(4): p. 433-40.
32. Östlund, N., et al., *Adaptive spatial filtering of multichannel surface electromyogram signals.* Medical and Biological Engineering and Computing, 2004. **42**(6): p. 825-831.
33. Pozzo, M., et al., *Sixty-four channel wearable acquisition system for long-term surface electromyogram recording with electrode arrays.* Medical and Biological Engineering and Computing, 2004. **42**(4): p. 455-466.

34. Reucher, H., G. Rau, and J. Silny, *Spatial Filtering of Noninvasive Multielectrode EMG: Part I-Introduction to Measuring Technique and Applications.* Biomedical Engineering, IEEE Transactions on, 1987. **BME-34**(2): p. 98-105.

35. Reucher, H., J. Silny, and G. Rau, *Spatial Filtering of Noninvasive Multielectrode EMG: Part II-Filter Performance in Theory and Modeling.* Biomedical Engineering, IEEE Transactions on, 1987. **BME-34**(2): p. 106-113.

36. Zwarts, M.J. and D.F. Stegeman, *Multichannel surface EMG: Basic Aspects and Clinical utility.* Muscle & Nerve, 2003. **28**(1): p. 1-17.

37. Hogrel, J.Y., *Use of surface EMG for studying motor unit recruitment during isometric linear force ramp.* Journal of Electromyography and Kinesiology, 2003. **13**(5): p. 417-423.

38. Hogrel, J.Y., *Clinical applications of surface electromyography in neuromuscular disorders.* Neurophysiologie Clinique, 2005. **35**(2-3): p. 59-71.

39. Hogrel, J.Y., I. Ledoux, and J. Duchêne, *Reliability of muscle fibre conduction velocity distribution estimation from surface EMG.* Biomedical Signal Processing and Control, 2008. **3**(2): p. 118-125.

40. Olson, W.H., *Basic Concepts of Medical Instrumentation*, in *Medical Instrumentation Application and Design*, J.G. Webster, Editor. 1992, Houghton Mifflin Company: Boston, MA, USA. p. 1-55.

41. Marieb, E.N., *Essentials of Human Anatomy & Physiology*. 8th ed. 2006, Benjamin Cummings, San Francisco: Pearson Benjamin Cummings.

42. Netter, F.H., J.P. Iannotti, and R.D. Parker, *The Netter Collection of Medical Illustrations: Musculoskeletal System, Volume 6, Part III - Biology and Systemic Diseases*. 2nd ed. 2013, Philadelphia, PA: Saunders.

43. Widmaier, E.P.R.H., *Vander's human physiology :the mechanisms of body function*. 11th ed, ed. H. Raff. 2008, Boston: McGraw-Hill Higher Education.

44. Kamen, G. and D.A. Gabriel, *Essentials of Electromyography*. 2010, USA: Human Kinetics.

45. Bernstein, J., *Musculoskeletal medicine*. 1st ed, ed. J. Bernstein. 2003, Rosemont, Ill.: American Academy of Orthopaedic Surgeons.

46. Bullock, J., J. Boyle, and M.B. Wang, *Physiology*. 3rd ed. 1995, Philadelphia: Williams & Wilkins.

47. Chaffin, D.B., *Localized Muscle Fatigue - Definition and Measurement.* Journal of Occupational Medicine Article author, 1973. **15**(4): p. 346-354.

48. Kilby, J., K. Prasad, and G.A. Mawston, *Multi-Channel Surface Electromyography Electrodes: A Review.* IEEE Sensors Journal, 2016(14): p. 5510-5519.

49. Garfield, E., *Journal impact factor: a brief review.* CMAJ: Canadian Medical Association Journal, 1999. **161**(8): p. 979-980.

50. Smith, E.R., *The journal impact factor.* The Canadian Journal of Cardiology, 2006. **22**(9): p. 787-788.

51. Vucovich, L.A., J. Blaine Baker, and J.T. Smith, *Analyzing the impact of an author's publications.* Journal of the Medical Library Association : JMLA, 2008. **96**(1): p. 63-66.

52. Zwarts, M.J., G. Drost, and D.F. Stegeman, *Recent progress in the diagnostic use of surface EMG for neurological diseases.* Journal of Electromyography and Kinesiology, 2000. **10**(5): p. 287-291.

53. Merletti, R., D. Farina, and M. Gazzoni, *The linear electrode array: a useful tool with many applications.* Journal of Electromyography and Kinesiology, 2003. **13**(1): p. 37-47.

54. Drost, G., et al., *Clinical applications of high-density surface EMG: A systematic review.* Journal of Electromyography and Kinesiology, 2006. **16**(6): p. 586-602.

55. Felici, F., *Neuromuscular responses to exercise investigated through surface EMG.* Journal of Electromyography and Kinesiology, 2006. **16**(6): p. 578-585.

56. Falla, D., et al., *Repeatability of surface EMG variables in the sternocleidomastoid and anterior scalene muscles.* European Journal of Applied Physiology, 2002. **87**(6): p. 542-549.

57. Farina, D., et al., *Standardising surface electromyogram recordings for assessment of activity and fatigue in the human upper trapezius muscle.* European Journal of Applied Physiology, 2002. **86**(6): p. 469-478.

58. Bazzucchi, I., et al., *Differences in the force/endurance relationship between young and older men.* European Journal of Applied Physiology, 2005. **93**(4): p. 390-397.

59. Holtermann, A., et al., *Changes in agonist EMG activation level during MVC cannot explain early strength improvement.* European Journal of Applied Physiology, 2005. **94**(5-6): p. 593-601.

60. Hummel, A., et al., *Relationship between perceived exertion and mean power frequency of the EMG signal from the upper trapezius muscle during isometric shoulder elevation.* European Journal of Applied Physiology, 2005. **95**(4): p. 321-326.

61. Schulte, E., et al., *Upper trapezius muscle conduction velocity during fatigue in subjects with and without work-related muscular disorders: a non-invasive high spatial resolution approach.* European Journal of Applied Physiology, 2006. **96**(2): p. 194-202.

62. Klaver-Król, E.G., et al., *Distribution of motor unit potential velocities in short static and prolonged dynamic contractions at low forces: use of the within-subject's skewness and standard deviation variables.* European Journal of Applied Physiology, 2007. **101**(5): p. 647-658.

63. Mulder, E.R., et al., *Characteristics of fast voluntary and electrically evoked isometric knee extensions during 56 days of bed rest with and without exercise countermeasure.* European Journal of Applied Physiology, 2008. **103**(4): p. 431-440.

64. Rainoldi, A., M. Gazzoni, and R. Casale, *Surface EMG signal alterations in Carpal Tunnel syndrome: a pilot study.* European Journal of Applied Physiology, 2008. **103**(2): p. 233-242.

65. Samani, A., et al., *Active biofeedback changes the spatial distribution of upper trapezius muscle activity during computer work.* European Journal of Applied Physiology, 2010. **110**(2): p. 415-423.

66. Sbriccoli, P., et al., *Neuromuscular control adaptations in elite athletes: the case of top level karateka.* European Journal of Applied Physiology, 2010. **108**(6): p. 1269-1280.

67. Piitulainen, H., et al., *Muscle fiber conduction velocity is more affected after eccentric than concentric exercise.* European Journal of Applied Physiology, 2011. **111**(2): p. 261-273.

68. Schmitz, J.P.J., et al., *Unchanged muscle fiber conduction velocity relates to mild acidosis during exhaustive bicycling.* European Journal of Applied Physiology, 2012. **112**(5): p. 1593-1602.

69. Gallina, A., R. Merletti, and M. Gazzoni, *Uneven spatial distribution of surface EMG: what does it mean?* European Journal of Applied Physiology, 2013. **113**(4): p. 887-894.

70. Rainoldi, A., et al., *Geometrical factors in surface EMG of the vastus medialis and lateralis muscles.* Journal of Electromyography and Kinesiology, 2000. **10**(5): p. 327-336.

71. Farina, D., M. Gazzoni, and R. Merletti, *Assessment of low back muscle fatigue by surface EMG signal analysis: methodological aspects.* Journal of Electromyography and Kinesiology, 2003. **13**(4): p. 319-332.

72. Cescon, C., et al., *Non-invasive characterization of single motor unit electromyographic and mechanomyographic activities in the biceps brachii muscle.* Journal of Electromyography and Kinesiology, 2006. **16**(1): p. 17-24.

73. Castroflorio, T., et al., *Reproducibility of surface EMG variables in isometric sub-maximal contractions of jaw elevator muscles.* Journal of Electromyography and Kinesiology, 2006. **16**(5): p. 498-505.

74. Campanini, I., et al., *Effect of electrode location on EMG signal envelope in leg muscles during gait.* Journal of Electromyography and Kinesiology, 2007. **17**(4): p. 515-526.

75. Farina, D., et al., *Correlation of average muscle fiber conduction velocity measured during cycling exercise with myosin heavy chain composition, lactate threshold, and VO2max.* Journal of Electromyography and Kinesiology, 2007. **17**(4): p. 393-400.

76. Kleine, B.U., et al., *Using two-dimensional spatial information in decomposition of surface EMG signals.* Journal of Electromyography and Kinesiology, 2007. **17**(5): p. 535-548.

77. Gerdle, B., et al., *Firing rate and conduction velocity of single motor units in the trapezius muscle in fibromyalgia patients and healthy controls.* Journal of Electromyography and Kinesiology, 2008. **18**(5): p. 707-716.

78. Kleine, B.U., et al., *Inter-operator agreement in decomposition of motor unit firings from high-density surface EMG.* Journal of Electromyography and Kinesiology, 2008. **18**(4): p. 652-661.

79. Maathuis, E.M., et al., *Motor unit tracking with high-density surface EMG.* Journal of Electromyography and Kinesiology, 2008. **18**(6): p. 920-930.

80. Merletti, R., A. Holobar, and D. Farina, *Analysis of motor units with high-density surface electromyography.* Journal of Electromyography and Kinesiology, 2008. **18**(6): p. 879-890.

81. Rainoldi, A., et al., *Myoelectric manifestations of fatigue in vastus lateralis, medialis obliquus and medialis longus muscles.* Journal of Electromyography and Kinesiology, 2008. **18**(6): p. 1032-1037.

82. Kallenberg, L.A.C., et al., *Reproducibility of MUAP properties in array surface EMG recordings of the upper trapezius and sternocleidomastoid muscle.* Journal of Electromyography and Kinesiology, 2009. **19**(6): p. e536-e542.

83. Mesin, L., et al., *A bi-dimensional index for the selective assessment of myoelectric manifestations of peripheral and central muscle fatigue.* Journal of Electromyography and Kinesiology, 2009. **19**(5): p. 851-863.

84. Staudenmann, D., et al., *Heterogeneity of muscle activation in relation to force direction: A multi-channel surface electromyography study on the triceps surae muscle.* Journal of Electromyography and Kinesiology, 2009. **19**(5): p. 882-895.

85. Barbero, M., et al., *Reliability of surface EMG matrix in locating the innervation zone of upper trapezius muscle.* Journal of Electromyography and Kinesiology, 2011. **21**(5): p. 827-833.

86. Melchiorri, G. and A. Rainoldi, *Muscle fatigue induced by two different resistances: Elastic tubing versus weight machines.* Journal of Electromyography and Kinesiology, 2011. **21**(6): p. 954-959.

87. Minetto, M.A., et al., *Feasibility study of detecting surface electromyograms in severely obese patients.* Journal of Electromyography and Kinesiology, 2013. **23**(2): p. 285-295.

88. Rodriguez-Falces, J., et al., *Spatial distribution of surface action potentials generated by individual motor units in the human biceps brachii muscle.* Journal of Electromyography and Kinesiology, 2013. **23**(4): p. 766-777.

89. Bosch, T., et al., *The effect of work pace on workload, motor variability and fatigue during simulated light assembly work.* Ergonomics, 2011. **54**(2): p. 154-168.

90. Kleine, B.U., et al., *Magnetic stimulation-induced modulations of motor unit firings extracted from multi-channel surface EMG.* Muscle & Nerve, 2000. **23**(7): p. 1005-1015.

91. Wood, S.M., et al., *Surface electromyography using electrode arrays: A study of motor neuron disease.* Muscle & Nerve, 2001. **24**(2): p. 223-230.

92. Merletti, R., et al., *Effect of age on muscle functions investigated with surface electromyography.* Muscle & Nerve, 2002. **25**(1): p. 65-76.

93. Bazzucchi, I., et al., *Differences between young and older women in maximal force, force fluctuations, and surface emg during isometric knee extension and elbow flexion.* Muscle & Nerve, 2004. **30**(5): p. 626-635.

94. Drost, G., et al., *Motor unit characteristics in healthy subjects and those with postpoliomyelitis syndrome: A high-density surface EMG study.* Muscle & Nerve, 2004. **30**(3): p. 269-276.

95. Pozzo, M., et al., *Muscle-fiber conduction velocity estimated from surface emg signals during explosive dynamic contractions.* Muscle & Nerve, 2004. **29**(6): p. 823-833.

96. Beck, R.B., et al., *Tracking motor unit action potentials in the tibialis anterior during fatigue.* Muscle & Nerve, 2005. **32**(4): p. 506-514.

97. Blok, J.H., et al., *Motor unit action potential topography and its use in motor unit number estimation.* Muscle & Nerve, 2005. **32**(3): p. 280-291.

98. Bazzucchi, I., et al., *Coactivation of the elbow antagonist muscles is not affected by the speed of movement in isokinetic exercise.* Muscle & Nerve, 2006. **33**(2): p. 191-199.

99. Van Beekvelt, M.C.P., et al., *Na+-K+-ATPase is not involved in the warming-up phenomenon in generalized myotonia.* Muscle & Nerve, 2006. **33**(4): p. 514-523.

100. Mulder, E.R., et al., *Knee extensor fatigability after bedrest for 8 weeks with and without countermeasure.* Muscle & Nerve, 2007. **36**(6): p. 798-806.

101. Kleine, B.U., et al., *Interspike interval analysis in a patient with peripheral nerve hyperexcitability and potassium channel antibodies.* Muscle & Nerve, 2008. **37**(2): p. 269-274.

102. Kallenberg, L.A.C. and H.J. Hermens, *Motor unit properties of biceps brachii in chronic stroke patients assessed with high-density surface EMG.* Muscle & Nerve, 2009. **39**(2): p. 177-185.

103. Piitulainen, H., et al., *Effect of electrode location on surface electromyography changes due to eccentric elbow flexor exercise.* Muscle & Nerve, 2009. **40**(4): p. 617-625.

104. Bazzucchi, I., et al., *Caffeine improves neuromuscular function during maximal dynamic exercise.* Muscle & Nerve, 2011. **43**(6): p. 839-844.

105. Kallenberg, L.A.C. and H.J. Hermens, *Motor unit properties of biceps brachii during dynamic contractions in chronic stroke patients.* Muscle & Nerve, 2011. **43**(1): p. 112-119.

106. Bonfiglioli, R., et al., *Surface electromyography features in manual workers affected by carpal tunnel syndrome.* Muscle & Nerve, 2012. **45**(6): p. 873-882.

107. Bouillard, K., et al., *Prediction of time-to-exhaustion in the first dorsal interosseous muscle from early changes in surface electromyography parameters.* Muscle & Nerve, 2012. **45**(6): p. 835-840.

108. Klaver-Król, E.G., et al., *Muscle fiber velocity and electromyographic signs of fatigue in fibromyalgia.* Muscle & Nerve, 2012. **46**(5): p. 738-745.

109. McIntosh, K.C.D. and D.A. Gabriel, *Reliability of a simple method for determining muscle fiber conduction velocity.* Muscle & Nerve, 2012. **45**(2): p. 257-265.

110. Menotti, F., et al., *Neuromuscular function after muscle fatigue in Charcot–Marie–Tooth type 1A patients.* Muscle & Nerve, 2012. **46**(3): p. 434-439.

111. Watanabe, K., et al., *Motor unit firing pattern of vastus lateralis muscle in type 2 diabetes mellitus patients.* Muscle & Nerve, 2013. **48**(5): p. 806-813.

112. Hermens, H.J. and R. Merletti, *SENIAM 1: European Activities on Surface Electromyography: Proceedings of the first general SENIAM workshop, Torino, Italy, September 6-7 1996*. 1996: Roessingh Research and Development.

113. Hermens, H., G. Hägg, and B. Freriks. *SENIAM 2: European Applications on Surface ElectroMyography*. in *Proceedings of the Second General SENIAM Workshop, Stockholm, Sweden, ISBN*. 1997.

114. Hermens, H.J., et al. *SENIAM 3: Surface ElectroMyography Application Areas and Parameters*. in *Proceedings of the third general SENIAM (Surface EMG for Non Invasive Assessment of Muscles) workshop, May*. 1998.

115. Hermens, H. and B. Freriks, *SENIAM 4: Future Applications of Surface ElectroMyography.* Roessingh Research and Development, Enschede, 1999.

116. Hermens, H. and B. Freriks, *SENIAM 5: The State of the Art on Sensors and Sensor Placement Procedures for Surface ElectroMyography: A proposal for sensor placement procedures.* Roessingh Research and Development, Enschede, 1997.

117. Hermens, H., et al., *SENIAM 6: State of the Art on Modelling Methods for Surface ElectroMyography.* Roessingh Research and Development, Enschede, 1998.

118. Hermens, H.J., et al., *SENIAM 7: The State of the Art on Signal Processing Methods for Surface ElectroMyography.* Roessingh Research and Development, Enschede, 1999.

119. Hermens, H.J., et al., *SENIAM 8: European recommendations for surface electromyography.* Roessingh Research and Development, Enschede, 1999.

120. Freriks, B. and H.J. Hermens, *SENIAM 9: European recommedations for surface electromyography (CDROM).* Roessingh Research and Development, Enschede, 1999.

121. Bronzino, J.D., *The Biomedical Engineering Handbook*. 2006, 6000 Broken Sound Parkway NW, Suite 300: CRC Press.

122. Webster, J.G., *Medical Instrumentation: Application and Design*. 4th ed, ed. J.G. Webster. 2009, USA: Wiley.

123. Robertson, D.G.E., et al., *Research Methods in Biomechanics*. Second ed. 2014, Champaign, IL: Human Kinetics.

124. Merletti, R., D. Farina, and A. Granata, *Non-invasive assessment of motor unit properties with linear electrode arrays*, in *Clinical Neurophysiology: From Receptors to Perception*. 1999, Elsevier: Amtersdam. p. 293-300.

125. Merletti, R., B. Afsharipour, and G. Piervirgili, *High Density Surface EMG Technology*, in *Converging Clinical and Engineering Research on Neurorehabilitation*, L.J. Pons, D. Torricelli, and M. Pajaro, Editors. 2013, Springer Berlin Heidelberg: Berlin, Heidelberg. p. 1205-1209.

126. Rau, G. and C. Disselhorst-Klug, *Principles of high-spatial-resolution surface EMG (HSR-EMG): single motor unit detection and application in the diagnosis of neuromuscular disorders.* Journal of Electromyography and Kinesiology, 1997. **7**(4): p. 233-239.

127. Farina, D., et al., *Comparison of spatial filter selectivity in surface myoelectric signal detection: Influence of the volume conductor model.* Medical and Biological Engineering and Computing, 2004. **42**(1): p. 114-120.

128. Bahm, J., et al., *High spatial resolution electromyography and video-assisted movement analysis in children with obstetric brachial plexus palsy.* Hand Clinics, 2003. **19**(3): p. 393-399.

129. Farina, D., et al., *Single motor unit analysis from spatially filtered surface electromyogram signals. Part I: Spatial selectivity.* Medical and Biological Engineering and Computing, 2003. **41**(3): p. 330-337.

130. Schulte, E., et al., *Single motor unit analysis from spatially filtered surface electromyogram signals. Part 2: Conduction velocity estimation.* Medical and Biological Engineering and Computing, 2003. **41**(3): p. 338-345.

131. Farina, D., E. Fortunato, and R. Merletti, *Noninvasive estimation of motor unit conduction velocity distribution using linear electrode arrays.* Biomedical Engineering, IEEE Transactions on, 2000. **47**(3): p. 380-388.

132. Merletti, R., A. Rainoldi, and D. Farina, *Surface Electromyography for Noninvasive Characterization of Muscle.* Exercise and Sport Sciences Reviews, 2001. **29**(1): p. 20-25.

133. Huigen, E., A. Peper, and C. Grimbergen, *Investigation into the origin of the noise of surface electrodes.* Medical and biological engineering and computing, 2002. **40**(3): p. 332-338.

134. Clancy, E., E.L. Morin, and R. Merletti, *Sampling, noise-reduction and amplitude estimation issues in surface electromyography.* Journal of Electromyography and Kinesiology, 2002. **12**(1): p. 1-16.

135. *Standards for Reporting EMG Data.* Journal of Electromyography and Kinesiology, 2014. **24**(1): p. I-II.

136. Schwartz, M.S. and F. Andrasik, *Biofeedback: A Practitioner's Guide*. 3rd ed. 2003, New York: The Guildford Press.

137. Dvir, Z., *Isokinetics : Muscle Testing, Interpretation, and Clinical Applications*. Second ed. 2004, New York: Churchill Livingstone.

138. Ritter, D.J., *LabVIEW GUI: Essential Techniques*. 2002: McGraw-Hill.

139. Pincivero, D.M., et al., *Angle- and gender-specific quadriceps femoris muscle recruitment and knee extensor torque.* Journal of Biomechanics, 2004. **37**(11): p. 1689-1697.

140. Shenoy, S., P. Mishra, and J.S. Sandhu, *Peak Torque and IEMG Activity of Quadriceps Femoris Muscle at Three Different Knee Angles in a Collegiate Population.* Journal of Exercise Science & Fitness, 2011. **9**(1): p. 40-45.

141. De Ruiter, C.J., et al., *Relative torque contribution of vastus medialis muscle at different knee angles.* Acta Physiologica, 2008. **194**(3): p. 223-237.

142. Toonstra, J. and C.G. Mattacola, *Test-retest reliability and validity of isometric knee-flexion and -extension measurement using 3 methods of assessing muscle strength.* Journal Of Sport Rehabilitation, 2013. **Technical Notes**(7).

143. Konrad, P., *The ABC of EMG: A Practical Introduction to Kinesiological Electromyography*. 2004, Arizona: Noraxon USA, Inc.

144. Merletti, R., et al., *Advances in surface EMG: recent progress in detection and processing techniques.* Critical Reviews In Biomedical Engineering, 2010. **38**(4): p. 305-345.

145. Petrofsky, J., *The effect of the subcutaneous fat on the transfer of current through skin and into muscle.* Medical Engineering and Physics, 2008. **30**: p. 1168-1176.

146. Nordander, C., et al., *Influence of the subcutaneous fat layer, as measured by ultrasound, skinfold calipers and BMI, on the EMG amplitude.* European Journal of Applied Physiology, 2003. **89**(6): p. 514-9.

147. Selkow, N.M., B.G. Pietrosimone, and S.A. Saliba, *Subcutaneous Thigh Fat Assessment: A Comparison of Skinfold Calipers and Ultrasound Imaging.* Journal

of Athletic Training (National Athletic Trainers' Association), 2011. **46**(1): p. 50-54.

148. Lin, H.-T., et al., *Comparison of EMG Activity Between Maximal Manual Muscle Testing and Cybex Maximal Isometric Testing of the Quadriceps Femoris.* Journal of the Formosan Medical Association, 2008. **107**(2): p. 175-180.

149. Reinking, M.F., et al., *Assessment of quadriceps muscle performance by hand-held, isometric, and isokinetic dynamometry in patients with knee dysfunction.* Journal of Orthopaedic & Sports Physical Therapy, 1996. **24**(3): p. 154-159 6p.

150. Krishnan, C. and G.N. Williams, *Variability in antagonist muscle activity and peak torque during isometric knee strength testing.* The Iowa Orthopaedic Journal, 2009. **29**: p. 149-158.

151. Eugenijus, K., *Biomedical Signals and Sensors I: Linking Physiological Phenomena and Biosignals*. 2012, New York: New York.

152. Peters, T.M. and J. Williams, *The Fourier Transform in Biomedical Engineering*. 1998, Boston, USA: Birkhäuser.

153. Cohen, A., *Biomedical Signal Processing: Volume 1 Time and Frequency Domain Analysis*. Vol. 1. 1986, Boca Raton, FL: CRC Press.

154. Smith, S.W., *The Scientist and Engineer's Guide to Digital Signal Processing*. 1997: California Technical Publishing.

155. Vegte, J.V.d., *Fundamentals of Digital Signal Processing*. 2002, Sydney: Prentice Hall.

156. Ives, J.C. and J.K. Wigglesworth, *Sampling rate effects on surface EMG timing and amplitude measures.* Clinical Biomechanics, 2003. **18**(6): p. 543-552.

157. Durkin, J.L. and J.P. Callaghan, *Effects of minimum sampling rate and signal reconstruction on surface electromyographic signals.* Journal of Electromyography and Kinesiology, 2005. **15**(5): p. 474-481.

158. Larivière, C., A. Delisle, and A. Plamondon, *The effect of sampling frequency on EMG measures of occupational mechanical exposure.* Journal of Electromyography and Kinesiology, 2005. **15**(2): p. 200-209.

159. Shannon, C.E., *Communication In The Presence Of Noise.* Proceedings of the IEEE, 1998. **86**(2): p. 447-457.

160. Beaulieu, N.C., *Introduction to "Certain topics in telegraph transmission theory".* Proceedings of the IEEE, 2002. **90**(2): p. 276-279.

161. Nyquist, H., *Certain topics in telegraph transmission theory.* Proceedings of the IEEE, 2002. **90**(2): p. 280-305.

162. Semmlow, J.L., *Biosignal and Bomedical Image Processing: MATLAB-based Applications*. Signal processing and communications ;22. 2004, New York: CRC Press.

163. Addison, P.S., J. Walker, and R.C. Guido, *Time-Frequency Analysis of Biosignals.* IEEE Engineering in Medicine and Biology Magazine, 2009. **28**(5): p. 14-29.

164. Addison, P.S., *The Illustrated Wavelet Transform Handbook*. 2002, Institute of Physics Publishing: Bristol.

165. De Luca, C.J. and E.J. van Dyk, *Derivation of some parameters of myoelectric signals recorded during sustained constant force isometric contractions.* Biophysical Journal, 1975. **15**(12): p. 1167-1180.

166. Farina, D. and R. Merletti, *Comparison of algorithms for estimation of EMG variables during voluntary isometric contractions.* Journal of Electromyography and Kinesiology, 2000. **10**(5): p. 337-349.

167. Luca, C.J.D., *Physiology and Mathematics of Myoelectric Signals.* IEEE Transactions on Biomedical Engineering, 1979. **BME-26**(6): p. 313-325.

168. De Luca, C.J., *The Use of Surface Electromyography in Biomechanics.* Journal of Applied Biomechanics, 1997. **13**(2): p. 135-163.

169. Payton, C. and R. Bartlett, *Biomechanical Evaluation of Movement in Sport and Exercise: The British Association of Sport and Exercise Sciences Guide*. 2008, New York, USA: Taylor & Francis.

170. Hägg, G., *Electromyographic fatigue analysis based on the number of zero crossings.* Pflugers Archiv European Journal of Physiology, 1981. **391**(1): p. 78.

171. Inbar, G.F., et al., *Monitoring surface EMG spectral changes by the zero crossing rate.* Medical and Biological Engineering and Computing, 1986. **24**(1): p. 10-18.

172. Rice, S.O., *Mathematical analysis of random noise.* The Bell System Technical Journal, 1944. **23**(3): p. 282-332.

173. Sze-Hou, C., G.E. Pihl, and M.W. Essigmann, *Representations of Speech Sounds and Some of Their Statistical Properties.* Proceedings of the IRE, 1951. **39**(2): p. 147-153.

174. Hägg, G.M. and J. Suurküla, *Zero crossing rate of electromyograms during occupational work and endurance tests as predictors for work related myalgia in the shoulder/neck region.* European Journal of Applied Physiology and Occupational Physiology, 1991. **62**(6): p. 436-444.

175. Cifrek, M., et al., *Surface EMG based muscle fatigue evaluation in biomechanics.* Clinical Biomechanics, 2009. **24**(4): p. 327-340.

176. Viitasalo, J.H.T. and P.V. Komi, *Signal characteristics of EMG during fatigue.* European Journal of Applied Physiology and Occupational Physiology, 1977. **37**(2): p. 111-121.

177. Gabriel, D.A., *Reliability of SEMG spike parameters during concentric contractions.* Electromyography and Clinical Neurophysiology, 2000. **40**(7): p. 423-430.

178. de Silva, C.W., *Sensors and Actuators: Engineering System Instrumentation*. Second Edition ed. 2015: Taylor & Francis.

179. Chidambaram, M., *Basics of Data Acquisition and Control*, in *Handbook of Networked and Embedded Control Systems*, D. Hristu-Varsakelis and W.S. Levine, Editors. 2005, Birkhäuser Boston: Boston, MA. p. 227-257.

180. Lindstrom, L.H. and R.I. Magnusson, *Interpretation of myoelectric power spectra: A model and its applications.* Proceedings of the IEEE, 1977. **65**(5): p. 653.

181. Stulen, F.B. and C.J. De Luca, *Frequency Parameters of the Myoelectric Signal as a Measure of Muscle Conduction Velocity.* IEEE Transactions on Biomedical Engineering, 1981. **BME-28**(7): p. 515.

182. Gabor, D., *Theory of communication. Part 1: The analysis of information.* Electrical Engineers - Part III: Radio and Communication Engineering, Journal of the Institution of, 1946. **93**(26): p. 429-441.

183. Mertins, A., *Signal Analysis*. 1999, Chichester: John Wiley & Sons.

184. Akay, M., *Time Frequency and Wavelets in Biomedical Signal Processing*. 1998: IEEE Press series in biomedical Engineering.

185. Misiti, M., et al., *Wavelet Toolbox For Use with MATLAB*. 2000, Natick, MA: The MathWorks Inc. 1.1-2.56.

186. Meyer, Y., *Ondelettes, fonctions splines et analyses graduées.* Lectures given at the University of Torino, Italy, 1986.

187. Daubechies, I., *Orthonormal bases of compactly supported wavelets.* Communications on pure and applied mathematics, 1988. **41**(7): p. 909-996.

188. Mallat, S.G., *A theory for multiresolution signal decomposition: the wavelet representation.* IEEE Transactions on Pattern Analysis and Machine Intelligence, 1989. **11**(7): p. 674-693.

189. Mallat, S., *A Wavelet Tour of Signal Processing: The Sparse Way*. 2008: Academic press.

190. Kilby, J. and H.G. Hosseini. *Wavelet analysis of surface electromyography signals*. in *Engineering in Medicine and Biology Society, 2004. IEMBS '04. 26th Annual International Conference of the IEEE*. 2004.

191. Constable, R. and R.J. Thornhill, *Using the Discrete Wavelet Transform For Time-Frequency Analysis of the Surface EMG Signal.* ISA, 1993. **16**: p. 121-127.

192. Broman, H., G. Bilotto, and C.J. De Luca, *Myoelectric signal conduction velocity and spectral parameters: influence of force and time.* J Appl Physiol (1985), 1985. **58**(5): p. 1428-37.

193. Arendt-Nielsen, L. and M. Zwarts, *Measurement of muscle fiber conduction velocity in humans: techniques and applications.* J Clin Neurophysiol, 1989. **6**(2): p. 173-90.

194. Zwarts, M.J., *Evaluation of the estimation of muscle fiber conduction velocity. Surface versus needle method.* Electroencephalography and Clinical Neurophysiology, 1989. **73**(6): p. 544-548.

195. Sollie, G., et al., *The measurement of the conduction velocity of muscle fibres with surface EMG according to the cross-correlation method.* Electromyogr Clin Neurophysiol, 1985. **25**(4): p. 193-204.

196. Winter, D.A., A.J. Fuglevand, and S.E. Archer, *Crosstalk in surface electromyography: Theoretical and practical estimates.* Journal Of Electromyography And Kinesiology: Official Journal Of The International Society Of Electrophysiological Kinesiology, 1994. **4**(1): p. 15-26.

197. Rababy, N., R.E. Kearney, and I.W. Hunter, *Method for EMG conduction velocity estimation which accounts for input and output noise.* Medical & Biological Engineering & Computing, 1989. **27**(2): p. 125-9.

198. Fiorito, A., S. Rao, and R. Merletti, *Analogue and digital instruments for non-invasive estimation of muscle fibre conduction velocity.* Medical & Biological Engineering & Computing, 1994. **32**(5): p. 521.

199. Broman, H., G. Bilotto, and C.J. De Luca, *A note on the noninvasive estimation of muscle fiber conduction velocity.* IEEE Trans Biomed Eng, 1985. **32**(5): p. 341-4.

200. Sacco, I.C.N., et al., *A method for better positioning bipolar electrodes for lower limb EMG recordings during dynamic contractions.* Journal of Neuroscience Methods, 2009. **180**(1): p. 133-137.

201. Rainoldi, A., G. Melchiorri, and I. Caruso, *A method for positioning electrodes during surface EMG recordings in lower limb muscles.* Journal of Neuroscience Methods, 2004. **134**(1): p. 37-43.

202. Kirkwood, B.R., J.A.C. Sterne, and B.R. Kirkwood, *Essential Medical Statistics*. 2003, Massachusetts: Blackwell Science.

203. Vogt, W.P., *Selecting the Right Analyses for Your Data : Quantitative, Qualitative, and Mixed Methods*. 2014, New York: The Guilford Press.

204. *Linear Circuit Design Handbook*, ed. H. Zumbahlenas. 2008, Amsterdam; Boston: Elsevier/Newnes Press.

205. *INA118 Precision, Low Power Instrumentation Amplifier*. Available from: http://www.ti.com/lit/ds/symlink/ina118.pdf.

206. Horowitz, P. and W. Hill, *The Art of Electronics*. Second ed. 1989: Cambridge University Press, USA.

207. Bartel, T.W. and S.L. Yaniv, *Creep and creep recovery response of load cells tested according to U.S. and international evaluation procedures.* Journal of Research of the National Institute of Standards and Technology, 1997. **102**(3): p. 349-362.

208. Javier;, M.R.F., et al. *Procedure for load cell calibration at ELSA Reaction Wall*. 2013.

209. King, R.H., *Introduction to Data Acquisition with LabVIEW*. 2nd ed. 2012, New York: McGraw-Hill. 288.